Clinical Phenotypes in Heart Failure Defined by Cardiac Magnetic Resonance Feature Tracking and Parametric Mapping



Radu Tanacli

Medical Sciences Division DTC, Linacre College
University of Oxford

Supervisors:
Professor Sebastian Kelle
Professor Robert JC Gilbert

A thesis submitted for the degree of Doctor of Philosophy
Trinity Term 2022

This thesis is dedicated to my wife, Barbara,

for all her unconditional love and patience and sacrifices

ὣς εἰποῦσα θεὰ σκέδασ᾽ ἠέρα, εἵσατο δὲ χθών:
γήθησέν τ᾽ ἄρ᾽ ἔπειτα πολύτλας δῖος Ὀδυσσεύς,
χαίρων ᾗ γαίῃ, κύσε δὲ ζείδωρον ἄρουραν.
αὐτίκα δὲ νύμφῃς ἠρήσατο, χεῖρας ἀνασχών:
νύμφαι νηϊάδες, κοῦραι Διός, οὔ ποτ᾽ ἐγώ γε
ὄψεσθ᾽ ὔμμ᾽ ἐφάμην: νῦν δ᾽ εὐχωλῇς ἀγανῇσι χαίρετ᾽

Odyssea, book 13, lines 352-358, Homeri Opera, Ed. Thomas W Allen (OUP, Oxford, 1975)

There is no Frigate like a Book
To take us Lands away,
Nor any Coursers like a Page
Of prancing Poetry –
This Traverse may the poorest take
Without oppress of Toll –
How frugal is the Chariot
That bears a Human soul.

The Poems of Emily Dickinson, Variorum Edition. Ed. R. W. Franklin (Belknap Press, Harvard, 1998)

Table of Contents

Acknowledgements 6
Published articles and manuscripts in preparation arising from this work 7
Abbreviations and Acronyms 9
Declaration 11
Thesis Abstract 12
Chapter One: General Introduction, Aims 14
1.1 Heart Failure: definition, epidemiology, classification 15
1.1.1 Classification based on disease progression 15
1.1.2 Difference in pathophysiology between HFrEF and HFpEF 16
1.1.3 ESC Classification of HF based on EF 18
1.1.4 Conceptual distinction between HF and Cardiac Remodeling 20
1.2 Role of CMR in Early Detection and Assessment of Cardiac Remodelling 22
1.2.1 Ventricular dilatation 22
1.2.2 Hypertrophy: definition, types, molecular mechanisms 23
1.2.3 Cardiomyocyte loss. 24
1.2.4 Cardiac fibrosis: definition, types, molecular mechanisms 24
1.2.5 Cardiac mechanical deficit: classification, molecular mechanisms 26
1.2.6 Infection, Inflammation 28
1.2.7 Left atrium and Right Ventricle – particularities, significance 29
1.3 CMR diagnostic role in Diastolic Dysfunction 29
1.4 Atrial remodelling in Heart Failure 31
1.5 Feature tracking – theoretical basis, usefulness in HF, limitations 35
1.6 Parametric mapping 40
1.7 Phenylketonuria: pathogenesis, cardiac phenotype 46
1.8 COVID-19 and cardiac damage. Role of CMR 48
1.9 Hypotheses, objectives and aims 52
Chapter Two: Methods 54
2.1 Study populations 55
2.2 Cardiac magnetic resonance: systems and protocols of image acquisition 60
2.3 CMR image analysis 62
2.5 Blood Samples and Biochemistry 68
2.6 Bioelectrical impedance 68
2.7 Endomyocardial Biopsy Samples 69
2.8 WHO Score of COVID-19 Severity Description 70
Chapter Three: Multilayer Strain in Heart Failure 72
3.1 Abstract 73
3.2 Background 74
3.3 Specific Methods 76
3.4 Results 78
3.4.1 Study population characteristics 78
3.4.2 Comparison between Endo, Myo, Epi layers 81
3.4.3 Comparison between pathology groups 85
3.4.4 ROC analyses. Comparative analysis of HF progression 86
3.4.5 Complementary diagnostic role of GCS and GLS in HF 86

3.5 Discussion 88
3.6 Limitations 94
3.7 Conclusions 94
Chapter Four: Left Atrial Function in Heart Failure 96
4.1 Abstract 97
4.2 Background 98
4.3 Specific Methods 99
4.3.1 Study population 99
4.3.2 CMR and Echocardiography 99
4.3.3 Image analysis 99
4.3.4 Definition of Atrial Failure 101
4.3.5 Statistical Analysis. 101
4.4 Results 102
4.4.1 Study population 102
4.4.2 Comparison between different groups of HF 103
4.4.3 Correlates of atrial dysfunction. Bivariate regressions. 106
4.4.4 Comparison between HF without atrial failure and HF with atrial failure . 107
4.5 Discussion 111
4.6 Limitations 114
4.7 Clinical implications 115
Chapter Five: CMR vs. LVEDP 116
5.1 Abstract 117
5.2 Introduction 118
5.3 Specific Methods 119
5.3.1 Study Population 119
5.3.2 Cardiac magnetic resonance 120
5.3.4 Echocardiography 120
5.3.5 Image analysis 120
5.3.6 Left Ventricular End-Diastolic Pressure 120
5.3.6 Statistical Analysis 121
5.4 Results 122
Chapter Six: Cardiac Phenotype in PKU: Baseline 136
6.1 Abstract 137
6.2 Background 138
6.3 Specific Methods 139
6.3.1 Study Population 139
6.3.2 Cardiac magnetic resonance. 140
6.3.3 Image analysis 140
6.3.4 Echocardiography 140
6.3.5 Biochemistry 140
6.3.6 Statistical Analysis 141
6.4 Results 142
6.5 Discussion 153
6.6 Limitations 158
6.7 Conclusions 159
Chapter Seven: Cardiac Phenotype in PKU: Follow-up 160
7.1 Abstract 161
7.2 Introduction 162

7.3 Specific Methods 163
7.3.1 Study Population 163
7.3.2 Cardiac magnetic resonance 164
7.3.3 Image analysis 164
7.3.5 Biochemistry 164
7.3.6 Statistical Analysis 165
7.4 Results 165
7.4.1 Population Characteristics 165
7.4.2 Cardiac anatomy, function and structural modfications 172
7.4.3 Cardiac deformation and Hemodynamic forces 172
7.4.4. Relation between phenylalanine levels and cardiac phenotype 173
7.5 Discussion 175
7.6 Limitations 180
7.7 Conclusions 180
Chapter Eight: CMR in COVID-19 and Acute Myocarditis 182
8.1 Abstract 183
8.2 Background 184
8.3 Specific Methods 186
8.3.1. Study population 186
8.3.2. WHO Score Description 187
8.3.3 Cardiac magnetic resonance 188
8.3.4 Image analysis 188
8.3.5 Biopsy samples 189
8.3.6 Statistical analysis 189
8.4 Results 190
8.4.1 Study Population Characteristics 190
8.4.2 Comparison between COVID-19, myocarditis and healthy volunteers 192
8.4.3 CMR - Lake Louise Criteria and EMB histological analyses. 195
8.4.4 CMR parameters and WHO Classification 199
8.4.5 CMR parameters. Comparison follow-up 199
8.5 Discussion 203
8.6 Limitations 207
8.7 Conclusions 208
Chapter Nine: Summary and Perspectives 209
References 215

Acknowledgements

The work presented here is the result of several years of strenuous work that would have not been possible without the constant support, understanding and kindness of the people that I would like to wholeheartedly thank here. For me this thesis is a boat to bring me back home after a tormenting personal odyssey.

First, I would like to thank my supervisors: Sebastian, for providing me with the right tools, scientific guidance and friendship that have been a great gift, thank you for offering me the chance to work together in a tranquil and productive atmosphere when very few others did; and Rob for his generous and completely altruistic support in a moment of crisis and further on throughout this endeavour, thank you for always finding a good word of comfort or encouragement, it really have meant a lot. To Athanasia, for her generous support in designing and accomplishing the PKU projects in difficult times, for her joyfulness and enthusiasm.

To my bright and dedicated colleagues: Lukas, Alessandro, Alessio, Patrick, Jakob, Victoria, Mahsa, Jenny, Sarah, Djawid, Tomas, Paulius, Justina, Agneta, Anna, Gisela and Undine, you were of such a great help, it has been a great experience meeting you all and working together these years.

This thesis and my career altogether would not have been possible without the protective wings of my parents, Adrian and Luminita-Georgeta, notwithstanding the geographical distance you were always with me and due to the strength of your love, I have felt your presence all the time, ever stronger in moments of disillusion and doubt. Because of you and your sacrifices and endurance, the little candle of goodness, burning all this time, prevailed over the heart of darkness. To the rest of my family and friends, in Bucharest and Catania, who believed in me and surrounded me with comfort and their love.

Published articles and manuscripts in preparation arising from this work

Published articles:

1. Doeblin P, Hashemi D, **Tanacli R**, Lapinskas T, Gebker R, Stehning C, Motzkus LA, Blum M, Tahirovic E, Dordevic A, Kraft R, Zamani SM, Pieske B, Edelmann F, Dungen HD and Kelle S. **CMR Tissue Characterization in Patients with HFmrEF.** *J Clin Med*. 2019;8.
2. Pedrizzetti G, **Tanacli R**, Lapinskas T, Zovatto L, Pieske B, Tonti G and Kelle S. **Integration between volumetric change and strain for describing the global mechanical function of the left ventricle**. *Med Eng Phys*. 2019;74:65-72.
3. **Tanacli R**, Hashemi D, Lapinskas T, Edelmann F, Gebker R, Pedrizzetti G, Schuster A, Nagel E, Pieske B, Dungen HD and Kelle S. **Range Variability in CMR Feature Tracking Multilayer Strain across Different Stages of Heart Failure**. *Sci Rep*. 2019;9:16478.
4. Bucius P, Erley J, **Tanacli R**, Zieschang V, Giusca S, Korosoglou G, Steen H, Stehning C, Pieske B, Pieske-Kraigher E, Schuster A, Lapinskas T and Kelle S. **Comparison of feature tracking, fast-SENC, and myocardial tagging for global and segmental left ventricular strain**. *ESC Heart Fail.* 2020;7:523-532.
5. Erley J, **Tanacli R**, Genovese D, Tapaskar N, Rashedi N, Bucius P, Kawaji K, Karagodin I, Lang RM, Kelle S, Mor-Avi V and Patel AR. **Myocardial strain analysis of the right ventricle: comparison of different cardiovascular magnetic resonance and echocardiographic techniques**. *J Cardiovasc Magn Reson*. 2020;22:51.
6. Faragli A, **Tanacli R**, Kolp C, Abawi D, Lapinskas T, Stehning C, Schnackenburg B, Lo Muzio FP, Fassina L, Pieske B, Nagel E, Post H, Kelle S and Alogna A. **Cardiovascular magnetic resonance-derived left ventricular mechanics-strain, cardiac power and end-systolic elastance under various inotropic states in swine**. *J Cardiovasc Magn Reson*. 2020;22:79.
7. Faragli A, **Tanacli R**, Kolp C, Lapinskas T, Stehning C, Schnackenburg B, Lo Muzio FP, Perna S, Pieske B, Nagel E, Post H, Kelle S and Alogna A. **Cardiovascular magnetic resonance feature tracking in pigs: a reproducibility and sample size calculation study.** *Int J Cardiovasc Imaging. 2020;36:703-712.*
8. **Tanacli R**, Hashemi D, Pieske B, Dungen HD and Kelle S. **Multilayer myocardial strain improves the diagnosis of heart failure with preserved ejection fraction**. *ESC Heart Fail*. 2020;7:3240-3245.
9. **Tanacli R**, Hassel J.-H., Gebker R, …Tacke F, Pieske B, Spranger J, Plöckinger U, Ziagaki A., Kelle S. **Cardiac Magnetic Resonance Reveals Incipient Cardiomyopathy Traits in Adult Patients with Phenylketonuria**, *J Am Heart Assoc.* 2021 Sep 7;10(17):e020351.
10. **Tanacli R**, Doeblin P,Götze C, Zieschang V, Faragli, Stehning C, …,Van Linthout S, Pieske B, Tschöpe C, Kelle S. **COVID-19 versus classical myocarditis associated myocardial injury evaluated by Cardiac Magnetic Resonance and Endomyocardial Biopsy**. *Front Cardiovasc Med.* 2021 Dec 24;8:737257. doi: 10.3389
11. Chen W, Doeblin P, Al-Tabatabaee S, Klingel K, **Tanacli R**, Jakob Weiß K, Stehning C, Patel AR, Pieske B, Zou J, Kelle S. **Synthetic Extracellular Volume in Cardiac Magnetic Resonance Without Blood Sampling: a Reliable Tool to**

Replace Conventional Extracellular Volume. *Circ Cardiovasc Imaging*. 2022 Apr 1:101161

12. Jahnke C, Doeblin P, **Tanacli R**, Witt U, Schneider M, Stehning C, Pieske B, Kelle S. **Case Series of Potential Cardiac Inflammation Associated With Various SARS-CoV-2 Vaccinations Assessed by Cardiac MRI**. *Front Cardiovasc Med.* 2022 Apr 8; 9:829392.

Publications in press, manuscripts under review or submitted:

13. **Tanacli R**, Doeblin P, Faragli A, Weiss J, Hashimi D, Tacke F, Pieske B, Spranger J, Plöckinger U, Ziagaki A, Kelle S - **Phenylalanine Levels are Determinant for the Cardiac Phenotype in Adult Patients with Phenylketonuria**
14. **Tanacli R**, Weiss J, Savova Y, Doeblin P… Pieske B, Kelle S - **CMR Role in the Assessment of Patients with elevated LVEDP**
15. **Tanacli R**, Schulz-Menger J, Parker M, Blaszczyk E, Armstrong P, Butler J, Lam Carolyn, Pieske B, Kim RJ, Kelle S - **CMR insights from the VICTORIA Trial – valid basis for sample size calculations for future clinical trials in patients with severe heart hailure.**
16. **Tanacli R**, Hashemi D, Doeblin P, Neye M, Motzkus LA, Blum M, Kraft R, Zamani SM, Pieske B, Düngen HD, Kelle S - **CMR diagnosis of Left Atrial Failure: characterising a distinct clinical feature in Heart Failure patients.**

Abbreviations and Acronyms

2Ch, 3Ch, 4Ch – 2 chamber, 3 chamber, 4 chamber view
ACC – American College of Cardiology
ACS – acute coronary syndromes
AHA – American Heart Association
Ao – aorta (aortic)
AUC – area under curve
CI – cardiac index
CMR – cardiac magnetic resonance
CO – cardiac output
COVID-19 – Coronavirus disease 2019
CR – cardiac remodeling
CT – computer tomography
DNA – desoxyribonucleic acid
E – transmitral flow velocity
e' – early diastolic tissue velocity
ECV – extracellular volume
EDV – end-diastolic volume
EF – ejection fraction
EMB – endomyocardial biopsy
Endo – sub-endocardial layer
Epi – sub-epicardial layer
ESC – European Society of Cardiology
ESV – end-systolic volume
FGF – fibroblast growth factor
FMD – flow mediated dilation
FT – feature tracking
GCS – global circumferential strain
GLS – global longitudinal strain
HD, HDF – hemodynamic, hemodynamic forces
HDL – high-density lipoproteins cholesterol
HF – heart failure
HFmrEF – heart failure with mid-range reduced ejection fraction
HFpEF – heart failure with preserved ejection fraction

HFrEF – heart failure with reduced ejection fraction

IGF – insulin-like growth factor, IGF-BP – Insulin-like growth factor-binding protein

LA – left atrium / atrial

LDL – low-density lipoproteins cholesterol

LGE – late gadolinium enhancement

LLC – Lake Louise Criteria

LV – left ventricle / ventricular

LVM – left ventricular mass

MI – myocardial infarction

MMP – Matrix metalloproteinase

MOLLI – modified Look-Locker Inversion-recovery

Myo – mid-myocardial layer

NT-proBNP – N-terminal pro-B type natriuretic peptide

PAH – phenylalanine hydroxylase

PDGF – platelet-derived growth factor

Phe – phenylalanine

PKU – phenylketonuria

PLN – phospholamban

RA – right atrium / atrial

RNA – ribonucleic acid

RV – right ventricle / ventricular

RVM – right ventricular mass

SARS-CoV-2 – severe acute respiratory syndrome coronavirus 2

SENSE - sensitivity encoding

SERCA – sarcoplasmic reticulum Ca^{2+}-ATPase

SSFP – steady-state free precession imaging

SV – stroke volume

TE – echo time

TIMP – tissue inhibitor of metalloproteinases

TR – repetition time

Tyr – tyrosine

VEGF-C – Vascular Endothelial Growth Factor C

WHO – World Health Organisation

Declaration

The work presented here is my own. Contribution of collaborators and colleagues is specified individually at the beginning of each chapter. The contents of Chapters 3, 6 and 8 have been previously published in peer-reviewed journals as detailed. For all previously published articles I designed the study in dialogue with my supervisors, collected the data, performed the analysis, wrote the manuscript and have been the corresponding author. The echocardiography scans were performed by Dr Djawid Hashemi and Dr Robin Kraft for the Empathy Cohort (Chapters 3 and 4), and Dr Michael Gräfe (Chapter 6). For Chapter 5, echocardiography data and analysis were collected and performed by Dr Yoanna Savova. For Chapter 8, Professor Karin Klingel and her team, performed the histological and molecular analysis of endomyocardial biopsy samples.

Thesis Abstract

In this thesis I applied cardiovascular magnetic resonance (CMR) feature tracking (FT) and parametric mapping, along with more general CMR and echocardiography methods and other specific methods (e.g. biochemistry, endomyocardial biopsy) to characterize various types of cardiac remodelling associated with heart failure (HF) or conditions that create cardiac dysfunction potentially associated to a preclinical phenotype of HF (patients with elevated left ventricular filling pressures, treated phenylketonuria and convalescent patients recovered from COVID-19).

My results indicate the important and specific role of FT CMR in quantification of functional deficit associated with HF. A multilayer systolic peak strain comparison individuates subendocardium as a particularly sensitive region of the myocardium for quantification of myocardial strain. I showed that Endo-Epi circumferential strain gradients, in particular, are progressively blunted in HFmrEF (Heart Failure with mid-range Ejection Fraction) and HFrEF (Heart Failure with reduced Ejection Fraction) but remain at physiological levels in HFpEF (Heart Failure with preserved Ejection Fraction). I further showed the feasibility and importance of this technique in assessing phasic emptying fractions and strains of the left atrium and proposed CMR criteria for the diagnosis of a newly described clinical entity, atrial failure. Following this line, I characterized what elements of LV remodelling related to atrial failure or phasic dysfunction. I further applied FT and derived mathematical models for systolic and diastolic hemodynamic forces approximation to characterize CMR surrogates of catheter-measured LV end-diastolic pressure. Here, I characterized for the first time the cardiac phenotype of adult patients with phenylketonuria, who demonstrate reduced myocardial mass and structural modifications related to their persistent metabolic abnormalities and showed the importance of life-long phenylalanine control

in preventing adverse cardiac remodelling. I compared the cardiac manifestations of COVID-19 with the ones observed in non-SARS-CoV2 viral myocarditis and point to a slower functional recovery in patients with more severe disease presentation and intense hospital care.

Chapter One:
General Introduction

1.1 Heart Failure: definition, epidemiology, classification

Heart failure (HF) is a generic term used to describe an insufficient circulatory support of adequate blood supply to the body, leading to specific signs and symptoms such as dyspnoea, central or peripheric oedema and progressive multi-organ functional deterioration. Even if HF can have extracardiac (pre and postcardiac) mechanisms, in this thesis I will refer strictly to the HF that is cardiac in origin, i.e. that involves a certain degree of cardiac remodelling. Despite remarkable progress being made in its medical treatment [1-3] with the therapeutic arsenal of effective drugs increasing practically every year and the advent of invasive strategies to improve rate control and prevent malignant arrhythmic events [4], heart failure continues to represent a massive burden for health systems around the world. In the last 10 years, the total number of patients with HF increased with 12%,[5] and the total prevalence is predicted to augment with 46% before 2030.[6] Almost one in two Americans suffers from at least one cardiovascular disease and the prevalence of heart failure raised progressively with the general aging of population to 6 million in 2021.[7] In the UK, prevalence is estimated currently at 4 million (1.6%)[5] and, globally, is reported to affect currently as many as 11.8% of individuals over 65 years living in developed countries.[8] These figures are expected to rise in the next decade, due to a general aging of populations and improved survivability after acute coronary syndromes or malignant arrhythmias.

1.1.1 Classification based on disease progression

In most cases the etiology of HF is multifactorial (e.g. coronary artery disease coexists often with diabetes, obesity, dyslipidemia, hypertension etc. with each of these factors contributing to the HF phenotype). Current ACC/AHA guidelines[2,3,9] classify HF

Table 1.1 Stages of Heart Failure according to ACC/AHA guidelines

Stage	Description	Examples
A	Patients at high risk of developing HF because of the presence of conditions that are strongly associated with the development of HF. Such patients have no identified structural or functional abnormalities of the pericardium, myocardium, or cardiac valves and have never shown signs or symptoms of HF.	Systemic hypertension; coronary artery disease; diabetes mellitus; history of cardiotoxic drug therapy or alcohol abuse; personal history of rheumatic fever; family history of cardiomyopathy.
B	Patients who have developed structural heart disease that is strongly associated with the development of HF but who have never shown signs or symptoms of HF.	Left ventricular hypertrophy or fibrosis; left ventricular dilatation or hypocontractility; asymptomatic valvular heart disease; previous myocardial infarction.
C	Patients who have current or prior symptoms of HF associated with underlying structural heart disease.	Dyspneea or fatigue due to left ventricular systolic dysfunction; asymptomatic patients who are undergoing treatment for prior symptoms of HF.
D	Patients with advanced structural heart disease and marked symptoms of HF at rest despite maximal medical therapy and who require specialized interventions.	Patients who are frequently hospitalized for HF or cannot be safely discharged from the hospital; patients in the hospital awaiting heart transplantation; patients at home receiving continuous intravenous support for symptom relief or being supported with a mechanical circulatory assist device; patients in a hospice setting for the management of HF.

Reproduced from Yancy CW et al., *Circulation*. 2017;136:e137-e161

according to presence of risk factors, symptoms, and structural heart disease elements (LVH, LV dilatation, hypocontractility, fibrosis) in 4 classes of severity (**Table 1.1.**). Cardiac imaging has an important role in early diagnosis, ideally before the onset of symptoms.

1.1.2 Difference in pathophysiology between HFrEF and HFpEF

Starting from this classification and integrating recent breakthrough data about the molecular mechanism HF, Pezel et al.[10] have proposed a dichotomy in the transition from Stage A HF (asymptomatic and reversible) to Stage B HF (asymptomatic and largely reversible) based on distinct phenotypes, dichotomy that persists and accentuates in more advanced stages of the disease, C and D. (**Figure1.1**). This scheme takes into account a different pathophysiological mechanism for patients in which pump function and presumably, contractility of the heart is preserved up to a very late burn-out stage in evolution. In 2013 Paulus and Tschöpe proposed a new pathogenic sequence for HF with preserved ejection fraction (HFpEF) including:

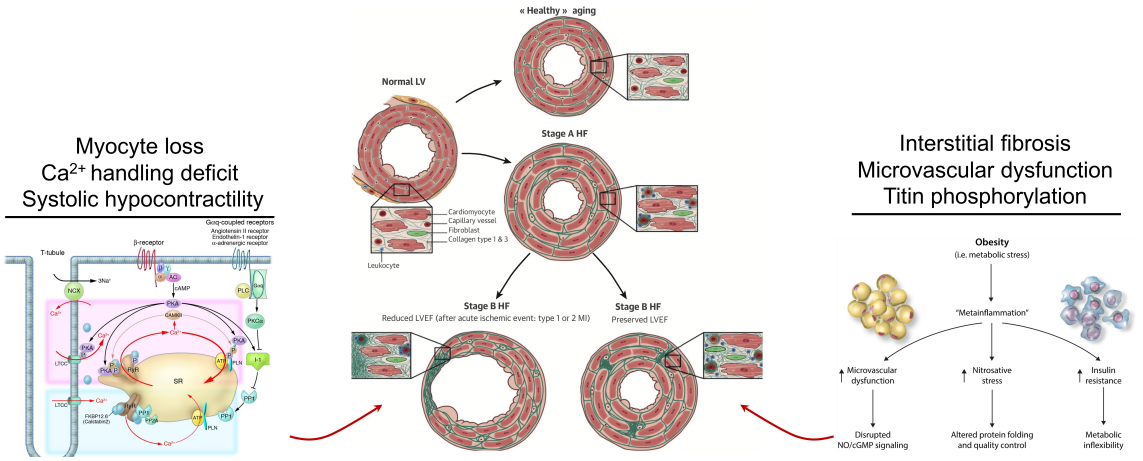


Figure 1.1 Left Ventricular Macrostructural and Microstructural Remodelling in Healthy Aging, Stage A and Stage B Heart Failure. Phenotypic dichotomy from Stage A HF – common, reversible phenotype where in nuce myocyte hypertrophy, interstitial fibrosis and microvascular remodelling are present toward either Stage B HF with reduced EF where hypocontractility and focal fibrosis dominate the phenotype or Stage B HF with preserved EF where systemic inflammation leads to activated myofibroblast and expansion of interstitial fibrosis and to endothelial dysfunction and subendocardial ischaemia. Depiction of the main molecular mechanisms responsible for the cardiac phenotype differ fundamentally between patients with HFrEF (left) and patients with HFpEF (right). HFrEF phenotype is characterised by focal myocyte loss and intracellular Ca^{2+}handling abnormalities leading concurrently to systolic contractile impairment, in contrast in HFpEF, the major pathogenic mechanisms are triggered by risk factors induced metafflamation leading to microvascular dysfunction, interstitial fibrosis and changes in titin phosphorylation, determining diastolic stiffness but preserving systolic contraction force. Adapted from Pezel, T. et al., *J Am Coll Cardiol Img.* 2021;14(5):1038–52, Yano, M. et al., *J Clin Invest.* 2005 Mar;115(3):556-64, Schiattarella et al., *Cardiovasc Res.* 2021 Jan 21;117(2):423-434.

comorbidities generating proinflammatory states leading to endothelial dysfunction, increased endothelial production of oxygen species and amplification of cGC/sGMP/PKG signal within the myocytes leading to myocardial hypertrophy, and respectively, amplification of TGF-β pathway with myofibroblast activation and diffuse collagen fibers deposition in the interstitial space. [11] Since then, a plethora of experimental and clinical data augmented our understanding about HFpEF and reinforced the initial paradigm's assumptions that given its largely different pathophysiology in comparison with HFrEF, HFpEF will require different therapeutic targets and overall strategies. [12] Indeed, pharmacological agents such as beta

blockers, angiotensin-converting-enzyme inhibitors, angiotensin receptor blockers and aldosterone antagonists efficient in treatment of HFrEF failed to demonstrate a consistent effect in HFpEF. [13-17] The Pezel model significance is twofold: 1. it presents two distinct phenotypes that can be identified in the course of HF development, 2. it indicates the salient role of imaging in Stages A and B of HF where the majority of pathological modifications could be curbed or reversed. Corollary, this window of opportunity for adequate treatment can be opend wider by increasing the ability of our tools to detect early changes such as modifications in function or structure of the myocardium and by clustering these changes to indicate the phenotype.

It is important to underline here that the dichotomic model described by Pezel et al. does not account for the modifications seen in inherited cardiomyopathies[18], infiltrative disease such as sarcoidosis or amyloidosis, or various forms of direct cardiotoxicity (e.g. chemo- or radiotherapy induced cardiomyopathy) where more complex, sui-generis myocardial remodeling occurs, generating distinct patterns of hypertrophy, fibrosis, changes in microvascular architecture and cardiac mechanics. As a consequence, imaging phenotype in these diseases is atypical and cannot be directly compared with canonical HF phenotype.

1.1.3 ESC Classification of HF based on EF

Establishing the severity stage and respectively the preponderant phenotype is quintessential for guiding an adequate therapeutic approach in patients with HF. Several pharmacological lines (beta-blockers, ACE inhibitors or angiotensin receptor blockers, aldosterone receptor inhibitors) showed a significant benefit in improving survival in patients with HFrEF but in contrast they showed no benefit in patients with EF>50%. On the other hand, these findings are based on clinical trials that included only patients with a definite systolic impairment i.e. EF<40% and therefore a large gray

Table 1.2 Stages of Heart Failure according to ESC guidelines

Type of HF		HFrEF	HFmrEF	HFpEF
CRITERIA	1	Symptoms ± Signs[a]	Symptoms ± Signs[a]	Symptoms ± Signs[a]
	2	LVEF < 40%	LVEF 40-49%	LVEF ≥ 50%
	3	–	1. Elevated levels of natriuretic peptides[b] 2. At least one additional criterion: a. Relevant structural heart disease (LVH and/or LAE) b. diastolic dysfunction (Left atrial volume index (LAVI) >34 mL/m2 or a left ventricular mass index (LVMI) ≥115 g/m2 for males and ≥95 g/m2 for females, E/e′ ≥13 and a mean e' septal and lateral wall<9 cm/s. Other criteria: impaired longitudinal strain or reduced tricuspid regurgitation velocity (TRV).	1. Elevated levels of natriuretic peptides[b] 2. At least one additional criterion: a. Relevant structural heart disease (LVH and/or LAE) b. diastolic dysfunction (Left atrial volume index (LAVI) >34 mL/m2 or a left ventricular mass index (LVMI) ≥115 g/m2 for males and ≥95 g/m2 for females, E/e′ ≥13 and a mean e' septal and lateral wall<9 cm/s. Other criteria: impaired longitudinal strain or reduced tricuspid regurgitation velocity (TRV).

Abbrieviations: BNP B-type natriuretic peptide; HF heart failure; HFmrEF heart failure with mid-range ejection fraction; HFpEF heart failure with preserved ejection fraction; HFrEF heart failure with reduced ejection fraction; LAE left atrial enlargement; LVEF left ventricular ejection fraction; LVH left ventricular hypertrophy; NT-proBNP N-terminal pro-B type natriuretic peptide.
[a] Signs may not be present in the early stages of HF (especially in HFpEF) and in patients treated with diuretics.
[b] BNP > 35 pg/ml and/or NT-proBNP > 125 pg/mL.
Adapted from Ponikowski et al., *Eur Heart J.* 2016;37:2129-2200.

area in between HFrEF and HFpEF ranges exists where the benefits observed in HFrEF and respectively not observed in HFpEF cannot be precisely ascertained. To incorporate these grey areas in order to give a unitary view over the entire spectrum of HF subtypes, the European Society of Cardiology proposed a new classification[19] with divides the patients with HF in 3 distinct groups of patients based primarily on EF and supported by other clinical and imaging parameters and biomarkers (**Table 1.2**) that includes a newly classified group, termed HFmrEF (HF with mid-range EF). HFmrEF comprises patients with an EF of 40-49% and specific data about disease progression, prognosis and response to therapy in this group are warranted. The ESC classification represents a step forward towards a phenotype-based classification of HF, however further detailed functional and structural characterization of currently proposed groups (HFpEF, HFmrEF and HFrEF) is now warranted in order to particularize therapy management and clinical evolution. Recent data analyzing comparatively the proteomic signatures of these 3 distinct classes of HF patients bring up new evidence

regarding the distinctiveness of the specific pathophysiological pathways involved in each subgroup and suggest novel therapeutic targets that may be effectively mended within a specific subgroup but less so in others (e.g. IGF/IGFBP signaling and MMP activity in HFrEF, VEGF-C angiogenesis in HFpEF or mPAK/JNK signaling in HFmrEF). [20]

1.1.4 Conceptual distinction between HF and Cardiac Remodeling

In its pathophysiological evolution, HF affects the heart structure and function, determining cardiac remodelling. Cardiac remodelling represents the totality of changes, intricate and frequently interdependent produced as a result of an acute or chronic cardiac injury and further exacerbated by various local and systemic molecular mechanisms mobilised in order to preserve as much as possible cardiac function at normal or acceptable standards. It consists of modifications at the level of every histological component of the heart: myocytes, fibroblasts, interstitium, coronary macro and microcirculation. Cardiac remodelling occurs sometimes physiologically as part of healthy aging and in specific cases such as constant strenuous physical exercise (athlete's heart). Pathologic, maladaptive, cardiac remodelling is reversible in its earlier stages and therefore understanding its molecular mechanisms and developing tools for an early diagnostic are warranted targets for research. Diagnosis of cardiac remodelling is difficult because of the intricacy and compensatory nature of the processes involved that tend to maintain unchanged the physiological, "macro", parameters such as cardiac volumes and ejection fraction. In some forms of cardiac remodelling and even type A HF, these "classical" diagnostic parameters remain unchanged.

A terminological distinction must be made between HF and cardiac remodeling (CR): HF represent a complex clinical syndrome with a clinical diagnosis based primarily on

the presence of dyspnea of cardiac origin and other symptoms and signs of cardiac functional decompensation (peripheral edema, hepatic congestion, raised JVP etc.), while CR represents any structural or functional modification of the heart. HF is invariably associated with a degree of CR which in turn can vary widely from subtle modifications in only diastolic parameters to massively hypertrophied and/or dilated heart. In the great majority of cases, subclinical CR precedes HF for years and therefore it is crucially important to develop tools able to (1) identify, as early as possible, CR, (2) discriminate and characterize in detail the pathological features of CR to allow a prompt intervention, able to rescue or reduce the pathophysiological loops contributing to HF development.

One of the key objectives of the clinical cardiology is the early diagnosis of a maladaptive cardiac remodelling that leads to progressive dysfunction and ultimately to HF and decompensation. Associated aims are to characterise and ideally quantify specific components of cardiac remodelling (dilatation, hypertrophy, hypocontractility, fibrosis), group them in phenotypes, and analyse specific treatment schemes and reversibility conditions and establish prognosis. Benefitting from a tailored approach in image acquisition obtained through variations in both the range of emitted radiofrequency pulses and receiver coils, CMR is the actual state-of-the-art device for assessing cardiac remodelling. Using the classification models presented above, CMR holds the promise to detect early transitions between normal LV and Stage A HF and respectively between Stage A HF and Stage B HF with the correct identification of distinct phenotypic traits. This would allow the clinician to commence an (1) early and (2) tailored therapeutic approach, able to mend specific pathophysiological changes and therefore to be more efficient in reversing or stalling the progression of the disease.[21]

I will present here succinctly the most important traits of CR and subsequently how each of these traits of cardiac remodelling can be assessed by CMR also emphasizing the current limitations and pitfalls. Consequently, I will comment on the advantages brought by two new emerging CMR techniques – respectively FT derived myocardial strain and respectively Parametric Mapping – in the diagnosis of cardiac remodelling. These 2 techniques and their applicability in patients with different types of HF and several conditions that predispose to HF are the central topic of my thesis.

1.2 Role of CMR in Early Detection and Assessment of Cardiac Remodelling

1.2.1 Ventricular dilatation

Ventricular dilatation results from chronically increased mechanical stress that myocytes and interstitial cells, in particular fibroblasts, have to uphold. In a healthy heart, following the Frank-Starling law, according to which the contraction force proportionally relates to the end-diastolic fibre length, a first mechanism available to adapt cardiac work to an increased afterload is to increase the elongation of fibres as far as possible and this is physiologically possible by increasing the end-diastolic volume.[22] However in pathology, chronically increased contractile demands trigger signalling pathways that progressively contribute to loss of contractile reserve of the heart and finally to mechanical decompensation. Ventricular dilatation precedes the development of HF in a population with[23] or without[24] previous myocardial infarction (MI).

CMR is the most precise technique for the assessment of LV and RV volumes, offering a complete spatial coverage of the cavities and walls achieved through a no gap transversal segmentation of the heart. Biventricular cavity volumes[25] and myocardial mass[26] can be reliably calculated using Simpson's "stack of parallel disks" method.

1.2.2 Hypertrophy: definition, types, molecular mechanisms

To increase the force of contraction and reduce the wall stress, stimulated by a complex network of molecular signals[27], myocytes expand their volume to accommodate more serially disposed sarcomeres, a process called myocardial hypertrophy. Left ventricular hypertrophy (LVH) represents a pathological feature of CR in disease such as systemic hypertension, obesity, and valve disease. Believed initially to be in part a reactive compensation for the increased afterload, it is increasingly recognised now that in pathological conditions, myocardial hypertrophy contributes to progressive deterioration of CR by increasing perfusion and metabolic demands and diffuse fibrosis through activating pro-fibrotic pathways in the resident fibroblasts.

Ventricular hypertrophy and dilatation coexist and the preponderance of one over the other defines the geometrical patterns of the cardiac remodelling. Even subtle elevations of myocardial workload are able to trigger pro-hypertrophic[28] and pro-fibrotic[29] messages resulting in further remodelling. The best way to discriminate between dilatation and hypertrophy is the direct microscopical examination of cellular shape, where a parameter such as cardiomyocyte length/width ratio is diagnostic. As an example, while in patients with chronic ischaemic cardiomyopathy elongation of the cells contribute almost exclusively to remodelling [30], in persistent hypertension, the increase in width precedes by years or even decades the elongation. [31]

CMR can assess cardiac hypertrophy by offering a 3D coverage of the cardiac walls. The thickness of LV walls can be therefore measured at any level of LV, in practice the maximal wall thickness at the level of the intraventricular septum and posterior wall are largely used and routinely reported. Left ventricular mass (LVM) can be, in some conditions, a more clinically significant and global representation of ventricular

hypertrophy. It can be assessed by calculating the total myocardial volume at end-diastole and multiplying this with the specific myocardial tissue density. Using this method, it is assumed that the expansion in the myocardial volume is mainly due to an increased volume of the myocytes, however significant expansions of the interstitial space caused by collagen deposition, oedema infiltration or structural changes (amyloid or sarcoid accumulation) can represent important confounding factors. Combining volumetric assessment with parametric imaging able to discriminate between normal myocardium and other tissue compositions holds promise in offering a more accurate account of LVH by indirectly assessing average myocyte dimensions.[32]

1.2.3 Cardiomyocyte loss.

Cardiomyocytes death occurs in most of the cases through necrosis, apoptosis or a combination of these two processes called necroptosis. This distinction is important in establishing the phenotype of HF: ischaemia/reperfusion injury, a complication of CAD, triggers primarily a pro-necrosis pathway, while the diastolic stretch predisposes through an Ang/AT1R pathway, activation of p38MAPK-p53, DNase I activation and ROS production, predominantly to apoptotic cellular loss. In the absence of specific molecular tracers, current CMR protocols are not able to distinguish between necrosis and apoptosis[33] and can detect myocyte loss only indirectly by identifying focal fibrosis as areas of positive late gadolinium enhancement (LGE). [8,34] However, LGE is not always specific for focal fibrosis, in particular when active inflammation coexists.[35,36]

1.2.4 Cardiac fibrosis: definition, types, molecular mechanisms

Cardiac fibrosis represents excessive deposition of collagen fibres within the myocardium. It is a major contributor to HF progression, affecting directly cardiac

diastolic and systolic function, and associating with a higher incidence of adverse events such a haemodynamic decompensation or malignant arrhythmia. [37,38]

Collagen is produced mainly by activated resident cardiac fibroblasts[39,40], with potential additional sources such as endothelial or epithelial cells or bone marrow-derived precursors. Many factors including stress induced by excessive mechanical load but also proinflammatory cytokines, latent TGF-β, angiotensin II, FGF and PDGF are all able to activate local resident fibroblast, induce a myofibroblast phenotype, responsible for collagen fibre production. [41] Subsequently, cardiac collagen matrix is further controlled and restructured permanently by two families of tissue enzymes with opposing actions (matrix metalloproteinases (MMPs) and tissue inhibitors of matrix metalloproteinases (TIMPs)). A dysregulated MMPs/TIMPs balance is present in advanced cardiac remodelling and contributes to cardiac decompensation and HF. [42]

According to histopathological appearance myocardial fibrosis can be: (1) focal, where a continuous mass of collagen replaces completely the myocytes in a defined area of the myocardium, (2) diffuse, where the fibrosis is limited to the interstitial and perivascular spaces that can be, as a consequence, increased in size, (3) patchy, where collagen fibres are interspersed through the myocytes that appear rarefied, misaligned and irregular in shape and orientation, (4) reactive fibrosis, where fibrotic deposition is associated with the presence of acute or chronic intramyocardial inflammation.

Recognising the pattern and extent of fibrosis can give precious information about the predominant phenotype of HF. HFrEF patients tend to have at least some extent of focal fibrosis resulting from either acute coronary syndromes or by intense apoptosis as a result of increased myocardial load. In contrast, typical for HFpEF is the absence

of localised fibrosis and the development of diffuse fibrosis, putatively triggered by extensive proinflammatory stimuli.

In line with most of the current explanatory models, diffuse fibrosis is considered a secondary phenomenon resulting mainly from increased mechanical stress and neurohumoral stimuli that are in great part a consequence and posterior to pro-hypertrophic signals.[43] Additionally, in later stages diffuse fibrosis results from microischaemic events leading to focal necrosis or apoptosis, predominantly in subendocardial regions. [44] Intriguingly, some data indicate that the fibrosis-related gene expression programme may be rather activated as an early process, preceding myocyte hypertrophy development[45] and imaging is able to detect specific structural changes only late when the interstitial space is significantly expanded. [46] Early diastolic relaxation abnormalities reflect accurately the amount of collagen deposition and therefore represent an important and sensitive, albeit indirect, imaging assessment of interstitial fibrosis. [47]

1.2.5 Cardiac mechanical deficit: classification, molecular mechanisms

The two distinct phenotypes described above for Stage B HF (**Figure 1.1**) recognise two largely distinct patterns of mechanical deficit, produced as a consequence of distinct molecular downstream pathways. In the case of HFrEF, myocyte loss, as a result of a necrotic injury after myocardial infarction or apoptosis induced by increased mechanical stress, toxicity, or infection, leads to neurohumoral activation of the renin-angiotensin-aldosterone system, increased oxidative stress leading both through PKA, PKC pathways to deranged SERCA2a, RyR and PLN phosphorylation, intracellular Ca^{2+} mishandling and diminished systolic contraction. In turn, dysregulations of the SERCA2a/PLN regulatome exacerbates cell loss through apoptosis and aggravates the contractile deficit.[48] For HFpEF a radically different model has been proposed,

where potent inflammatory cytokines such as IL-6 and TNF-α determine through TGF-β myofibroblast activation and excessive diffuse fibrosis deposition and through inhibiting sGC-cGMP-PKG axis hypertrophy and titin N2BA to N2B isoform switch. [11] The same strong inflammatory drive and lipid abnormalities associated with obesity and insulin resistance, frequent triggers of HFpEF, contribute to endothelial dysfunction in microvasculature. [49,50]

Due to gigantic energetic demands, within the myocardium an efficient blood supply is required in order to provide large supplies of oxygen and metabolic fuel to the working myocytes. This is ensured by an arborescent coronary architecture formed by progressive intramural branching of coronary arteries from the epicardial surface towards the epicardium. [51]

Two thirds of the human myocardial cells are represented by non-myocytic cells such as fibroblast that together with an abundant collagen network ensure stability and rigidity of the heart tissue, endothelial cells, pericytes, neurons, adipocytes, myeloid and lymphoid cells. [52] Among the ventricular myocytes there is a marked heterogeneity.

Several traits individuate the subendocardial myocardium from other layers: (1) it is in proximity to the blood pool and therefore undergoes the influence of the steep variations of intracardiac pressures during the cardiac cycle, (2) its vascularization is represented by the most distal ramifications of the coronary circulation, with the smallest calibre but with the largest variation of calibre and flow during the cardiac cycle[53], (3) In physiological conditions, intracellular Ca^{2+} concentrations are significantly higher in the subendocardium with a transmural gradient towards the subepicardium. [54] In both ischemic heart failure and dilated cardiomyopathy, the gene expression of SERCA2a and PLN are more decreased in the subendocardial myocardium compared with mid-myocardium and subepicardial regions. [55] As

discussed above, these two proteins are essential in intracellular Ca^{2+} handling and their decreased activity associates with a marked plateau in systolic action potential and hypocontractility. [56]

Taken together these findings support the idea that subendocardium is particularly vulnerable in the progression of heart failure and a selective or comparative assessment of this layer may be able to detect earlier cardiac dysfunction in comparison with global parameters, assessed over the entire myocardial volume. This idea led me to hypothesize that a selective evaluation of myocardial deformation at endocardial/sub-endocardial level may be more sensitive in detecting contractile impairment.

1.2.6 Infection, Inflammation

Infectious pathogens or systemic inflammatory conditions can frequently have damaging effects on cardiac structures. In these cases, inflammation involving cardiac structures can reflect tissue damage, an infection or a reactive reaction to a distant or systemic pathogenic trigger and can be either acute or chronic. On the other hand, intrinsic cardiac conditions such as acute MI or inherited cardiomyopathies can elicit an inflammatory response at the level of the myocardium. Therefore, detecting the presence, nature and pattern and being able to measure the amplitude and extent of inflammation in the heart tissue are important information improving risk stratification and guiding treatment. Of note and of particular importance for the investigation presented in this thesis, the fine intramural microvasculature of the subendocardial myocardium is more vulnerable to pro-inflammatory pathways and oxidative stress upregulation leading to localised endotheliitis or microvascular dysfunction. Tools to collate information regarding subendocardial mechanics (such as multilayer evaluation of strain) and regional volumetric distribution of elevated T2 times (achieved by T2

mapping) would augment the current standard of diagnostic (e.g. updated Lake Louise Criteria (LLC) in acute myocarditis) and pave the way for a more specific, ideally quantitative approach to risk stratification with CMR.

1.2.7 Left atrium and Right Ventricle – particularities, significance

Additionally to the LV parameters, and due to its excellent spatial resolution and the wide possibility to plan the acquired images, CMR extends greatly the abilities of imaging investigations of the other 3 cardiac chambers – right ventricle (RV), left (LA) and right atrium. In particular RV and LA assessment, provides crucial information that can guide diagnosis and treatment in a variety of cardiac disease. Both RV and LA functions are important independent markers of mortality in the HF population. RV volumes and internal diameters can be assessed in a similar manner with the LV. For best results, LA volumes require a dedicated full SA stack to cover transversally the chamber followed by Simpson's method estimation, but this is not routinely acquired. However atrial phasic volumes estimated with a biplane-area method applied to CMR 4Ch and 2Ch LA SSFP cine showed satisfactory correlation with gold-standard Simpson's method. [57] In this thesis we used biplane-area method to quantify atrial volumes and emptying fractions (details in Chapter 2 Methods and Specific Methods sections of individuals chapters). Similarly, as previously described [58,59], CMR FT was applied to both RV and LA to determine various types of strain. Even if in theory possible, due to irregular shape and highly trabeculated structure (RV) [60] or thin walled cavity (AF) [61], parametric imaging is just at an experimental stage at this moment.

1.3 Diastolic Dysfunction and Increased Ventricular Filling Pressures. Emerging role of CMR.

In tandem with systole, diastole is the other phase of the cardiac cycle when heart ventricles fill, progressively and in a coordinate rhythm, with blood following gradients

of pressure created through mechanical activity of each of the ventricles and homolateral atrium. Briefly it has an early phase, when the extension of ventricular fibres through longitudinal and circumferential elongation and base-apex untwisting create a negative pressure that draws blood inside the ventricular chambers, and a late phase when atrial contraction actively pushes more blood into the ventricles. Between and after these phases there are variably long intervals of ventricular diastasis when volume and pressure are maintained. Abnormalities in any of these phases determine diastolic dysfunction. Independently of systolic parameters, diastolic dysfunction is proportionally related to cardiovascular mortality[62,63], therefore developing adequate and practical tools to assess part of the clinical routine is desirable.

Diastolic function of the heart can be most accurately assessed using a complex invasive protocol that measures over the entire cardiac cycle the relation between LV volume and intraventricular pressure (PV loops). Diastolic dysfunction is generally associated with elevated LV filling pressures resulting from impaired lusitropy (metabolically active process of LV fibre relaxation), chamber stiffness and decreased atrial pump function.

So far, echocardiography proved an efficient albeit imperfect tool to diagnose and quantify diastolic deficit. This can be satisfactorily achieved through a combination of cut-off values such as early and late mitral flow velocities, early diastolic tissue velocities (E/e' is a particularly useful index), peak tricuspid regurgitation velocity and indexed maximal atrial volume [64], however a significant gap remains between echocardiographical estimation and invasively measured LV filling pressures. [65] In a comprehensive meta-analysis E/e' falls short of ensuring a reliable diagnostic accuracy. [66] Comparatively CMR has a relatively lower temporal resolution and in the

absence of a Doppler quantification of blood and tissue velocities offered by echocardiography, can currently assess diastolic function only indirectly [67].

A hallmark parameter for DD is elevated LV end-diastolic pressure that can be measured invasively either directly through left heart catheterization[68] or indirectly through the evaluation of related pressures such as pulmonary capillary wedge pressure (PCWP) in the right heart through a venous approach. [69] Given the inherent practical difficulties and risks of invasive procedures, there is a justified interest in developing imaging tools able to approximate LV filling pressures, LVEDP in particular. So far, only a complex algorithm using several echocardiography parameters, reached at best moderate results, while the role of CMR in this endeavour remains largely unexplored.

1.4 Atrial remodelling in Heart Failure

Atrial dilatation or dysfunction are important independent factors associated with increased mortality and incidence of stroke in the general population[70-74]. (**Figure 1.2.A**) Extensive atrial remodelling leading to mechanical and structural remodelling contributes in time to a reduced cardiac output and increases the burden of atrial arrythmia, in particular atrial fibrillation (AF). On the other hand, a significant but variable degree of atrial remodelling is present in many patients with HF[75], but the pathophysiological mechanisms and their relative contribution in HF subgroups (HFpEF, HFmrEF and HFrEF) are not well established.[76] A proposed model to explain the pathophysiological interdependence between HF and AF is illustrated in **Figure 1.2. B**. Indexed left atrial volume (LAVi) is associated with a higher rate of hospitalization and death in HF patients, independently of LV systolic or diastolic function, with incremental value added by LA emptying fraction (LAEF). [77] Moreover, increase in atrial size is tightly correlated to the incidence of atrial fibrillation[78], which

can precipitate or complicate HF symptomatology and clinical evolution. [79] An impaired atrial function can anticipate a decline in LV diastolic function and further development of HF symptoms. [80]

Atrial fibrosis represents an important histological marker of atrial remodelling directly related to mechanic dysfunction and propensity for electric abnormalities causing arrhythmia. [81] The shorter more fusiform shape of atrial myocytes and the thin walls of atrial chambers, make cellular hypertrophy inefficient to compensate for an increase in mechanical load and determine the cavity to dilate in response to an increase in volume

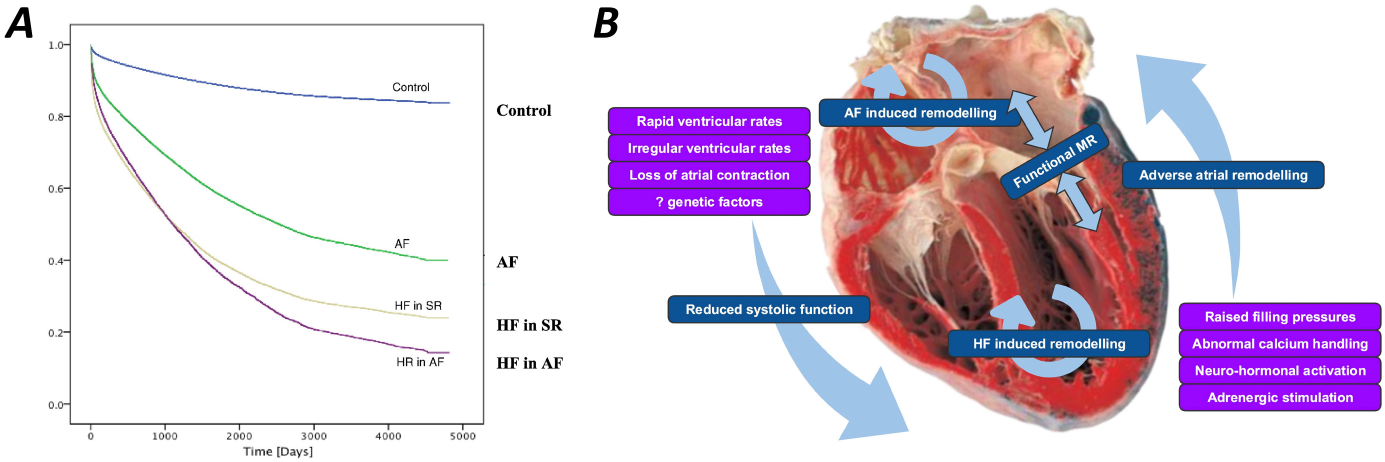


Figure 1.2 Intercausal relation between Heart Failure (HF) and Atrial Fibrillation (AF). **A.** Epidemiologically, the coexistence of HF and AF have a cumulative effect on mortality, data from a large cohort of patients (approximately 1 million patients recruited) included between 2000 and 2013 in the United Kingdom (UK) Algorithm for Co-morbidity, Associations, Length of stay, and Mortality (ACALM) registry. **B.** Proposed pathophysiological links between HF and AF: (i) chronically raised filling pressures, abnormal intracellular calcium handling, neuro-hormonal activation and excessive adrenergic stimulation determine all concurrently progressive atrial remodelling with dilatation, fibrosis and mechano-electrical deficit and (ii) atrial remodelling leads to paroxysmal and then persistent AF which through irregular, incoordinated, rapid ventricular rates and loss of atrial pump function exacerbates ventricular remodelling with progressive diastolic and systolic mechanical impairment and perfusion deficit. Adapted from Ziff OJ. et al. *Int J Cardiol.* 2018 Feb 1;252:117-121. and Prabhu S et al., *Heart, Lung and Circulation* (2017) 26, 967–974. with permission from the authors.

or pressure. [82] Atrial fibroblasts are more sensitive to pro-fibrotic pathways in particular the TGF-β1/SMAD2/3 pathway triggered by elevated renin-angiotensin-aldosterone drive.[83]

Atrial and ventricular functions are connected and concur to ensure an adequate blood output during every cardiac cycle and their synchronised functions are coordinated by the electrical conduction system. [84] Atrial physiology can be therefore be described by three distinct phases: reservoir – corresponding to the relaxation of the atrial myocardial fibres and filling with blood of the atrial cavity, passive contraction – corresponding to the emptying of the atrium under the influence of ventricular suction force (negative pressure obtained through relaxation and untwisting of the ventricular fibres during early diastole) and gravitation, pump or booster contraction – corresponding to active contraction of the atrial fibres and propulsion of the remaining atrial blood towards the ventricle. [85]

All of the three phases described above reflect different aspects of atrioventricular physiology and their assessment is potentially important for the cardiac phenotype as a whole. For each of these, maximal and minimal volumes, emptying fractions and myocardial strain can be estimated. [86] Even if echocardiography is a good technique to assess and quantify atrial parameters, through its posterior position within the thorax, pyramidal irregular shape and conic insertion of pulmonary veins that is hard to delineate without high spatial resolution, imaging LA carries significant limitations. [87] CMR is the imaging gold standard for atrial imaging, closer to the real dimensions measured by histopathological methods and more reproducible. [88] Therefore, it is desirable to apply CMR methods for the characterisation of atrial parameters (volumes, fractions, strain) and to indicate their role in HF. Of importance is also to understand what is the relation between ventricular remodelling (dilatation, hypertrophy, systolic or diastolic impairment, fibrosis) and atrial parameters.

Novel approaches allow a direct visualisation and quantification of atrial fibrosis with CMR[89], however, the imaging protocol is complex requiring a dedicated complete atrial

stack (several short axis slices to cover the entire atrial volume), specific LGE acquisition parameters and offline analysis. Moreover, the reproducibility remains low and a comprehensive histological validation is currently insufficient[90], particularly for diffuse fibrosis. Alternatively, atrial deformation can represent a good surrogate marker of diffuse atrial fibrosis.[91] In particular, reservoir strain as a global index of atrial relaxation and filling and conduit strain, related to atrio-ventricular coupling are likely to be affected by excessive atrial fibrosis. [92]

Starting from the observation that severe atrial dysfunction or remodelling can exist independently or even in the absence of any significant ventricular pathology, a new clinical entity has been recently proposed, the authors coining the name “atrial failure”.[93] Recognising and diagnosing atrial failure would have major implication for guiding a targeted therapy against complications associated with it such as higher risk of atrial fibrillation, thromboembolic complications such as stroke or HF.

Recent data[94-96] support the hypothesis that, an underlying cardiomyopathy, triggered by common molecular downstream pathways could affect simultaneously but in a variable degree atria and ventricles. This is further supported by the epidemiological relation between heart failure and atrial fibrillation. [79] On the other hand, atrial remodelling[75] and prevalence of AF differ among the subgroups of HF[97]. Taken together these findings lead to the assumption that molecular mechanisms responsible for atrial remodelling differ with the subtype of HF. [98]

To date, no study using CMR evaluated comparatively the LA remodelling among the subgroups of patients with HF. Looking at a well characterised group of patients with HF (containing 3 matched subgroups with HFpEF, HFmrEF, HFrEF) and control subjects, I plan to characterise the atrial remodelling using phasic volumetry, emptying fractions and strain in each of these groups and interrogate which parameters routinely

used to characterise CR in HF, are related to atrial dysfunction. This study is presented below in Chapter 4.

1.5 Feature tracking – theoretical basis, usefulness in HF, limitations

In practice, HF is frequently evaluated as ejection fraction (EF). Initially proposed by Roland Folse and Eugene Braunwald[99] in the early 60s, EF is calculated as the volume ratio between the systolic output and the initial, maximal end-diastolic volume of blood. For the patients with a clear-cut reduction in systolic function, EF proved to be a versatile and clinically highly relevant parameter able to predict and stratify the risk groups for various indexes of morbidity and mortality. [100,101] However, for borderline values, considered to range between 45% and 55%, the ability of EF to risk stratify the HF patients is uncertain.[102] On the other hand, approximately half of the patients with a clinical diagnosis of heart failure maintain a normal EF but their prognostic remains poor and clinical management challenging. [103] From these considerations results the demand to seek for alternative approaches for estimating the contractile ability of the heart and help the clinical decision making.

Over the last three decades, several techniques have competed to offer the best imaging approach to characterise myocardial mechanics. Firstly described, myocardial tagging [104] has been progressively less prominent in recent years due to long dedicated acquisition protocols, laborious image analysis techniques, and incomplete information about diastolic phase where the tags applied at the beginning of systole become less precise leading to errors in quantification. [105,106] Validated against tagging, echocardiography-based methods[107-109], in particular, speckle tracking still represents a versatile method to tissue-track infinitesimal segments of the myocardium and renders 3D deformation properties. The advantages of echocardiography methods are an excellent temporal resolution offered by the ultrasound-based acquisition, and the

Doppler support able to quantify directly the velocity of blood flow through the valves and respective specific myocardial segments. [110,111] However, compared with CMR it has a reduced spatial resolution and is in many instances is hampered by poor-windowing, artefacts, and operator and examination related variability.[112,113]

Myocardial strain can be estimated through the formula $E(t) = \frac{L(t) - L_0}{L_0}$, where E is the myocardial strain, L_0 initial length of the segment, $L(t)$ the dimension of the segment at a time *t*. As the rate of change varies with time in our case, in each moment of time, over the entire cardiac cycle, a value of strain can be obtained through the formula $E = \frac{\partial(L - L_0)}{\partial L_0}$,and strain rate through the formula $ER = \frac{d(L - L_0)}{dL_0 \cdot dt}$. Per convention, the 3 directions in which an infinitesimal volume of myocardium is deformed during the cardiac systole are named longitudinal (E_{LL}), circumferential (E_{cc}) and radial (E_{RR}). Of note, the three-dimensional movement is described by composition of these three vectors only if we assume that there is no movement in between the layers, a movement called shearing. If shearing is taken into account, another 3 rotational vectors contribute to deformation E_{CL}, E_{CR}, E_{RL}. In this way, myocardial deformation can be assessed in three distinct spatial directions: longitudinal, circumferential and radial. (**Figure 1.3**).

One of the important limitations of CMR in comparison with echocardiography is the low temporal resolution (with a frame frequency of 20-30ms, in contrast with less than 5ms offered by echocardiography), which become particularly important in the assessment of diastole. Developed in the early 90s myocardial tagging was the first to quantify myocardial strain and remained the gold standard against which Doppler echocardiography methods were developed subsequently. Tagged CMR images usefulness for clinical practice is hampered by several disadvantages: image

acquisition is laborious and artefacts are frequent, offline image analysis is laborious and, for magnetic field strength used in cardiac MRI (1.5 and 3T), the tags tend to fade away during the diastole and drastically compromise the consistency of data. While speckle-tracking Doppler echocardiography resolved at least in part these inconveniences, inherent limitations related to echocardiography and in particular its inferior inter-observer and inter-study reproducibility, made the quantification of systolic myocardial strain still received with reservation by clinical cardiologists. Comparative analysis and validation against a gold-standard method to evaluate diastolic dysfunction, invasively measured LV end-diastolic pressures, rendered E/e'

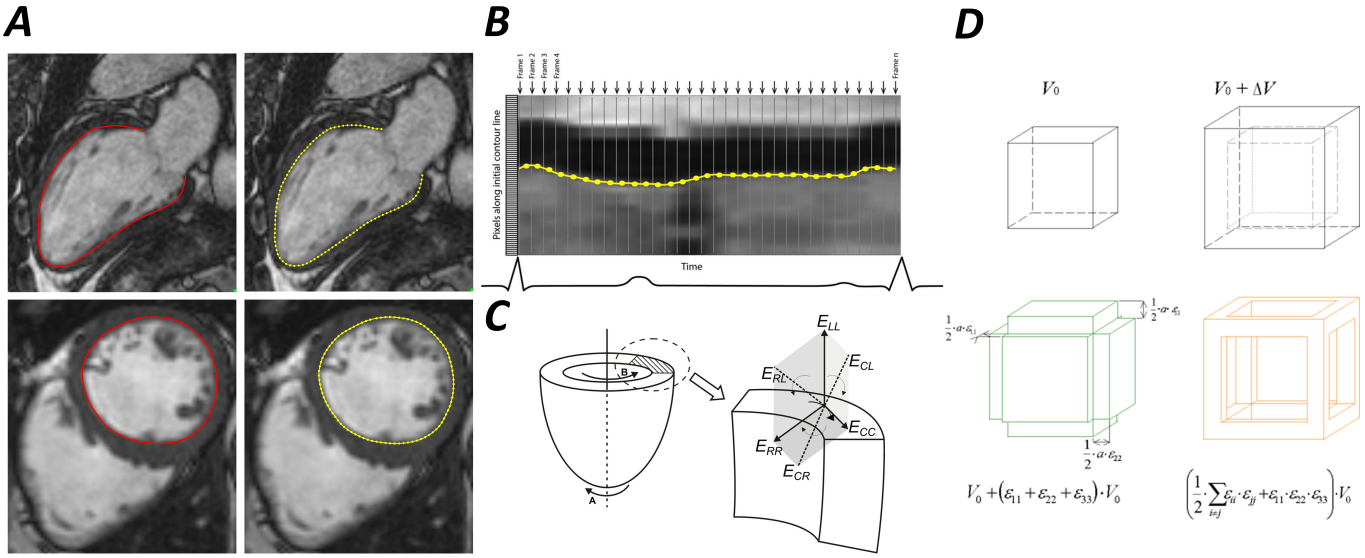


Figure 1.3 Illustration of CMR Feature Tracking Method and Myocardial Deformation Assessement. **A.** operator traced or automatic myocardial segmentation defines the endocardial (and others: midmyocardial, epicardial) contours in various cine sequences (here 2Ch and basal short-axis orientation) which can be further divided in a linear network of points that are identified and tracked over the cardiac cycle **B.** (copyright Berthold Klas, TomTec, Unterschleissheim, Germany, reproduced here with permission) space-time (M-mode like) reconstruction of tracking over a cardiac-cycle of an individual point defined previously **C.** for each such point 6 vectors representing translational movement (simple strain) and inter-plane sliding (shear), in all our analyses shear amplitude was considered negligible and not included in numeric estimation of strain D. volumetric strain leading to volume expansion, in the case of infinitesimal strain theory the variation of volume (ΔV) is negligible between consecutive phases and strain refers only to deformation in three spatial directions. Adapted from Schuster A. et al., *Circ Cardiovasc Imaging.* 2016 Apr;9(4) and Shehata M.L. et al, *J Cardiovasc Magn Reson.* 2009 Dec 21;11(1):55.

(a ratio between early diastolic trans-mitral blood flow and para-mitral tissue velocities) as the most reliable imaging parameter to evaluate LV diastolic properties and recognise the progression of diastolic function. However, correlation is not always satisfactory and prone to become insignificant for some pathologies, such as inherited cardiomyopathies and severe restrictive cardiomyopathies.

One of the key advantages of CMR FT is the extensive applicability on any routinely acquired cine SSFP cine sequences with minimal variability dependent on the clinical system used, mode and time of acquisition and spatial parameters or resolution. The theoretical basis is that a superimposed contour, consisting in a very fine linear vector of points, (or a matrix of points if multiple contours are provided), can be tracked over a period of time, in this case, over the entire cardiac cycle, based on assigned spatial relations of vicinity with other points and with clearly identifiable features such as line of contrast between other obvious features e.g. between myocardium and blood pool or pericardium.

CMR FT can be thus applied retrospectively on previously acquired images, and offers a complex set of data about myocardial mechanics: velocities, relative displacement, deformation (strain) or rate of deformation (strain-rate). Therefore, longitudinal interrogations and long-follow-up studies are possible.

Myocardial deformation of any defined region can be assessed spatially (three-dimensionally) through the evaluation of longitudinal, circumferential and radial strain. Benefiting from the excellent spatial resolution of cine SSFP images and increasing temporal resolutions, CMR FT has the capacity to extend the assessment of myocardial deformation to discrete myocardial regions (e.g. subendocardial layer, ventricular base or apex) and, respectively, through spatial reconstruction and tracking,

assess 3D interplane deformation such as systolic twisting or diastolic untwisting amplitudes.

In contrast with tagging[105], FT covers very well the cardiac cycle, maintaining the a constant high spatial resolution and thus yielding excellent resolution for the diastolic phase. Using FT parameters such as early and late diastolic strain and strain-rate, deceleration times can be computed. Moreover, these can be combined with LV volume or dV/dt curves to render the ratio between myocardial deformation and volume capacitance in early diastole.[67] As for the systole, FT diastolic strain and strain-rate can be assessed in longitudinal, circumferential and radial directions. [114] In addition, reconstructing the 3D mechanics between basal and apical planes, diastolic untwisting amplitude and rate can be measured with FT, using a similar approach to the one validated with speckle tracking echocardiography. [115]

Progressively blunted systolic and diastolic interventricular pressure gradients[116] and 4-D flow disturbances[117] were identified in the failing heart supporting the clinical importance of a thorough and feasible hemodynamic assessment. Applying the first principle of fluid mechanics and Navier-Stokes equation and assuming an ideal valvular impedance of blood flow, mathematical modelling of LV intraventricular pressure gradients and hemodynamic (HD) forces can be derived from spatial myocardial deformation (CMR FT strain) and measurements of inflow and outflow valvular surfaces (mitral and aortic valve). [118] These parameters have been previously validated against four-dimensional (4D) flow MRI which is the non-invasive reference imaging standard[119], and more recently in a pilot test against invasive right heart catheter measurements. [120] To quantify HD forces and derived parameters (HD work and power) in systole, early and late diastole[118], I used here a commercially available tool, integrated to the offline analysis platform (details regarding the software platform,

image acquisition, post-processing, analysis and numeric expression, previous validation of the method and preliminary studies in patients with HF are briefly reviewed and presented in **Chapter 2**).

For all the reasons highlighted above, CMR FT emerges as a much warranted investigation tool, perfectly adapted to be used as the main imaging outcome in multicentric large scale clinical trials and big data national databases (such as UK Biobank). To apply CMR-FT to patients with cardiac remodelling resulting from several distinct conditions is a major purpose of our investigation. Using this methodology, we assessed myocardial deformation in all three directions of space: longitudinal, circumferential and radial. Because of the low reproducibility [121] and relatively minor contribution [122] and in keeping with other studies previously published and using this methodology, I chose to exclude radial deformation from my assessment. Further, I assessed not only the longitudinal and circumferential strain at the mid-myocardial level but also at the level of subendocardium and subepicardium, and, in some cases, evaluated the gradient between the deformation amplitude between subendocardial and subepicardial layers. In addition to LV strain assessment, in this thesis, I applied CMR FT to assess the RV, LA and in some cases RA deformations.

1.6 Parametric mapping in HF – an insight into structural modifications, proposed new roles

Parametric imaging is the representation pixel by pixel of two fundamental magnetic properties: longitudinal relaxation time (T1) and respectively, transverse relaxation time (T2) of all the protons (H^1) contained in every correspondent unit of volume, after being excited intermittently by radiofrequency pulses. After the appliance of radiofrequency pulses, the longitudinal and transversal magnetizations recover following exponential curves which describe different slopes (equations) determined

by the quantity of H^1 contained inside the respective tissue composition and by specific structural modifications of the myocardium such as enlarged interstitial space, interspersed collagen fibres, inflammatory infiltrate, iron or lipid deposition, gadolinium-based contrast agents. [123] As proposed by Bloch, the time of recovery of longitudinal magnetization is called T1 and is calculated when longitudinal magnetization reaches the reference level $M = M_0\left(1 - e^{-t/T1}\right)$, approximately 63% of M_0 and, respectively the time of recovery of transversal magnetization is called T2 and is calculated when transversal magnetization reaches the reference level $M = M_0 e^{-t/T2}$, approximately 37% of M_0.[124] **(Figure 1.4)**. Mapping uses a colour coded pixel by pixel rendition of the entire myocardium to compare the T1, T2 and derived values such as ECV, of adjacent regions and emphasise abnormal regions and quantify the amplitude of the changes in any precisely circumscribed region of interest (**Figure 1.5 A**). The acquired signal is proportional to the density of protons in the unit of volume, most of these representing water molecules. In this way it can discriminate with excellent spatial resolution between histological compartments where the water composition differs significantly such as blood pool, myocytes, oedema, fibrosis and other infiltrative substrates such as sarcoid or amyloid, or lipid deposition **(Figure 1.5 B)**. Various sequences were developed and tailored to identify a specific structural element or saturate confounding components in order to highlight the desired target.

Therefore, parametric mapping brings a number of unique advantages for the clinical management of heart disease:

1.It is based on a numeric expression and, in this way, allows a standardized approach and criteria of severity. It makes possible thus, a transition from semi-quantitative (relative volume, surfaces) to a quantitative approach, opening also the possibility of a

more reliable longitudinal evaluation and follow-up of the histological development through continuous variables.

2. A more defined topology – a. place in the myocardium but also adjacent structures, b. more precise spatial pattern

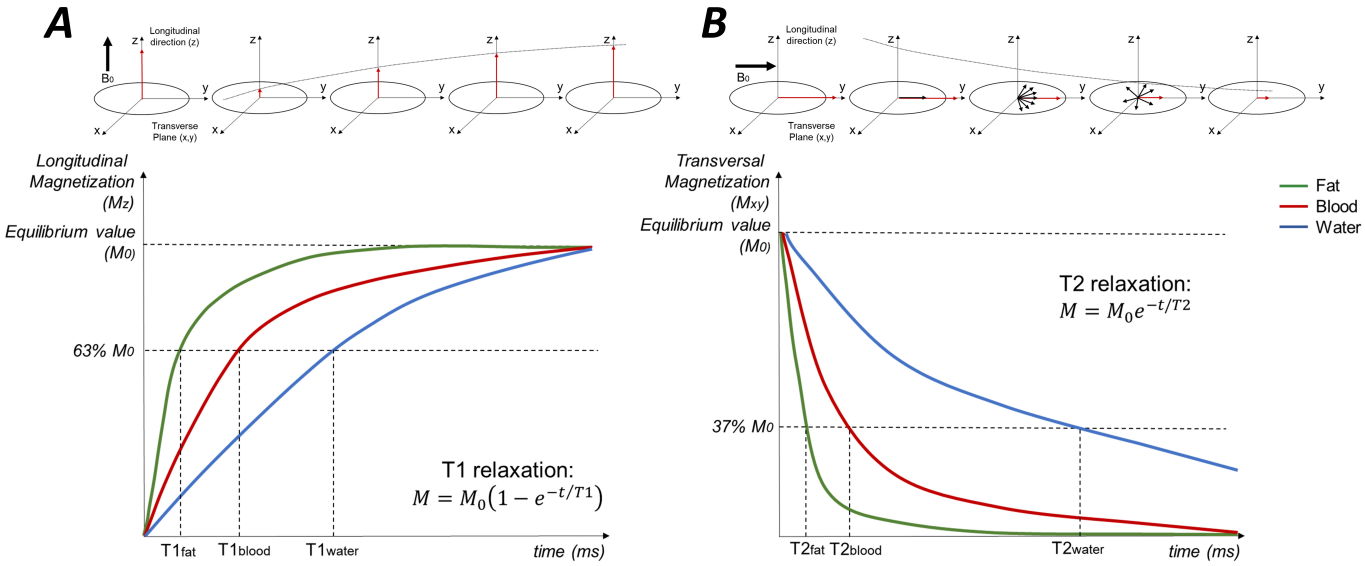


Figure 1.4 Illustration of the Principle of Parametric Mapping. **A.** T1 maps are based on colour coding of different times, distinct for different histological substrates (e.g. fat, blood, water, muscle etc.) measured as the time necessary of the protons in a unit of volume to relax in a longitudinal plan after an initial excitatory magnetic pulse (with the intensity B0) applied. **B.** Similarly T2 maps represent the times necessary for the protons to relax in a transverse plane after an initial excitatory magnetic pulse.

3. It allows the identification of a spectrum of changes rather than a simple area of positive signal (e.g. relationship between fibrosis, oedema, no flow area-viable myocardium) in complicated ACS [35,36] This is particularly important as the usefulness can be extended towards other tissues e.g. fat infiltration that decreases the T1 times.[125]

4. As a corollary, the possibility emerges to characterise and monitor not only one lesion area but multiple related areas of lesion and the relation between them (e.g. fibrosis plus perilesional oedema post MI, cardiac lipidosis and adjacent fibrosis in obesity).

Fibrosis appearance and pattern of focal fibrosis rendered by contrast-enhanced CMR are in practice very important diagnostic criteria. Diffuse fibrosis is more insidious and difficult to detect, localize and quantify with standard post-contrast enhancement techniques. The advent of T1 mapping offers the great prospect of reducing the threshold for recognising diffuse fibrosis, improving localization and offering a quantitative scale of local fibrosis content – comparable with histological methods.

The presence of oedema (increased water content in a unit of volume) prolongs T2 times making the evaluation of this parameter a unique tool for the in-vivo identification of localised active inflammation within cardiac tissue and pericardium. [126] As reviewed above, inflammation is a feature and frequently a therapeutic target in cardiovascular disease and therefore monitoring and quantifying it are helpful elements of a diagnostic. Similarly as with T1, T2 signal can be mapped to cover the entire myocardial volume and this offers similar advantages in terms of more precise localisation, pattern identification and semi-quantitative assessment.

In particular, T2 mapping proves a very useful diagnostic tool in myocarditis and myopericarditis reflected by recognising these methods as an essential part of the current guidelines of diagnostic (Lake Louise Criteria[127] firstly implemented in 2009, subsequently revised[128] to include T1 and T2 mapping in 2018).

As discussed above, LGE or T1 mapping can often overestimate myocardial irreversible damage with cellular loss, in particular when inflammation coexists[35,36], therefore a contemporaneous quantification of both T1 and T2 signal with the

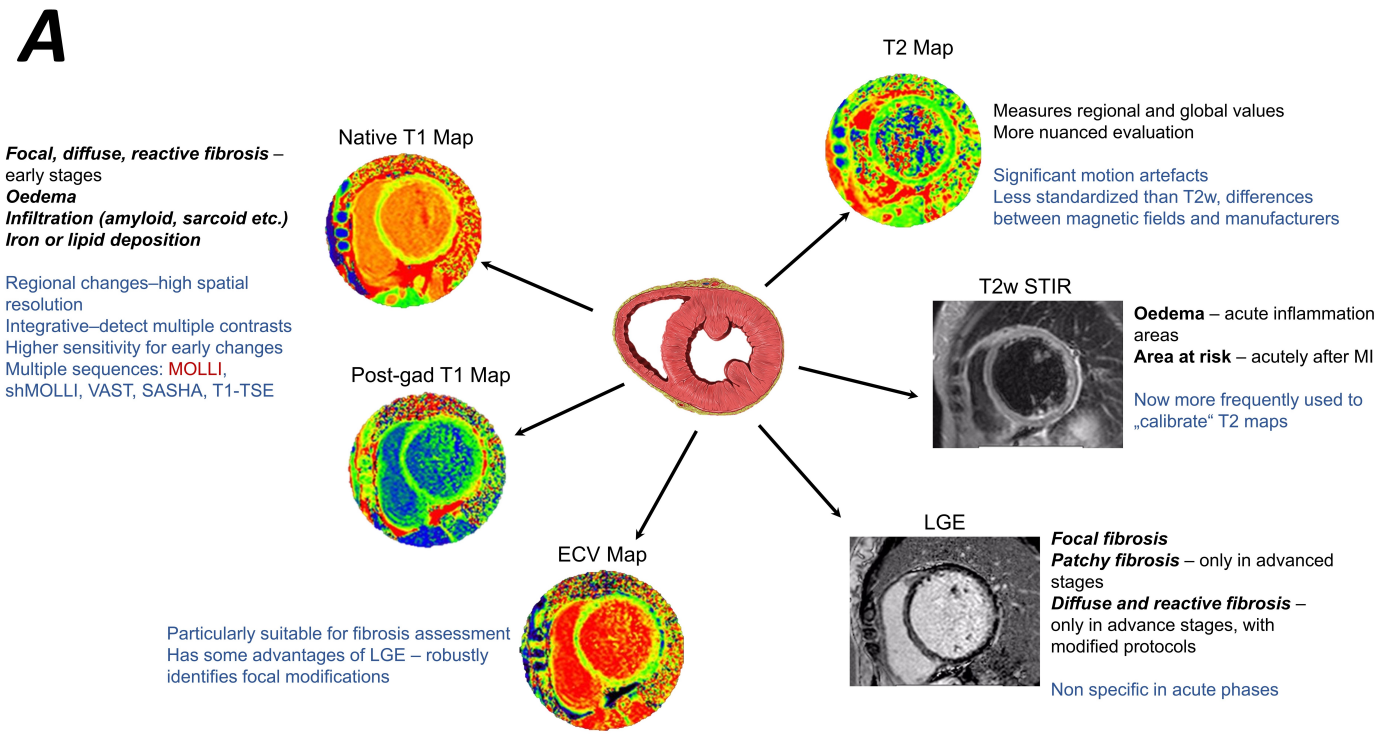


Figure 1.5 A. Parametric Mapping and Structural Imaging with CMR. T1 maps are excellent in defining all types of myocardial fibrosis, infiltration, iron or lipid deposition through a great discriminative capcity of T1 times for various types of histological modifications involved. T2 maps are ideal to detect inflammation and oedema. **B.** Parametric Mapping Diagnostic Role. Evaluation of T1 native, T2 and ECV taken together confers information regarding the histological substrate of myocardial modifications. These diagnostic potential is supported by increased spatial resolution and standardized continuous numerical scale for each individual volume unit. (B. reproduced with permission from Puntmann, V.O. et al., *Circ Res* 2016 Jul 8;119(2):277-99.)

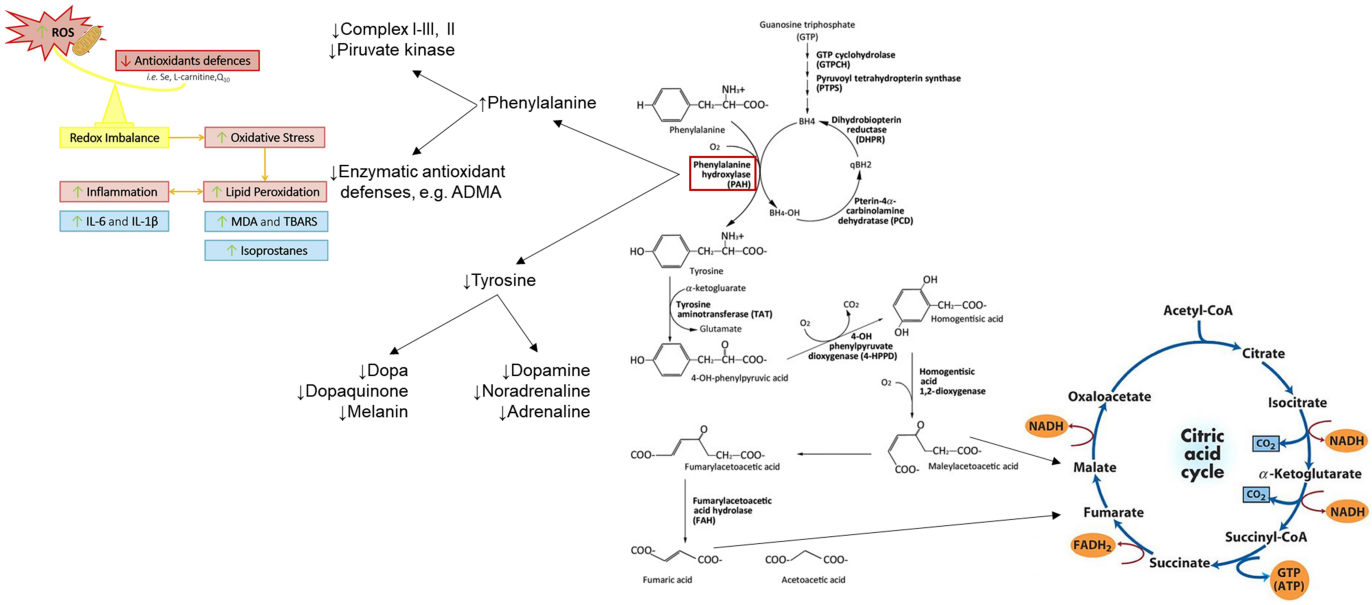


Figure 1.6 Schematic representation of biochemical modifications in „classical" phenylketonuria. A genetic defect abolishing phenylalanine hydroxilase (PAH) enzymatic activity leads to high concentrations of phenylalanine (Phe) and respectively, to reduced levels of tyrosine (Tyr). Increased concentrations of Phe: a. interfere with cellular energetic homeostasis by inhibition of mitochondrial respiratory chain complex I-III and II and inhibition of pyruvate kinase, a key effector of the glycolitic pathway, b. through a deficit of anti-oxidant barriers such as asymmetric dimethylarginine (ADMA), L-carnitine, selenium associates an increase in oxidative stress and pro-inflammatory downstream. Reduced levels of Tyr determine a. complex interference with citric acid cycle (Krebs cycle) resulting in an imbalance in fumarate-malate ratio and b. reduced levels of neuromediators such as noradrenaline, adrenaline and dopamine. (Adapted from DeArmond P.D. et al., *Amino acids disorders,* in *Biomarkers in Inborn Errors of Metabolism*, 2017, Guerra, I.M.S. et al., *Arch Biochem Biophys.* 2020 Jul 30;688:108431).

possibility to superpose reliably the corresponding maps increases the accuracy of assessing myocyte loss (e.g. using indexes such as myocardial salvage index). [129]

Notwithstanding the great promise several limitations need to be acknowledged: sequences are relatively longer, in particular those used to acquire T1 maps, and require patient cooperation to avoid moving artefacts[130]; the most frequently used protocols require inclusion of contrast administration to quantify post-contrast T1 times (T1 post) and extracellular volume (ECV), however non-contrast alternatives are under development[36]; the range of normal values vary significantly between manufacturers

and magnetic field strengths, in particular for T1 and T2 native values[131,132] and therefore pooling large multicentric data could lead to skewed results.

1.7 Phenylketonuria: pathogenesis, cardiovascular risk factors, cardiac phenotype

Phenylketonuria (PKU) is an autosomal recessive inborn metabolic defect causing mutations in the gene for phenylalanine hydroxylase (PAH). [133] In humans, PAH is found mostly in liver and kidney[134], where it has a role in the metabolization of amino-acid phenylalanine to tyrosine. [135] Consequently, an absence of this enzyme, leads to high plasma levels and intra-tissular accumulation of phenylalanine and other compounds resulting from alternative catabolic pathways such as phenylpyruvate produced through transamination.[135] The natural evolution of the disease involves, most importantly, structural and functional modification in the brain leading to severe neuropsychological deficit, seizures, behavioural problems and mental disorders [136] and therefore, the therapeutic efforts have been principally directed towards mitigating these effects.

Current clinical approach to the disease is early diagnosis, in most countries a screening at birth for PKU is instituted followed by a prompt diet control of phenylalanine intake, part of a complex plan of drastically reducing animal protein and supplementing with phenylalanine free compounds and tyrosine. [137] While this strategy proved highly successful in drastically decreasing plasma levels and tissue deposition of phenylalanine, avoiding thus developmental and neuropsychological complications[136], a number of biochemical abnormalities persist (**Figure 1.6**) and their long-term consequences are largely unknown.

While it is widely demonstrated that a higher compliance with the diet control and medically-recommended dietary supplements is associated with lower levels of Phe and higher levels of Tyr[138,139] (the latter obtained through targeted dietary supplements[140]), this is not the only factor that finally determines the Phe and Tyr plasma concentration but also genetic subtypes and complex metabolic interactions are partially responsible. [141] Maintaining lower plasma concentrations of Phe has been widely correlated in children and adults with lower incidence of neurological complications and better psychological prognosis. [142]

Several known cardiovascular and systemic risk factors, described previously, and other metabolic conditions associated with altered metabolic pathways support the hypothesis that a certain degree of cardiac remodelling may be present in adults with PKU, putatively but not necessarily, related to the plasma levels of Phe and Tyr.

One of the potential culprits in PKU pathophysiology is the higher blood and tissue level of oxidative stress, resulting from both excessive expression and activity of NADPH oxidases and 'uncoupled' NOS enzymes[143], depletion of antioxidant enzymatic defence (such as lower levels of asymmetric dimethylarginine[144] or superoxide dismutase[145]) and scarcity in metabolic substrates such a L-carnitine and selenium. [146] The evidence that oxidative stress causes neuronal and white matter damage is compelling[147], however if this plays a role in the development of cardiovascular disease remains still incompletely explored. Only recently, a study brings conclusive evidence regarding FMD impairment and endothelial dysfunction in adult PKU patients and relates them quantitatively to the levels of oxidative stress. [148] A relation between oxidative stress levels and cardiac remodelling, even if mechanistically plausible, is currently missing.

On the other hand, a mechanistic study demonstrated premature senescence-like modifications in the heart of mice with chronically elevated levels of Phe that are partially reversible after a subsequent restriction in Phe intake.[149] At biochemical levels, excessive intracellular Phe organises itself in amyloid-like deposits able to trigger apoptotic signals and thus determine localised lesions. [150] It may be therefore implied that a direct toxic effects of higher concentrations plasma and excessive intracellular influx can be a valid explanation for tissular toxicity in PKU. Moreover, alternative catabolic pathways for Phe are responsible for production of toxic metabolites such as phenylpyruvate, phenyllactate, and phenylacetate. [151] In support of this hypothesis, metabolomic screening indicates higher phenylalanine concentrations as directly related to a higher incidence of heart failure in the general population. [152]

Many adult PKU patients present higher BMI and variable degrees of dyslipidemia, however the nature and prevalence of these conditions vary widely between concurrent studies. [153-155] However, most studies point toward a pro-atherogenic raised LDL/HDL ratio and for higher plasma concentrations of triglycerides. [153] Independently of their vascular effects, raised total cholesterol and LDL/HDL ratio are also metabolic traits associated with cardiomyocyte hypertrophy, diffuse fibrosis, and diastolic and systolic deficit. [156-159] To date a comprehensive study to investigate the cardiac phenotype of adult patients with PKU is missing.

1.8 COVID-19 and cardiac damage. Role of CMR

Since the outbreak of the COVID-19 pandemic, in December 2019, numerous clinical reports[160] bring increasing evidence of serious multiorgan lesions associated with the

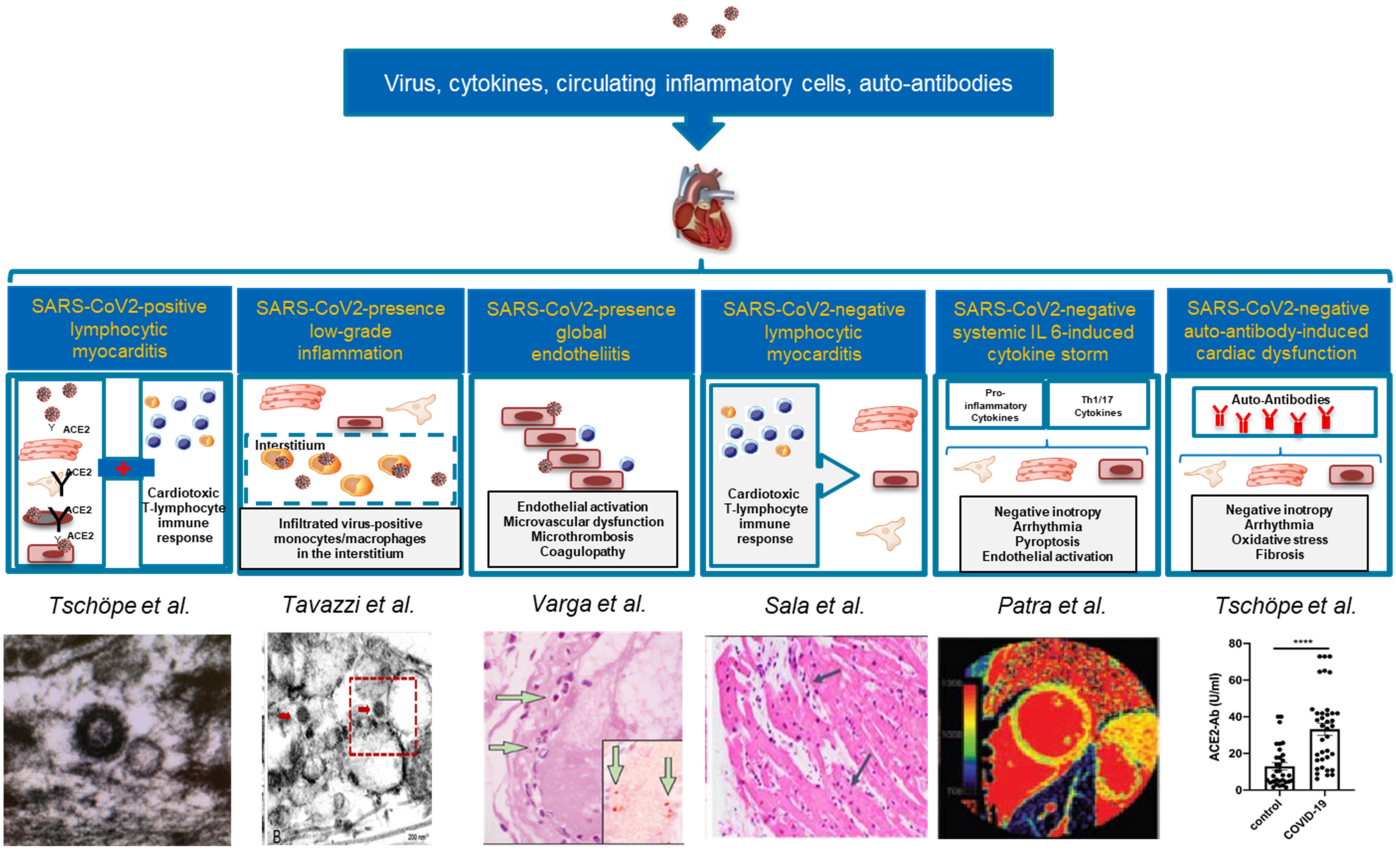


Figure 1.7 Potential mechanism explaining cardiovascular pathogenesis in patients with COVID-19. According to reported data, COVID-19 can associate cardiovascular features of acute myocarditis that can results either from a direct infection with viral particles of the myocardium and local triggering of an immune reaction: lymphocitic myocarditis, low grade inflammation or global endotheliitis or from an indirect immune reaction involving cardiotoxic effect of CD3+ lymphocytes in the absence of cardiac presence of viral particles, an IL-6 mediated cytokine storm trigerred by infected endothelial cells or tissue damage and fibrosis induced by auto-antibodies. (Figure is courtesy from Professors Tschöpe and Kelle and reproduced here with permission).

infection SARS-CoV2, including worrying accounts of cardiovascular features identified post-mortem but also in recovered convalescent patients. Lately described, long COVID-19 syndrome[161] comprises also a number of cardiovascular abnormalities[162] potentially responsible for slow recovery of functional and exertional abilities and other persistent general symptoms and comorbidities. The pathophysiological and molecular aspects of these cardiovascular modifications

determined by COVID-19 are however less well understood and a number of concurrent mechanisms are described (**Figure 1.7**):

1. Entry of the SARS-CoV2 in cardiomyocytes via angiotensin-converting enzyme 2 (ACE-2) membrane receptor was characterised using a pluripotent stem cell-derived cardiomyocyte model[163] and in isolated cases demonstrated in vivo[164], however in a larger study, viral structures were identified mostly in the macrophages or other interstitial cells. [165]
2. Viral structures present at cardiac level and a low-grade myocardial inflammation may be contained inside migrating infected alveolar macrophages[166] and triggered further inflammation and cellular damage.
3. Taking into account the abundance of ACE-2 expression and supporting data from a series of case reports with direct identification of the virus inside endothelial cells[167], a pan-endotheliitis predisposing to microvascular dysfunction, microthrombosis and coagulopathy has been proposed as an alternative pathogenic mechanism. [168]
4. Another possible explanation is a reactive diffuse CD3+ T cells lymphocytic inflammatory infiltrate in the absence of a direct colonisation by SARS-CoV2[169].
5. SARS-CoV2 through the S1 region of its spike protein, activates, in the endothelial cells, intracellular transcription orchestrators such as NF-κB, c-Fos, and MAPK leading to overactivation of immune mediators, particularly IL-6 leading to a cytokine storm and exacerbated inflammatory response. [170]
6. Presence of auto-antibodies, such as those targeting angiotensin II type I receptors[171] or ACE-2 [172] are higher in patients infected with SARS-CoV2 and their levels are correlated with the severity of the disease, with increased pro-inflammatory, pro-fibrotic and pro-thrombotic response. [173]

Given its non-invasive and low risk character, CMR plays an important role in defining the extent and the longitudinal evolution of cardiovascular lesions in patients with COVID-19[174] and indeed, the Society for Cardiovascular Magnetic Resonance (SCMR) promptly launched an international multicentric initiative and guideline[175] to include and follow-up a large number of patients affected by COVID-19. In a large multicentric cohort, 62.3% of the patients requiring hospitalisation had biochemical evidence of myocardial injury (elevated troponin), and 2/3 of these presented also echocardiographic evidence of cardiac dysfunction (RV impairment, global or regional LV impairment, grade II or III diastolic dysfunction, pericardial effusion) that additionally associated with a higher risk of death. [176] Preliminary CMR reports characterised persistent oedema and structural modifications similar to those described in “classical” myocarditis with increased T1 and T2 signals, which, intriguingly persist at mid-term (on average 3-6 months follow-up) [177] and associated functional deficit in LV and RV functions in patients with additional evidence of sustained structural lesions. [178] The distribution pattern of LGE or areas of increased T1, T2 signal is compatible with non-ischaemic injury. [178] However other subsequent studies provide conflicting data describing these cardiac lesions and questioned the parallel between these changes and more drastic ones observed in acute viral myocarditis according to updated Lake Louise Criteria[128], the current recommended CMR based diagnostic criteria. These discrepancies were partly due to an absence of appropriate control against, on one hand, healthy matched subjects but on the other, equally, to patients with “classical” non-SARS CoV2 viral myocarditis. Furthermore, histological evidence of viral presence at the level of the myocardium will need to be specifically interrogated with endomyocardial biopsies (EMB), widely accepted as the gold standard diagnosis for viral myocarditis [179], followed by immunohistochemistry and PCR diagnostic screening. [160] Moreover, a thorough LLC based diagnostic in COVID-19 patients, including T1 and

T2 mapping and numeric evaluation, will bring conceptual clarification regarding the CMR criteria of acute myocarditis applied to COVID-19.

1.9 Hypotheses, objectives and aims

Myocardial strain quantified by CMR holds the promise to delineate better so far incompletely explored mechanistic questions about the early progression of heart failure. We hypothesize that CMR FT can reliably assess regional, layer specific myocardial deformation and offer new parameters to evaluate myocardial systolic and diastolic mechanics.

1. In Chapter 3 we aim to answer the question if there are differences between myocardial systolic strain and strain-rate between sub-endocardium, mid-myocardium and sub-epicardium between the 3 subgroups of HF patients (HFpEF, HFmrEF and HFrEF) and what is their respective contribution to the transition between control, HFmrEF and HFrEF.
2. In Chapter 4 we explore the atrial volumes and phasic functions with CMR FT.
3. In Chapter 5 we investigate if the CMR FT parameters are able to give information about the LV diastolic function and how these compare with better established criteria such as invasively measured LVEDP, Doppler echocardiography derived E/e', and NT-proBNP.
4. In Chapter 6 and 7 we explore the cardiac phenotype of adult patients with phenylketonuria, a genetic condition that is associated with well known cardiovascular risk factors such as oxidative stress, dyslipidaemia and ectopic fat deposition. With multiparametric CMR and echocardiography we investigated a cohort of patients with "classical" PKU and compare them with age and sex matched controls and

5. In Chapter 8 we used data offered by multilayer FT and parametric mapping to investigate the cardiac modifications produced by the infection with the SARS CoV2 virus during the 2019 pandemic in convalescent patients, recovered from COVID-19 disease, who still present cardiac symptoms (some with persistent traits of long COVID syndrome) and compare them with, on one hand healthy controls and on the other hand patients with non-SARS CoV2 viral myocarditis. This double comparison allows us a better understanding of the severity and dynamics of these changes and gives a hint regarding further therapeutic or clinical surveillance approaches.

Chapter Two:

Methods

2.1 Study populations

In this thesis I investigated several groups of patients and in some cases control volunteers, each of them recruited following the Ethics approval of the home institution

1. For Chapters 3 and 4 patients included for analyses were recruited as part of Empathy-HF clinical study.
2. For Chapter 5, validation against haemodynamics was performed in a group of patients who underwent an invasive catheter study with LV pressure measurements – the LVEDP Cohort.
3. For Chapters 6 and 7, PKU cohort and age- and gender matched controls were included. Some of these patients had a second follow-up visit.
4. For Chapter 8, 32 patients with COVID-19, 22 patients with acute myocarditis and 16 control subjects were included. Of these 10 patients with COVID-19 and 13 with acute myocarditis had a follow-up scan which was included in our study.

All individuals were fully informed about the aim, rationale and detailed protocol of the study (subject information leaflet) and consequently written informed consent was obtained before participation. Inclusion and exclusion are detailed below and also available online at Deutsches Register Klinischer Studien (German Clinical Trials Register) www.drks.de.

2.1.1 Inclusion Criteria – All patients

All patients included in the studies presented in this thesis are adult men and women of any age who provided written informed consent for prospectively recruited patients or verbal consent after receiving full information either in writing or verbally. Below are presented the detailed inclusion and exclusion criteria for each cohort used.

2.1.2 Empathy HF-Inclusion Criteria

Age >45 years and presence of signs and symptoms of heart failure NYHA II-IV (at least 30 days prior to screening), in clinically stable condition defined as no i.v. therapy with diuretics or inotropics and no hospitalization within the last 7 days and unchanged medication at least 7 days prior to screening.

Subgroup HFpEF:

HFpEF - Baseline- echocardiography[180] with the following findings: EF ≥50% and NT-proBNP ≥ 220 pg/ml while in sinus rhythm at screening and one of the following: indexed LA volume > 34 ml/m2 or E/e´ > 13 (medial or lateral mitral anulus) **or** LVH: septal wall thickness or posterior wall thickness ≥ 13mm).

Subgroup HFrEF:

EF <40% in echocardiography during screening, individualized optimized and unchanged (at least 7 days prior to screening) heart failure therapy (must include Beta-Blocker, ACE-Inhibitor/ AT1-Inhibitor, aldosterone-antagonist as long as no contraindications exist), EF <40% in imaging within 90 days of screening.

Sub-group HFmrEF

EF 40-49%, NT-proBNP ≥ 220 pg/ml while in sinus rhythm on screening **and** (LAVI > 34 ml/m^2 **or** E/e´ > 13 (medial or lateral para-mitral segments) **or** LV hypertrophy - assessed as septal wall thickness or posterior wall thickness ≥ 13 mm).

Sub-group healthy controls:

The healthy control groups included subjects with no clinically relevant structural heart disease, no symptoms of heart failure, no symptoms of CAD, no relevant arrhythmia, no valve defects >I°, LVEF ≥ 55%, able to provide written informed consent, age >45 years.

2.1.3 Inclusion Criteria – PKU study

For the PKU cohort study the following inclusion criteria were used: age >18 years, absence of any generic contraindication for CMR (claustrophobia, cardiac pacemakers or defibrillators, metallic implants, such as artificial valves or cerebral aneurysm clips, and morbid obesity), and signed consent to participate in all the stages of our protocol. Patients with any cardiac pathology (more than trivial valve disease, uncontrolled systemic hypertension, coronary artery disease, previous myocardial infarction, and cardiac arrhythmias) were excluded from the study. Four patients were excluded because of incomplete compliance with the protocol. Thus, a final number of 39 patients completed all the stages of our protocol, and their data were available for the functional analysis of the cardiac phenotype. A complete set of parametric imaging of sufficient quality to characterize the myocardial phenotype was obtained in 36 of 39 patients. For comparison, an age- and sex-matched group of 39 volunteers who underwent a similar protocol was included in the study. Controls were investigated without the administration of contrast medium and, therefore, T1 post and ECV could not be assessed directly. Controls were selected from our volunteer database at German Heart Centre Berlin.

15 out of 36 patients who had a complete initial set of CMR data (see **Chapter 6**, Methods) agreed to participate in a follow-up CMR study. Additionally, to compare the phenylalanine and tyrosine and respectively the lipid profile all 39 patients agreed and gave permission to access retrospectively all the clinical and laboratory data available on the dedicated database.

2.1.4 Inclusion Criteria – COVID-19 study

All post-COVID-19 patients referred to our clinic with suspected cardiac pathology (palpitations, angina, persistent high troponin levels, persistent breathlessness and reduced capacity of effort) and who consented to participate were enrolled. Healthy control subjects were identified from an existing database available. [181] This study was reviewed and approved by the Charité–Universitätsmedizin Berlin Ethics Committee and complies with the Declaration of Helsinki.

In total, 32 patients with a previous COVID-19 infection were included in the study. For comparison, we retrospectively included 22 patients with a clinically confirmed diagnosis of acute non-COVID-19 myocarditis and an available baseline CMR scan, along with 16 healthy volunteers. Ten of the post-COVID-19 patients underwent a clinically indicated follow-up scan. Thirteen of the 22 patients with acute myocarditis had an available follow-up CMR on file. Inclusion criteria for the post-COVID-19 patients were as follows: (I) a previously diagnosed SARS-CoV-2 infection with COVID-19 disease; (II) clinical indication for CMR such as suspected myocardial injury (elevated troponin), reduced LVEF and/or presence of pericardial effusion on echocardiogram, persistent arrhythmia, persistent dyspnoea, reduced exercise capacity, or fatigue; and (III) resolution of acute COVID-related symptoms to allow the end of self-isolation or a confirmation of a negative PCR test. The non-COVID-19 viral myocarditis cases were retrospectively identified from our local database and inclusion criteria followed the ESC recommendations. [179]

2.1.5 Exclusion Criteria – All patients

In agreement with SCMR guidelines and following our local safety recommendations we excluded all the patients or volunteers falling in any of these categories: contractual incapacity, pregnant or breastfeeding women, additional generic MRI contraindications (history of claustrophobia, impaired hearing >30 dB, history of tinnitus, implanted

pump-devices, recently implanted joint prothesis, metal coils within the brain, neurostimulators, Cochlea-Implantation, magnetically attached teeth prothesis, metals plinters present in any part of the body, history of neurosurgery using metal clips, early pregnancy <3 months), documented previous allergic reactions to the contrast agent used or impaired renal function (GFR<40ml/min/1.73m^2 BSA), unstable cardiorespiratory state within last 4 weeks.

2.1.6 Exclusion Criteria – Empathy-HF study

Atrial Fibrillation, symptomatic CAD with angina pectoris > CCS II, recent PCI within 4 weeks or planned PCI/CABG-surgery, myocardial infarction within the last 3 months, stroke within the last 3 months, relevant valve defect > II°, hypertrophic obstructive or infiltrative cardiac disease (e.g.: HOCM, Amyloidosis), complex congenital heart defect, ongoing myocarditis, significant pulmonary disease in investigators discretion, significant arrhythmia in investigators discretion, persistent atrial fibrillation, planned changes of concomitant medication, planned heart transplantation, status post heart transplantation, Cardiac Resynchronisation Therapy begun within last 3 months, ICD/Pacemaker implanted within last 4 weeks, uncontrolled Hyper-/Hypotension (systolic BP > 180 mmHg/ diastolic BP > 95mmHg), enrolled in rehabilitation program, known malignant disease limiting life expectancy <1 year, anaemia (defined as Hb < 10 mg/dl), untreated clinically significant disease of the thyroid, i.v. administration of diuretics or inotropics within 7 days prior to screening, myocardial infarction within 4 days prior to inclusion.

2.1.7 Exclusion Criteria – COVID-19 study

Exclusion criteria applied for this study were largely similar: coexistence of underlying cardiac pathology (myocardial infarction, cardiomyopathy, and/or haemodynamically

relevant valvulopathy). Specifically, we screened for and excluded all the COVID-19 patients with a known history of acute or chronic non-COVID-19 myocarditis, or any autoimmune conditions with a potential impact on the heart (rheumatoid arthritis, systemic lupus erythematosus, antiphospholipid syndrome, Sjögren's syndrome, systemic sclerosis).

2.2 Cardiac magnetic resonance: systems and protocols of image acquisition

For the studies presented in this thesis different CMR scanners were used as follows:

For the data presented in Multilayer Strain in HF (**Chapter**3), Left Atrial Function in HF (**Chapter 4**), PKU Baseline (**Chapter 6**) and Follow-up (**Chapter 7**) studies, CMR images were acquired using a 1.5T (Achieva, Philips Healthcare, Best, The Netherlands). For LVEDP Study (data presented in **Chapter 5**), CMR images were acquired using a 1.5T system (Achieva, Philips Healthcare, Best, the Netherlands) and a 3T system (Ingenia, Philips Healthcare, Best, the Netherlands). For the COVID-19 vs acute myocarditis Study (**Chapter 8**) CMR images were acquired using three clinical MRI scanners: a clinical 1.5T system (Achieva, Philips Healthcare, Best, the Netherlands), a clinical 3T system (Ingenia, Philips Healthcare, Best, the Netherlands), and a clinical 1.5T system (Magnetom Aera, Siemens Inc.). More details about the specific groups of patients that were scanned on each of these systems are given in the Specific Methods section of **Chapter 8**.

All study participants were scanned with a comprehensive imaging protocol and appropriate local receiver coil arrays in accordance with the most recent Society for Cardiovascular Magnetic Resonance (SCMR) guidelines. [182]

All CMR scans were acquired with ECG gating or retrospective gating (cine) in one breath hold (8–15 s). Typical imaging parameters are summarized as follows: Long-

axis cine-imaging (Philips 3T): balanced steady state free precession (bSSFP), TR = 2.9 ms, TE = 1.45 ms, flip angle = 45°, acquisition voxel size = 1.9 × 1.9 × 6.0 mm^3, acquired/reconstructed heart phases = 27/40, parallel imaging (SENSE) acceleration = 2. Long axis cine-imaging (Philips 1.5T): TR = 3.4 ms, TE = 1.7 ms, flip angle = 60° , acquisition voxel size = 1.6 × 1.6 × 6.0 mm^3 , acquired/reconstructed heart phases = 25/50, parallel imaging (SENSE) acceleration = 2. T2-weighted short tau inversion recovery STIR (Philips 1.5T / 3T): black blood prepared turbo spin echo (TSE) imaging, TE = 100 ms, flip angle 90°, refocusing angle 160°, acquisition voxel size = 1.5 × 1.5 × 8.0 mm^3, half-Fourier factor 0.65, acquisition every other heart beat to allow for optimal blood signal suppression. T2 mapping: (Philips 1.5T / 3T): black blood prepared gradient and spin echo (GraSE) imaging, flip angle 90°, refocusing angle 180°, 9 echoes, echo times = n × 8.8 ms, EPI-factor 7, acquisition voxel size = 2.0 × 2.0 × 10.0 mm^3, parallel imaging (SENSE) acceleration = 2.3. Siemens 1.5T Magnetom Aera: repetition time (TR) = 40.8 ms, echo time (TE) = 1.07 ms, flip angle = 55°, acquisition voxel size = 1.9 × 1.9 × 8.0 mm3.[34]

Native and 15 min post-contrast T1-mapping were performed using modified Look-Locker imaging (MOLLI) in two left ventricular short-axis slices (basal and mid-ventricle), as described previously.[183] Patients received 15 mmol/kg of gadolinium-based contrast agent (Gadobutrol 1.0 mmol/ml, Gadovist R , Bayer AG, Leverkusen, Germany). Segmented inversion-recovery fast gradient–echo imaging was used to assess late gadolinium enhancement (LGE) 10 min after the administration of contrast substance [34]. mDixon-imaging was used to differentiate pericardial enhancement from fat.[184]

2.3 CMR image analysis

I present here an exhaustive protocol used for the image analysis representing the local standards of practice, for each individual study, modifications or adaptations of these methods are presented in the Specific Methods subchapter. Image analysis were carried out in agreement with the post-processing guidelines published by the SCMR. [185,186]

All images were analyzed offline using commercially available software (Medis Suite, version 3.1, Leiden, The Netherlands) in accordance to recent consensus document for quantification of LV function using CMR. [187]

LV and RV volumes and mass were derived identifying the ED and ES phases for both LV and RV on a SSFP short-axis stack covering the entire ventricular myocardium. At ED level, endocardial and epicardial contours were manually drawn, at ES level the endocardial contours were similarly manually drawn. The Simpson method was used to derive LV and RV volumes and masses and cardiac output. Left atrial (LA) volumes were assessed using a biplane area length method after segmentation of atrial contour in long-axis 4Ch and 2Ch views and exclusion of LA appendage.

All volumes are presented indexed with body surface area (BSA) throughout the thesis, unless otherwise specified. BSA was calculated using Mosteller formula. [188]

LV strain analysis included 2Ch, 3Ch and 4Ch cine images, and respectively, 3 preselected slices from the LV short-axis stack to correspond to basal, mid-ventricular and apical levels. The endocardial and epicardial contours drawn on cine images with QMass version 8.1 were transferred to QStrain RE version 2.0, where, after the application of tissue tracking algorithm, endocardial and epicardial borders were detected throughout all the cardiac cycle. These long-axis cine images were further

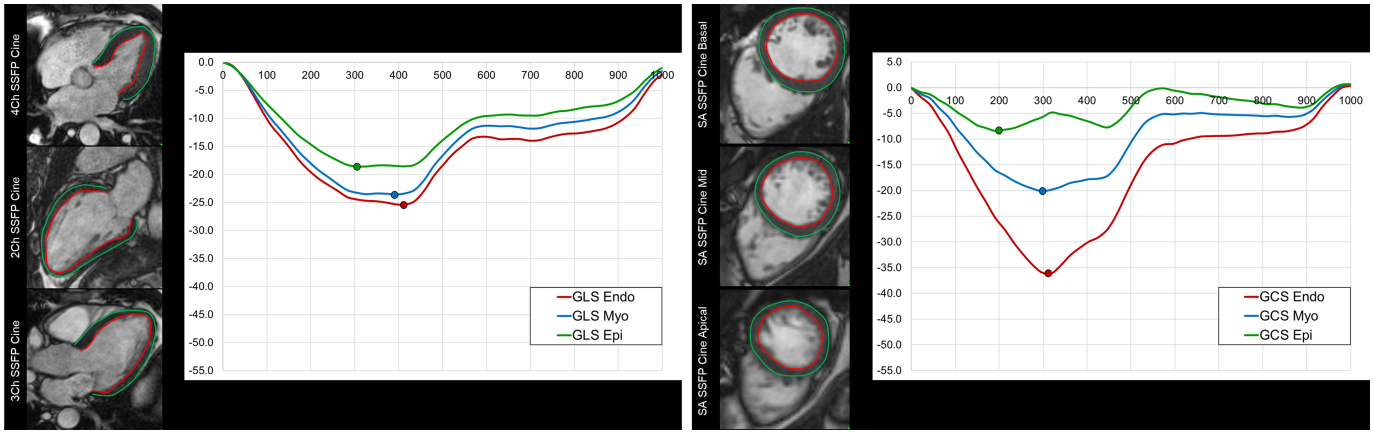


Figure 2.1 Multliyer assessment of longitudinal (GLS) left side and circumferential (GCS) myocardial strain. Endocardial and epicardial contours are drawn in end-diastolic and end-systolic phases in long-axis 4Ch, 3Ch and 2Ch SSFP Cine and respectively in short-axis basal, mid-ventricle and apical SSFP Cine and propagate along the cardiac cycle. GLS and GCS Strain curves can be measured at three distinct levels of the myocardium: subendocardial (Endo), mid-myocardial (Myo) and subepicardial (Epi). In the figure the point of peak systolic deformation is indicated with a dot on all strain curves.

used to compute global myocardial longitudinal (GLS) and, respectively, short-axis images were used to compute circumferential (GCS) strain and strain-rate at 3 distinct levels within the myocardial volume: Endo subendocardial myocardium, Myo mid-myocardium, and Epi subepicardial myocardium (**Figure 2.1**). The global values for each layer were respectively obtained through averaging the values according to an American Heart Association (AHA) 17 segments model[189], apex being excluded, as follows: GCS from averaging CS for 6 basal, 6 mid and 4 apical segmental individual values; GLS from 2Ch, 3Ch and 4Ch averaging 6 basal, 6 mid and 4 apical segments using a bull-eye view algorithm. Of note, I report Endo, Myo and Epi values for the specific multilayer strain project (**Chapter 3**), for all the other studies the standard Endo values or Endo and Myo were computed. We used a commercially available tool (Medis Suite, version 3.1, Leiden, The Netherlands) to derive LV intraventricular hemodynamic forces. [119]

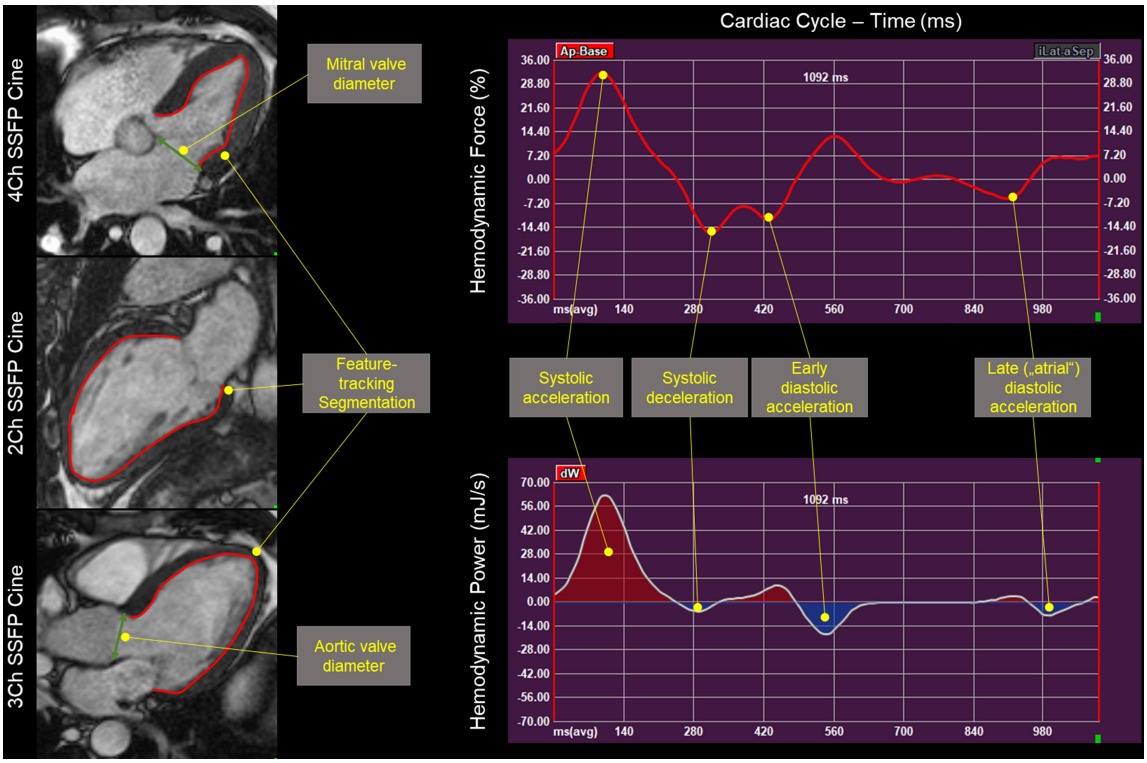


Figure 2.2 Left ventricular hemodynamic (HD) forces can be modelled integrating information obtained from long-axis (GLS)and short-axis (GCS) myocardial strain and the estimation of mitral and aortic valve. On the HD force graph (upper row) four phases can be identified: systolic acceleration corresponding to the systolic thrust, systolic deceleration – recoil phase, early diastolic acceleration (suction), late (atrial) diastolic deceleration. On the HD work graph (lower row), three corresponding amplitudes (HD Power) and areas under curve (HD Work) can be identified and measured: HD systolic HD early diastolic and HD late diastolic.

These parameters were previously validated and tested for inter and intra-observer reproducibility with excellent results. [190] Propagating the previously segmented long-axis 4Ch, 3Ch and 2Ch SSFP cine and further drawing the maximal mitral (visible in 4Ch view) and aortic valve diameter (visible in 3Ch), we were able to estimate hemodynamic (HD) forces and respectively HD power and work in 3 different phases of the cardiac cycle as follows: systole, early diastole and late diastole. (**Figure 2.2**). HD forces can be quantified in 3 directions corresponding to the main axes of the LV as follows: basal- apical, septal-lateral, and inferior-anterior. A complex list of

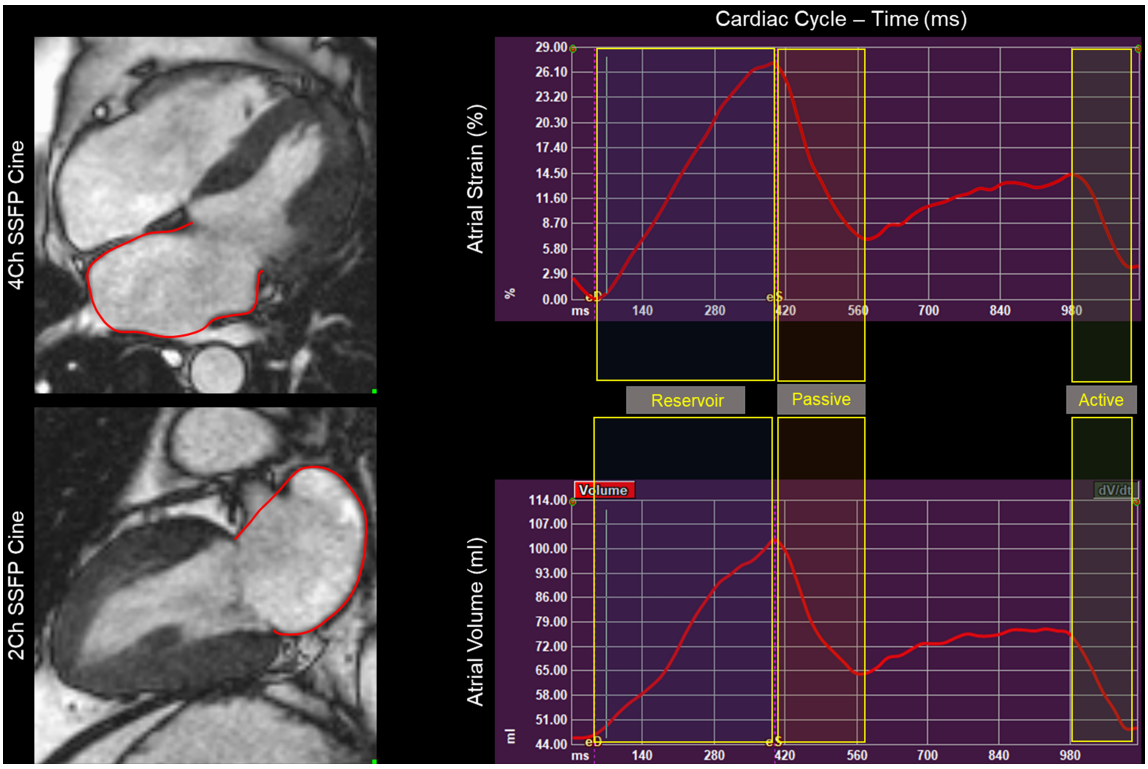


Figure 2.3 Phasic left atrial (LA) strain and volume:contours are drawn in both 4Ch and 2Ch SSFP cine images at the points of maximal and minimum volume and propagated along the cardiac cycle. Three phases describing atrial physiology are delineated as follows: reservoir – filling with blood of LA between LA minimal volume (corresponding to the closing of mitral valve at the end of the LV diastole) and LA maximal volume, passive emptying – emptying of LA from the opening of the mitral valve till the atrail diastasis, active emptying – emptying of LA through active contraction of atrial myocardium, between the commencement of the P wave on the ECG and closing of the mitral valve. Corresponding to these 3 phases LA phasic volumes and LA phasic strain can be derived.

parameters able to quantify distinct amplitudes (HD forces), their derivative over time (HD power), timing, areas under curve (equating with work of a certain HD force) and orientation parameters can be derived for each phase of the cardiac cycle. [118,191] For each study presented here we retain the most significant and pathophysiologically relevant values and specify them accordingly in tables. Given its magnitude and therefore physiological importance and superior reproducibility, in this thesis we quantified and refer exclusively to HD forces, work and power recorded along the

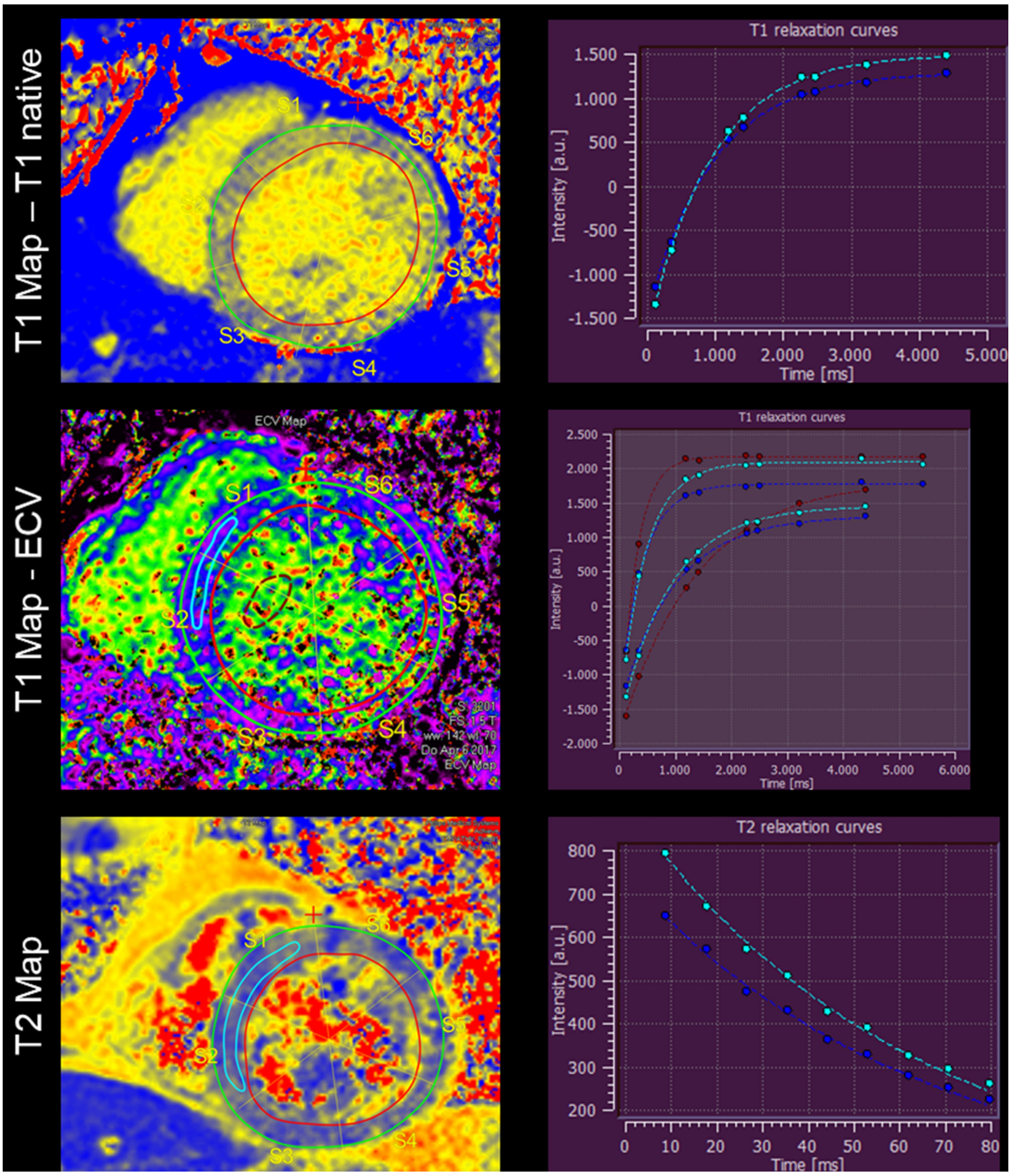


Figure 2.4 Colour mapping of T1 native, extracellular volume (ECV) and T2. For every pixel a curve of magnetic recovery is drawn. Calculation of average signal value for the entire LV volume or discrete region of interest can be performed.

basal-apical axis. [118] As numeric expression, HD forces are given as percentage (positive in systole and negative in early and late diastole) which reflects the indexed

value (taking into account the surface on which this force acts – intraventricular surface derived from EDV, fluid density and gravity acceleration). Indexing the absolute values, expressed in newtons facilitates the comparison between patients or groups of patients, taking into account intrinsic differences in body and heart size.

Similarly, RV strain was determined through drawing of the endocardial and epicardial contours at ED and ES phases in a long-axis 4Ch SSFP cine image followed by propagation through the cardiac cycle and loading in the QStrain RE version 2.0. Only the RV free wall segments were included in the analysis, RV GLS represents the averaged peak systolic value.

LA strain was determined using the endocardial and epicardial contours for maximal and minimal atrial volume and propagation through the cardiac cycle and loading in the QStrain RE version 2.0. This was done separately for 2Ch and 4Ch long-axis views and the values of strain averaged. **(Figure 2.3)**

Mapping parameters were measured using QMap RE version 2.0 (Medis Medical Imaging Systems bv, Leiden, the Netherlands). For parametric imaging, pre- and post-contrast MOLLI images were manually adjusted for in-plane motion and T1 native and post-contrast relaxation times were determined using nonlinear fitting with a maximum likelihood estimator. [183] Extracellular volume (ECV) was computed from pre- and postcontrast T1 and hematocrit values as previously described. [192] Global T1 native, ECV, and T2 values were calculated by averaging individual segmental values derived for each patient from mapping of two distinct ventricular short-axis slices at basal and mid-ventricular levels. [183] The presence of LGE was established by visual assessment evaluated in all the slices of the short axis stack and three long axis views. An illustration of T1, ECV and T2 maps and derived average and ROI signal curves are presented in **Figure 2.4**.

2.4 Echocardiography

Transthoracic echocardiographic imaging was per-formed using an iE33 system with the X5–1 probe (Philips Healthcare, Best, the Netherlands). To characterize parameters related to the valvular and diastolic function, early (E) and late trans-mitral flow (A) and E/A ratio were assessed. Doppler tissue imaging was used to assess the velocity of para-mitral segments (e′) and calculate E/e′ ratio, an imaging parameter evaluating noninvasively LV filling pressures. Image analysis was performed using a dedicated post-processing software (IntelliSpace Portal V11.1, Koninklike Philips N.V., Amsterdam, The Netherlands).

2.5 Blood Samples and Biochemistry

All determinations were performed performed by the local hospital platform (Labor Berlin—Charité Vivantes GmbH) and collected from Charité – Universitätsmedizin Berlin. For the PKU Baseline and Follow-up Studies plasma levels of Phe and Tyr were calculated using all the data available, obtained from the Interdisciplinary Centre for Metabolism of the Charité University Berlin in agreement with the Ethical Approval. These average concentrations were based on at least 20 single determinations (range, 20–60 determinations for each patient with phenylketonuria).

2.6 Bioelectrical impedance

For PKU patients, routine assessments of bioelectrical impedance analysis (BIA) with a single frequency bioimpedance analyser were performed with a ViScan measurement system (Tanita Corporation). We collected these data (fat, fat-free, muscle, water and visceral mass components, basal metabolic rate) from the available database of Interdisciplinary Centre for Metabolism of the Charité University Berlin in agreement with the Ethical Approval.

2.7 Endomyocardial Biopsy Samples: collection, processing, immunohistochemistry, DNA/RNA extraction, PCR.

Endomyocardial biopsy was performed in a selected number of COVID-19 and non-SARS-CoV-2 acute myocarditis subjects (data presented in Chapter 8). In all patients, including those with COVID-19 undergoing EMB, myocarditis was clinically suspected, following the recent guideline recommendations.[179] Myocardial biopsy was performed in all COVID-19 and myocarditis cases as described previously. Briefly, endomyocardial samples were collected through femoral vein access using either a 7F long sheath with angulated tips (from the RV surface of the interventricular septum) or a 7F long-sheath without angulation using a retrograde approach (from the LV surface of the interventricular septum). At least four pieces per patient were collected with which Fluoroscopic guidance was used to identify the region of interest. Vital parameters and ECG were closely monitored during the procedure. A routine echocardiogram was performed at the end of the procedure to exclude iatrogenic pericardial effusion. Analysis of endomyocardial biopsy (EMB) samples was performed in specialized laboratories by experienced cardio-pathologists as described previously.[193] Myocardial inflammation was considered to be present when ≥ 20 infiltrating immune cells/mm2 were observed (CD3 T-lymphocytes and/or CD68 macrophages). Additionally, enhanced HLA class II expression in antigen-presenting immune cells was evaluated. Screening for viral genomes was performed after extraction of deoxyribonucleic acid (DNA) and ribonucleic acid (RNA) with Proteinase-K digestion and phenol/chloroform. Reverse transcriptase-polymerase chain reaction was used subsequently to detect virus presence within cardiac tissue samples, e.g., COVID-19 and, respectively, viruses frequently involved in myocarditis, such as enteroviruses (including coxsackieviruses of group A and B and echoviruses), parvovirus B19

(PVB19), adenoviruses, human cytomegalovirus, Epstein-Barr virus, and human herpesvirus type 6 (HHV6). Oligonucleotide sequences were chosen from the glyceraldehyde-3-phosphate-dehydrogenase gene as a control for successful extraction of DNA and RNA. Negative and positive controls were included in each PCR reaction. Automatic DNA sequencing was used to confirm the specificity of all viral amplification products. Masson trichrome staining was used for histological examination of various types of fibrosis (multifocal fibrosis/scarring without inflammation/diffuse collagen deposition). Congo-red staining was used to exclude amyloid deposition.

2.8 WHO Score of COVID-19 Severity Description

World Health Organization (WHO) guidance on clinical management of COVID-19 (https://www.who.int/publications/i/item/WHO-2019-nCoV-clinical-2021-2) was used to define disease severity as follows: mild and moderate disease–symptomatic patients meeting the case definition for COVID-19 without evidence of viral pneumonia, hypoxia, or some clinical signs of pneumonia (fever, cough, dyspnoea, and/or fast breathing) without other criteria of severity and SpO2 ≥ 90% on room air. Severe and critical disease were defined as presence of additional severity signs and respiratory distress as follows: respiratory rate > 30 breaths/min; severe respiratory distress; or SpO2 <90% at room air or presence of acute respiratory distress syndrome or specific signs on radiograph, CT scan, or lung ultrasound (e.g., bilateral opacities, not fully explained by volume overload, lobar or lung collapse, or nodules).

2.9 Statistical analysis

Statistical analysis was carried out with SPSS IBM statistics, versions 25 and 26. For the graphical representation of the results I used SPSS IBM statistics versions 25 and

26, GraphPad Prism version 8 (GraphPad Software, San Diego) and Microsoft Excel. The details of statistical analysis used in every individual study are presented in detail in the Specific Methodology part of every chapter.

Chapter Three:

Multilayer Evaluation of Myocardial Mechanics using Feature Tracking Cardiac Magnetic Resonance

The work presented in this chapter referring to multilayer assessment of LV strain is based on two articles previously published in *Scientific Reports* 2019 Nov 11;9(1):16478. [194] and *ESC Heart Fail.* 2020 Oct;7(5):3240-3245. [195] on both of which I am the first author. I was involved in CMR data collection, analysis and in writing the manuscripts. The echocardiographic data were collected by Dr Djawid Hashemi and Dr Robin Kraft from the Charité – Universitätsmedizin Berlin.

3.1 Abstract

Heart failure (HF) is associated with progressive ventricular remodeling and impaired contraction that affects distinctly various regions of the myocardium. Our study applied cardiac magnetic resonance (CMR) feature tracking (FT) to assess comparatively myocardial strain at 3 distinct levels: subendocardial (Endo), mid-myocardial (Myo) and subepicardial (Epi) myocardium across an extended spectrum of patients with HF.

59 patients with HF, divided into 3 subgroups as follows: preserved ejection fraction (HFpEF, N=18), HF with mid-range ejection fraction (HFmrEF, N=21), HF with reduced ejection fraction (HFrEF, N=20) and a group of age- gender- matched volunteers (N=17) were included. Using CMR FT we assessed systolic longitudinal and circumferential strain and strain-rate at Endo, Myo and Epi levels.

Strain values were the highest in the Endo layer and progressively lower in the Myo and Epi layers respectively, this gradient was present in all the patients groups analyzed but decreased progressively in HFmrEF and further on in HFrEF groups. GLS decreased with the severity of the disease in all 3 layers: Normal>HFpEF>HFmrEF>HFrEF (Endo: -23.0±3.5>-20.0±3.3>-16.4±2.2>-11.0±3.2, $p<0.001$, Myo: -20.7±2.4>-17.5.0±2.6>-14.5±2.1>-9.6±2.7, $p<0.001$; Epi: -15.7±1.9>-12.2±2.1>-10.6±2.3>-7.7±2.3, $p<0.001$). In contrast, GCS was not different between

the Normal and HFpEF (Endo: -34.5±6.2 vs -33.9±5.7, p=0.51; Myo: -21.9±3.8 vs -21.3±2.2, p=0.39, Epi: -11.4±2.0 vs -10.9±2.3, p=0.54) but was, as well, markedly lower in the systolic heart failure groups: Normal>HFmrEF>HFrEF (Endo: -34.5±6.2>-20.0±4.2>12.3±4.2, p<0.001; Myo: -21.9±3.8>-13.0±3.4>-8.0±2.7. p<0.001; Epi:-11.4±2.0>-7.9±2.3>-4.5±1.9. p<0.001).

CMR feature tracking multilayer strain assessment identifies large range differences between distinct myocardial regions. Our data emphasizes the importance of sub-endocardial myocardium for cardiac contraction and corollary, its predilect role in imaging detection of functional impairment.

3.2 Background

As discussed in Chapter 1, a fundamental trait of cardiac remodelling is hypocontractility. While contractility per se cannot be directly quantified in vivo with imaging methods, proxy parameters evaluating deformation properties of the myocardium are likely more accurate in evaluating myocardial mechanics than volumetric approaches such as EF or EDV. [196] By analysing with great spatial accuracy myocardial deformation, CMR offers currently several tools to approximate cardiac contractility and hold the promise to detect early-on subtle abnormalities in the cardiac mechanics. [197] Using FT, we assess here myocardial strain and strain rate at the level of three distinct layers and compare these values in a cohort of patients with different types of HF.

Over the cardiac cycle, human heart undergoes a complex multiplane dynamics consisting of: descent on a longitudinal axis from base to apex of the mitral valve plane, concentric transversal plane contraction with a reduction of cavity horizontal diameter, and a wringing movement with clockwise twist towards the base and anticlockwise

towards the apex. To accomplish this complex spatial mechanics human myocardium contains multiple layers of myofibers with different calibre, orientation and contractile properties. [198,199]

One of the essential challenges of clinical cardiology is the detection as early as possible of mechanical deficit of the heart. Due to complex remodelling triggered to compensate incipient hypocontractility and maintain the output, using volumetric parameters such as EDV, or EF or even global deformation (strain) may be inefficient in recognising these early modifications.

Following the three spatial coordinates, myocardial strain can be classified as longitudinal, circumferential and radial for each individual volume unit and through vector summing, values corresponding to certain segments or globally for the whole LV myocardium can be calculated. Benefiting from an excellent spatial resolution of cine SSFP images (average resolution of 1.8×1.8 ×6.0 mm^3 for a standard 1.5T clinical system [200]) FT CMR has the ability to render at pixel level the deformation properties of myocardial tissue and in this way to differentiate between more superficial (epicardial) and more profound (endocardial) layers. [201]

Structural remodelling of the heart, in particular hypertrophic remodelling and microvascular dysfunction associated with hypertension, obesity, diabetes or coronary artery disease, conditions that all lead to heart failure, affect primordially the subendocardial myocardium first and quantitatively more. Moreover, in heart failure, at a molecular level, mechanisms directly responsible for force generation and muscular contraction such as adrenergic beta receptors distribution, downstream cAMP and phosphodiesterase activity, levels of expression of sarcoplasmic reticulum Ca^{2+} ATPase, become more reduced in the subendocardium. [202]

CMR FT technique has been presented in **Chapter 1** (description of the method) and **Chapter 2** (image acquisition and offline analysis) of the thesis. In this study we applied CMR FT to assess myocardial strain and strain rate at the level of three distinct myocardial layers, compared these values and demonstrated the potential advantages of this approach to assess patients with HF.

3.3 Specific Methods

The general lines of image acquisition and analysis protocols were described in **Chapter 2**.

Briefly, for this study, we included prospectively, patients with a diagnosis of HF who were subdivided according to recent ESC guidelines [19] into 3 groups, as follows: (1) patients with HF with preserved ejection fraction (HFpEF), where EF≥50% but diastolic dysfunction is present (an E/e′ ≥13 and a mean e' septal and lateral wall <9 cm/s) and plasma levels of NT-proBNP >125 pg/mL, (2) patients with HF with mid-range ejection fraction (HFmrEF), where EF=40-49% and similar additional criteria were present, (3) patients with HF with reduced ejection fraction (HFrEF) where EF<40%. The complete inclusion and exclusion criteria are presented in Chapter 2.

For this study, all CMR images were acquired using a 1.5 T (Achieva, Philips Healthcare, Best, The Netherlands) MRI scanner with a 5-channel cardiac surface coil in a supine position. The specific acquisition parameters for this system and image analysis principle for FT are described in **Chapter 2**. Specific for a multilayer approach, strain and SR were evaluated separately at 3 distinct levels of the myocardium: after segmenting the long-axis images (2Ch, 3Ch and 4Ch SSFP cines) and short-axis (three distinct basal, mid and apical SA SSFP cines, as described previously) identifying the endocardial and epicardial contour and propagating over the cardiac

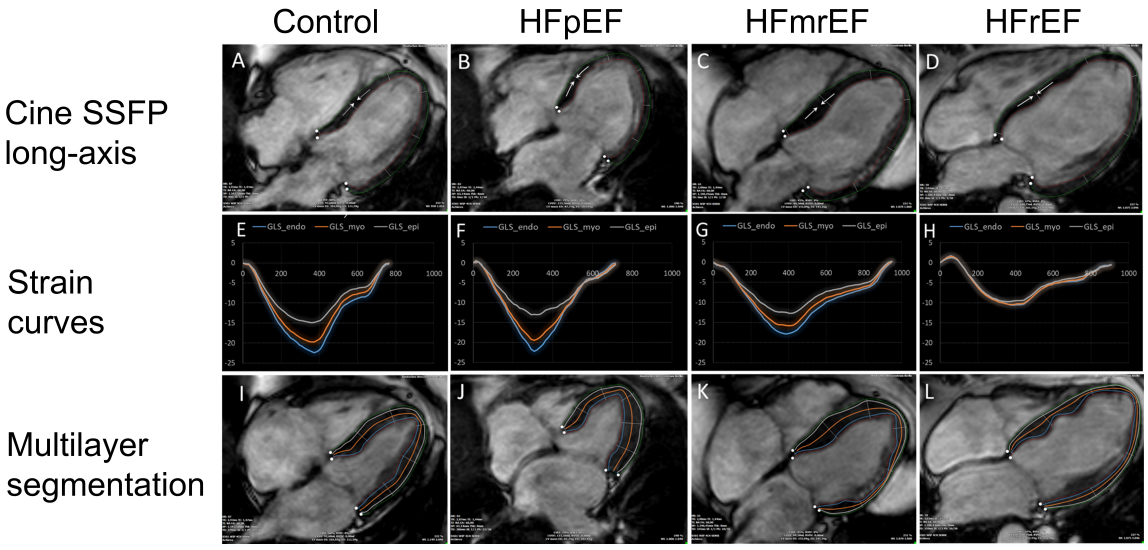


Figure 3.1 Multilayer global longitudinal strain in representative cases (from left to right: healthy controls, HFpEF, HFmrEF and HFrEF): **A,E,I** – Control **B,F,J** – HF with preserved EF, **C,G,K** – HF with mid-range reduced EF, **D,H,L** – HF with reduced EF. For each case on the vertical, from up to down, are shown, respectively : long-axis 4Ch SSFP cine in end-diastole, GLS curves at 3 distinct myocardial layers: Endo, Myo, Epi, long-axis 4Ch SSFP cine in end-systole segmented according to Endo, Myo, Epi myocardial layers.

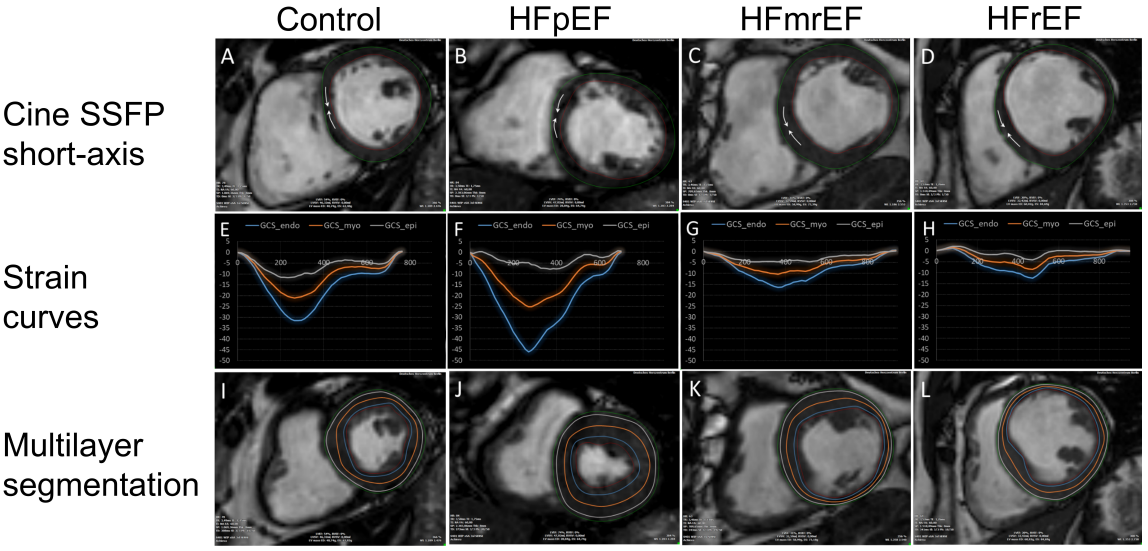


Figure 3.2 Multilayer global circumferential strain (GCS) in representative subjects (from left to right: healthy controls, HFpEF, HFmrEF and HFrEF): **A,E,I** – Control **B,F,J** – HF with preserved EF, **C,G,K** – HF with mid-range reduced EF, **D,H,L** – HF with reduced EF. For each case on the vertical, from up to down, are shown, respectively : short-axis basal SSFP cine in end-diastole, GLS curves at 3 distinct Endo, Myo, Epi myocardial layers, short-axis basal SSFP cine in end-systole segmented according to Endo, Myo, Epi myocardial layers.

cycle with QStrain RE suite, 3 lines of reference were determined and values for each layer returned by the software.(**Figures 3.1 and 3.2**) Global values were obtained through averaging separately these values following an AHA 17 segments model. [189]

3.4 Results

3.4.1 Study population characteristics

(A total number of 140 patients with a diagnosis of HF were screened for the inclusion criteria, as stated above, and a resultant number of 56 patients were finally recruited for the study, as follows: 20 were diagnosed with HFpEF, 19 with HFmrEF and 17 with HFrEF. Demographics, relevant laboratory tests, comorbidities, functional tests and an inventory of current cardiovascular relevant medication are presented in **Table 3.1**. Incidence of relevant comorbidities was certainly higher than in controls, but demonstrated a uniform distribution between the HF subgroups. Similarly, the functional tests showed significantly worse results in HF patients compared with Control but on average were equivalent between the HF subgroups.

CMR and echocardiography baseline parameters are presented in **Table 3.2**. There were no differences between the control group and HFpEF for LV ED or ES volumes, EF was borderline decreased in HFpEF but this did not reach statistical significance. As expected LV end-diastolic volume was progressively larger in patients with HFmrEF and HFrEF respectively. Patients with HFmrEF and HFrEF had a more dilated ventricle and left atrium. LV wall thickness was slightly larger in all 3 HF groups compared with normal measured at septum level but there was no difference in the free wall, LV mass was higher in HFmrEF and HFrEF groups but the difference was not significant between HFpEF and Normal. On echocardiography, E/A and E/e' were

Table 3.1 Study Population: Daemographics, Laboratory Values, Functional Tests, Comorbidities, Current Medication

	Pathology Group				
	Control N=19	HFpEF N=20	HFmrEF N=19	HFrEF N=17	P Value ANOVA
Daemographics					
Age, y	67±7	72±7	68±9	68±9	0.24
Male Subjects, N (%)	10 (53)	10 (50)	11 (61)	10 (59)	0.88
Heart rate (bpm)	60±9	62±9	65±9	67±9	0.71
BMI (kg/m²)	25±3	27±4	27±5	28±4	0.20
NYHA Class II, N (%)	0(0)	12(60)	16(84)	12 (71)	
Class III, N (%)	0(0)	8(40)	3(16)	5(29)	
Laboratory Values					
NT-proBNP (ng/l)	92±67	429±503	899±1161	2278±3761	***0.008***
logNT-proBNP (ng/l)	1.86±0.30	2.66±0.32	2.74±0.36	3.01±0.53	***<0.001***
Creatinin (mg/dl)	0.87±0.20	0.92±0.18	1.07±0.33	1.09±0.38	0.02
GFR (ml/min)	81±10	71±16	70±18	72±21	0.44
Troponin T (ng/l)	7±3	16±12	19±20	18±12	***<0.001***
CRP (mg/dl)	1.3±1.4	2.9±2.7	3.0±4.2	1.0±0.7	***<0.001***
Hemoglobin (g/dl)	14±1	13±1	14±1	15±1	0.51
Hematocrit	0.40±0.03	0.38±0.03	0.40±0.03	0.43±0.04	0.86
WBC (n/nl)	6.1±1.6	7.2±2.4	8.5±2.4	8.4±2.3	***<0.001***
Platelets (n/nl)	263±66	261±73	261.5±75	211±51	0.07
Cholesterol (mg/dl)	204±34	182±47	156±44	152±37	***<0.001***
LDL (mg/dL)	133±39	114±40	96±41	82±25	***<0.001***
HDL (mg/dL)	67±2	55±15	48±11	51±19	***0.019***
Triglycerides (mg/dL)	130±80	130±48	131±81	185±159	0.28
HbA1c (%)	5±1	6±1	6±1	6±1	0.16
Functional Tests					
6 min walking test	524±126	345±122	414±85	412±130	***<0.001***
Borg Score	7.5±1.7	12.4±2.4	10.6±2.3	11.0±2.6	***<0.001***
Minessota QoL Score	5.0±5.9	27.3±22.7	27.4±22.5	29.6±25.3	***0.002***
Comorbidities, risk factors					
CAD, N(%)	0 (0)	12 (60)	14 (74)	11 (65)	***<0.001***
Previous MI, N(%)	0 (0)	7 (35)	12 (63)	8 (47)	***<0.001***
Peripheric Artery Disease, N(%)	0 (0)	5 (25)	3 (16)	2 (12)	0.11
Hypertension, (N%)	6 (32)	12 (60)	15 (79)	12 (71)	0.12
Diabetes, (N%)	2 (11)	4 (20)	5 (26)	3 (18)	0.72
Hypercholesterolemia, N(%)	4 (21)	12 (60)	14 (74)	11 (65)	***0.031***
COPD, N(%)	0 (0)	1 (5)	3 (16)	1 (6)	0.34
Smokers, N(%)	6 (32)	7 (35)	8 (42)	6 (35)	0.94
Medication					
ACE-inhibitors or ARBs	6 (32)	15 (75)	15 (79)	17 (100)	***<0.001***
Calcium Antagonists	4 (21)	3 (15)	3 (16)	1 (6)	0.64
MRA	0 (0)	2 (10)	4 (21)	11 (65)	***<0.001***
ARNi	0 (0)	0 (0)	0 (0)	3 (18)	***0.015***
Beta-blockers	6 (32)	10 (50)	15 (79)	17 (100)	***<0.001***
Statins	1 (5)	8 (40)	16 (84)	10 (59)	***<0.001***
Diuretics	4 (21)	7 (35)	9 (47)	7 (41)	0.31

Abbreviations: HFpEF – heart failure with preserved ejection fraction, HFmrEF – heart failure with mid-range ejection fraction, HFrEF – heart failure with reduced ejection fraction, NT-proBNP – N-terminal prohormone of brain natriuretic peptide, GFR – estimated glomerular filtration rate, CRP – C reactive protein, WBC – white blood cells, CAD – coronary artery disease, MI – myocardial infarction, COPD – chronic obstructive pulmonary disease, ACEi – Angiotensin converting enzyme inhibitors, ARB – Angiotensin receptor blocker, MRA - Mineralocorticoid receptor Antagonists, ARNi – Angiotensin Receptor-Neprilysin inhibitor.

not on average different from control in any of the HF subroups but the early diastolic tissue velocity (e'), particularly at septal level, was lower.

Table 3.2 CMR and Echocardiography Baseline Parameters

	Pathology Group				
	Control N=19	HFpEF N=20	HFmrEF N=19	HFrEF N=17	P Value ANOVA
CMR					
LVEDV (ml/m²)	64±11	66±21	94±15	116±31	***<0.001***
LVESV (ml/m²)	23±8	29±9	53±6	78±24	***<0.001***
LVSV (ml/m²)	41±11	38±13	42±6	38±27	0.91
LVEF (%)	64±6	60±7	44±4	31±6	***<0.001***
Cardiac Index (L/min/m²)	2.82±0.50	2.71±0.55	2.72±0.49	2.86±0.49	0.99
LV-EDD (mm)	49±4	51±4	57±5	65±7	***<0.001***
Septum (mm)	9±2	11±2	12±2	12±3	***<0.001***
Lateral Wall (mm)	7±1	8±1	7±2	8±2	0.35
LVM (g/m2)	42±15	47±8	61±18	71±15	***<0.001***
RVEDV (ml/m²)	75±18	69±16	72±15	84±19	0.07
RVESV (ml/m²)	32±9	30±9	35±12	36±12	0.29
RVSV (ml/m²)	43±10	40±9	38±10	48±11	***0.013***
RVEF (%)	58±5	57±6	53±11	58±10	0.14
Parametric Mapping					
T1 native (ms)	972±31	985±32	1021±46	1041±47	***<0.001***
ECV (%)	*27.0±4.0	27.3±2.6	29.0±2.6	29.5±3.4	0.08
T2 (ms)	50.6±2.1	52.6±3.6	55.0±3.6	56.4±5.9	***<0.001***
Echocardiography					
E velocity (cm/s)	0.65±0.17	0.73±0.14	0.76±0.28	0.75±0.25	0.63
A velocity (cm/s)	0.71±0.18	0.87±0.37	0.79±0.25	0.75±0.29	0.59
Deceleration Time (ms)	197±45	200±42	163±37	155±48	***0.018***
E/A	0.94±0.22	0.98±0.49	0.95±0.42	1.02±0.49	0.51
e' Septal (cm/s)	7.4±2.1	5.5±1.0	5.9±2.0	4.6±1.3	***0.002***
e' Lateral (cm/s)	9.8±2.7	6.8±1.7	8.3±2.4	6.7±2.4	***0.008***
E/e´	10.1±3.7	12.0±4.3	10.8±1.9	14.2±5.9	0.07

Abbreviations: HFpEF – heart failure with preserved ejection fraction, HFmrEF – heart failure with mid-range ejection fraction, HFrEF – heart failure with reduced ejection fraction, LV – left ventricle (left ventricular), EDV – end-diastolic volume, ESV – end-systolic volume, SV – stroke volume, EF – ejection fraction , EDD end-diastolic diameter, LVM – left ventricular mass, Endo- subendocardial layer, Myo- mid-myocardial layer, GLS – global longitudinal strain, GCS – global circumferential strain, ECV – extracellular volume, E – early diastolic mitral transmitral inflow velocity, A – late diastolic transmitral inflow velocity, e‘ – paramitral segments tissue velocity.

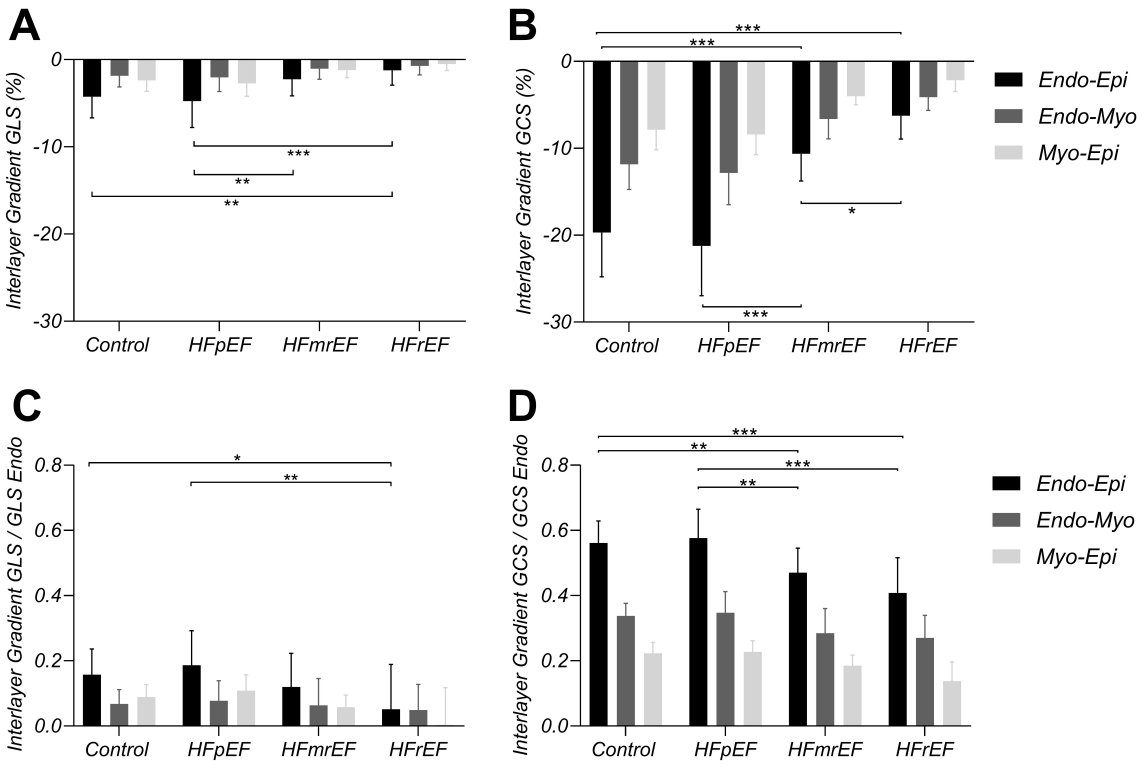


Figure 3.3 Representation of differences (Δ) between strain values measured at different myocardial layers (absolute values and relative values indexed with GLS Endo and GCS Endo) **A.** Intralayer gradient GLS and **B.** Intralayer gradient GCS **C.** Intralayer gradient GLS / GLS Endo Ratio, **D.** Intralayer gradient GCS / GCS Endo Ratio, between Endo-Epi, Endo-Myo and Myo-Epi respectively in the 4 groups: Control, HFpEF, HFmrEF, HFrEF, The gradient is larger for ΔGCS than for ΔGLS and decreases in both ΔGLS and ΔGCS progressively in HFmrEF and HFrEF from Control levels, while in HFpEF both ΔGLS and ΔGCS gradients are preserved. There is no difference in GLS or GCS gradients between Control and HFpEF. Differences are maintained when Interlayer Gradient Values were indexed with GLS Endo and respectively with GCS Endo.

3.4.2 Longitudinal and Circumferential Strain. Comparison between Endo, Myo, Epi layers

We initially looked for intrasubject paired comparisons between Endo, Myo and Epi layers of the myocardium. In all 4 groups, GLS is more pronounced in the Endo layer compared with Myo and Epi, a difference that remains significant even if tends to diminish in HFmrEF and is the lowest in HFrEF (**Table 3.3**). Comparatively the Endo-Epi interlayer gradient (ΔGLS) was borderline higher in Control compared to HFmrEF

(ΔGLS =-4.3±2.4% vs -2.3±1.9%, p=0.05) and significantly higher compared with HFrEF ((ΔGLS=-4.3±2.4% vs -1.2±1.7%, p=0.001) but was not different between Normal and HFpEF (ΔGLS=-4.3±2.4 vs -4.8±3.0, p=0.90) or between HFmrEF and HFrEF (ΔGLS =-2.3±1.9% vs -1.2±1.7%, p=0.56) (**Figure 3.3 A** and **B**). To investigate the relative changes in contractile reserve we compared in a similar fashion these gradient values, indexed with the respective value of subendocardial strain values (**Figure 3.3 C** and **D**). For GLS, there were significant differences in relative values between Interlayer Gradient GLS Endo-Epi / GLS Endo between Control and HFrEF (0.16±0.08 vs 0.05±0.014, P=0.022) and between HFpEF and HFrEF (0.19±0.11 vs 0.05±0.014, P=0.002) but not between any other groups. For GCS, there were differences in relative values between Interlayer Gradient GCS Endo-Epi / GCS Endo between Control and both HFmrEF (0.56±0.07 vs 0.47±0.08, P=0.009) and HFrEF (0.56±0.07 vs 0.41±0.11, P<0.001) and between HFpEF and both HFmrEF (0.58±0.09 vs 0.47±0.08, P=0.001) and HFrEF (0.58±0.09 vs 0.41±0.11, P<0.001) but not between HFmrEF and HFrEF.

For the GCS there is a more pronounced significant gradient Endo-Myo-Epi in all the 4 groups with largest differences seen in subjects with preserved EF (Control and HFpEF). The Endo-Epi interlayer gradient is overtly higher in Control than HFmrEF and progressively than in HFrEF (ΔGCS =-19.7±5.1% vs -10.6±3.1% vs -6.3±2.7%, p<0.001) but not different from HFpEF (ΔGCS =-19.7±5.1% vs -21.2±5.7%, p=0.81). Of note, with this software platform, we could not assess multilayer values for radial strain and radial SR.

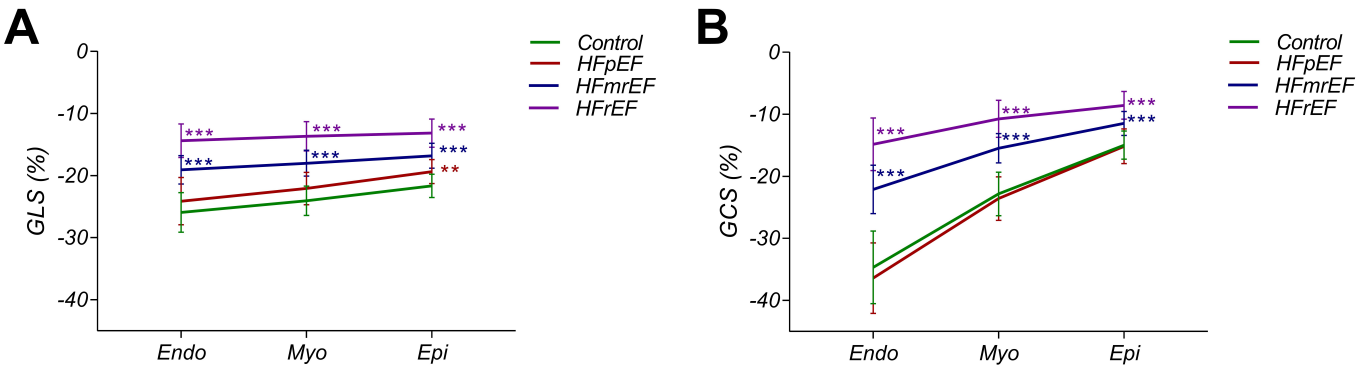


Figure 3.4 Multilayer assessment (Endo, Myo, Epi layers of left ventricular myocardium) of: **A.** global longitudinal strain (GLS), and **B.** global circumferential strain in 4 groups: Normal, HFpEF, HFmrEF, HFrEF. There is a marked difference between Control and HFmrEF and HFrEF at all levels: Endo, Myo and Epi. GLS is reduced only in the Epi layer and GCS is similar between HFpEF and Control in all three layers.

Table 3.3 Mulitlayer Left Ventricular Global Strain and Strain Rate (SR)

	Pathology Group					P Value					
	Control N=19	HFpEF N=20	HFmrEF N=19	HFrEF N=17	ANOVA	Control vs HFpEF	Control vs HFmrEF	Control vs HFrEF	HFpEF vs HFmrEF	HFpEF vs HFrEF	HFmrEF vs HFrEF
Longitudinal Strain and SR											
Endo GLS (%)	-25.9±3.2	-24.1±3.8	-19.1±2.3	-14.4±2.7	***<0.001***	0.26	***<0.001***	***<0.001***	***<0.001***	***<0.001***	***<0.001***
Myo GLS (%)	-24.1±2.4	-22.1±2.6	-18.0±2.2	-13.3±2.6	***<0.001***	0.05	***<0.001***	***<0.001***	***<0.001***	***<0.001***	***<0.001***
Epi GLS (%)	-21.7±1.9	-19.4±1.9	-16.8±2.0	-13.2±2.3	***<0.001***	***0.003***	***<0.001***	***<0.001***	***<0.001***	***<0.001***	***<0.001***
GLS Gradient Endo-Epi (%)	-4.3±2.4	-4.8±3.0	-2.3±1.9	-1.2±1.7	***<0.001***	0.90	0.05	***0.001***	***0.007***	***<0.001***	0.56
Endo GLSR (%/s)	-1.66±0.28	-1.69±0.42	-1.34±0.24	-1.13±0.26	***<0.001***	0.99	***0.012***	***<0.001***	***0.005***	***<0.001***	0.21
Myo GLSR (%/s)	-1.54±0.20	-1.52±0.33	-1.26±0.23	-1.06±0.23	***<0.001***	0.99	***0.008***	***<0.001***	***0.012***	***<0.001***	0.10
Epi GLSR (%/s)	-1.55±0.22	-1.54±0.37	-1.32±0.26	-1.09±0.23	***<0.001***	0.99	0.07	***<0.001***	0.09	***<0.001***	0.07
GLSR Gradient Endo-Epi (%/s)	-0.11±0.18	-0.15±0.21	-0.01±0.13	-0.04±0.13	0.07	0.89	0.32	0.67	0.07	0.26	0.95
Circumferential Strain and SR											
Endo GCS (%)	-34.7±5.8	-36.4±5.7	-22.1±3.9	-14.8±4.2	***<0.001***	0.70	***<0.001***	***<0.001***	***<0.001***	***<0.001***	***<0.001***
Myo GCS (%)	-22.8±3.5	-23.6±3.5	-15.5±2.3	-10.7±3.0	***<0.001***	0.88	***<0.001***	***<0.001***	***<0.001***	***<0.001***	***<0.001***
Epi GCS (%)	-15.0±2.3	-15.2±2.8	-11.5±1.9	-8.6±2.2	***<0.001***	0.99	***<0.001***	***<0.001***	***<0.001***	***<0.001***	***0.002***
GCS Gradient Endo-Epi (%)	-19.7±5.1	-21.2±5.7	-10.6±3.1	-6.3±2.7	***<0.001***	0.81	***<0.001***	***<0.001***	***<0.001***	***<0.001***	***<0.001***
Endo GCSR (%/s)	-2.13±0.43	-2.41±0.62	-1.49±0.28	-1.20±0.39	***<0.001***	0.22	***<0.001***	***<0.001***	***<0.001***	***<0.001***	0.22
Myo GCSR (%/s)	-1.38±0.23	-1.54±0.32	-1.09±0.18	-0.93±0.29	***<0.001***	0.24	***0.005***	***<0.001***	***<0.001***	***<0.001***	0.30
Epi GCSR (%/s)	-1.17±0.24	-1.32±0.33	-1.02±0.19	-0.93±0.27	***<0.001***	0.30	0.30	***0.039***	***0.004***	***<0.001***	0.73
GCSR Gradient Endo-Epi (%/s)	-0.95±0.37	-1.09±0.46	-0.47±0.22	-0.26±0.19	***<0.001***	0.59	***<0.001***	***<0.001***	***<0.001***	***<0.001***	0.26
Radial Strain and SR											
GRS (%)	95.0±28.4	100.6±28.5	50.9±16.8	36.0±17.5	***<0.001***	0.90	***<0.001***	***<0.001***	***<0.001***	***<0.001***	0.30
GRSR (%/s)	3.02±0.55	3.08±0.60	2.11±0.29	1.85±0.62	***<0.001***	0.98	***<0.001***	***<0.001***	***<0.001***	***<0.001***	0.44

Abbreviations: HFpEF – heart failure with preserved ejection fraction, HFmrEF – heart failure with mid-range ejection fraction, HFrEF – heart failure with reduced ejection fraction, GLS – global longitudinal strain, GCS – global circumferential strain, GLSR – global longitudinal strain rate, GCSR – global circumferential strain rate, GRS – global radial strain, GRSR – global radial strain rate, Endo, Myo, Epi – subendocardial, mid-myocadial, subepicardial myocardial layers.

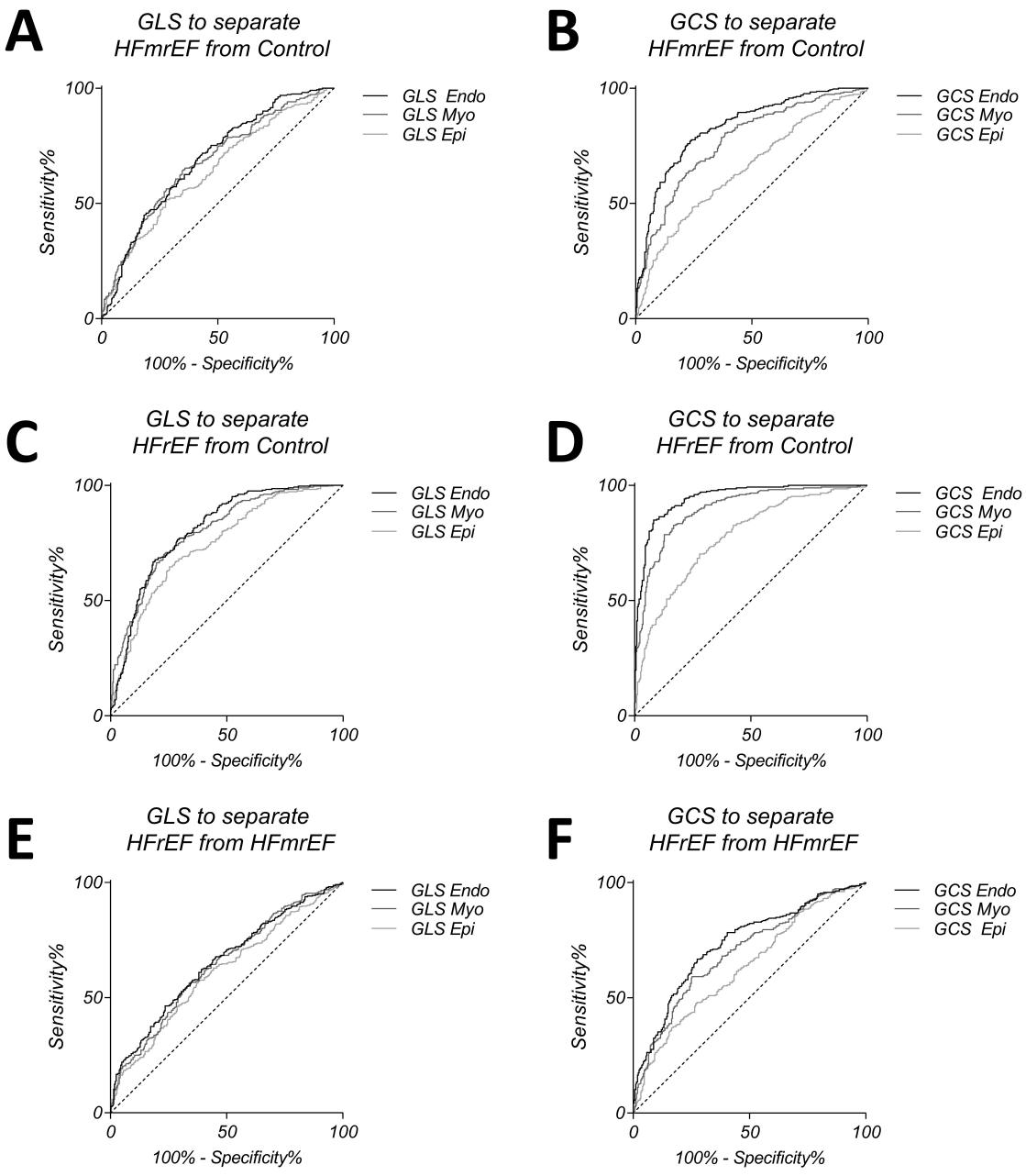


Figure 3.5 ROC analysis to compare discriminative ability of multilayer global longitudinal (GLS) and circumferential (GCS) strain between patients with HFmrEF, HFrEF and Control. On the left side: **A.** GLS to discriminate HFmrEF from Control, **B.** GCS to discriminate HFmrEF from Control, **C.** GLS to discriminate HFrEF from Control, **D.** GCS to discriminate HFrEF from Control, **E.** GLS to discriminate HFrEF from HFmrEF, **F.** GCS to discriminate HFrEF from HFmrEF. GCS Endo demonstrated the highest ability to separate between Control, HFmrEF and HFrEF and therefore represents the most sensitive parameter to stratify the risk in patients with HF when EF is lower than normal.

Table 3.4 Mulitlayer Strain – comparative ROC to discriminate contractile deficit in HFmrEF and HFrEF patients

	AUC	P Value	Threshold	Sensitivity, %	Specificity, %		P Value
			HFmrEF vs Control				
GLS Endo	0.69(0.65-0.73)	***<0.001***	-23.5	71.5	57		GLS Endo vs
GLS Myo	0.68(0.64-0.72)	***<0.001***	-19.7	64.4	65.3	GLS Myo	0.75
GLS Epi	0.64(0.60-0.68)	***<0.001***	-15.6	51.7	72.1	GLS Epi	0.10
						GCS Endo	***<0.001***
GCS Endo	0.83(0.80-0.86)	***<0.001***	-28.94	77.6	76		GCS Endo vs
GCS Myo	0.77(0.73-0.81)	***<0.001***	-21.02	80.6	61.5	GCS Myo	***0.015***
GCS Epi	0.65(0.61-0.70)	***<0.001***	-9.71	48.4	75.7	GCS Epi	***<0.001***
			HFrEF vs Control				
GLS Endo	0.81(0.78-0.84)	***<0.001***	-17.41	67.8	80.8		GLS Endo vs
GLS Myo	0.80(0.77-0.83)	***<0.001***	-16.97	70.9	76.5	GLS Myo	0.70
GLS Epi	0.75(0.71-0.78)	***<0.001***	-14.88	64.7	74.6	GLS Epi	***0.016***
						GCS Endo	***<0.001***
GCS Endo	0.94(0.93-0.96)	***<0.001***	-22.18	84.9	91.8		GCS Endo vs
GCS Myo	0.90(0.87-0.92)	***<0.001***	-16.06	82.7	83.2	GCS Myo	***0.006***
GCS Epi	0.77(0.74-0.81)	***<0.001***	-10.53	70.2	72.04	GCS Epi	***<0.001***
			HFrEF vs HFmrEF				
GLS Endo	0.65(0.61-0.69)	***<0.001***	-15.57	62.2	60.9		GLS Endo vs
GLS Myo	0.64(0.60-0.69)	***<0.001***	-15.68	56.4	66.1	GLS Myo	0.77
GLS Epi	0.61(0.57-0.65)	***<0.001***	-14.29	57	62.3	GLS Epi	0.19
						GCS Endo	***0.007***
GCS Endo	0.73(0.69-0.77)	***<0.001***	-18.44	66.8	72.4		GCS Endo vs
GCS Myo	0.70(0.65-0.74)	***<0.001***	-14.15	58.9	75.0	GCS Myo	0.22
GCS Epi	0.63(0.59-0.68)	***<0.001***	-11.18	47.4	73.2	GCS Epi	***0.001***

Abbreviations: ROC – receiver operating characteristic curve, AUC – area under curve, HFmrEF – heart failure with mid-range ejection fraction, HFrEF – heart failure with reduced ejection fraction, GLS – global longitudinal strain, GCS – global circumferential strain, Endo, Myo, Epi – subendocardial, mid-myocadial, subepicardial myocardial layers.

3.4.3 Longitudinal and Circumferential Strain. Comparison between pathology groups

We further compared the GLS values between the groups at each of the 3 multilayer levels between the 4 pathology groups (results are summarized in **Table 3.3**). Both GLS and GCS were able to discriminate progressively between Control, HFmrEF and HFrEF, also between HFmrEF and HFrEF groups (**Figure 3.4**). Radial strain was also much lower in HFmrEF and HFrEF than in Control and HFpEF but between Control and HFpEF and respectively between HFmrEF and HFrEF, the values were not different. In the same sense but with more fluctuant values (higher SD), SR values are decreased in HFmrEF and HFrEF but not between Control and HFpEF and respectively between HFmrEF and HFrEF. (**Table 3.3**).

3.4.4 ROC analyses. Comparative analysis of HF progression

As both GLS and GCS measured at any myocardial layer (Endo, Myo or Epi) were different on average, progressively between Control, HFmrEF and HFrEF we wanted to test the diagnostic ability of each of these parameters to discriminate between these 3 groups. As in some patients, in particular HFrEF, larger differences between viable and non-viable segments is presumed, we opted to include for this analysis, for each subject all segmental values of peak systolic strain following an AHA model, rather than the mean global values. Results are presented in **Table 3.4** and **Figure 3.5**. As observed previously when we compared the mean values (see **Table 3.3**), in all 3 layers, GLS and GCS are progressively impaired from Control to HFmrEF and further to HFrEF. Corollary, in the ROC analysis, Endo, Myo, Epi GLS and respectively GCS discriminated all between Control and HFmrEF and HFmrEF and HFrEF. Comparatively, however, GCS Endo proved the most sensitive parameter to discriminate between Control and HFmrEF (AUC = 0.83(0.80-0.86), $p<0.001$), between Control and HFrEF (AUC= 0.94(0.93-0.96), $p<0.001$) and between HFmrEF and HFrEF (AUC = 0.73(0.69-0.77), $p<0.001$). In all these 3 cases, GCS Endo proved a better discriminator than GLS Endo (0.83(0.80-0.86) vs 0.69(0.65-0.73) $p<0.001$, 0.94(0.93-0.96) vs 0.81(0.78-0.84), $p<0.001$ and 0.73(0.69-0.77) vs 0.65(0.61-0.69), $p=0.007$).

3.4.5 Scatterplot. Complementary diagnostic role of GCS and GLS in HF

For each ROC curve described above, we used Youden's index to determine the threshold where a maximum sum between sensitivity and specificity is achieved (results are shown in **Table 3.4**). Further, we applied the threshold values of GLS Endo and GCS Endo resulted from the segmental ROC analysis to divide our cohort (**Figure 3.6**) according to the 4 quadrants defined by these reference values: subjects with

normal GCS and GLS values, subjects with subnormal GCS but normal GLS, subjects with subnormal GLS but normal GCS, subjects with subnormal GCS and subnormal GLS.

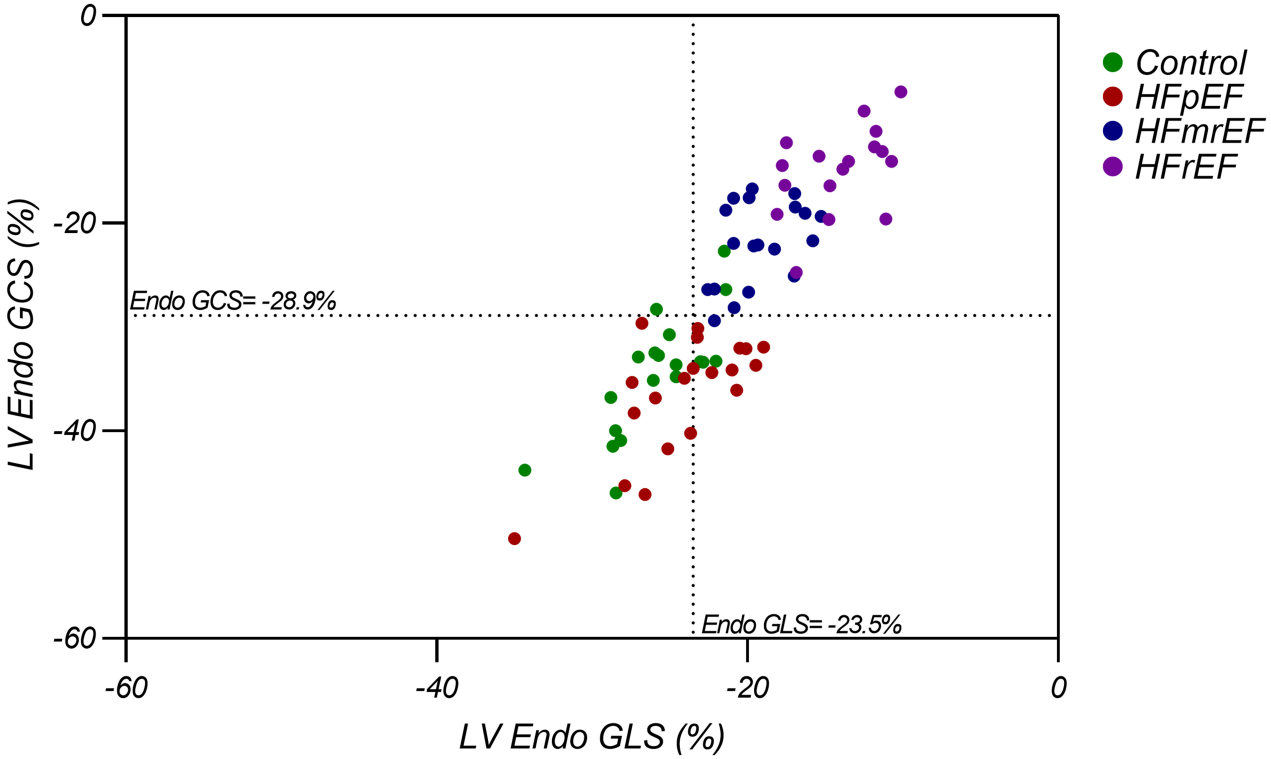


Figure 3.6 Scatterplot with GLS Endo and GCS Endo values in the 4 pathology groups: Control, HFpEF, HFmrEF, HFrEF. . Reference lines represent the threshold values obtained through ROC analysis and Youden´s index calculation. These GCS Endo (-28.9%) and GLS Endo (-23.5%) cut-off values offer an excellent sensitivity to detect systolic impairment and stratify HFmrEF and HFrEF patients. All the HFpEF patients have GCS Endo within normal range, and only some of them have a degree of GLS Endo impairment.

The graph gives an indication of the excellent sensitivity of both GCS and GLS values to diagnose patients with systolic impairment, practically all the patients with HFmrEF and HFrEF having their GLS Endo under the threshold value and only one of these had borderline normal GCS. According to these thresholds, 5(26%) of the Control subjects have subnormal GLS Endo, 3 (16%) have subnormal GLS Endo and 2 (11%) have both subnormal GLS Endo and GCS Endo. Interestingly, using the same reference thresholds, 10 (50%) of the HFpEF patients have a subnormal GLS Endo but all had normal GCS Endo. While GLS and GCS, proved their usefulness in

stratifying the patients with HFmrEF and HFrEF, they were not as efficient to identify patients with HFpEF (**Table 3.3**). However, while the GCS Endo, Myo, Epi were all not significantly different from Control, (GCS Endo: -36.4±5.7 vs -36.4±5.7, p=0.70; GCS Myo: -23.6±3.5 vs -22.8±3.5, p=0.88; GCS Epi: -15.2±2.8 vs -15.0±2.3, p=0.99), GLS Endo and GLS Myo showed a trend to be impaired in HFpEF, however they reached significance only for GLS Epi values (GLS Endo: -24.1±3.8 vs -25.9±3.2, p=0.26; GLS Myo: -22.1±2.6 vs -24.1±2.4, p=0.05; GLS Epi: -19.4±1.9 vs -21.7±1.9, p=0.003).

3.5 Discussion

Intrinsic assessment of contraction parameters rather than a volume-based estimation of cardiac performance remains an important desiderate of clinical cardiology as it would allow a necessary distinction between force generating myofiber contractility and loading pressures (pre and afterload). The novel concept of myocardial strain, based on assessing relative deformation of every infinitesimal myocardial segment, holds the promise to be a better approximator of myocardial contractile properties. Global values of longitudinal strain were previously shown to be a more reliable marker of mortality in patients with HF in comparison with EF[203] due to both an earlier recognition of regional or plane-specific mechanic deficit [204] and higher reproducibility. [205]

Several echocardiography studies assessed myocardial strain using a multilayer approach in normal subjects [206-209], coronary artery disease[210], aortic stenosis[211], hypertrophic cardiomyopathy[212,213] and underlined potential advantages of this method for clinical management. To date very few studies applied CMR tools to assess multilayer strain [214] and none of them assessed systematically patients with HF.

My findings can be summarized as follows:

- there is a marked heterogeneity of strain and strain values measured selectively at the level of Endo, Myo and Epi layers, with a significant gradient in deformation amplitude from endocardium (highest values) towards epicardium (lowest values). This gradient was preserved in Control and HFpEF but was blunted in HFmrEF and HFrEF.
- GLS and GCS Endo, Myo and Epi were impaired in HFmrEF and HFrEF compared to Controls.
- In a comparative ROC analysis, GCS Endo shows the best ability to progressively stratify HFmrEF and HFrEF from Control and respectively HFmrEF from HFrEF.
- GCS was not different between HFpEF and Control in any of the myocardial layers while GLS was on average impaired only in the Epi layer, which may represent a reliable diagnostic tool, while approximately only half of these patients have subnormal GLS Endo.

Firstly, I report an important difference of magnitude for both GLS and GCS values depending on the level at which these parameters were assessed. For both GLS and GCS there is a significant Endo-Epi gradient with the highest values found towards the endocardium and the lowest towards the epicardium. My findings supported the hypothesis that subendocardial fibres play a privileged role in maintaining a physiological contractile power with a greater quantitative contribution, compared with fibres with myocardial and epicardial distribution. Proportionally, the strain values measured at an endocardial level dropped more with the severity of heart failure and myocardial remodelling. These gradients were more pronounced for GCS than for GLS. Corollary, we showed that measuring GCS at an endocardial level offers the best parameter to discriminate patients with systolic impairment, even if milder, such as HFmrEF group, from a normal population. Data presented here confirms in part

previous results of Altiok et al. [214] who used a different acquisition method, strain-encoded magnetic resonance imaging (SENC) and assessed the strain values only at 2 layer-levels: subendocardial and subepicardial and extended them in assessing myocardial strain in the 3 distinct ESC subgroups described by recent guidelines.

The relative contribution of GCS and GLS to pump function of the human heart, in normal and pathologic conditions, is not very well established [215,216]. Histologically, circumferential fibres outnumber those with longitudinal and transversal orientation, especially at the base of the ventricle, with a ratio of 10:1 [217]. Recently, using a mathematical modelling of the LV, Stokke et al. [122] argued that GCS is accountable for generating two times more contractile force than GLS and with a steeper positive correlation with the EF. Our data indicate higher absolute values of circumferential than longitudinal strain and a more severe decrease of GCS in patients with systolic heart failure (HFmrEF and HFrEF), a decrease which is proportional to the baseline EF of the patients (i.e. in patients with lower EF, the Endo-Epi gradient is lower).

Based on a segmental approach we propose generic threshold values for both GCS and GLS able to identify patients with contractile impairment. We showed further excellent sensitivity of these combined values to identify patients with HF and moreover, to stratify the severity of disease.

While EF is a robust prognostic factor in a large number of patients with overt HF, with severely depressed cardiac contraction, its role per se in borderline subnormal and mid-range EF patients seems to be more controversial. [102] Recent ESC guidelines [19] identify HFmrEF as a potentially different pathologic entity from the more typical HFrEF group. HFmrEF class comprises patients with symptoms but not signs of HF, an intermediate degree of systolic dysfunction (EF between 40 and 50%) and with other traits of the disease present such as elevated natriuretic peptides, diastolic

dysfunction, enlarged left atrium. Initial echocardiography studies in HFmrEF showed mixed traits shared by both HFrEF and HFpEF such as the combination of LV dilatation with depressed contraction and respectively, increased stiffness and elevated diastolic filling pressures. Describing only discrete differences and similar patterns in strain values and interlayer gradients between HFmrEF and HFrEF, this study suggests that HFmrEF follows a similar pathophysiological pathway with HFrEF and likely represents a more incipient stage of HFrEF and not a distinct phenotype. However, these are just initial data, to confirm such a hypothesis, a tailored molecular and proteomic approaches is warranted.

Previous studies indicated that myocardial strain, particularly GLS, represents an important independent prognostic factor in the clinical evolution of patients with HF, bringing supplementary information from EF and LGE assessment, two major CMR derived parameters. [218-221] These intriguing findings could be explained by the fact that myocardial strain as a measure of tissue deformation is more sensitive than EF in detecting contractile dysfunction as it reflects more accurately the myocardial mechanical properties. Global strain (GLS, GCS or GRS) reflects an averaging of deformation amplitudes registered over the entire surface of LV and, is in this way less affected by geometric assumptions. In contrast, EF is calculated using CMR by applying Simpson's multiple disk volume approximation, taking into account subsequent endocardial contours in ED and ES. This method is also hampered by the presence of papillary muscles, trabeculations and areas of partial compaction of the ventricular wall, interplane sagittal movements and partial volume. Most importantly, the development of concentric LVH, with decreased ESV/ ED diameter ratio leads to higher EF values and systematic overestimation of contractile function. It is expected that in these patients GLS and GCS represent a more faithful classification than a

volumetric approach. In many patients with HF there is a significant LV dyssynchrony between different myocardial segments contributing further to global contractile insufficiency. An averaged graphic representation of strain for the entire cardiac cycle is more effective than EF, computed at 2 discrete time points (ED and ES) to take into account these rhythm abnormalities.

In a comparative analysis we propose further that GCS assessed selectively within a subendocardial myocardial layer (GCS Endo) is the most sensitive FT CMR parameter reaching the AUC to separate on one hand HFmrEF from Control and HFmrEF from HFrEF. In a scatter-plot representation we showed that estimating both GCS Endo and GLS Endo could provide a more nuanced approach to contractile dysfunction. While generally GLS and GCS values correlate with EF, there is a noticeable, albeit reduced, overlap between Control and HFmrEF patients with two Control subjects having both GLS Endo and GCS Endo under the cut-off values and two patients with HFrEF had both GLS and GCS Endo within the HFmrEF range rather than HFrEF There was also an important overlap between Control and HFpEF with a subgroup of 10 out 20 (50%) of HFpEF having reduced values of GLS Endo but normal GCS Endo. (**Figure 3.6**).

Approximately one half of the total number of patients diagnosed with HF have preserved EF where different mechanisms concur to cardiac dysfunction (certainly or mainly diastolic): endothelial dysfunction leading to microvascular disease of the myocardium, diffuse fibrosis resulting from elevated inflammatory pathways, chronically elevated renin-angiotensin-aldosterone response, systemic metabolic alterations, underlying renal failure. [11,222] Treating patients with HFpEF is difficult and targeting these specific causal mechanisms is warranted. Systolic contractility in patients with diastolic dysfunction is insufficiently explored and understood [223]. Importantly, in our study, GCS in the HFpEF group was not different from normal. In

agreement with previous echocardiography studies[224,225], we found that GLS is on average decreased in the HFpEF group compared with controls only at Epi level, however, due to a wider variation, its specificity to discriminate HFpEF patients from controls is low. We were particularly scrupulous with the inclusion of HFpEF patients: all were symptomatic and had elevated LV filling pressures (impaired E/e' ratio), however the underlying etiology was putatively diverse. Our findings support the idea that an underlying systolic impairment in patients with primarily diastolic heart failure is inconstant and, where present, tends to affect only the long-axis systolic contraction.

The discrepancy in magnitude of strain values between endocardium and epicardium warrants a very careful approach to the resulting data. Despite representing a powerful tool to assess regional and global cardiac function, the advent of strain imaging in day-by-day usage has been restricted so far by a modest concordance between methodologies to measure, compute and report these values.

Contractility is consistently impaired in patients with HFmrEF paralleling the degree of ventricular dilatation suggesting that drugs targeting the ventricular remodelling such as angiotensin converting enzyme inhibitors, Spironolactone or β-blockers maintain their beneficial effects, seen in HFrEF group, in this group of patients still insufficiently characterized. [212]

CMR has a great ability to integrate a detailed analysis of myocardial mechanics to methods that provide information about structural modifications of the heart such as fibrosis, inflammatory oedema, infiltrative disorders, perfusion abnormalities and spatial remodelling of myocardium (such as indexes of sphericity, fibre architecture and tractography framework).[226,227]

3.6 Limitations

We acknowledge several limitations of this study: (1) even if representative for a specific disease class, the groups of patients were small and more comprehensive studies are warranted to validate our findings in a widespread HF population, (2) in most of our patients the etiology of heart failure is related to coronary artery disease and previous acute coronary events, an extrapolation of our findings to a more complex group of HF patients, especially those affected by an intrinsic cardiomyopathy, is warranted, (3) larger populations are required to assess the prognostic importance of multilayer strain and establish their independent contribution for risk stratification.

From the all the subjects and patients included in the study, 0 (0%) in the Control Group, 7 (35%) in HFpEF, 12 (63%) in HFmrEF and 8 (47%) in HFrEF group had previous MI. The quantification of peak systolic strain took into account an average curve of strain deformation obtained from the computation of all 17 AHA segments strain curves. From these calculations we did not exclude hypokinetic, akinetic or dyskinetic segments from our analysis as we believed this represents an accurate approximation of global deformation of the myocardium in systole. The estimation of global values GLS and GCS Endo, Myo or Epi were not affected by the presence of wall motion abnormalities or LGE. As some of these previous MI were not transmural, but had a predominantly subendocardial pattern may have contributed to a higher differential of GCS Endo and GLS Endo between Control, HFmrEF and HFrEF respectively.

3.7 Conclusions

CMR FT multilayer evaluation of cardiac contraction is a convenient and fast procedure that can be easily derived from routinely acquired CMR cine SSFP images. Systolic

amplitudes vary significantly within the myocardium and therefore measurement of strain and strain rate must be performed cautiously and standards of practice regarding image analysis are required in order to unify and make more relevant large amounts of multicentric data. Sub-endocardial regions and respectively circumferential strain offer the best discriminative tool for early identification of patients with HFmrEF and HFrEF, however in HFpEF circumferential strain is unchanged and longitudinal strain is subnormal in only approximately half of these patients. HFpEF diagnostic imaging remains challenging and novel CMR parameters are required to account for cardiac remodelling in these patients.

Chapter Four:

Left Atrial Volumetric and Functional Remodelling in Heart Failure

4.1 Abstract

Atrial volume and function are important markers of mortality in heart failure patients. With an increased spatial resolution and versatility CMR feature tracking has the potential to precisely quantify atrial remodeling and function deficit. We applied here CMR FT to characterize atrial parameters in HF patients.

56 patients with HF divided as follows: 20 with preserved ejection fraction (HFpEF), 18 with mid-reduced EF (HFmrEF) and 17 with reduced EF (HFrEF). Atrial phasic (corresponding to reservoir, conduit and pump functions) volumes and emptying fractions were derived from 4Ch and 2Ch CMR SSFP cine images individually and then averaged using the biplane-area-length method. From the same SSFP cine images, atrial phasic strains were computed offline using a feature-tracking algorithm. Atrial maximal, total, passive or active volumes were not on average different between HF and control, only modest differences were observed in the HFrEF subgroup. In contrast, atrial expansion index, and total and passive emptying fractions were significantly impaired in HF patients but there was no significant difference between the 3 subgroups. LA active emptying fraction was impaired in HFpEF and HFrEF but not in HFmrEF. LA reservoir and conduit strain, but not pump strain, were impaired in HF. Atrial failure (defined as LA total emptying fraction <46% for males and <47% for females) was present in 20(36%) of 56 HF patients. Patients with HF and atrial failure had worse atrial emptying fractions and strain values than control and patients with HF without atrial failure.

CMR FT is a useful and highly accessible tool for a more detailed assessment of atrial function. Atrial failure is a potentially important risk factor in HF population and further prognostic studies are warranted to establish its role in clinical practice

4.2 Background

Left atrial volume [228] and function are important independent predictors of morbidity and mortality in the heart failure (HF) population. Molecular mechanisms responsible for ventricular remodeling in HF, produce similar effects on the atrial myocardium. [229] Most of these mechanisms are progressive in nature and lead to functional decompensation with myocyte hypocontractility and interstitial collagen deposition and, in more advanced stages, to aberrant conduction of electrical impulses and arrythmic events in both atria and ventricles. [81]

The atrium myocardium is structurally more sensitive to profibrotic remodeling[83] and pressure-overload dilatation[230], two central mechanisms leading to atrial fibrillation (AF). [231] Atrial active contribution to global cardiac output can be higher in HF patients, particularly in those cases where diastolic dysfunction is predominant and factors such as LV deficient lusitropy, increased stiffness and concentric hypertrophy reduce the ventricular suction pressure. Therefore, in many HF patients, once AF sets in and atrial active contraction is lost, this results, acutely, in rapid decompensation and overall constitutes an unfavorable factor of prognosis. [232] It is therefore a desiderate to be able to assess with non-invasive methods atrial remodeling in patients with HF and discriminate between ventricular and atrial impairment, in order to stratify the risk and manage the therapy in this group of patients.

Differences in incidence and clinical impact of atrial function on the clinical course and mortality in different subtypes of HF[97,233,234] raises the hypothesis that LA may be differently affected between these three subgroups warranting a comparative analysis of atrial remodeling in various entities of HF. We apply here CMR feature tracking (FT), a versatile offline image analysis algorithm, to quantify atrial phasic strain in distinct subgroups of patients diagnosed with HF and compare these results with a more basic

volumetric evaluation of atrial function and with other well-established markers of HF progression. We then investigated which of the imaging or molecular markers of cardiac remodeling are related to distinct components of atrial strain and could be involved in atrial failure.

4.3 Specific Methods

4.3.1 Study population

This study included all the HF patients and Controls included in the study presented in Chapter 3. Due to poor quality of atrial images, one patient with HF (HFmrEF subgroup) has not been considered for this substudy.

4.3.2 CMR and Echocardiography

The general lines of image acquisition and analysis protocols were described in Chapter 2.

4.3.3 Image analysis

All image analysis was performed using Medis Suite version 3.1 (Medis Medical Imaging Systems bv Leiden, The Netherlands). LA maximal and minimal volumes were first established visually in long-axis SSFP cine 4Ch and 2Ch views, respectively and drawn manually in QMass version 8.1 (**Figure 4.1 A**). All the values were averaged between those obtained in 4Ch and 2Ch images, respectively. Atrial volumetric and strain curves were recomposed and all atrial parameters derived, as follows: LA Max, maximal LA volume; LA Min, minimal LA volume; LApreA, volume at atrial diastasis) (**Figure 4.1 B**), LA emptying fraction (LAMax−LAMin)/LAmax, passive LA emptying fraction (LAMax− LApreA)/LAMax, active LA emptying fraction (LApreA−LAmin)/LAMax. Subsequently, these contours were further exported to a FT platform, QStrain RE version 2.0 and automatically propagated over the entire cardiac cycle. In a similar fashion, LA phasic strain was derived using LA Strain Max, Min and

LApreA strain at atrial diastasis (**Figure 4.1 C**). Similarly, the values were averaged between those obtained in 4Ch and 2Ch images, respectively.

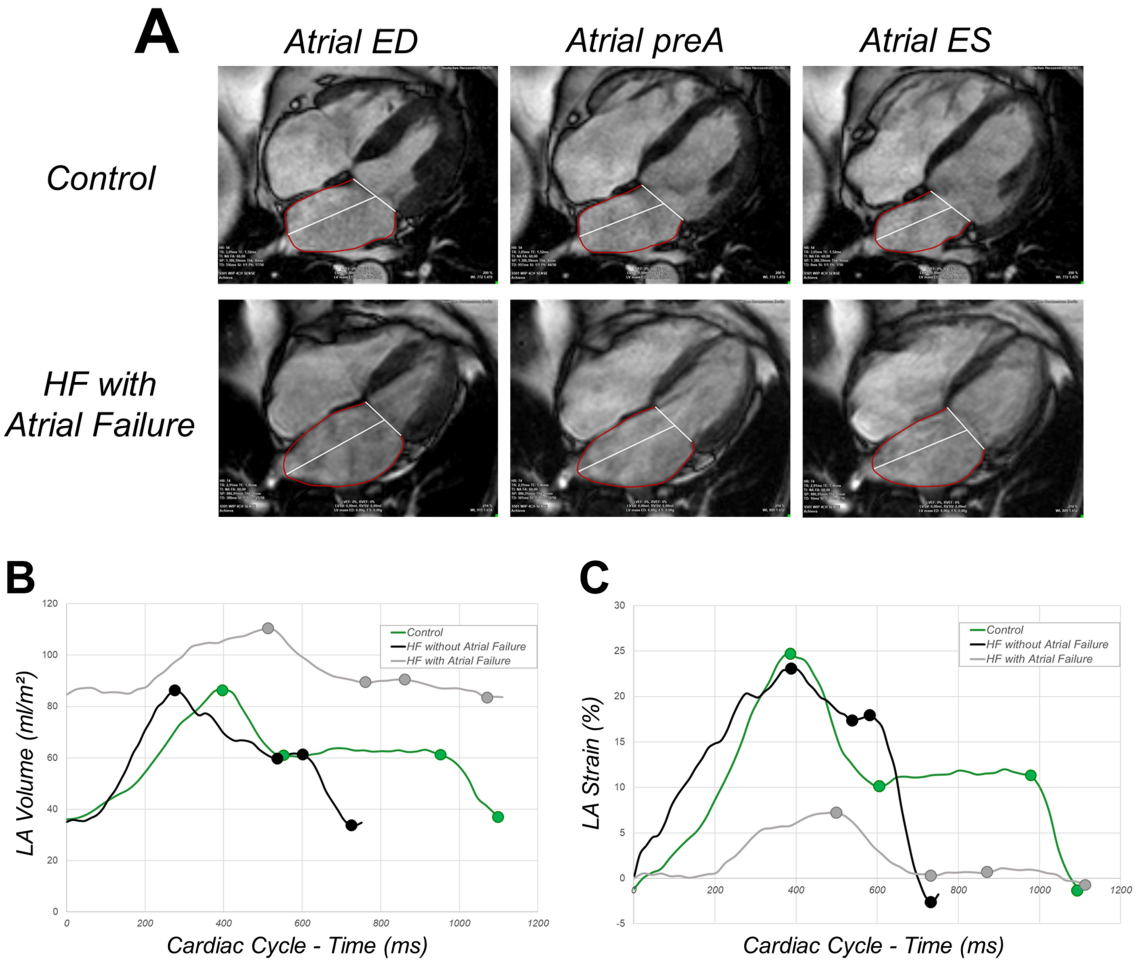


Figure 4.1 Illustrative Examples of Atrial Strain Quantification with CMR FT. **A.** Upper row – Control, Lower row – a HF with Atrial Failure patient. In both examples, LA end-diastolic (left), LA preA (center) and LA end-systolic (right) phases are represented. CMR FT follows the contour of atrial myocardium over the entire cardiac cycle generating the volumetric and strain curves for which phasic volumes and strains can be derived as shown below **B.** Volumetric curves in Control (green), HF without Atrial Failure (black), and HF with Atrial Failure (grey), **C.** Similarly, phasic strain reconstruction in Control (green), HF without Atrial Failure (black), and HF with Atrial Failure (grey). Each colored dot corresponds to the reference points for phasic volumetric (B.) and strain (C.) assessment. In this example is to be observed the significant atrial dilatation and impaired atrial function in a typical case of HF with Atrial Failure.

4.3.4 Definition of Atrial Failure

We used the most recent comprehensive JCMR meta-analysis that pooled several studies using a very similar method for the assessment of atrial volumes[188] as a reference for and defined accordingly the LAEF range of normality and respectively that corresponding to atrial failure. Four studies were included [235-238] comprising a total number of 534 males and 578 females and the average values and standard deviations were pooled and weighted accordingly. [188] Applying Neyman and Pearson 95% confidence interval assumption[239] we obtained values of LAEF <46% for males and <47% for females to be under the normal range and therefore to represent atrial failure (AFail).

4.3.5 Statistical Analysis.

Data were analysed using dedicated software packages IBM SPSS v27 (SPSS Inc, IL) and Medcalc v19 (MedCalc Software, Mariakerke, Belgium). All variables were tested for normality of distribution with Kolmogorov-Smirnov test. The equality of variances between subgroups was tested with Brown-Forsythe test. ANOVA one-way or non-parametric equivalent test were used to compare continuous variables between three or more groups and a Tukey post-hoc test with Bonferroni correction to compare further the mean between each two of these groups. Bivariate linear regressions were used to test the association between two variables. Multiple logistic regression models were built to determine factors involved in LV and cardiac remodeling and progression of HF that are associated with AFail as a categorical variable and multiple linear regressions were built to determine the association between these factors and LA EF and phasic atrial strain as continuous variables. All the independent variables were previously tested for collinearity, a variance inflation factor lower than 2 being considered satisfactory. A stepwise backward elimination of variables, with $p \leq 0.10$ criterium to enter and remain in the model, was applied to both logistic and linear regression

models. ROC analysis followed by determination of specific area under curve (AUC) and Youden's index calculation was used to determine the optimal cut-off value, sensitivity and specificity. Results are presented as mean ± SD. Values of $p<0.05$ were considered statistically significant.

4.4 Results

4.4.1 Study population

A summary of the subgroups that resulted after application of inclusion criteria and descriptive statistics of the parameters per each subgroup are shown in **Table 4.1**. There was no difference in age and gender distribution between subgroups however, as expected, there was a trend for the patients in the HFpEF to be older that the other 3 subgroups. NT-proBNP, Troponin and CRP were higher in HF population compared with controls. In the comorbidities comparison, while none of the controls had coronary artery disease this was commonly found in the HF group. Some risk factors were present in the Control group: 6 of 19 subjects were hypertensive, 2 had diabetes, 4 hypercholesterolemia and 6 were smokers.

CMR and some basic echocardiography parameters are presented in **Table 4.2**. HFmrEF and HFrEF patients presented a more significant ventricular remodeling with increased ventricular volumes, LVM, reduced ventricular systolic deformation, increased T1 and T2 times. HFpEF patients included in our study showed a reduced degree of ventricular remodeling and systolic deficit was insignificant when compared with control. T1 and T2 times were also within the normal range. The echocardiographic parameters that approximate ventricular relaxation and ventricular filling pressures (e' septal and lateral velocities, E/e' ratio) were on average not significant from control.

Table 4.1 Study Population: baseline characteristics

	Pathology Group				
	Control N=19	HFpEF N=20	HFmrEF N=18	HFrEF N=17	P Value
Daemographics					
Age, y	67±7	72±7	68±9	68±9	0.24
Male Subjects, N	10 (53%)	10 (50%)	11 (61%)	10 (59%)	0.88
Heart rate (bpm)	60±9	62±9	65±9	67±9	0.71
Laboratory Values					
NT-proBNP (ng/l)	92±67	429±503	899±1161	2278±3761	***0.008***
Log NT-proBNP (ng/l)	1.85±0.32	2.62±0.35	2.74±0.36	3.01±0.53	***<0.001***
Hemoglobin (g/dl)	13.9±1.1	12.8±1.2	13.6±1.1	15.0±1.1	0.51
Hematocrit	0.40±0.03	0.38±0.03	0.40±0.03	0.43±0.04	0.86
Creatinin (mg/dl)	0.87±0.20	0.92±0.18	1.07±0.33	1.09±0.38	0.02
GFR (ml/min)	81±10	71±16	70±18	72±21	0.44
Troponin T (ng/l)	7±3	16±12	19±20	18±12	***<0.001***
CRP (mg/dl)	1.3±1.4	2.9±2.7	3.0±4.2	1.0±0.7	***<0.001***
WBC (n/nl)	6.1±1.6	7.2±2.4	8.5±2.4	8.4±2.3	***<0.001***
Functional Tests					
6 min walking test	524±126	345±122	414±85	412±130	***<0.001***
Borg Score	7.5±1.7	12.4±2.4	10.6±2.3	11.0±2.6	***<0.001***
Minessota QoL	5.0±5.9	27.3±22.7	27.4±22.5	29.6±25.3	***0.002***
Comorbidities, risk factors					
CAD	0	12	14	11	***<0.001***
Peripheric Artery Disease	0	5	3	2	0.11
Hypertension	6	12	15	12	0.12
Diabetes	2	4	5	3	0.72
Hypercholesterolemia	4	12	14	11	***0.031***
COPD	0	1	3	1	0.34
Smokers	6	7	8	6	0.94
Medication					
ACE-inhibitors or ARBs	6	15	15	17	***<0.001***
Calcium Antagonists	4	3	3	1	0.64
Mineralocorticoid Receptor Antagonists	0	2	4	11	***<0.001***
Angiontensin Receptor Neprilysin Inhibitor	0	0	0	3	***0.015***
Beta-blockers	6	10	15	17	***<0.001***
Statins	1	8	16	10	***<0.001***
Diuretics	4	7	9	7	0.31

Abbreviations: HFpEF – heart failure with preserved ejection fraction, HFmrEF – heart failure with mid-range ejection fraction, HFrEF – heart failure with reduced ejection fraction, NT-proBNP – N-terminal prohormone of brain natriuretic peptide, GFR – estimated glomerular filtration rate, CRP – C reactive protein, WBC – white blood cells, CAD – coronary artery disease, COPD – chronic obstructive pulmonary disease, ACE – Angiotensin-converting enzyme. ARB – Angiotensin-receptor blocker. ANOVA-one way test was performed to test the difference between subgroups average for contnuous variables and Chi-squared or Fisher'S Exact Test to test the difference between subgroups for categorical variables. A P value <0.05 was considered statistically significant.

4.4.2 Comparison of atrial volumes emptying fractions and phasic strains between different groups of HF

We wanted first to compare the phasic atrial volumes between the different groups of patients with HF and controls, respectively. All these results are presented in **Table 4.3**. LA maximal volume was larger in HFrEF compared with Control (53.9±18.8 vs 39.5±7.7 ml/m^2, p<0.020), but not different on average in HFpEF and HFmrEF patients.

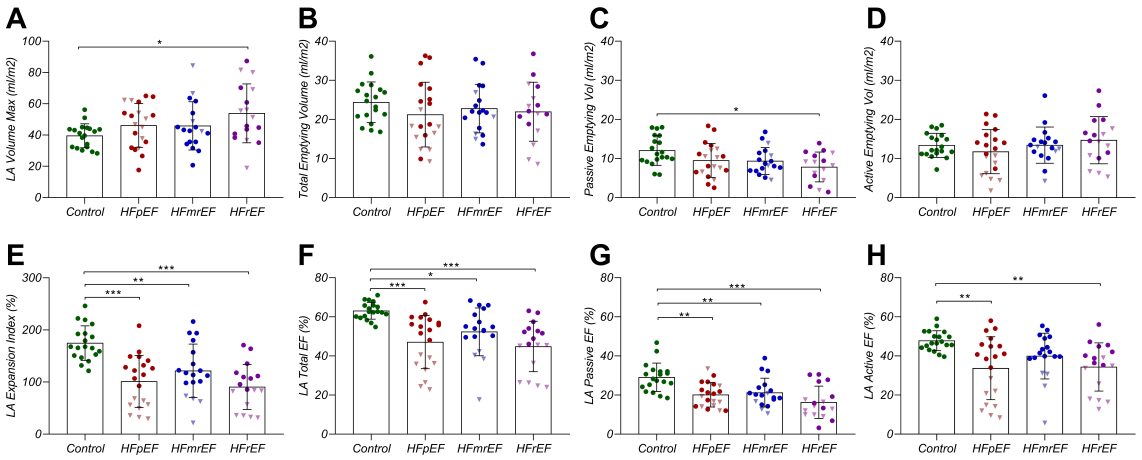


Figure 4.2 Left atrial maximal volume (**A.**) and phasic emptying volumes (**B.** total, **C.** passive, **D.** active), left atrial expansion index (**E.**) and phasic emptying fractions (**F.** total, **G.** passive, **H.** active) and in the four subgroups: Control (green), HFpEF (red), HFmrEF (blue), HFrEF (purple). For each subgroup, triangular shapes indicate patients with atrial failure, round circles patients without atrial failure.

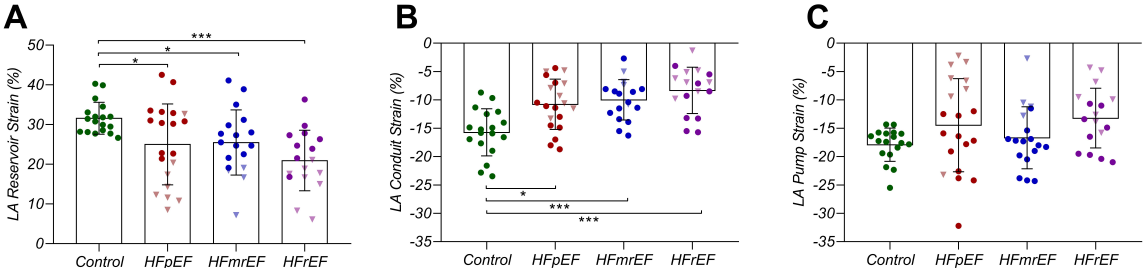


Figure 4.3 Left atrial phasic strain (**A.** reservoir, **B.** conduit, **C.** pump) in the four subgroups: Control (green), HFpEF (red), HFmrEF (blue), HFrEF (purple). For each subgroup, triangular shapes indicate patients with atrial failure, round circles patients without atrial failure.

Importantly, none of these parameters was different on average between the 3 subgroups of patients with HF (**Figure 4.2 A**, **B**, **C**, **D, E**). LAEF and LA passive EF were lower in all HF subgroups when compared with control (LAEF: 47±14, 52±12, 45±13 vs 63±4 %, p<0.001, LA passive EF: 20±6, 21±7, 16±8 vs 29±7 %, p<0.001, **Figure 4.2 F, G, H**) but there was no significant difference between the HF subgroups. Comparison of atrial strains between different groups of HF are also presented in **Table 4.3**. Similarly, as with the corresponding emptying fractions, LA Reservoir and Conduit

Table 4.2 CMR and Echocardiography: Left Ventricular Parameters.

	Pathology Group				
	Control N=19	HFpEF N=20	HFmrEF N=18	HFrEF N=17	p-Value ANOVA
CMR					
LVEDV (ml/m²)	64±11	62±14	90±15	116±31	***<0.001***
LVESV (ml/m²)	23±8	25±7	50±8	78±24	***<0.001***
LVSV (ml/m²)	41±11	37±10	40±12	38±27	0.91
LVEF (%)	64±6	60±7	44±4	31±6	***<0.001***
LV-EDD (mm)	49±4	51±4	57±5	65±7	***<0.001***
Septum (mm)	9.1±1.5	11.1±2.2	11.8±1.5	11.9±2.9	***<0.001***
Lateral Wall (mm)	7.2±1.0	7.5±1.4	7.1±1.6	8.2±2.2	0.35
LVM (g/m²)	42±15	47±8	62±18	71±15	***<0.001***
Endo- GLS (%)	-25.9±3.2	-24.1±3.8	-19.2±2.3	-14.1±2.7	***<0.001***
Myo- GLS (%)	-24.1±2.4	-22.1±2.6	-18.0±2.2	-13.3±2.6	***<0.001***
Endo- GCS (%)	-34.7±5.8	-36.4±5.7	-21.9±4.0	-14.8±4.2	***<0.001***
Myo- GCS (%)	-22.8±3.5	-23.6±3.5	-15.5±2.3	-10.7±3.0	***<0.001***
T1 native (ms)	972±31	985±32	1021±46	1041±47	***<0.001***
ECV (%)	*27.0±4.0	27.3±2.6	29.0±2.6	29.5±3.4	0.08
T2 (ms)	50.6±2.1	52.6±3.6	55.0±3.6	56.4±5.9	***<0.001***
Echocardiography					
E velocity (cm/s)	0.65±0.17	0.73±0.14	0.76±0.28	0.75±0.25	0.63
A velocity (cm/s)	0.71±0.18	0.87±0.37	0.79±0.25	0.75±0.29	0.59
Deceleration Time (ms)	197±45	200±42	163±37	155±48	***0.018***
E/A	0.94±0.22	0.98±0.49	0.95±0.42	1.02±0.49	0.51
e' Septal (cm/s)	7.4±2.1	5.5±1.0	5.9±2.0	4.6±1.3	***0.002***
e' Lateral (cm/s)	9.8±2.7	6.8±1.7	8.3±2.4	6.7±2.4	***0.008***
E/e´	10.1±3.7	12.0±4.3	10.8±1.9	14.2±5.9	0.07

Abbreviations: HFpEF – heart failure with preserved ejection fraction, HFmrEF – heart failure with mid-range ejection fraction, HFrEF – heart failure with reduced ejection fraction, LV – left ventricle (left ventricular), EDV – end-diastolic volume, ESV – end-systolic volume, SV – stroke volume, EF – ejection fraction , EDD end-diastolic diameter, LVM – left ventricular mass, Endo- subendocardial layer, Myo- mid-myocardial layer, GLS – global longitudinal strain, GCS – global circumferential strain, ECV – extracellular volume, E – early diastolic mitral transmitral inflow, A – late diastolic transmitral inflow, e‘ – paramitral segments tissue velocity.

Table 4.3 CMR: Left Atrial Phasic Volumes, Emptying Fractions and Strain.

	Pathology Group				P-Value					
	Control N=19	HFpEF N=20	HFmrEF N=18	HFrEF N=17	Control vs HFpEF	Control vs HFmrEF	Control vs HFrEF	HFpEF vs HFmrEF	HFpEF vs HFrEF	HFmrEF vs HFrEF
LA Phasic Volumes and Fractions										
LA Total Volume (ml/m²)	39.5±7.7	46.2±14.0	45.9±15.4	53.9±18.8	0.48	0.54	***0.020***	0.99	0.37	0.36
LA Total EV (ml/m²)	24.4±5.2	21.2±8.3	22.8±6.2	23.6±10.0	0.57	0.92	0.99	0.93	0.77	0.99
LA Passive EV (ml/m^2)	12.1±3.8	9.5±4.3	9.3±3.4	7.8±3.8	0.17	0.16	***0.010***	0.99	0.59	0.67
LA Active EV (ml/m^2)	13.4±3.1	11.8±5.6	13.4±4.6	14.7±6.0	0.73	0.99	0.85	0.73	0.28	0.87
LA Total EF (%)	63±4	47±14	52±12	45±13	***<0.001***	***0.030***	***<0.001***	0.50	0.93	0.22
Patients with Atrial Failure N (%)	0 (0)	8 (40)	4(22)	8 (47)						
LA Passive EF (%)	29±7	20±6	21±7	16±8	***0.002***	***0.009***	***<0.001***	0.97	0.37	0.19
LA Active EF (%)	48±5	34±16	40±12	34±12	***0.003***	0.20	***0.007***	0.39	0.99	0.53
LA expansion index (%)	175±33	101±50	122±51	91±43	***<0.001***	***0.003***	***<0.001***	0.50	0.90	0.18
LA expansion Time (%)	42±6	44±5	47±7	48±10	0.95	0.21	0.16	0.48	0.39	0.99
LA Strain Parameters										
LA Reservoir Strain (%)	33.1±7.6	25.0±10.2	25.5±8.2	20.9±7.6	***0.020***	***0.040***	***<0.001***	0.99	0.47	0.40
LA Conduit Strain (%)	-16.7±5.8	-10.8±4.4	-10.0±3.6	-8.3±4.1	***<0.001***	***<0.001***	***<0.001***	0.94	0.37	0.72
LA Pump Strain (%)	-17.3±3.9	-14.5±8.2	-16.7±5.5	-13.2±5.3	0.46	0.99	0.19	0.66	0.92	0.33

Abbreviations: HFpEF – heart failure with preserved ejection fraction, HFmrEF – heart failure with mid-range ejection fraction, HFrEF – heart failure with reduced ejection fraction, LA – left atrial, EV – emptying volume, EF – emptying/ejection fraction.

Strain were impaired in patients with all HF subgroups, with no significant difference between the 3 subgroups. (LA reservoir strain: 25.0±10.2, 25.5±8.2, 20.9±7.6 vs

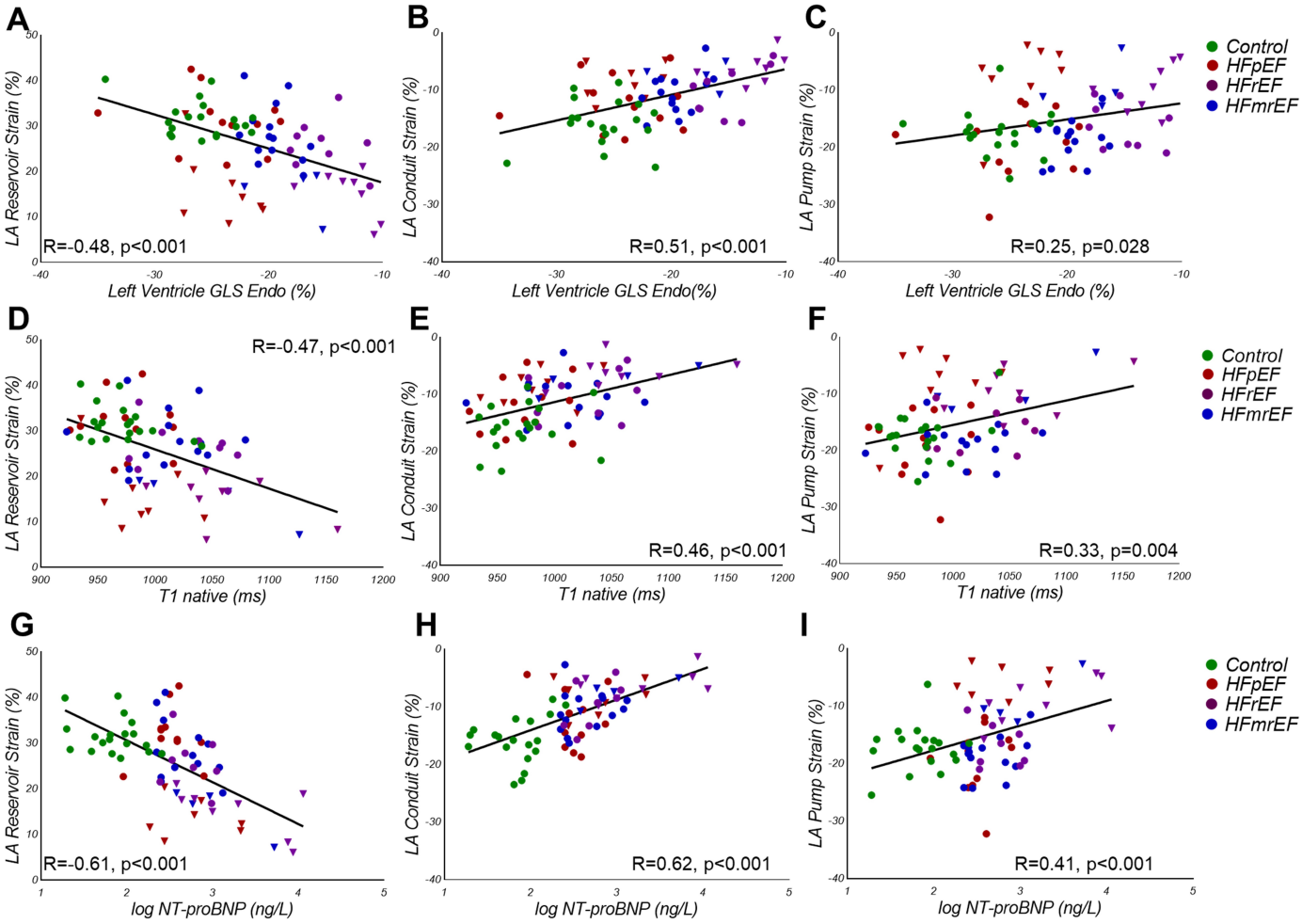


Figure 4.4 Scatterplots: Graphic representation of the relation between LA phasic strain and left ventricular global longitudinal strain (**A.,B.,C.**), T1 native (**D.,E.,F.**) and log NT-proBNP (**G.,H.,I.**). Triangular shapes indicate patients with atrial failure, round circles patients without atrial failure. Legend indicates the four subgroups of patients represented in each graph: Control (green), HFpEF (red), HFmrEF (blue) and HFrEF (purple). Reduced systolic deformation, longer T1 native times and higher NT-proBNP are associated with adverse functional modifications of LA.

33.1±7.6 %, p<0.001, LA conduit strain: -10.8±4.4, -10.0±3.6, -8.3±4.1 vs -16.7±5.8 %, p<0.001). In contrast, LA Pump Strain was not impaired in any of the HF subgroups (**Figure 4.3**).

4.4.3 Correlates of atrial dysfunction. Bivariate regressions.

In order to relate atrial dysfunction to the ventricular and systemic progression of HF, we compared LAEF, LA Reservoir, Conduit and Pump Strains with parameters

Table 4.4 Bivariate regressions with dependent variable: LA total emptying fraction, and LA phasic strains in patients with HF

	LA Total EF (%)		LA Reservoir Strain (%)		LA Conduit Strain (%)		LA Pump Strain (%)	
	Standardized Coefficient (β)	P Value	Standardized Coefficient (β)	P Value	Standardized Coefficient (β)	P Value	Standardized Coefficient (β)	P Value
General								
Age (y)	-0.20	0.14	-0.16	0.24	0.19	0.16	0.10	0.46
BMI (kg/m^2)	0.15	0.29	0.08	0.57	0.07	0.61	-0.15	0.30
LV Function								
LV EDV (ml/m^2)	-0.20	0.15	-0.21	0.12	0.13	0.34	0.21	0.12
LV ESV (ml/m^2)	-0.19	0.17	-0.24	0.07	0.18	0.20	0.21	0.12
LV SV (ml/m^2)	0.07	0.61	0.07	0.63	-0.21	0.12	0.21	0.11
LV EF (%)	0.09	0.54	0.19	0.16	-0.23	0.09	-0.08	0.55
CI (L/min/m^2)	0.10	0.47	0.05	0.72	-0.19	0.17	0.06	0.66
LV GLS Endo (%)	-0.20	0.14	-0.35	***0.008***	0.36	***0.006***	0.22	0.10
LV GLS Endo (%)	-0.25	0.07	-0.39	***0.003***	0.41	***0.002***	0.25	0.07
LV GCS Endo (%)	-0.11	0.44	-0.21	0.13	0.25	0.07	0.09	0.51
LV GCS Myo (%)	-0.17	0.22	-0.29	***0.034***	0.34	***0.012***	0.14	0.31
E/A	-0.52	***<0.001***	-0.34	***0.026***	0.17	0.29	0.39	***0.011***
E/e´	-0.33	***0.033***	-0.31	***0.047***	0.38	***0.012***	0.19	0.23
LV Structural Remodelling								
LVM (g/m^2)	-0.22	0.11	-0.36	***0.007***	0.27	***0.048***	0.29	***0.031***
T1 native (ms)	-0.30	***0.025***	-0.39	***0.004***	0.37	***0.006***	0.30	***0.028***
ECV (%)	-0.19	0.18	-0.24	0.09	0.19	0.17	0.16	0.26
T2 (ms)	-0.28	***0.036***	-0.27	***0.045***	0.22	0.10	0.20	0.14
Other Factors								
NT-proBNP (ng/l)	-0.42	***0.002***	-0.46	***<0.001***	0.39	***0.004***	0.36	***0.008***
log NT-proBNP (ng/l)	-0.53	***<0.001***	-0.54	***<0.001***	-0.07	***0.002***	0.44	***<0.001***
6 min WT (m)	-0.11	0.44	-0.06	0.70	-0.07	0.66	0.14	0.36
QoL	-0.22	0.13	-0.16	0.27	0.20	0.16	0.10	0.49
Borg Score	-0.28	***0.050***	-0.18	0.21	0.22	0.13	0.15	0.29

Abbreviations: EDD end-diastolic diameter, LVM – left ventricular mass, GLS – global longitudinal strain, GCS – global circumferential strain, ECV – extracellular volume, E – early diastolic mitral transmitral inflow, A – late diastolic transmitral inflow, e‘ – paramitral segments tissue velocity, NT-proBNP – N-terminal prohormone of brain natriuretic peptide.

relevant for the imaging and clinical assessment of HF. These results are presented in **Table 4.4**. GLS Endo and Myo were both correlated with LA Reservoir and Conduit Strain but not to Pump Strain (**Figure 4.4 A, B, C**) and E/e', an imaging marker of LV filling pressures and diastolic dysfunction, were correlated with LAEF, Reservoir and Conduit Strain but not to Pump Strain. T1 native and LVM were correlated with all phases of LA strain but not with LAEF. T1 native (**Figure 4.4 D, E, F**) and NT-proBNP levels (**Figure 4.4 G, H, I**) influenced all phasic LA strains and LAEF.

4.4.4 Comparison between HF without atrial failure and HF with atrial failure

Out of all 56 patients with HF included in the study, 20 (36%) had AFail, as follows: 8 (40%) are patients with HFpEF, 4(22%) are patients with HFmrEF and 8(47%) patients with HFrEF. In order to establish what parameters may be involved in the development

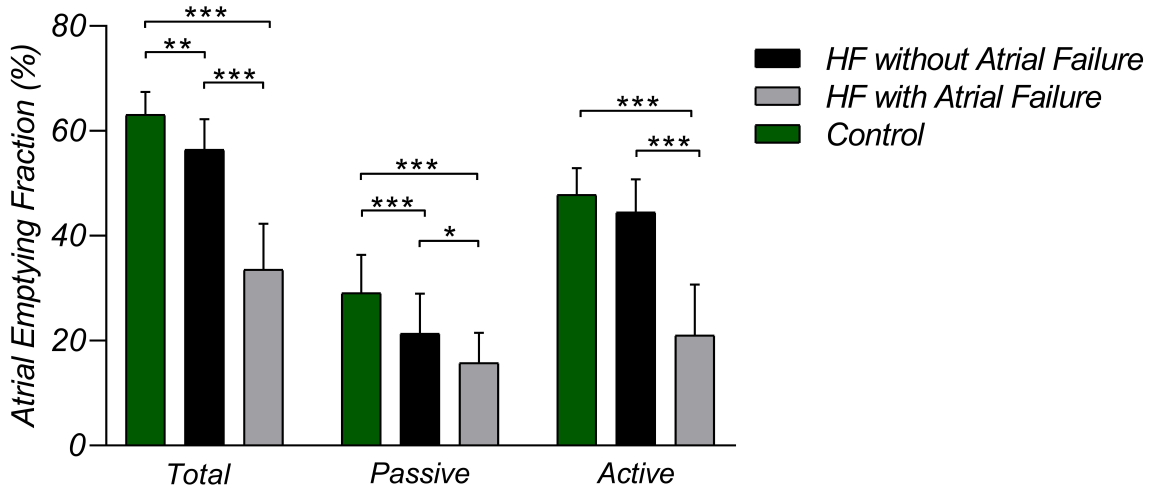


Figure 4.5 Comparison of total, passive and active emptying fractions between patients with HF with Atrial Failure, HF without Atrial Failure and Control. An important difference in Active emptying fraction exist between HF patients with and respectively without Atrial Failure, an indication that the LA is frequently spared and fully functional in a considerable number of patients with HF.

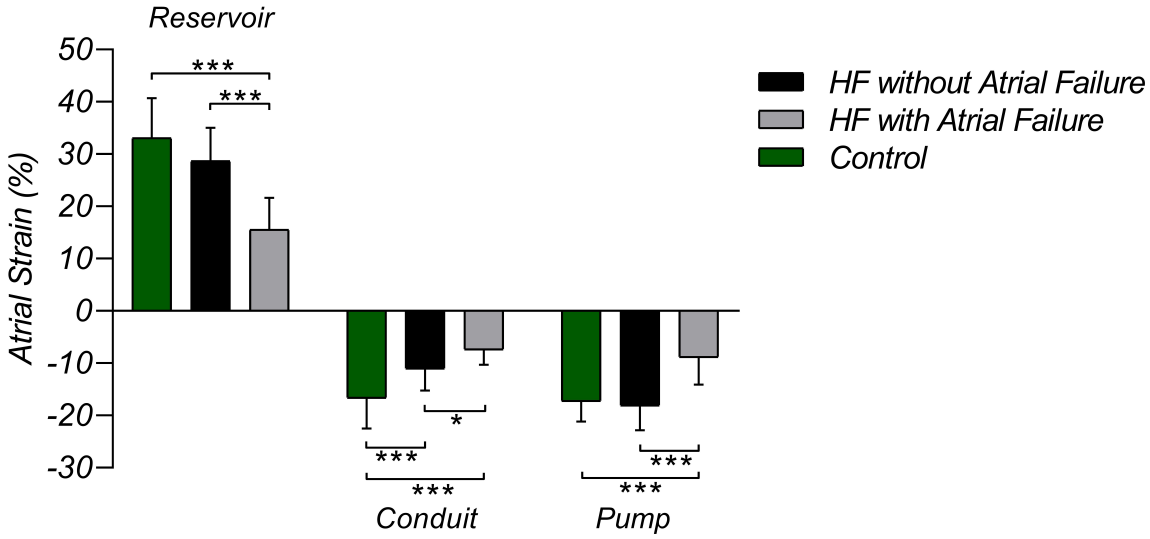


Figure 4.6 Comparison of reservoir, passive and pump strain between patients with HF with Atrial Failure, HF without Atrial Failure and Control. Atrial pump strain is significantly impaired when compared with control only in patients with HF and Atrial Failure. Patients with HF and atrial failure have significant deficit in mechanical strain affecting all three functional phases. In patients with HF without Atrial Failure, the active (pump) strain is preserved.

Table 4.5 Comparison between patients with HF without Atrial Failure, patients with HF with Atrial Failure and Control

	Pathology Group			P-Value		
	Control	HF-AFail	HF+AFail	Control vs HF-Afail	Control vs HF+Afail	HF-AFail vs HF+Afail
Patients in group, N	19	36	20			
Age, y	67±7	70±11	72±12	0.29	0.12	0.53
Male Subjects, N(%)	10 (53%)	19 (53%)	14 (60%)	0.99	0.33	0.26
LA Phasic Volumes and Fractions						
LA Total Volume (ml/m^2)	40±8	45±15	54±17	0.33	***0.006***	0.08
LA Total EV (ml/m^2)	25±5	25±8	18±6	0.98	***0.004***	***<0.001***
LA Passive EV (ml/m^2)	12±4	10±5	8±3	0.34	0.06	0.45
LA Active EV (ml/m^2)	13±3	15±5	9±4	0.20	***0.010***	***<0.001***
LA Total EF (%)	63±4	56±6	34±9	***0.002***	***<0.001***	***<0.001***
LA Passive EF (%)	29±7	21±8	16±6	***<0.001***	***<0.001***	***0.016***
LA Active EF (%)	48±5	44±6	21±10	0.24	***<0.001***	***<0.001***
LA expansion index (%)	175±33	134±34	53±20	***<0.001***	***<0.001***	***<0.001***
LA expansion Time (%)	42±6	47±6	44±10	0.07	0.74	0.32
LA Strain Parameters						
LA Reservoir Strain (%)	33.1±7.6	28.7±6.3	15.6±6.1	0.06	***<0.001***	***<0.001***
LA Conduit Strain (%)	-16.7±5.8	-11.1±4.2	-7.5±2.8	***<0.001***	***<0.001***	***0.011***
LA Pump Strain (%)	-17.3±3.9	-18.2±4.6	-8.9±5.2	0.77	***<0.001***	***<0.001***
Other Parameters						
LV EDV (ml/m^2)	78±13	93±32	102±40	0.07	0.10	0.35
LV ESV (ml/m^2)	29±7	53±25	60±36	***<0.001***	***0.003***	0.45
LV SV (ml/m^2)	41±11	41±7	40±13	***0.019***	0.05	0.82
LV EF (%)	64±6	47±12	45±14	***<0.001***	***<0.001***	0.68
LVM (g/m^2)	42±15	56±13	62±21	***0.010***	***0.008***	0.25
GLS Endo (%)	-25.9±3.2	-20.1±4.7	-18.2±5.7	***<0.001***	***<0.001***	0.20
GLS Myo (%)	-24.1±2.4	-18.7±3.8	-16.8±5.0	***<0.001***	***<0.001***	0.15
GCS Endo (%)	-34.7±5.8	-25.5±9.7	-23.8±11.4	***0.003***	***0.004***	0.56
GCS Myo (%)	-22.8±3.5	-17.6±5.9	-15.7±6.5	***0.005***	***<0.001***	0.27
T1 native (ms)	972±31	1005±41	1031±54	***0.035***	***<0.001***	0.06
ECV (%)	*27.0±4.0	28.4±2.9	28.7±3.0	0.14	0.14	0.70
T2 (ms)	50.6±2.1	54.1±3.9	55.6±5.7	***0.013***	***0.003***	0.26
Echo E/e´	10.1±3.7	11.6±3.5	13.6±5.9	0.58	0.11	0.25
NT-proBNP (ng/l)	91±62	521±325	2405±3335	***<0.001***	***<0.001***	***0.024***
Log NT-proBNP (ng/l)	1.85±0.32	2.62±0.27	3.04±0.53	***<0.001***	***<0.001***	***<0.001***
6 min walking test (m)	523±119	387±113	400±116	***<0.001***	***0.005***	0.86
Borg Score	7.5±1.7	10.8±2.5	12.4±2.0	***<0.001***	***<0.001***	***0.025***
Minessota QoL	5.0±5.9	25.3±24.3	33.2±20.9	***0.001***	***<0.001***	0.25

Abbreviations: HF-AFail - heart failure without atrial failure, HF+AFail – heart failure with atrial failure,EDD – end-diastolic diameter, LVM – left ventricular mass, ECV – extracellular volume, E – early diastolic mitral transmitral inflow, A – late diastolic transmitral inflow, e‘ – paramitral segments tissue velocity, NT-proBNP – N-terminal prohormone of brain natriuretic peptide.

of AFail we wanted then to compare various atrial, ventricular and functional parameters between patients with HF without atrial failure (HF+AFail) and patients with HF with atrial failure (HF-AFail). These data are summarized in **Table 4.5**. Total, passive and active emptying fractions as well as reservoir, conduit and pump atrial strains were more severely impaired in HF+AFail (**Figure 4.5**). Interestingly, LA pump strain and active emptying fraction were unchanged from control in patients with HF-AFail and LA pump strain mean was even slightly higher in HF-AFail, indicating a compensatory role.

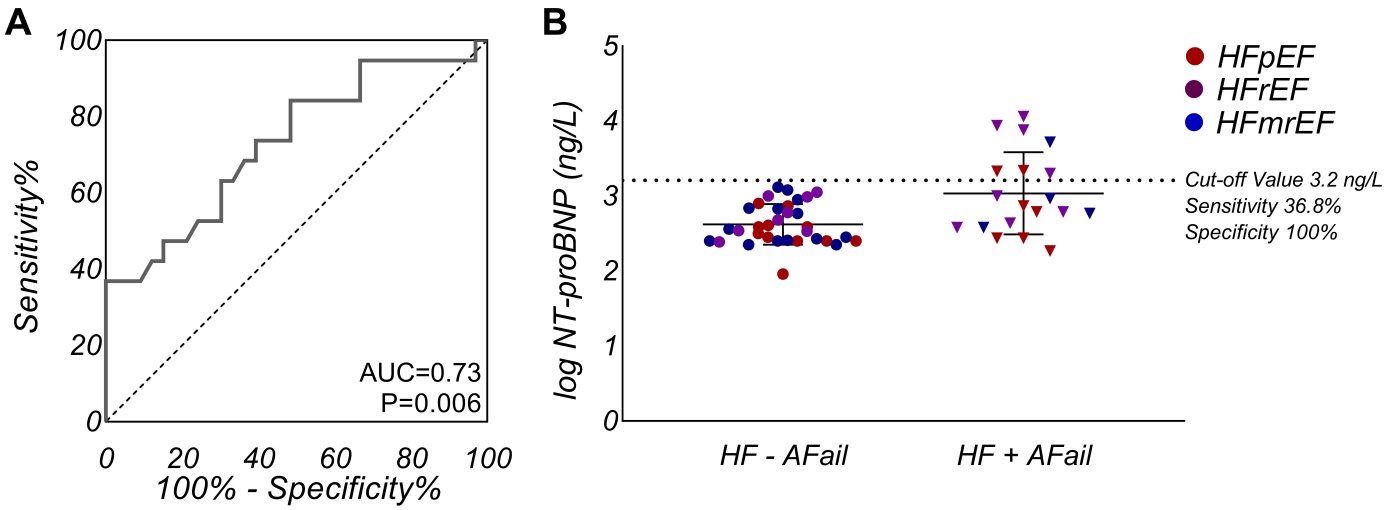


Figure 4.7 Log NT-proBNP is the only independent predictor of Atrial Failure (AF) in patients with Heart Failure (HF): **A.** ROC curve and **B.** comparison of individual values in patients with HF without AF and HF with AF. Dotted line represents the respective cut-off values obtained through Youden formula, specified numerically with the values of sensitivity and specificity obtained at this cut-off value of the predictor. A cut-off value of 3.2 ng/L reaches a 100 % specificity for detection of Atrial Failure and can be important as a new marker of severity in HF and prompt more detailed evaluation of atrial remodelling.

Also, LA Reservoir Strain was not significantly reduced in HF-AFail when compared with control (**Figure 4.6**). From all the parameters characterizing ventricular structure and function and the functional status in HF patients, only NT-proBNP plasma levels (for log NT-proBNP: 2.62±0.27 vs 3.04±0.53, p<0.001) and Borg Score (10.8±2.5 vs 12.4±2.0, p=0.025) were different between HF-AFail and HF+AFail groups.

Further, we wanted to compare different predictive models for AFail in HF patients building up a model of logistic regression where the dependent variable was considered AFail, as a yes/no categorical variable. We further applied multiple linear regressions to establish what variables approximate LA EF, LA reservoir, conduit and pump strain. The selection of predictive variables took in account the plausibility of a cause-effect relation between variables and of a significant effect, following the results of bivariate regressions presented in **Table 4.4**. As independent variables were included: LV GLS Endo, LV GCS Endo, LVM, T1 native, T2, log NT-proBNP and cofactors were considered age and BMI. Logistic regression model to predict AFail

retains only log NT-proBNP (B=2.62, p=0.006) which, in a ROC analysis yields an AUC=0.73 (p=0.006). A cut-off value of 3.2 ng/L has sensitivity of 36.8% and specificity of 100% in detecting AFail and can be used as an useful risk marker in a HF population. (**Figure 4.7**). Using a multiple linear regression model with LA EF as a continuous dependent variable and the same group of potential predictors, again, only log NT-proBNP is the only independent predictor (β=-0.53, p<0.001). LA reservoir strain is predicted by LVM (β=-0.24, p=0.048) and log NT-proBNP (β=-0.49, p<0.001), LA conduit strain by LV GLS Endo (β=0.43, p=0.004), T1 native (β=0.39, p=0.011), log NT-proBNP (β=0.34, p=0.028), age (β=0.47, p<0.001) and BMI (β=0.26, p=0.023) and LA pump strain only by log NT-proBNP (β=0.44, p=0.001).

4.5 Discussion

The findings of our study can be summarized as follows:

1. There was a significant degree of atrial remodeling in patients with HF compared with age and gender match control
2. On average, total and phasic atrial volumes are not different between control and HF making them unreliable. In contrast, functional parameters such as total and passive atrial emptying fractions and reservoir and passive atrial strains are different from control and significantly impaired in patients with HF. However, none of these parameters is different between the 3 groups of HF (HFpEF, HFmrEF, HFrEF).
3. In serial bivariate regression analysis, markers of LV remodeling such as LVM, T1 native, NT-proBNP are correlated with all three phases of atrial strain. LV systolic function (particularly longitudinal strain) and echocardiography-derived E/e', influenced LA reservoir and conduit strain but not LA pump strain.

4. According to the large amount of pooled data available, we proposed here a new criterion, based on LAEF, for the diagnosis of patients with atrial failure: LAEF<46% for males and <47% for females.
5. Using this criterion, from our total number of 56 patients with HF included in this study, 20 have atrial failure. These patients are characterized by significant emptying fraction and atrial strains compared with both controls and HF patients without atrial failure.
6. Elevated log NT-proBNP was an important factor associated with the prevalence of AFail in patients with HF, influencing all reservoir, conduit and pump atrial phasic functions.

LAV showed a superior prognostic ability when compared with LA area[240] and is a powerful predictor of cardiac mortality and morbidity in HF patients.[241] In our observational study we found however, that most of the patients with HF had LAV within the normal range and a significant dilatation from normal was observed only in HFrEF group. Similarly, all 3 atrial phasic emptying volumes were unmodified from control in HFpEF and HFmrEF and only the passive, but not the total and active emptying volume, is lower in HFrEF. These data suggest that a simple evaluation of atrial volume can be misleading and underestimate atrial pathology in HF.

According to the data presented here, atrial remodeling in HF is influenced by some factors that are markers of ventricular remodeling. E/e', a marker of LV filling pressures and quantifier of diastolic dysfunction stage, that is correlated with LA EF, reservoir and conduit strain but not with LA Pump strain. T1 native and LVM, markers of interstitial fibrosis and LV hypertrophy, respectively, have also an important contribution to atrial remodeling. In a comparative analysis of ROCs, an exhaustive model comprising a multitude of variables related to LV remodeling can predict with

some accuracy the presence of AFail, however, in a selective model only log NT-proBNP remains as an independent predictor. In several previous large scale studies[97,233,234], “de novo” AF incidence is higher in HFpEF group and much lower in HFrEF patients, in contrast we found that the prevalence of AFail is the highest in HFrEF. Our data indicate also that higher LVM and longer T1 native times are independently associated with worse atrial function and strain. As we previously showed LVM is higher in HFrEF and HFmrEF compared with Control and HFpEF and T1 is longer[183]. Taken together these data suggest that other risk factors involved in HFpEF pathogenesis may be responsible for the high prevalence of AF in this subgroup apart from ventricular remodeling. On the other hand, progressive atrial remodeling with lower emptying fraction and reduced atrial strain per se may be much more important as causal mechanisms for AF in HFrEF patients and therefore more significant to tackle in this subgroup.

In our study, in HFpEF subgroup, atrial functional impairment was significant, arguing that the left atrium is a functional mirror of increased LV filling pressures. Likely underlying pathophysiological changes associated with HFpEF such as interstitial fibrosis and microvascular dysfunction that increased ventricular stiffness, contribute through chronically increased atrial pressures to dilatation and contractile deficit. In the HFmrEF subgroup, LA was less affected and LAEF was on average the least different from normal. Only 4 (22%) of the HFmrEF have atrial failure compared with 40% in the HFpEF group and 47% in the HFrEF. Moreover, pump strain and active emptying fraction are preserved in HFmrEF. Reversing processes such as LV hypertrophy and interstitial fibrosis holds the potential to revert this subtler atrial dysfunction and ensure a restitutio ad integrum of the cardiac output. Also, as a consequence of this findings, HFmrEF patients may have a lower risk of developing AF compared with other patients with HF.

The concept of AFail has been recently proposed as a separate clinical entity[93,242], however so far there have been no numerical range and parameters proposed to define it. [93] We proposed here a widely available criteria based on global atrial emptying function, LAEF. Being an unitless measure it is easily translatable between different imaging methods such as CMR, CT, echocardiography. It offers a more adequate representation of atrial function compared to simple volumetric approach. LAEF is tightly correlated to LA reservoir strain and proportionally more influenced by the LA active (pump strain) than passive (conduit strain) deformation.

4.6 Limitations

Our study is a prospective cross-sectional study for which a relatively small number of patients with HF were included. Therefore, the main purpose of our investigation was to demonstrate the feasibility and applicability of FT for the assessment of LA size and function. To establish the relevance of FT-derived atrial phasic strains much larger longitudinal studies are warranted. With this study we could not establish the prognostic importance of AFail for major adverse cardiac events (MACEs) or new-onset AF in a HF population. However, we defined here AFail using very simple criteria, based only on parameters derived from widely available SSFP cine images and, therefore, large retrospective studies could be conveniently designed in the future to assess reliably the clinical importance of AFail. To estimate the atrial dimension and function we used in all cases presented here the biplane-area method, however with CMR or CT, ideally a multislice atrial transversal stack can be planned. Applying FT to this stack has the potential of quantifying the best regional and global deformation abnormalities and offering a more accurate overall estimation of LA function.

4.7 Clinical implications

Based on previously demonstrated prognostic role, atrial diameter or volume are widely used in clinical practice to assess atrial remodeling. However, with this study we showed that, on average, atrial volume is only different from control in HFrEF, but not in HFpEF or HFmrEF, moreover a significant number of patients with impaired atrial function have a normal LA volume. In contrast, atrial emptying fraction and global strain proved to characterize better the atrial physiology and therefore should be preferred to a simple volume estimation.

Atrial function is correlated with processes that characterize LV remodeling in HF such as LV hypertrophy and interstitial fibrosis. Targeting more aggressively these underlying processes in HF patients may lead to a delayed atrial dilatation or even reverse remodeling[98] and could in time reduce the prevalence of atrial fibrillation and cardiac decompensation. CMR offers thus an invaluable complex tool for evaluation of the LA, which should make soon part of the routine clinical assessment of the patients with HF. Using CMR and an extensive range of parameters to characterize the phasic details of atrial function to monitor evolution over time and response to specific HF therapy is warranted and holds the potential to instruct a better overall therapeutic approach in patients with HF.

Chapter Five:

CMR Role in the Assessment of Patients with elevated LVEDP

5.1 Abstract

Novel CMR-derived tools such as FT and mapping, integrating functional and structural details, hold particularly high promise to characterise precisely diastolic dysfunction and approximate LVFP with a higher accuracy than echocardiography-based algorithms, currently used as clinical standard. However, so far, a reduced number of cross-sectional studies compared CMR and invasively measured parameters in patients with preserved EF, and none of these used FT to characterise diastolic parameters.

We included 131 consecutive patients with normal systolic function and absence of any pre-existent significant cardiovascular pathology that underwent both CMR and invasive LV end-diastolic pressure (LVEDP) measurements within an interval of no more than a week between the examinations. We considered a cut-off value of ≥ 16mmHg and divided the patients in two groups accordingly. Conventional CMR parameters such as LV EDV, EF, LVM, LAVI were not different between the two groups, but global circumferential strain (GCS) (GCS Endo: -33.9±7.8 vs -37.9±8.5, p=0.014) and early diastolic hemodynamic forces and work (HD Early Diastolic Force: -13.0±6.8 vs -19.4±10.5, p<0.001) were stronger in patients with elevated LVEDP. GLS was comparable between groups. A mediation analysis and multiple regression, retain only these two parameters (GCS Endo: β=-0.189, p=0.035, HD Early Diastolic Force: β=-0.344, p=0.035) as independent approximators of LVEDP yielding a cumulative AUC of 0.70, p<0.001 in a ROC analysis.

We propose that CMR FT may represent an important adjuvant tool in the preliminary identification of patients with elevated LVEDP. We showed that both systolic and

diastolic LV functions relate to LVEDP and are exacerbated in patients with elevated LVEDP. In contrast with previous data, we did not find similar differences in ECV or LAVI.

5.2 Introduction

Increased LV filling pressures (LVFP) are correlated with a worse mortality independently of other markers of CR[243-245] and thus represent an important independent marker of cardiovascular risk. In pathology, raised LVEDP results from the discrepancy of increased preload and/or afterload burden and progressive LV chamber stiffness. An LVEDP above 16 mmHg is considered one of the hallmarks of HFpEF and has a confirming role in the recently proposed diagnostic algorithm.

However, direct assessment of LVFP requires left heart invasive catheter access and thus entails inherent risks and limitations. Imaging methods such as echocardiography and CMR offer the double advantage of being non-invasive and conveniently applicable in successive sessions and therefore better place for a longitudinal clinical evaluation and intermediary assessment of therapy results. Given its image acquiring and processing advantages and unique insight into structural modifications, such as diffuse fibrosis, CMR's role in assessing LV diastolic function is currently expanding and holds the promise to become the preeminent examination in patients with diastolic dysfunction and HFpEF. CMR FT has the advantage of evaluating not only the systolic but also early and late diastolic deformation. We previously showed that by combining the spatial assessment of LV deformation and, respectively, detailed visualization of mitral and aortic valve structures, allowing accurate measurements of valvular diameters over the cardiac cycle and applying mathematical modelling, a reliable estimation of intraventricular pressure gradients and hemodynamic forces is

feasible.[118] This method is presented in more detail in Chapter 1 (theoretical premises and previous validation) and Chapter 2 (method principles and quantification).

While for echocardiography, current expert recommendations select a group of several parameters such as E/A, E/e', left atrial volume, tricuspid regurgitation jet velocity, that taken together approximate LVFP[111,246] the role of CMR in diagnosis and staging of DD is so far insufficiently explored. CMR is becoming and increasingly powerful tool to characterize ventricular diastole[67], a direct comparison and validation of CMR parameters against invasively measured LVFP is currently missing.

In this chapter we compared LVEDP measured using invasive left heart catheterization and compare it with an extensive list of CMR parameters with the twofold purpose of providing CMR-derived indirect evaluation of LV hemodynamics and of gaining novel mechanistic insight into the pathophysiology of HFpEF. Using FT- derived strain curves we characterized in detail the systolic and phasic diastolic deformation properties of the LV and by applying a mathematical modelling of intraventricular systolic and diastolic hemodynamic forces we compared these non-invasively acquired data with the gold-standard invasively measured LVEDP.

5.3 Specific Methods

5.3.1 Study Population

We screened our local CMR general database at Deutsches Herzzentrum Berlin and identified all the consecutive patients registered in the time interval between 1st of January 2018 and 31st of December 2020 with respectively at least one CMR scan available and a contemporary left heart catheter assessment comprising measurement of LVEDP at rest. A maximal difference of one week between the CMR and interventional diagnostic visits was considered acceptable for inclusion. Exclusion

criteria were EF<50%, valvulopathy of any degree above trivial, permanent or persistent AF, diagnosis of inherited cardiomyopathy (DCM; HCM, ARVC), infiltrative cardiomyopathies, takotsubo cardiomyopathy, pericarditis (active or in resolution), previous myocarditis, significant CAD or previous transmural or hemodynamically significant MI, cardiac transplant, medical evidence of systemic conditions such rheumatoid arthritis or other autoimmune disease, low quality images or significant artefacts. Study protocol, inclusion of patients, data access and usage were reviewed and approved by the Charité–Universitätsmedizin Berlin Ethics Committee (Study Code: EA2/017/22) and fully complies with the Declaration of Helsinki.

5.3.2 Cardiac magnetic resonance

69 (53%) patients were scanned with a clinical 3T system (Ingenia, Philips Healthcare, Best, the Netherlands), and 62 (47%) with a 1.5T system (Achieva, Philips Healthcare, Best, the Netherlands). The details regarding image acquisition parameters and protocols are described in detail in Chapter 2.

5.3.4 Echocardiography

Contemporary transthoracic echocardiography reports were collected where available. As our inclusion criteria for these data comprised the assessment of e' tissue Doppler velocities for the calculation of E/e', only 39 of 131 patients had a satisfactory set of results. For all echocardiographic imaging iE33 with a X5–1 probe and EPIQ5 systems with a S5-1 probe (Philips Healthcare, Best, the Netherlands) were used.

5.3.5 Image analysis – details presented in Chapter 2.

5.3.6 Left Ventricular End-Diastolic Pressure

Left heart catheterization was performed with a 6F Impulse PIG pigtail catheter (Boston Scientific Corp, Massachusetts, US) using a femoral or brachial artery access by crossing the aortic valve. LV pressures were recorded, after a complete expiration over

at least four consecutive cardiac cycles and digitally plotted. LVEDP was estimated at end diastole corresponding to the nadir of the “a” segment on pressure tracing, averaging the measurements over three consecutive heart beats.

5.3.6 Statistical Analysis

Statistical analysis of the data and graphical representation were performed out using SPSS v28 (IBM SPSS Inc, Armonk, NY) and GraphPad Prism v9 (GraphPad Software, Inc, La Jolla, CA). For each continuous variable normality of distribution was tested using Kolmogorov-Smirnov and Shapiro-Wilk tests. All the parameters included in the study showed a normal pattern of distribution with the exception of NT-proBNP which were subsequently log transformed. For continuous variables comparison between groups was performed with a 2-sided, independent-samples Student t test for normally distributed data and Mann-Whitney and Kruskal-Wallis tests for skewed data. For categorical variables, comparison was tested with a $\chi 2$ test and statistical significance assessed with Fisher's exact test. Bivariate linear regressions were carried out to analyse the relation between imaging parameters and LVEDP. Mediation analysis was used, as described previously, to detect which of these variables can independently predict LVEDP and respectively which effect is mediated by a stronger cofactor. After exclusion of redundant variables, the independent predictors given by the mediation analysis were entered in a multiple linear regression model. Using the same set of variables, a logistic regression was applied in order to define a collective predictive variable. Receiver-operating characteristics (ROC) curves were generated to measure the predictive capacity of the model to LVEDP and cut-off values were derived and an illustrative scatter-plot analysis was plotted. For all analyses, a 2-tailed $P<0.05$ was considered statistically significant.

5.4 Results

5.4.1 Population Characteristics

We identified a total number of 131 patients (age 64±13 years, 79(60%) males, mean LVEDP 20±7 mmHg) who satisfied all the inclusion and exclusion criteria. We further divided them according to the established cut-off value [247] of LVEDP=16mmHg into two groups respectively: normal LVEDP (<16mmHg, N=38) and elevated LVEDP (≥16mmHg, N=93). The baseline demographics, clinical and medication characteristics of these two groups are presented and compared in **Table 5.1**. The basic laboratory values and in particular adjusted NT-proBNP levels were similar between the two groups (log NT-proBNP: 2.34±0.60 vs 2.26±0.63, p=0.55). Comorbidity distribution was also similar between groups. NYHA criteria indicated a higher total prevalence of symptoms in the elevated LVEDP group (17 (45%) vs 63 (68%), p=0.018) and tendency for a higher percentage of cases for all 4 classes. Even if we excluded patients with significant symptomatic CAD and those referred for surgical revascularisation, CAD was still prevalent among both groups, 23(61%) vs 62 (67%). Of note 30 (79%) of the normal LVEDP group and 70 (75%) of the elevated LVEDP group were on ACE inhibitors or angiotensin receptor blockers.

5.4.2 Comparison between patients with normal and elevated LVEDP

We further compared the two groups of patients in terms of generic CMR and echocardiography parameters routinely acquired and assessed. These results are shown in **Table 5.2**. Biventricular volumes and ejection fractions were equivalent between groups (LVEDV: 67±17 vs 68±20 ml/m^2, p=0.82, LVEF: 57±12 vs 60±11 %, p=0.30, RVEDV: 69±19 vs 74±20 ml/m2, p=0.17, RVEF= 51±12 vs 52±11 %, p=0.57). We did not find any differences between left atrial remodeling between groups (LAVI=

40±10 vs 43±12 ml/m^2, p=0.25, LAEF= 55±14 vs 57±12 %, p=0.45, LA Strain= 32.4±11.1 vs 34.5±10.5 %, p=0.31).

Table 5.1 Demographics, comorbidities and risk factors, medication

	Pathology Group		P Value
	LVEDP<16mmHg	LVEDP≥16mmHg	
	N=38	**N=93**	
Daemographics			
Age, y	66±10	64±12	0.39
Male Subjects, N (%)	21 (55)	58 (62)	0.45
Heart rate (bpm)	63±11	64±6	0.43
Laboratory Values			
NT-proBNP (ng/l)	476±571	634±1616	0.61
Log NT-proBNP (ng/l)	2.34±0.60	2.26±0.63	0.55
Hemoglobin (g/dl)	14±1	14±1	0.65
Hematocrit	40±4	40±4	0.81
Creatinin (mg/dl)	0.97±0.18	1.39±3.42	0.46
GFR (ml/min)	78±15	79±22	0.70
Troponin T (ng/l)	16±9	18±11	0.32
Chol total	195±50	191±52	0.74
Chol HDL	54±16	50±13	0.18
Chol LDL	120±45	120±45	0.95
Triglycerides	149±84	150±98	0.96
Glucose	125±50	119±51	0.53
HbA1C	6.1±1.2	6.1±1.3	0.93
CRP (mg/dl)	2.9±1.8	3.1±2.4	0.64
WBC (n/nl)	7.3±2.0	7.0±1.9	0.57
Comorbidities, risk factors, N(%)			
NYHA Class			
Class I	4 (11)	13 (14)	0.59
Class II	9 (24)	29 (31)	0.39
Class III	4 (11)	19 (20)	0.18
Class IV	0 (0)	2 (2)	0.36
Total	17 (45)	63 (68)	***0.018***
CAD	23 (61)	62 (67)	0.50
Peripheric artery disease	4 (11)	18 (19)	0.22
MI	12 (32)	24 (26)	0.50
Hypertension	32 (84)	77 (83)	0.84
Diabetes	12 (32)	26 (28)	0.68
COPD	7 (18)	15 (16)	0.75
Smokers	10 (26)	29 (31)	0.58
Medication, N(%)			
ACE-inhibitors or ARBs	30 (79)	70 (75)	0.65
Calcium Antagonists	12 (32)	32 (34)	0.76
MR Antagonists	2 (5)	7 (8)	0.64
Beta-blockers	21 (55)	54 (58)	0.77
Statins	24 (63)	66 (71)	0.38
Diuretics	10 (26)	33 (35)	0.31
Nitrates	9 (24)	10 (11)	0.06

Abbreviations: NT-proBNP N-terminal prohormone of brain natriuretic peptide, GFR glomerular filtration rate, Chol cholesterol, HbA1C glycated haemoglobin, CRP protein reactive C, WBC white blood cells, CAD coronary artery disease, MI myocardial infarction, COPD chronic obstructive pulmonary disease, ACE angiotensin converting enzyme, ARB – angiotensin receptor blockers. MR mineralocorticoid receptor. N represents the number of subjects included in the analysis.

Table 5.2 CMR Parameters: LV and RV Volumes, LA volume, LA EF and strain

	Pathology Group		P Value
	LVEDP<16mmHg	LVEDP≥16mmHg	
CMR Left Ventricle	**N=38**	**N=93**	
LVEDV (ml/m2)	67±17	68±20	0.82
LVESV (ml/m2)	28±9	27±10	0.77
LVSV (ml/m2)	39±11	42±11	0.24
LVEF (%)	57±12	60±11	0.30
LVCI (L/min/m2)	2.90±0.85	2.99±0.82	0.59
LVEDD (mm)	51±6	50±7	0.41
Septum (mm)	12±3	12±3	0.82
Lateral Wall (mm)	8±2	8±2	0.84
LVM (g/m2)	49±12	48±12	0.93
ECV (%)	25.6±5.5	26.2±4.7	0.47
CMR Right Ventricle			
RVEDV (ml/m2)	69±19	74±20	0.17
RVESV (ml/m2)	33±11	35±13	0.40
RVSV (ml/m2)	36±10	39±11	0.11
RVEF (%)	51±12	52±11	0.57
RVCI (L/min/m2)	2.63±0.78	2.80±0.82	0.27
RVEDD (mm)	32±6	32±4	0.82
CMR Left Atrium			
LAV (ml/m2)	40±10	43±12	0.25
LAEF (%)	55±14	57±12	0.45
LA Strain (%)	32.4±11.1	34.5±10.5	0.31

Abbreviations: LV left ventricular, EDP end-diastolic pressure, EDV end-diastolic volume, ESV end-systolic volume, EF ejection fraction, CI cardiac index, EDD end-diastolic diameter, LVM left ventricular mass, ECV extracellular volume, RV right ventricular, LA left atrial, LAV left atrial volume.

We further used FT to compare deformation properties of the LV over the cardiac cycle. In addition to the Endo and Myo values of peak systolic deformation (GLS and GCS) (two illustrative examples are shown in **Figure 5.1**) we included in the analyses derived parameters to characterize diastolic properties of the LV (two illustrative examples are shown in **Figures 5.2 and 5.3**), described in detail in **Chapter 2**. All these results are listed here in **Table 5.3**. GLS was not different (GLS Endo: -24.3±5.3 vs -25.6±5.3 %, p=0.23) between the two groups but GCS was significantly lower in patients with elevated LVEDP (GCS Endo: -33.9±7.8 vs -37.9±8.5, p=0.014).

Table 5.3 CMR Parameters: LV myocardial deformation, hemodynamic forces, quantification of LV diastolic function

	Pathology Group		P Value
	LVEDP<16mmHg	LVEDP≥16mmHg	
	N=38	**N=93**	
Left Ventricle			
GLS Endo (%)	-24.3±5.3	-25.6±5.3	0.23
GLS Myo (%)	-21.4±3.6	-22.4±4.1	0.18
GCS Endo (%)	-33.9±7.8	-37.9±8.5	***0.014***
GCS Myo (%)	-20.1±4.4	-22.9±4.5	***0.002***
GCS Endo-Epi gradient (%)	-13.8±4.2	-15.1±4.7	0.15
GCS/GLS Endo	1.42±0.30	1.52±0.44	0.19
GCS/GLS Myo	0.94±0.18	1.04±0.24	***0.037***
E dV/dt (ml/s)	270±116	322±125	***0.032***
A dV/dt (ml/s)	347±109	346±129	0.97
E/A dV/dt	0.97±0.86	1.40±2.40	0.29
Diast Peak GLSR (%/s)	1.10±0.45	1.21±0.52	0.26
Diast Peak GCSR (%/s)	1.65±0.73	1.93±0.84	0.08
Ratio (E dV/dt / Diast Peak GLSR) (ml/%)	135±58	156±93	0.21
Ratio (E dV/dt / Diast Peak GCSR) (ml/%)	97±56	97±51	0.98
HD Systolic Force (%)	31.0±13.9	34.0±16.7	0.33
HD Systolic Work (%)	6.2±6.4	6.9±5.8	0.52
HD Systolic Work (mJ)	3.4±2.0	4.9±3.7	***0.004***
HD Systolic Power (mJ/s)	37.7±24.0	46.9±36.2	0.16
HD Early Diastolic Force (%)	-13.0±6.8	-19.4±10.5	***<0.001***
HD Early Diast Work (%)	-1.1±0.9	-1.8±1.4	***0.009***
HD Early Diast Work (mJ)	-0.6±0.4	-1.1±0.8	***<0.001***
HD Early Diast Power (mJ/s)	-9.5±8.9	-16.3±13.1	***0.001***
HD Late Diast Force (%)	-10.9±8.4	-10.9±7.0	0.99
Echo Left Ventricle	**N=15**	**N=24**	
E/e' septal	10.7±4.0	12.1±4.6	0.37
E/e' lateral	7.4±3.1	9.7±3.4	0.12
E/e' mean	8.4±3.4	10.1±3.4	0.14

Abbreviations: LVEDP – left ventricular end-diastolic pressure, GLS global longitudinal strain, GCS global circumferential strain, Endo – subendocardial layer, Myo mid-myocardial layer, E early diastolic, A “atrial” late diastolic, Diast diastolic, GLSR global longitudinal strain rate, GCSR global circumferential strain, HD hemodynamic, E/e’ ratio between early diastolic mitral flow velocity and early diastolic paramitral tissue velocity.

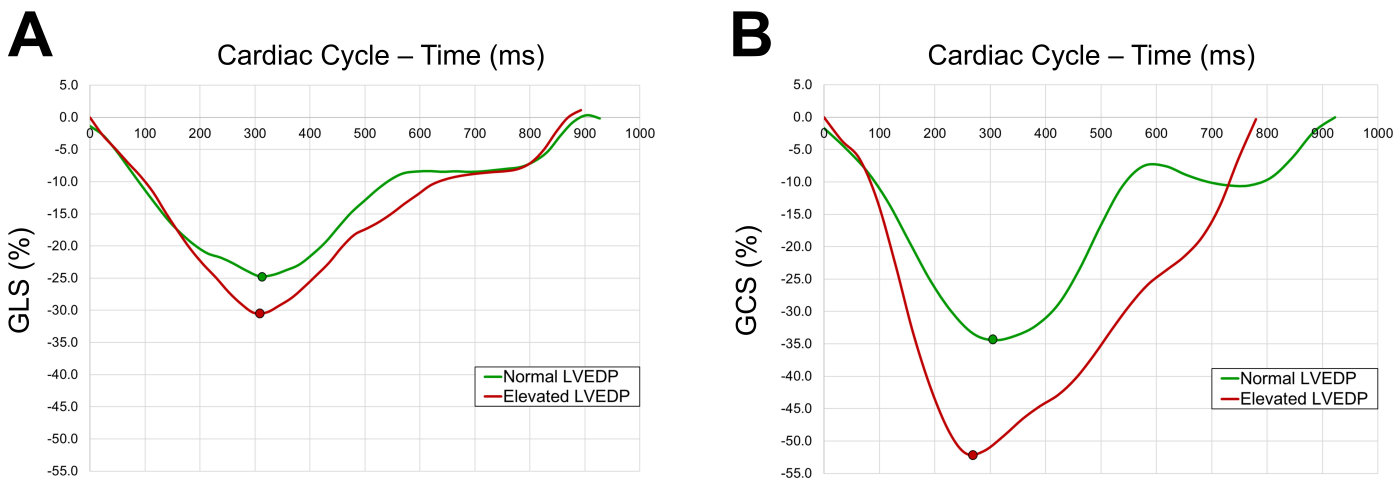


Figure 5.1 Illustrative examples of **A.** global left ventricular longitudinal strain (GLS) and **B.** global left ventricular circumferential strain (GCS) in a patient with elevated LVEDP (red) and a patient with normal LVEDP (green). On each curve the peak systolic values of GLS and GCS effectively used in the study are indicated.

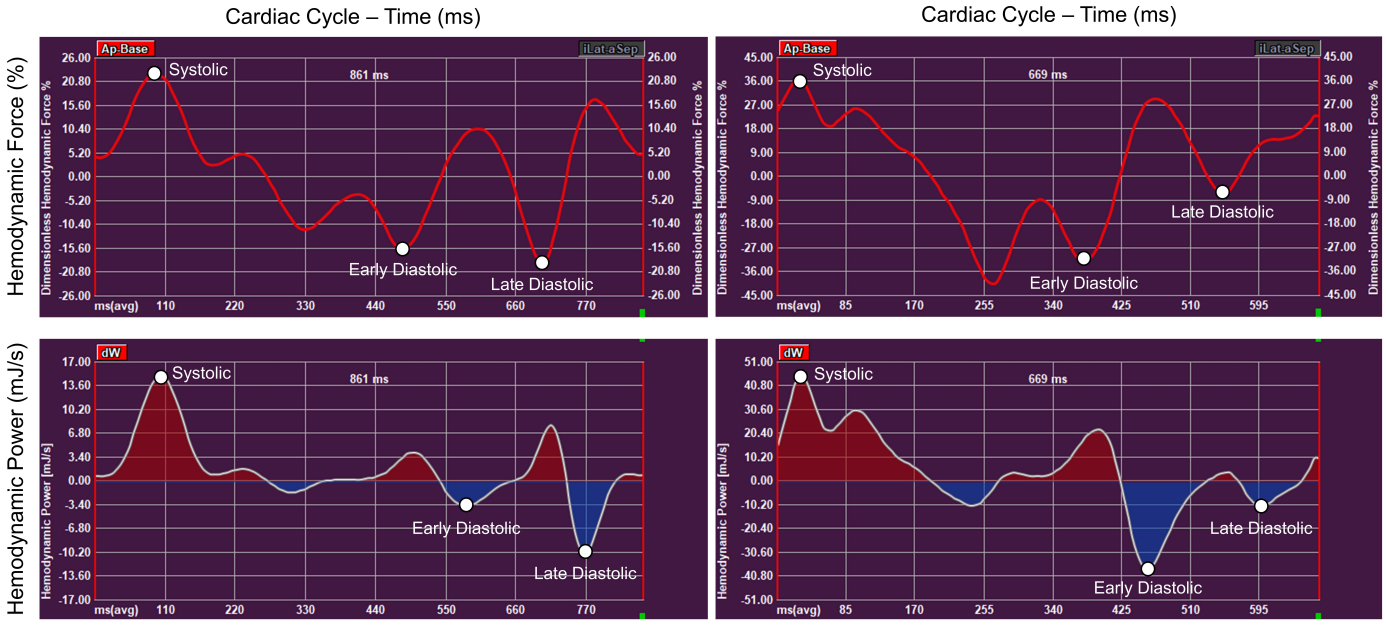


Figure 5.2 Illustrative examples of hemodynamic forces (%) and hemodynamic power (mJ/s) in a patient with normal values of LVEDP at rest (left) and in a patient with elevated LVEDP (right), measured along all the phases of the cardiac cycle (white dots correspond to the points of maximal amplitude of systolic, early diastolic and late diastolic phases). Phasic hemodynamic work was calculated as the area under curve: red for systolic phase (numerically positive) and blue for early diastolic phase (numerically negative).

Table 5.4 Relation between LVEDP and various CMR and echocardiography parameters all patients (left rows) and patients with elevated LVEDP (right rows)

	All Patients		Only Patients with LVEDP≥16mmHg	
	Standardized Coefficient (β)	P Value	Standardized Coefficient (β)	P Value
Daemographics	**N=131**		**N=93**	
Age, y	-0.076	0.39	-0.058	0.58
Log NT-proBNP (ng/l)	0.013	0.90	0.079	0.55
CMR Left Ventricle				
LVEDV (ml/m2)	-0.026	0.77	-0.152	0.15
LVEF (%)	0.155	0.08	0.124	0.24
LV Septum (mm)	-0.015	0.87	-0.018	0.86
LVEDD (mm)	-0.058	0.51	-0.079	0.45
LVM (g/m2)	-0.028	0.75	-0.102	0.33
ECV (%)	0.053	0.57	-0.124	0.27
CMR Strain and HDF				
GLS Endo (%)	-0.189	***0.033***	-0.234	***0.026***
GLS Myo (%)	-0.161	0.07	-0.159	0.13
GCS Endo (%)	-0.341	***<0.001***	-0.340	***<0.001***
GCS Myo (%)	-0.351	***<0.001***	-0.296	***0.004***
Gradient GCS (%)	-0.279	***0.001***	-0.335	***0.001***
GCS/GLS Endo	0.156	0.08	0.097	0.36
GCS/GLS Myo	0.221	***0.012***	0.132	0.21
E dV/dt (ml/s)	0.168	0.06	0.035	0.74
Diast Peak GLSR (%/s)	0.147	0.09	0.118	0.27
Diast Peak GCSR (%/s)	0.240	***0.006***	0.185	0.08
HD Systolic Force (%)	0.094	0.29	0.050	0.64
HD Systolic Work (%)	0.167	0.06	0.191	0.07
HD Systolic Work (mJ)	0.196	***0.026***	0.064	0.55
HD Systolic Power (mJ/s)	0.087	0.33	-0.018	0.87
HD Early Diastolic Force (%)	-0.427	***<0.001***	-0.389	***<0.001***
HD Early Diast Work (%)	-0.334	***<0.001***	-0.332	***0.004***
HD Early Diast Work (mJ)	-0.315	***<0.001***	-0.158	0.13
HD Early Diast Power (mJ/s)	-0.281	***0.001***	-0.168	0.11
HF Late Diastolic Force (%)	0.002	0.98	-0.059	0.58
CMR Right Ventricle				
RVEDV (ml/m2)	0.063	0.47	-0.141	0.18
RVEF (%)	0.149	0.09	0.161	0.12
RVEDD (mm)	-0.031	0.73	-0.135	0.21
CMR Left Atrium				
LAVI (ml/m2)	0.140	0.11	0.065	0.54
LAEF (%)	-0.060	0.50	-0.120	0.25
LA Strain (%)	0.010	0.91	-0.063	0.55
Echo Left Ventricle	**N=39**		**N=24**	
E/e' septal	0.210	0.21	0.098	0.63
E/e' lateral	0.415	***0.049***	0.356	0.23
E/e' mean	0.280	0.09	0.137	0.52

Abbreviations: LV left ventricular, EDP end-diastolic pressure, EDV end-diastolic volume, ESV end-systolic volume, EF ejection fraction, CI cardiac index, EDD end-diastolic diameter, LVM left ventricular mass, ECV extracellular volume, GLS global longitudinal strain, GCS global circumferential strain, Endo subendocardial layer, Myo mid-myocardial layer, E early diastolic, A “atrial” late diastolic, Diast diastolic, GLSR global longitudinal strain rate, GCSR global circumferential strain, HD hemodynamic RV right ventricular, LA left atrial, LAV left atrial volume, E/e’ ratio between early diastolic mitral flow velocity and early diastolic paramitral tissue velocity.

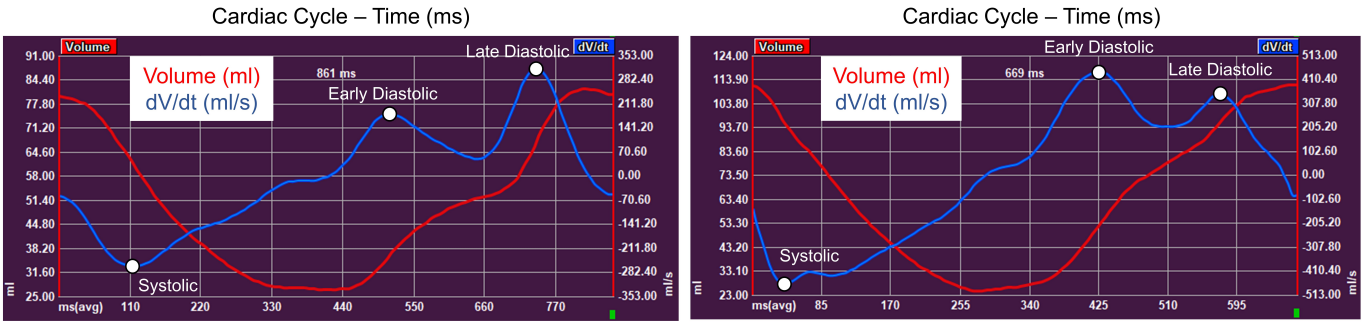


Figure 5.3 Illustrative examples of LV volume (ml) – in red – and LV volume derivative (ml/s) – in blue – curves in a patient with normal values of LVEDP at rest (left) and in a patient with elevated LVEDP (right), measured along all the phases of the cardiac cycle (white dots correspond to the points of maximal amplitude of systolic, early diastolic and late diastolic phases) for the LV volume derivative curve. In this study we assessed only early diastolic (E dV/dt) and late diastolic values (A dV/dt), considering that systolic function is better evaluated by systolic strain (GLS and GCS).

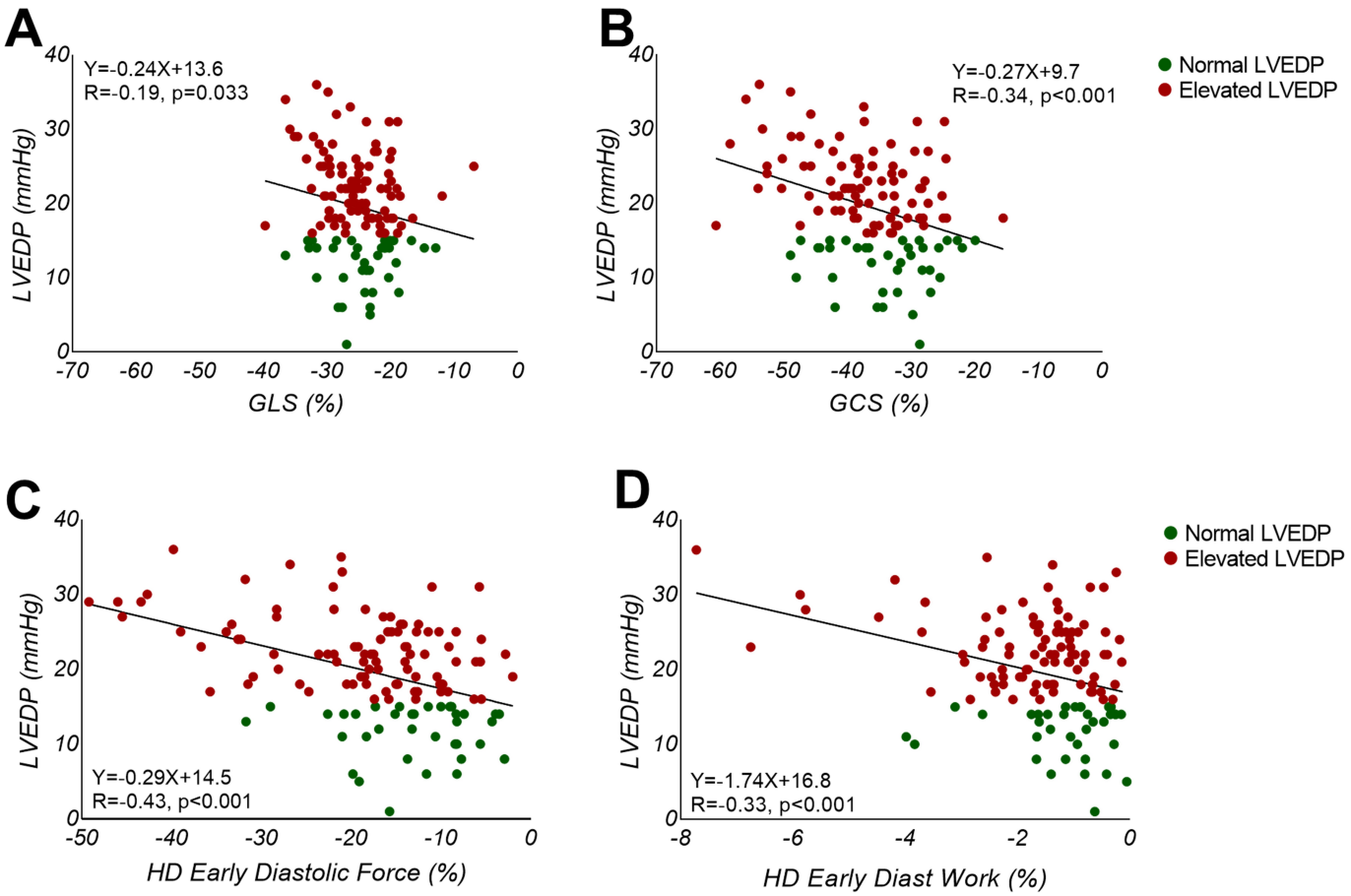
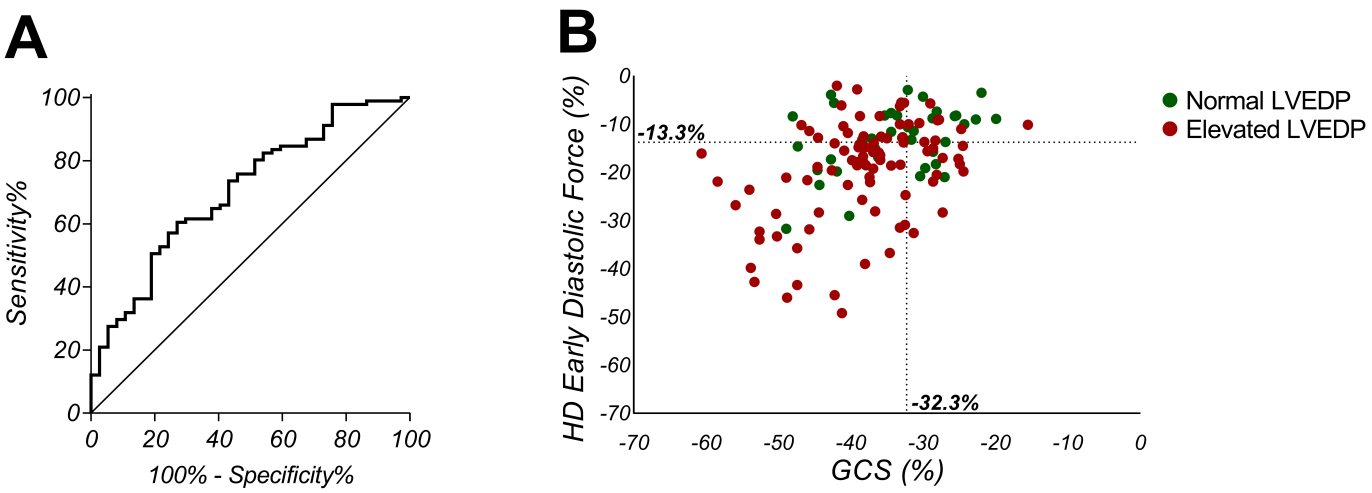


Figure 5.4 Relation between peak systolic strain A. GLS Endo B. GCS Endo C. hemodynamic early diastolic force and D. hemodynamic early diastolic work and left ventricular end-diastolic pressure (LVEDP) in all patients included in the study. Green dots represent patients with normal LVEDP and red dots patients with elevated LVEDP. and left ventricular end-diastolic pressure (LVEDP) in all patients included in the study. Green dots represent patients with normal LVEDP and red dots patients with elevated LVEDP.

Patients with elevated LVEDP had also an increased early diastolic volume gradient (E dV/dt: 270±116 vs 322±125 ml/s, p=0.032), suggestive of an increased early diastolic mitral inflow. Hemodynamic force, work and power were all exacerbated in early diastole in patients with elevated LVEDP (HD Early Diastolic Force= -13.0±6.8 vs -19.4±10.5 %, p<0.001). Echocardiography Doppler data were available for a minority of patients (15 with normal and 24 with elevated LVEDP), however in these patients the differences were not significant for E/e'.

5.4.3 Relation between imaging parameters and LVEDP

As a next step we wanted to investigate which of these parameters are able to offer a good approximation for the invasively measured LVEDP. We ran a series of univariate regressions including as predictive variable every relevant imaging parameter. First we included the whole group of patients and then subsequently we ran similar regressions only in the group of patients with elevated LVEDP. A summary of these data is presented in **Table 5.4**. GLS Endo (β=-0.189, p=0.033) (**Figure 5.4 A**), GCS Endo (β=-0.341, p<0.001) (**Figure 5.4.B**) and Myo (β=-0.351, p<0.001), GCS Endo-Epi gradient (β=-0.279, p=0.001), HD systolic work (β=-0.196, p=0.026) and respectively, hemodynamic early diastolic circumferential strain-rate (β=-0.240, p=0.006) and all early diastolic hemodynamic parameters (HD Early Diastolic Force: β=-0.427, p<0.001 (**Figure 5.4.C**), HD Early Diastolic Work (β=-0.334, p<0.001) (**Figure 5.4.D**), HD Early Diastolic Power (β=-0.281, p=0.001)) were significant predictors for LVEDP. Observing that parameters characterizing both LV systole and diastole predict LVEDP we further performed a mediation analysis to determine which of these factors remains an independent predictor and which effect can be mediated by a stronger co-variate. Among parameters characterizing LV systole only GCS Endo proved to have the strongest independent effect, GCS Endo-Epi gradient (β=0.249, p=0.25) and HD



	AUC	95% CI	Significance	Cut-off value	Sensitivity (%)	Specificity (%)
GCS Endo (%)	0.63	0.53-0.74	0.017	-32.3	78	51
HD Early Diastolic Force (%)	0.69	0-59-0.79	<0.001	-13.3	68	62
Combined	0.70	0.61-0.80	<0.001		60	73

Figure 5.5 The role of CMR parameters as predictors of LVEDP: **A.** area under curve for a combined variable integrating global circumferential strain and hemodynamic early diastolic force **B.** scatter plot representing HD Early Diastolic Force and GCS in all patients and the discrimination ability of the cut-off values obtained through ROC analysis. Green dots represent patients with normal LVEDP and red dots patients with elevated LVEDP. Relative and cumulative AUC and numerical details are presented in the table below.

Table 5.5 Multiple linear regression models in all patients included in the study (upper rows) and only in patients with elevated LVEDP (lower rows).

	All Patients (N=131)				
			95% CI		
	Standardized Coefficient (β)	Unstandardized Coefficient (B)	Lower Bound	Upper Bound	P Value
Constant	10.035		5.330	14.740	***<0.001***
GCS Endo (%)	-0.189	-0.149	-0.288	-0.011	***0.035***
HD Early Diastolic Force (%)	-0.344	-0.232	-0.350	-0.114	***<0.001***
	Patients with LVEDP≥16mmHg (N=93)				
			95% CI		
	Standardized Coefficient (β)	Unstandardized Coefficient (B)	Lower Bound	Upper Bound	P Value
Constant	15.515		11.332	19.697	***<0.001***
GCS Endo (%)	-0.216	-0.122	-0.240	-0.004	***0.044***
HD Early Diastolic Force (%)	-0.300	-0.138	-0.234	-0.042	***0.005***

Abbreviations: GCS global circumferential strain, Endo subendocardial layer, HD hemodynamic, CI confidence interval

systolic work (β=0.099, p=0.26) lost significance when forced in a multiple regression with GCS Endo. Similarly, the HD early diastolic work proved the only independent predictor of LVEDP. We therefore included GCS Endo and HD Early Diastolic Force in a multiple regression analysis. These results are presented in **Table 5.5**.

5.4.4 Cut-off values and ROC analysis. Comparison with echocardiography

To establish what cut-off values are optimal in order to reach a maximal discrimination capacity between patients with normal and elevated LVEDP, we used the predictive variable resulting from the multiple regression (Y= - 0.149*Endo GCS - 0.232*HD Early Diast Force + 10.035) and plotted the ROC curve. We calculated using Youden's method, the cut off vales for maximal sensitivity and specificity which were GCS Endo= -32.3% and HD Early Diastolic Force=-13.3% (**Figure 5.5**).

Discussion

The role of CMR in assessing LV diastolic function is currently increasingly bringing the expectation of new capabilities to visualize ventricular mechanics and hemodynamics.

Here we bring new evidence about a connection between invasively measured LVEDP, a hallmark of diastolic hemodynamic stress and non-invasive CMR parameters. These can be summarized as follows:

1. There is no clear distinction between patients with normal and elevated LVEDP, in terms of cardiac remodeling or structure when generic CMR parameters, such as volumes, EF, LV mass, ECV or atrial volume or function, are considered.
2. CMR FT derived myocardial systolic strain is on average more pronounced in patients with elevated LVEDP, with a subgroup of these patients exhibiting higher than normal values of GLS and GCS

3. CMR FT derived myocardial diastolic properties (in particular modelled HD Early Diastolic Force) are also more pronounced in patients with elevated LVEDP, suggesting an increased early diastolic stress to maintain circulatory demands
4. Integrating Systolic GCS and HD Early Diastolic Force in a predictive model offers a promising new tool for non-invasive identification of patients with elevated LVEDP, comparable with the current diagnostic algorithms offered by electrocardiography.

Elevated LVEDP is an established risk factor for developing HF and is directly associated with a higher cardiovascular mortality. The mechanisms that lead to an increase in LV filling pressures are only partially known and complex. Similarly, the relation between chronically elevated LV filling pressures and cardiac remodeling are insufficiently explored, one of the main reasons being the lack of adequate tools to estimate LV filling pressures in vivo. To date, available imaging methods are not equipped to measure hemodynamic pressure therefore surrogate markers of either cardiac mechanics (such as systolic and diastolic myocardial strain and strain-rate), or blood flow velocity (based on Bernoulli equation the dynamic pressure in a fluid is a function of velocity). In this sense, systematic attempts to reliably approximate LV filling pressure using a battery of echocardiography derived parameters have been made, however the accuracy of such approaches remains low and as yet far-fetched for daily clinical practice.

In agreement with previous studies, using a porcine model we indicated that when challenged by increased tissular metabolic requirements (physical effort, obesity etc.), cardiac inotropic function in normal conditions becomes higher than baseline in order to satisfy elevated demands. [248] So far, some studies shown mildly decrease LV systolic function in HFpEF and most of them, including ours (Chapter 3) indicated that

systolic strain remains largely unchanged when compared with healthy counterparts. Previous studies underlined the revealing role played by stress imaging or invasive hemodynamics in the diagnostic of HFpEF[249,250] and, on the other hand, the reduced contractile reserve. [251] More recently, cardiac energetic deficit (measured using MR spectroscopy as phosphocreatine/ATP ratio) was shown to be frequently present in patients with HFpEF or predisposing conditions (hypertension, type 2 diabetes), elicited by minor physical effort and correlated to the systolic and diastolic contractile reserve. [252] We showed here, against current paradigms, that in patients with higher LVEDP there was proportionally more systolic deformation in both longitudinal (GLS) and circumferential axes (GCS) at rest (**Figure 5.4 A** and **B**). It is therefore intriguing to speculate that reduced augmentation of contractile force from rest to stress observed in HFpEF may be due to higher baseline levels of systolic contraction. Moreover, it can be speculated that elevated LVEDP represents an early stage that precedes functional decompensation at rest and development of HF symptoms.

The main pathogenic mechanism described in HFpEF are triggered by a complex of often interrelated risk factors such as obesity, insulin-resistance, endothelial dysfunction with increased oxidative stress which increase inflammation and further determine myofibroblast activation leading to diffuse fibrosis, endotheliitis and microvascular dysfunction. [253] Myocytes physiology remains intact until later when impaired relaxation and ‘stiffening’ produced by a phosphorglyceratkinase (PGK) mediated switch in titin subtypes determines impaired diastolic relaxation and chamber filling. Increased stiffness is produced mainly through increased deposition of diffuse fibrosis [254,255] Previous studies have shown increased ECV in HFpEF patients and underlined the potential role it can have as a diagnosis e.g. against hypertensive heart without HF. [256] Raised ECV is likely due to an increase in diffuse collagen deposition[257],

however current guidelines are focused on early commencement of disease modifying agents such as ACEi or ARB with an efficient anti-fibrotic action[258] and on early institution of firmer limitation of the risk factors (obesity, diabetes, hypertension, dyslipidemia). In our cohort, only 32 out 131 (24%) patients had elevated ECV, 8 out of 38 (21%) in LVEDP<16 and 24 out of 93 (26%) in LVEDP≥16 groups, respectively. Additionally, we observed similar trends in the HFpEF subgroup analysed in the study presented in Chapter 3, where only 5 out of 20 (25%) patients had raised ECV.

Limitations

Contemporaneous echo data were available in a limited number of patients and therefore we cannot offer here a comparative analysis between the accuracy of echocardiographic and CMR methods in estimating LVEDP. Our data however suggest an important additional role of CMR FT in the assessment of diastolic function.

We did not assess velocity encoded mitral blood flow, feasible with CMR, that would have given us the possibility to assess directly these two important parameters used to estimate diastolic properties of the heart. To overcome this limitation, we used for our study accurate LV volume and volume-rate curves resulting from a Simpson approximation of the intraventricular blood over the cardiac cycle. Previous studies attribute to this method a good approximation ability of velocity-encoded measured flow. LVEDP represents just a discrete value of the pressure-volume curve and therefore a normal LVEDP at rest does not exclude completely a certain degree of diastolic dysfunction or HFpEF and it is possible that among these exist a significant number of patients with markedly reduced exercise capacity and contractile reserve.[259] An inherent selection bias results from the study design, we only included patients that were referred for both CMR and left heart catheterization, which implies a higher

burden of cardiovascular risk factors and symptoms than in a generic population of patients with diastolic dysfunction.

Clinical Implications

Non-invasive routine assessment of LVEDP in patients with cardiovascular risk factors would allow to early recognition of this specific phenotype and the tailoring of specific treatments such as diuretics, able to decongest the systemic circulation and reduce afterload. Betablockers are frequently prescribed in HFpEF for comorbidities such as CAD or AF, however their benefit in improving mortality in HFpEF patients has been shown to be uncertain by randomized clinical trials [260]. Our data suggest that an exacerbated systolic and diastolic contractility may be a therapeutic target in patients with elevated LVEDP. CMR holds the promise to pave the way for a phenotypic classification of HFpEF much warranted in clinical practice and for in this endeavor concomitant non-invasive evaluation of intracardiac hemodynamics may maintain a preeminent role.

Chapter Six:

Cardiac Phenotype in Adult Patients with Phenylketonuria

The work presented in this chapter is based on the article “Cardiac Magnetic Resonance Reveals Incipient Cardiomyopathy Traits in Adult Patients With Phenylketonuria” previously published in the Journal of the American Heart Association. I am the first author of this study and had the main contribution in study design, analysis and presentation of scientific data and in writing the manuscript.

6.1 Abstract

Phenylketonuria (PKU) is the most common inborn error of amino-acid metabolism where oxidative stress and collateral metabolic abnormalities are likely to cause cardiac structural and functional modifications. We aim here to characterize the cardiac phenotype of adult subjects with PKU using advanced cardiac imaging.

Thirty-nine adult patients with PKU (age 30.5±8.7 years old, mean 10 years phenylalanine concentration (Phe) 924±330 µmol/L) and thirty-nine age- and sex-matched healthy controls were investigated. Participants underwent a comprehensive cardiac magnetic resonance (CMR) and echocardiography examination. 10-year-averaged plasma levels of Phe and Tyrosine (Tyr) were used to quantify disease activity and adherence to treatment.

PKU patients had thinner LV walls (Septal end-diastolic (ED) thickness 7.0±17 vs 8.8±1.7 mm, p<0.001, lateral thickness 6.1±1.4 vs 6.8±1.2 mm, p=0.004), more dilated LV cavity (EDV: 87±14 vs 80±14 mL/m2, p=0.0178, ESV: 36±9 vs 29±8 mL/m2, p<0.001), lower EF (59±6 vs 64±6%, p<0.001) and reduced systolic deformation (global circumferential strain (GCS): -29.9±4.2 vs -32.2±5.0, p=0.027) and lower LV mass (38.2±7.9 vs 47.8±11.0, p<0.001). T1 native values were decreased (936±53 vs 996±26 ms, p<0.001), with particular low values in patients with Phe >1200µmol/L (909±48 ms). Both mean Phe (p=0.013) and Tyr (p=0.035) levels were

independently correlated with T1 and in a multiple regression model, higher Phe levels and higher LVM associate lower T1.

Cardiac phenotype of adult patients with PKU reveals some traits of an early stage cardiomyopathy. Regular cardiology follow-up, tighter therapeutic control and prophylaxis of cardiovascular risk factors, in particular dyslipidemia, are recommended.

6.2 Background

With an incidence of approximately 1:10.000-1:15.000, Phenylketonuria is the most common inborn error of amino-acid metabolism.[133], which is characterized by a low activity of phenylalanine hydroxylase (PAH), an enzyme responsible for the conversion of the essential amino acid phenylalanine (Phe) to tyrosine (Tyr). Lack of PAH activity in untreated individuals leads to severe structural brain damage, with complex psychological alterations and mental retardation, seizures and spasticity. [261-263] Since the institution of newborn screening strategies in 1960s[264] followed by immediate beginning a Phe-low diet combined with Phe-free amino-acid supplementation[139], excellent progresses has been made regarding the neuropsychological complications and intellectual development. This diet should be followed by PKU patients lifelong,[265] however, a good constant adherence during adulthood is sometimes difficult to achieve. Moreover, little is known about the long-term efficacy of the PKU diet and about putative consequences of this highly selective food intake supported by periodic intermittent Phe-free aminoacid supplementations.

A series of potential cardiovascular risk factors have been associated with the disease, triggered by persistent metabolic abnormalities or by special, restrictive diet. Several studies identified increased levels of oxidative species resulting from the abnormal

cellular metabolism[146] as well as from weaker cellular anti-oxidative defense (in particular, PKU patients have lower levels of selenium, ubiquinone-10 and L-carnitine).[266] Corollary, increased levels of pro-inflammatory plasma cytokines such as interleukin-6 and interleukin-1β contribute to protein oxidation and lipid peroxidation. [267] Most studies agree that adult PKU patients frequently display a certain degree of dyslipidemia[154] but not necessarily overt obesity or insulin resistance[268], despite their vegan diet, in principle anti-atherogenic[139]. Several studies found previously lower HDL cholesterol concentrations[269,270] and higher concentrations of LDL Cholesterol [148,271] and triacylglycerol [269]. Recently, a vascular phenotype consisting in endothelial dysfunction and increased arterial stiffness, measured non-invasively with ultrasound, was identified in adult PKU patients. [148]

So far, no study evaluated comprehensively the cardiac phenotype in adults with PKU. Cardiac magnetic resonance (CMR) is the current gold standard to evaluate cardiac dimensions and function[113]. In addition, novel protocols based on parametric mapping, provide crucial information about cardiac structural modifications such as interstitial fibrosis, inflammation and substrate accumulation in the extracellular space. [272]

Here we characterized a cohort of adult patients with classical PKU, using advanced CMR and echocardiography and compared their cardiac phenotype to that of age- and sex-matched healthy individuals.

6.3 Specific Methods

6.3.1 Study Population

A total number of 43 adult patients with an established diagnostic of PKU were recruited prospectively from the Interdisciplinary Center for Metabolism: Endocrinology, Diabetes and Metabolism of Charité University Berlin. The following

inclusion criteria were used: age over 18 years, absence of any generic contraindication for CMR (claustrophobia, cardiac pacemakers or defibrillators, metallic implants such as artificial valves or cerebral aneurysm clips, morbid obesity), signed consent to participate in all the stages of our protocol. Patients with any cardiac pathology (more than trivial valve disease, uncontrolled systemic hypertension, coronary artery disease, previous myocardial infarction, cardiac arrhythmias) were excluded from the study. Four patients were excluded due to incomplete compliance with the protocol. Thus, thirty-nine patients completed all the stages of our protocol and their data were available for the functional analysis of the cardiac phenotype. A complete set of parametric imaging of sufficient quality to characterize the myocardial phenotype was obtained in 36/39 patients. For comparison an age- and sex- matched group of 39 volunteers who underwent a similar protocol was included in the study. Controls were investigated without the administration of contrast medium and, therefore T1 post-contrast and ECV could not be assessed directly. Controls were selected from our volunteer database at German Heart Center Berlin and partially characterized previously. [183,273]

6.3.2 Cardiac magnetic resonance – details presented in Chapter 2.

6.3.3 Image analysis – details presented in Chapter 2.

6.3.4 Echocardiography – details presented in Chapter 2.

6.3.5 Biochemistry

During the visits routine haematological and biochemical parameters were determined. Median values of Phe and Tyr plasma concentrations were calculated using all the data available covering a period of approximately 10 years before the date of the CMR scan, obtained from the Interdisciplinary Center for Metabolism of the Charité University Berlin. These average concentrations were based on at least 20 single

determinations (range 20-60 determinations for each PKU patient). Phe and Tyr concentrations were measured in dried blood spots using mass spectrometry. In addition, data obtained in the same laboratory unit, the most recent serum levels of total cholesterol, low-density lipoprotein (LDL) cholesterol, high-density lipoprotein (HDL) cholesterol, triglycerides, carnitine free fraction and total, and glucose were obtained. All determinations were performed in duplicate by the Hospital laboratory as part of the routine clinical evaluation of the patients (Labor Berlin - Charité Vivantes GmbH.)

6.3.6 Statistical Analysis

Statistical analysis was carried out with IBM SPSS version 26. Normality of variables was assessed by visual assessment of normality curves and the Shapiro-Wilk test. Comparison between groups for continuous variables was performed with a 2-sided, independent-samples Student t test for normally distributed data and Mann-Whitney and Kruskal-Wallis tests for skewed data. For categorical variables, comparison was done with a $\chi 2$ test and statistical significance evaluated with Fisher's exact test. Univariate and bivariate regressions models with T1 native as dependent variable and Phe and Tyr as predictors were used. To further test the dependency of T1 native on Phe levels, we built a stepwise multiple regression with T1 native as dependent variable T1, and Phe levels as independent, controlled for several clinically relevant covariates: plasma concentrations of lipids, LVmass, EF, age and sex, and having criteria for entry 0.05 and for removal 0.10. Unstandardized regression coefficients (B) were reported for univariate and bivariate regression models, unstandardized and standardized coefficients (B) for multiple regression model. To compare the three subgroups of PKU patients divided according to the Phe concentrations, a one-way ANOVA for normally distributed data and, respectively Kruskal-Wallis for non-normally

distributed data were performed followed by Tukey post-hoc tests to compare differences among subgroups. Results are presented as mean±SD. Values of P <0.05 were considered statistically significant.

6.4 Results

6.4.1 Population Characteristics

A complete set of these values is presented in **Table 6.1**. There was an equivalent distribution of comorbidities between the PKU and the control group. PKU patients have a slightly higher BMI when compared with the control group (25.7±5.0 vs 23.7±3.3 kg/m2, p=0.03). Among the PKU patients, 10 years median Phe concentration was 924±330 µmol/L. However, 21 out of 39 (54%) of the PKU patients had poor adherence with Phe values above 900 µmol/L. [274] Moreover, 27 out of 39 patients had a Phe concentration above the critical concentration of 800 µmol/L, associated with high oxidative stress and tissue damage [275] and specific structural and functional cerebral modifications. [261] 17 out of 39 (44%), of PKU patients had a certain degree of dyslipidemia, most frequently reduced HDL-cholesterol levels (14 out of 17, 82%). In addition, elevated concentrations of triglycerides (8 out of 17, 47%) or LDL-cholesterol (10 out of 17, 59%) were observed.

6.4.2 Cardiac anatomy and function in PKU patients.

All quantitative date are presented in **Table 6.2**. We primarily compared the PKU cohort and controls with respect to the size, structure and function of the heart. PKU subjects had a more dilated heart than controls: (EDV 87±14 vs 80±14 ml/m^2, p=0.018, ESV 36±9 vs 29±8 ml/m2, p<0.001) (**Figure 6.1 A, B**) with thinner walls (septal WT 7.0±17 vs 8.8±1.7 mm, p<0.001, lateral WT 6.1±1.4 vs 6.8±1.2 mm, p=0.042) and an important reduction in LV mass (38.2±7.9 vs 47.8±11.0 g/m2, p<0.001) (**Figure 6.1 G**). LV mass

Table 6.1 Characteristics of Study Population

	PKU Patients (n=39)	Control (n=39)	P*
Demographics			
Age, y	30.5±8.7	31.3±8.9	0.43
Males, n (%)	23 (55%)	21 (50%)	0.82
Smokers, n (%)	11 (26%)	12 (29%)	0.98
Anthropometrics			
Height, cm	172±10	174±10	0.42
Weight, kg	76±17	72±14	0.19
BMI, kg/m2	25.7±5.0	23.7±3.3	***0.030***
BSA, m2	1.86±0.37	1.86±0.21	0.99
Bioelectrical impedance			
Fat mass, kg	18.3±9.3		
Fat-free mass, kg	56.2±11.0		
Ratio fat / fat-free mass	0.34±0.19		
Visceral fat, kg	5.1±3.0		
BMR, J/(h·kg)	1670±305		
Muscle mass, kg	53.4±11.0		
Body Water, kg	41.1±8.0		
Clinical			
Heart Rate, bpm	64±9	62±11	0.39
Systolic BP, mmHg	114±15	112±8	0.75
Diastolic BP, mmHg	66±9	67±7	0.87
Pulse pressure, mmHg	47±11	46±8	0.57
Biochemistry			
Phe Mean, µmol/L	924±330		
Phe Median, µmol/L	915±326		
Phe SD, µmol/L	200±80		
Tyr Mean, µmol/L	80±23		
Tyr Median, µmol/L	76±25		
Tyr SD, µmol/L	33±14		
Carnitin free, mg/dL	34.9±10.9		
Carnitin total, mg/dL	50.5±14.0		
Carnitin ratio free/total	0.71±0.16		
Cholesterol total, mg/dL	164±33		
HDL-Cholesterol, mg/dL	47.3±13.7		
LDL-Cholesterol, mg/dL	92.8±26.3		
Triglycerides, mg/dL	150±98		
Glucose, mg/dL	78±16		

Abbreviations: BMI – body mass index, BSA – body surface area, BMR – basal metabolic rate, BP – blood pressure, Phe – phenylalanine, Tyr – tyrosine. Values as are given as mean±SD unless stated otherwise. P* PKU patients versus age and sex matched controls.P values were adjusted with the Bonferroni method. Abbreviations: Phe – 10 years average plasma phenylalanine, Tyr – 10 years average plasma tyrosine

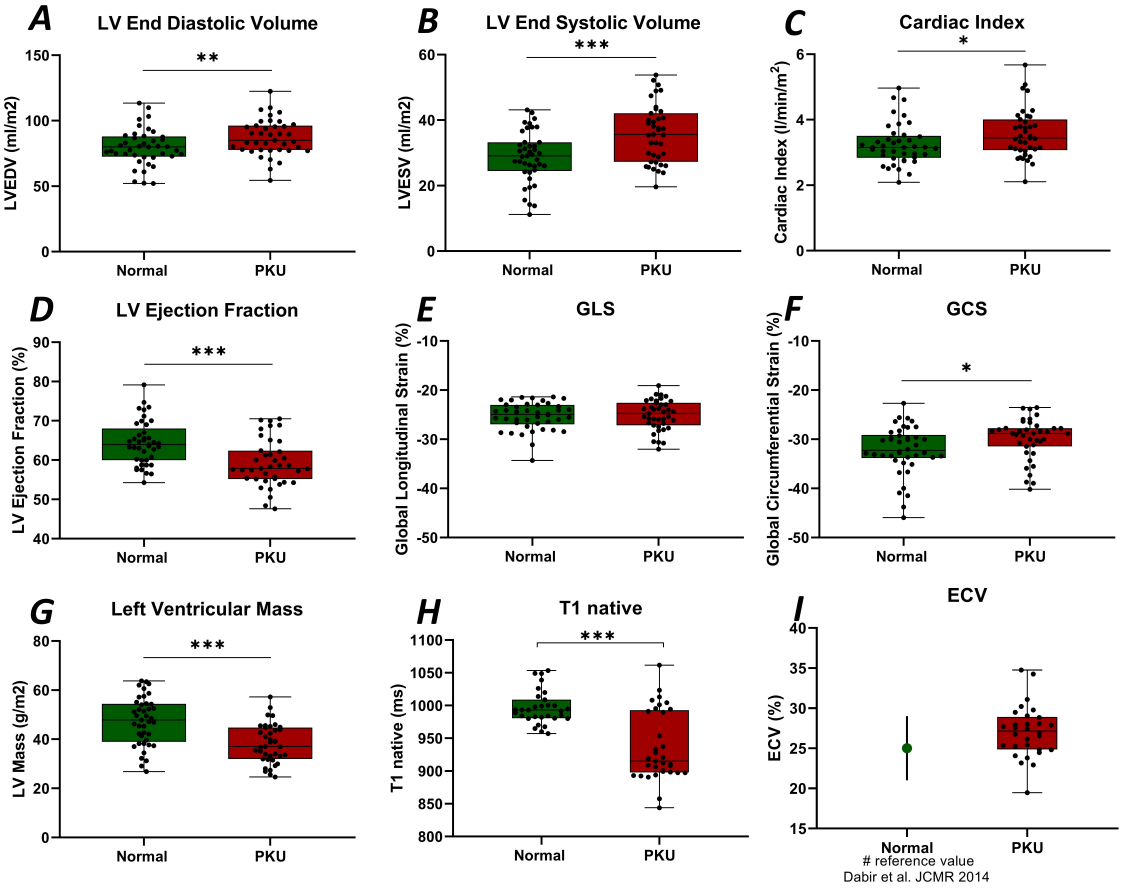


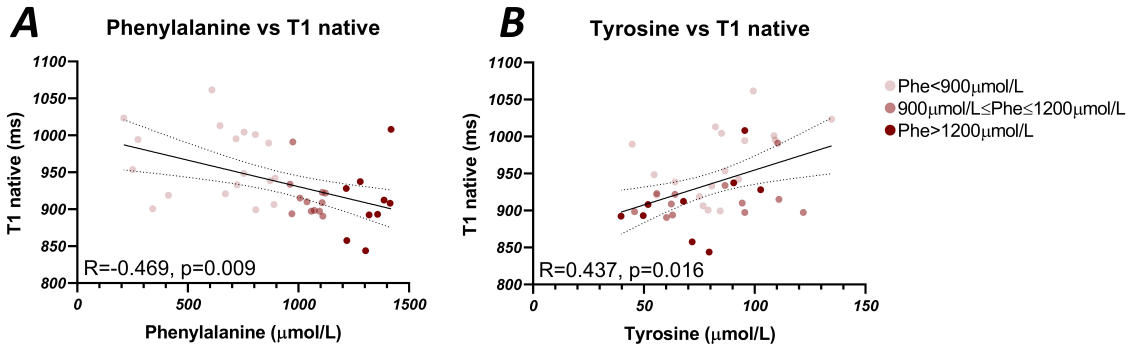
Figure 6.1 Cardiac Structural and Functional Remodeling in Adult Patients with Phenylketonuria and age- and sex- matched Control. **A.** LV end-diastolic volume, **B.** LV end-systolic volume, **C.** Cardiac Index, **D.** LV ejection fraction, **E.** Global Longitudinal Strain, **F.** Global Circumferential Strain, **G.** LV Mass, **H.** T1 native, **I.** ECV (# mean and SD referenced in literature (Dabir et al., *J Cardiovasc Magn Reson.* 2014; 16:69) for similar scanner and magnetic field strength). A P<0.05 was considered statistically significant. *P<0.05, **P<0.01, ***P<0.001. Abbreviations: LV – left ventricle, GLS – Global Longitudinal Strain, GCS – Global Circumferential Strain, ECV – extracellular volume, SD – standard deviation.

deficit remained significant even when indexed with EDV (0.44±0.06 vs 0.61±0.12 g/mL, p<0.001). LV EF (59±6 vs 64±6%, p<0.001) and LV GCS (-29.9±4.2 vs -32.2±5.0%, p=0.027) are reduced but not GLS (**Figure 6.1 D, E, F**). E/A ratio was within normal limits, with an increased early trans-mitral flow velocity. LA volumes were not different from control, but LA emptying fraction and LA strain were increased suggesting increased atrial pressures. RV ejection fraction was not significantly

Table 6.2 Cardiac structure and function in PKU patients.

	PKU Patients (n=39)	Control (n=39)	P*
Left Ventricle			
ED volume, mL/m^2	87±14	80±14	***0.018***
ES volume, mL/m^2	36±9	29±8	***<0.001***
Stroke volume, mL/m^2	51±8	51±8	0.83
Ejection fraction, %	59±6	64±6	***<0.001***
Cardiac Index, L/min/m^2	3.57±0.74	3.25±0.63	***0.037***
GLS Endo %	-25.1±3.1	-25.3±2.8	0.74
GLS Myo, %	-24.1±2.8	-24.1±2.1	0.94
GLS Endo-Epi Gradient, %	-2.6±1.8	-3.3±2.2	0.13
GCS Endo %	-29.9±4.2	-32.2±5.0	***0.027***
GCS Myo, %	-20.7±3.3	-21.7±3.2	0.09
GCS Endo-Epi Gradient, %	-15.0±3.2	-17.7±4.3	***0.001***
Septal ED WT, mm	7.0±17	8.8±1.7	***<0.001***
Lateral ED WT, mm	6.1±1.4	6.8±1.2	***0.042***
Relative WT	1.15±0.15	1.32±0.23	***<0.001***
LV Mass (g/m^2)	38.2±7.9	47.8±11.0	***<0.001***
LV Mass/ED volume, g/mL	0.44±0.06	0.61±0.12	***<0.001***
LV ED maximal diameter mm	53±4	52±5	0.10
HD Systolic Force (%)	37.7±13.5	31.4±10.1	***0.021***
HD Systolic Work (%)	5.1±2.2	5.4±4.6	0.74
HD Systolic Work (mJ)	4.8±2.5	4.0±1.8	0.09
HD Systolic Power (mJ/s)	57.8±37.3	42.1±22.1	***0.024***
HD Early Diastolic Force (%)	-24.3±9.8	-17.6±9.0	***0.002***
HD Early Diast Work (%)	-1.9±1.0	-1.2±0.7	***0.001***
HD Early Diast Work (mJ)	-1.6±0.6	-0.9±0.7	***<0.001***
HD Early Diast Power (mJ/s)	-26.5±11.4	-15.5±14.0	***<0.001***
HD Late Diast Force (%)	-6.8±3.8	-8.5±4.6	0.09
Left Atrium			
LA max Vol mL	37.2±8.0	35.1±9.3	0.29
LA min Vol mL	10.7±3.3	11.3±5.7	0.57
LA emptying fraction %	71±5	67±8	***0.012***
LA strain %	49.5±12.5	40.5±15.5	***0.008***
Right Ventricle			
RV Vol max	46.2±11.2	42.2±10.7	0.11
RV Vol min	17.2±6.7	14.8±5.0	0.07
RV ejection fraction %	62.7±7.9	65.4±6.7	0.11
RV longitudinal strain %	-25.0±5.5	-29.0±5.7	***0.002***
Ascending Aorta			
Systolic aortic diameter, mm	45.5±0.9	41.9±1.0	0.25
Diastolic aortic diameter, mm	35.2±0.9	32.7±0.8	0.38
Aortic distensibility, 10^{-3}mmHg^{-1}	6.76±2.60	6.40±1.54	0.64
Echocardiography			
MV E Vmax (cm/s)	80±14	71±17	***0.020***
MV A Vmax (cm/s)	52±13	61±19	***0.046***
MV E/A	1.61±0.43	1.32±0.60	***0.027***
E/e‘	6.36±2.27	5.18±1.44	0.11
	PKU Patients (n=36)	Control (n=39)	P*
Parametric Imaging			
T1 native	936±53	996±26	***<0.001***
T1 post contrast	592±45		
ECV (%)	26.5±4.4	25.0±4.0#	0.15

Values as are given as mean±SD unless stated otherwise. P* PKU patients versus age and sex matched controls. All P values were adjusted with the Bonferroni method. A P value < 0.05 was considered statistically significant and marked with § Abbreviations: ED end-diastolic, ES end-systolic, LV left ventricle, LA left atrium, RV right ventricle, HD hemodynamic, MV mitral valve, ECV extracellular volume. (# mean and SD referenced in literature (Dabir et al., *J Cardiovasc Magn Reson.* 2014; 16:69) for similar scanner and magnetic field strength



C

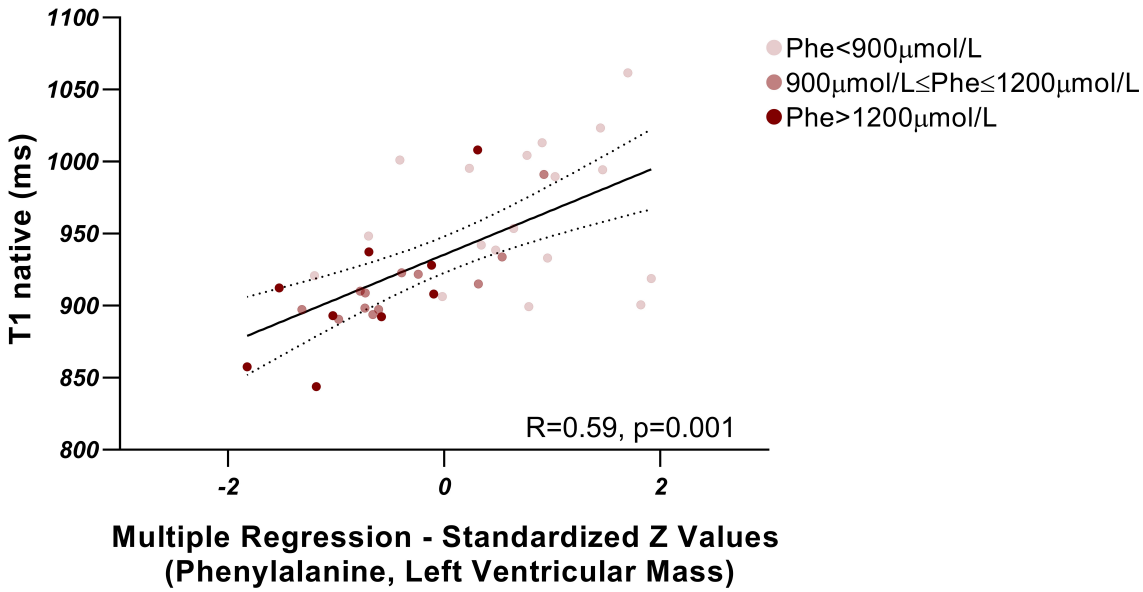
	B coefficient (per T1 unit)	95% Confidence Interval Lower Bound	Upper Bound	P Value
Univariate Regression				
Phenylalanine, μmol/L	-0.072	-0.115	-0.028	0.002 §
Tyrosine, μmol/L	0.943	0.302	1.583	0.005 §
Bivariate Regression (Phenylalanine and Tyrosine)				
Phenylalanine, μmol/L	-0.056	-0.100	-0.013	0.013 §
Tyrosine, μmol/L	0.679	0.049	1.309	0.035 §

Figure 6.2 Uni- and bivariate regression to determine the relation between 10 years average levels of phenylalanine and tyrosine and T1 native values. **A.** Linear regression between phenylalanine plasma levels and T1, **B.** Linear regression between tyrosine plasma levels and T1, (continuous line represents the regression best fit equation line and the dotted lines the 95% confidence limits) **C.** Regression parameters and B coefficients. A P<0.05 was considered statistically significant – Phenylalanine (Phe) and Tyrosine (Tyr) plasma levels predict independently T1 values indicating that therapeutic intervention not only to reduce Phe levels but also to augment the Tyr levels may be beneficial to correct cardiac changes. § indicates P<0.05 considered statistically significant.

decreased, however the means for RV ejection fraction and RV GLS were lower in the PKU group (**Table 6.2**).

6.4.3 Parametric imaging and correlations with plasma Phe concentrations.

Compared with control, T1 native relaxation time was shorter in the PKU group (936±53 vs 996±26ms, p<0.001) (**Figure 6.1 H**). We did not administer contrast to the volunteers participating in the study, and for comparing ECV data, we used reference values, corresponding to the scanner model and protocol used in our center, published elsewhere. [132] There was no difference in the ECV between the PKU patients and this reference value (26.5 ± 4.4 vs 25.0 ± 4.0%, p=0.15) (**Figure 6.1 I**). T1 values were negatively correlated with Phe (r=-048, p=0.002) (**Figure 6.2 A**) and positively with Tyr



	β coefficient (standardized)	B coefficient (per T1 unit)	95% Confidence Interval Lower Bound	Upper Bound	P Value
Multiple Regression					
Phenylalanine, µmol/L	-0.34	-3.20	-5.95	-0.46	0.024 §
Left Ventricular Mass (g/m²)	-0.43	-2.54	-4.27	-0.80	0.005 §

Figure 6.3 In a multivariate regression model the independent predictors of T1 native are the averaged levels of plasma Phe (B coefficient standardized: -0.34) and respectively Left Ventricular Mass (β coefficient standardized: -0.43), both negatively correlated with T1 native times. These data suggest that the pathologic substrate that may be responsible for lower T1 times is associated with a higher LVM and a poor control of the disease or adherence to specific diet (leading to chronically elevated Phe concentrations). § indicates P<0.05 considered statistically significant.

(r=0.44, p=0.005) (**Figure 6.2 B**) suggesting that shorter, more abnormal, T1 values associate with poor dietery adherence among PKU patients. To establish the individual and cumulative effect of Phe and Tyr concentrations for T1 values we performed univariate and bivariate multiple regression, results are presented in **Figure 6.2 C**.

On the other hand, T1 values correlated negatively with LVM (r=-0.50, p=0.004) (**Figure 6.3**), septal WT (r=-0.52, p=0.001) and lateral WT (r=-0.49, p=0.001) indicating that lower relaxation times correspond to an increase in mass and wall thickness of the myocardium. There was no association between T1 values and parameters characterizing LV systolic function but T1 was correlated with E/e' ratio (R=-0.487, p=0.004), suggesting that an incipient LV impaired lusitropy may be related

Table 6.3 Cardiac structure and function in PKU patient subgroups divided according to 10 year mean phenylalanine plasma concentrations: Phe≤900µmol/L, 900<Phe≤1200 µmol/L, Phe>1200 µmol/L

	Phe≤900µmol/L (n=18)	900<Phe≤1200 µmol/L (n=12)	Phe>1200 µmol/L (n=9)	P ANOVA	P†	P‡	P#
Left Ventricle							
ED Volume, mL/m²	84±14	92±13	86±14	0.31			
ES Volume, mL/m²	35±9	37±9	37±10	0.75			
Stroke volume, mL/m²	50±8	56±8	49±7	0.09			
Ejection Fraction, %	59±6	61±6	57±6	0.45			
GLS Endo %	-25.4±3.4	-25.6±2.3	-23.9±3.3	0.41			
GLS Myo, %	-24.8±3.2	-24.1±2.0	-22.8±2.5	0.23			
GLS Endo-Epi Gradient, %	-2.1±1.9	-3.3±1.8	-2.6±1.2	0.22			
GCS Endo %	-30.3±4.1	-30.1±3.6	-28.9±4.0	0.69			
GCS Myo, %	-21.2±3.4	-21.3±3.5	-19.0±2.4	0.20			
GCS Endo-Epi Gradient, %	-15.0±3.2	-15.0±3.5	-15.3±2.8	0.97			
Cardiac Index	3.4±0.6	3.9±0.7	3.5±1.0	0.27			
Septal ED WT, mm	6.7±1.7	6.9±1.6	7.8±1.9	0.26			
Lateral ED WT, mm	5.8±1.4	6.1±1.1	6.8±1.7	0.26			
Relative WT	1.16±0.15	1.13±0.15	1.16±0.15	0.82			
LV Mass g/m²	36.7±8.3	40.1±6.7	38.5±8.7	0.52			
LV Mass/ED volume, g/mL	0.43±0.07	0.44±0.06	0.45±0.06	0.90			
LV ED max Diam, mm	52±5	53±4	56±4	0.10			
HD Systolic Force (%)	36.9±13.6	40.2±15.9	35.8±10.6	0.73			
HD Systolic Work (%)	5.0±2.2	5.5±2.4	4.9±2.0	0.79			
HD Systolic Work (mJ)	4.1±1.6	5.6±3.2	5.1±2.6	0.26			
HD Systolic Power (mJ/s)	51.5±29.9	69.0±52.2	-55.3±26.3	0.45			
HD Early Diastolic Force (%)	-25.8±11.8	-24.5±6.2	-21.2±9.5	0.54			
HD Early Diast Work (%)	-2.1±1.2	-1.8±0.7	-1.5±0.7	0.26			
HD Early Diast Work (mJ)	-1.7±0.7	-1.6±0.5	-1.4±0.6	0.55			
HD Early Diast Power (mJ/s)	-27.7±13.2	-27.1±10.3	-23.4±9.2	0.65			
HD Late Diast Force (%)	-6.6±2.6	-8.0±4.3	-5.3±5.2	0.30			
Left Atrium							
LA max Vol mL/m²	37±6	39±7	34±12	0.37			
LA min Vol mL/m²	11±3	11±3	10±4	0.29			
LA emptying fraction %	70±6	73±4	73±5	0.37			
LA strain %	49.1±15.3	51.0±9.8	48.0±9.6	0.87			
Right Ventricle							
RV Vol max mL/m²	45±10	49±14	45±11	0.51			
RV Vol min mL/m²	17±7	18±7	18±5	0.97			
RV ejection fraction %	62±9	64±8	61±6	0.65			
RV longitudinal strain %	-25.2±4.8	-26.5±4.9	-22.5±7.2	0.26			
Ascending Aorta							
Systolic Ao. Diam., mm	46.2±9.4	44.2±9.2	45.2±10.1	0.81			
Diastolic Ao. Diam., mm	36.0±9.4	33.4±8.3	35.7±10.3	0.91			
Ao. distens. 10^{-3}mmHg^{-1}	7.96±2.99	6.48±1.84	6.48±3.04	0.39			
Echocardiography							
MV E Vmax (cm/s)	75±12	80±14	80±13	0.52			
MV A Vmax (cm/s)	49±13	54±7	50±15	0.56			
MV E/A	1.64±0.38	1.51±0.38	1.70±0.48	0.50			
E/e‘	5.24±1.62	5.87±1.57	8.33±1.74	***<0.001***	0.62	***<0.001***	***0.001***
Plasma Lipids							
Total Chol (mg/dL)	155±31	161±31	173±43	0.47			
Trigylcerides (mg/dL)	126±57	113±83	241±111	***0.002***	0.91	***0.004***	***0.003***
HDL Chol (mg/dL)	52±14	48±10	42±13	0.17			
LDL Chol (mg/dL)	86±19	94±28	99±31	0.41			
LDL/HDL Chol	1.70±0.34	2.03±0.68	2.54±0.82	***0.008***	0.32	***0.006***	0.15
	Phe≤900µmol/L	900<Phe≤1200 µmol/L	Phe>1200 µmol/L				
Parametric Imaging	(n=18)	(n=9)	(n=9)				
T1 native	964±48	915±27	909±48	***0.003***	***0.012***	***0.001***	0.94
T1 post contrast	591±56	613±33	577±25	0.25			
ECV	27±9	27±4	26±2	0.72			

Values as are given as mean±SD unless stated otherwise. PANOVA analysis between the 3 groups, divided according to median 10 years value of plasma phenylalanine (Phe) concentrations: group 1 – Phe≤15mg/dL, group 2 – 15<Phe≤20mg/dL, group 3 – Phe>20mg/dL. P† comparison between group 1 and group 2, P‡ comparison between group 1 and group 3, P# comparison between group 2 and group 3. All P values were adjusted with the Bonferroni method. A P value < 0.05 was considered statistically significant. Abbreviations: ED end-diastolic, ES end-systolic, LV left ventricle, LA left atrium, RV right ventricle, Ao. aorta, Diam. diameter, MV mitral valve, ECV extracellular volume.

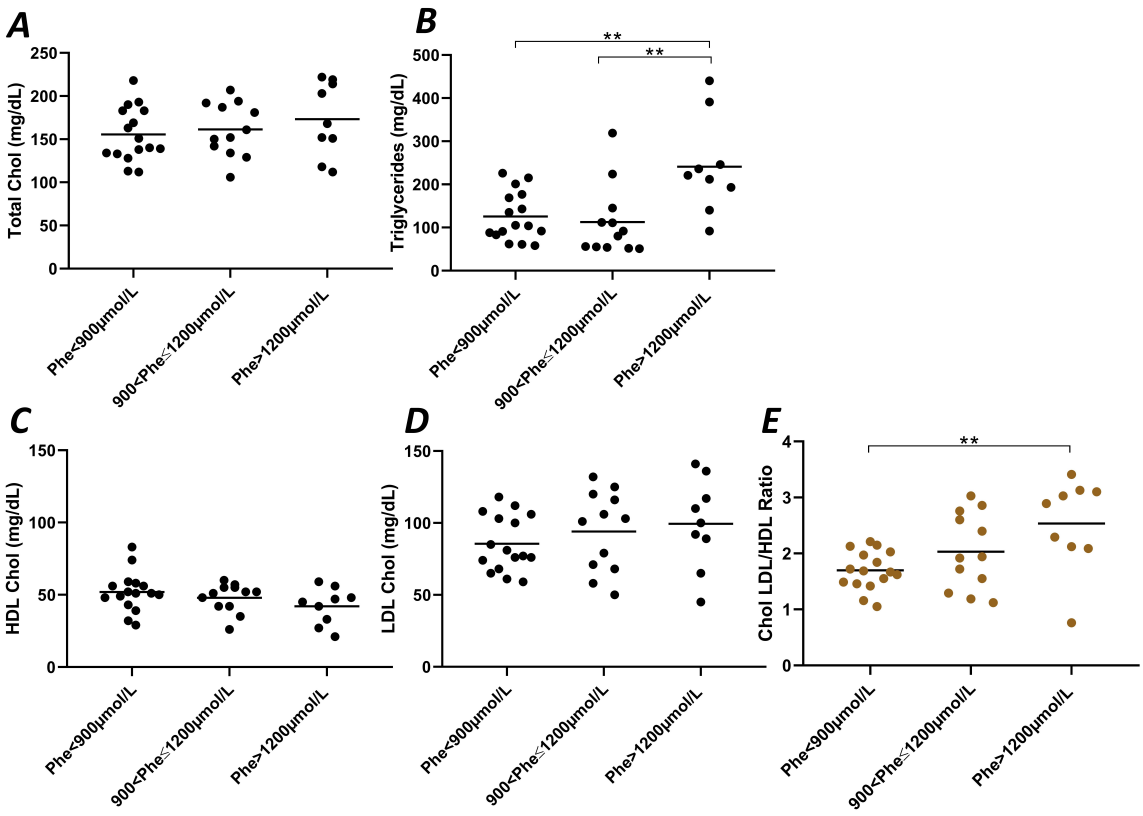


Figure 6.4 Lipid profile in 3 subgroups of adult Phenylketonuria patients divided according to the 10 years mean Phe level (from left to right in each graph: group 1 – Phe≤900µmol/L, group 2 – 900<Phe≤1200µmol/L, group 3 – Phe>1200µmol/L): **A.** Total cholesterol, **B.** Triglycerides, **C.** HDL Cholesterol, **D.** LDL Cholesterol, **E.** LDL/HDL Cholesterol Ratio. Significant differences were recorded between the level of Triglycerides and LDL/HDL Cholesterol Ratio, with a more pronounced dyslipidemic profile observed in patients with poor control of the disease (i.e. higher mean Phe values). Abbreviations: Phe – phenylalanine, HDL – high-density lipoprotein, LDL – low-density lipoprotein, Chol – cholesterol.

to these presumed structural abnormalities. In a multivariable regression model T1 as dependent variable was predicted by Phe (standardized beta -0.34, p=0.024) and LVM (standardized beta -0.43, p=0.005) with a resultant R=0.59, p=0.001 **(Figure 6.3)**.

To test any association with the cardiac phenotype, we compared the lipid plasma concentrations with structural and functional parameters. Total cholesterol (r=-0.40, p=0.021) and HDL fraction (r=-0.45, p=0.009) but not LDL fraction or triglyceride concentration, correlated inversely with LVM. Taken together these findings indicate that reduced levels of HDL-cholesterol, which is most frequently seen in PKU subjects,

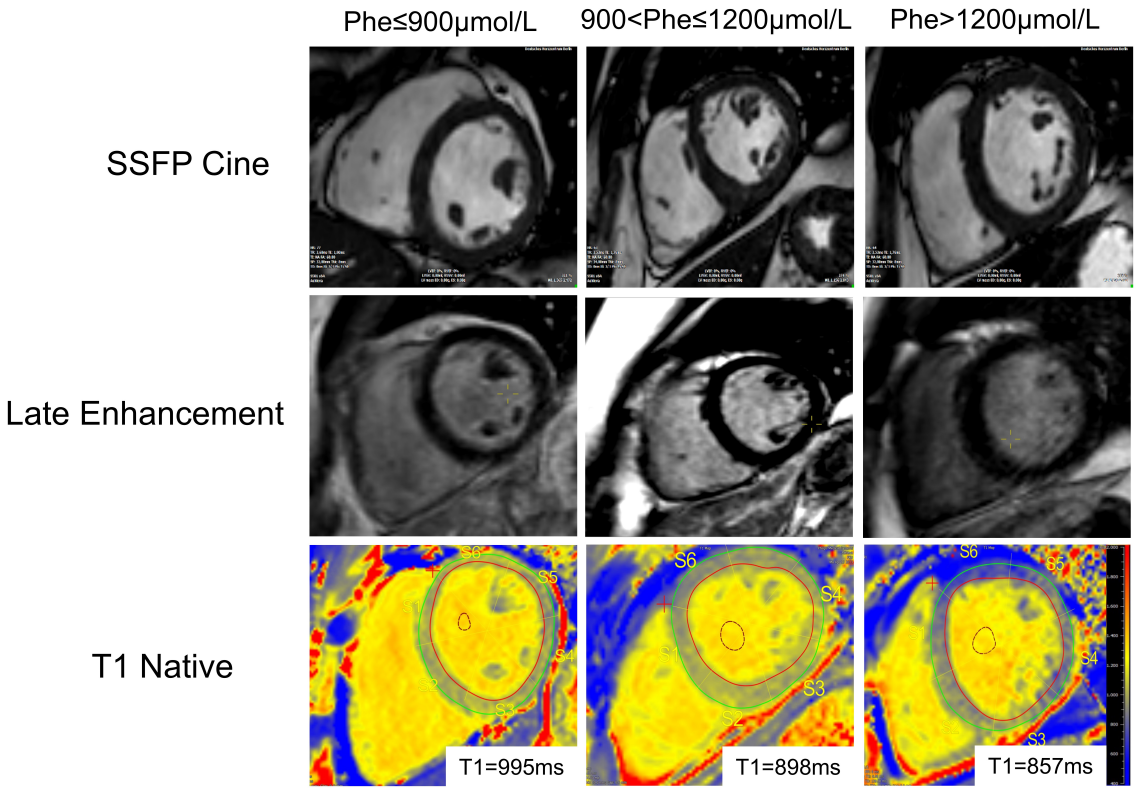


Figure 6.5 Representative SSFP Cine (first row), Late Gadolinium Enhancement (middle row) and T1 native maps (lower row) of 3 Phenylketonuria subjects from 3 groups, divided according to mean 10 years value of plasma phenylalanine (Phe) concentrations: group 1 – Phe≤900μmol/L, group 2 – 900<Phe≤1200μmol/L, group 3 – Phe>1200μmol/L, displayed as follows: group 1 subject (left column), group 2 subject (middle column) and group 3 subject (right column). In the absence of any focal lesion there is a diffuse process that shortens T1 native times in patients in which the therapeutic control of Phe is suboptimal. Abbreviations: Phe – phenylalanine, SSFP – steady-state free precession.

may play an important role to promote dyslipidemia and thus, enhance lipid accumulation in the heart.

6.4.4 Analysis of subgroups.

To test if persistently higher concentrations of Phe influenced the cardiac structure and function in the patients we divided the PKU cohort according to Phe levels recorded before the CMR scan into 3 subgroups as follows: PKU patients with Phe<900μmol/L, patients with Phe between 900 and 1200μmol/L, patients with Phe>1200μmol/L (data presented in **Table 6.3**) There were no significant differences between these 3

Table 6.4 Cardiac structure and function in PKU patient subgroups divided according to lipid plasma concentrations: normolipidemic and dyslipidemic

	Normolipidemic PKU (n=22)	Dyslipidemic PKU (n=17)	P‡
Left Ventricle			
ED volume, mL/m^2	83±14	93±12	***0.019***
ES volume, mL/m^2	33±7	40±10	***0.012***
Stroke volume, mL/m^2	50±9	53±7	0.23
Ejection fraction, %	60±5	58±7	0.16
GLS Endo %	-25.9±2.5	-24.0±3.5	***0.052***
GLS Myo, %	-24.7±2.0	-23.3±3.4	0.10
GLS Endo-Epi Gradient, %	-2.9±1.7	-2.3±1.9	0.29
GCS Endo %	-30.7±3.7	-28.9±4.6	0.20
GCS Myo, %	-21.2±2.5	-20.1±4.1	0.34
GCS Endo-Epi Gradient, %	-15.3±2.7	-14.7±3.7	0.56
HD Systolic Force (%)	39.0±13.3	36.0±14.0	0.51
HD Systolic Work (%)	5.3±2.2	4.8±2.2	0.48
HD Systolic Work (mJ)	4.5±1.9	5.3±3.1	0.31
HD Systolic Power (mJ/s)	54.1±28.9	62.5±46.6	0.50
HD Early Diastolic Force (%)	-25.6±9.2	-22.7±10.5	0.36
HD Early Diast Work (%)	-2.0±1.1	-1.7±0.8	0.24
HD Early Diast Work (mJ)	-1.5±0.7	-1.6±0.6	0.65
HD Early Diast Power (mJ/s)	-26.3±12.3	-26.8±10.5	0.89
HD Late Diast Force (%)	-7.6±3.8	-5.8±3.8	0.14
Cardiac Index, L/min/m^2	3.6±0.8	3.6±0.6	0.89
Septal ED WT, mm	6.4±1.2	7.8±2.0	***0.011***
Lateral ED WT, mm	5.6±1.1	6.9±1.5	***0.003***
Relative WT	1.16±0.14	1.13±0.16	0.59
LV Mass g/m^2	36.1±0.06	40.8±8.2	0.07
LV Mass/EDV, g/mL	0.44±0.06	0.44±0.07	0.96
LV ED diameter mm	51±9	55±4	***0.017***
Left Atrium			
LA max Vol mL/m^2	37±8	38±8	0.56
LA min Vol mL/m^2	10±3	11±4	0.48
LA emptying fraction %	72±5	71±6	0.75
LA strain %	49±13	50±13	0.79
Right Ventricle			
RV Vol max mL/m^2	44±11	49±11	0.2
RV Vol min mL/m^2	16±7	20±6	0.08
RV ejection fraction %	64±8	61±7	0.23
RV longitudinal strain %	-25.3±5.1	-24.5±6.2	0.65
Ascending Aorta			
Systolic Ao. Diam., mm	43.8±7.7	47.7±10.7	0.20
Diastolic Ao. Diam., mm	34.4±8.2	36.2±9.9	0.53
Ao. distens. 10^{-3}mmHg^{-1}	6.36±2.47	7.26±2.73	0.29
Echocardiography			
MV E Vmax (cm/s)	84±15	76±12	0.06
MV A Vmax (cm/s)	55±14	49±11	0.18
MV E/A	1.60±0.49	1.61±0.34	0.96
E/e‘	5.99±1.75	6.83±1.74	0.19

Table 6.4 Cardiac structure and function in PKU patient subgroups divided according to lipid plasma concentrations: normolipidemic and dyslipidemic (cont.)

Plasma Lipids			
Total Chol (mg/dL)	161±32	163±37	0.85
Trigylcerides (mg/dL)	131±108	174±70	0.15
HDL Chol (mg/dL)	53±8	42±15	***0.010***
LDL Chol (mg/dL)	88±25	97±26	0.30
LDL/HDL Chol	1.69±0.53	2.43±0.61	***<0.001***
	Normolipidemic PKU (n=19)	Dyslipidemic PKU (n=17)	
Parametric Imaging			
T1 native	935±52	938±47	0.87
T1 post contrast	585±53	599±36	0.39
ECV	26.0±5.3	27.0±3.4	0.51

Values as are given as mean±SD unless stated otherwise. P‡ comparison between non-dyslipidemic and lipidemic patients. P values were adjusted with the Bonferroni method. A P value < 0.05 was considered statistically significant. Abbreviations: GLS global longitudinal stress, GCS global circumferential strain, HD hemodynamic, ED end-diastolic, ES end-systolic, LV left ventricle, LA left atrium, RV right ventricle, Ao. aorta, Diam. diameter, MV mitral valve, Chol – cholesterol, ECV extracellular volume.

subgroups in total, HDL or LDL cholesterol, however in patients with a poorer control of the disease (Phe>1200μmol/L), triglycerides and LDL/HDL ratio were higher than in patients with optimal control (Phe<900μmol/L). Detailed data are given in **Table 6.3** and represented in **Figure 6.4**. Age was only modestly correlated with total (R^2=0.21, p=0.004), HDL (R^2=0.15, p=0.019), and LDL (R^2=0.13, p=0.027) cholesterol but not with tryglicerides and LDL/HDL ratio or with Phe levels.

21 out of 39 (54%) patients had Phe values above 900μmol/L and 9 out of 39 (23%) patients had Phe values above 1200μmol/L. Parameters characterizing cardiac size and systolic function were not different between the subgroups, however there were some trends in the means of several of these parameters such as a tendency to higher thickness of the cardiac walls and LV diameters in the subgroups characterized by higher Phe levels. T1 native values were comparatively lower (964±48 vs 915±27 vs 909±48, p<0.003) in subgroups with high Phe levels, while ECV was comparable among the groups (**Figure 6.5**) E/e', an echocardiographical biomarker of abnormal LV filling pressures and diastolic dysfunction was higher in patients with higher Phe (5.24±1.62 vs 5.87±1.57 vs 8.33±1.74, p<0.001).

Importantly, within-subject Phe levels standard deviation recorded for the same time frame as the median (on average 10 years) correlated positively with both EDV (R=0.357, p=0.026) and ESV (R=0.359, p=0.025). This would suggest that with a tighter control of Phe values over time may be efficient in preventing adverse LV remodeling seen in PKU subjects.

Similarly, to establish if abnormal concentrations of lipids were correlated with cardiac phenotype we compared a subgroup of the PKU patients with at least one abnormal lipid plasma level (normal range reference values were considered: total Cholesterol < 200mg/dl, HDL-Cholesterol > 45mg/dL, LDL-Cholesterol < 130mg/dl, Triglycerides < 180mg/dl) and respectively a subgroup composed of patients with normal levels of lipids. These data are presented in **Table 6.4**. In the dyslipidemic group, LV walls were thicker (septal WT: 7.8±2.0 vs 6.4±1.2 mm, p=0.011, lateral WT: 6.9±1.5 vs 5.6±1.1 mm, p=0.003) and the cavity was significantly more dilated (EDV: 93±12 vs 83±14 mL/m2, p =0.0019, ESV: 40±10 vs 33±7 mL/m2, p=0.012) but EF was equivalent. However, there is a trend that GLS, GCS and EF are all lower in the dyslipidemic than in the normolipidemic subgroup.

6.5 Discussion

Our findings can be summarized as follows:

1. PKU patients had thinner cardiac walls, a more dilated LV and a lower myocardial mass than their healthy counterparts.

2. A functional deficit was also notable with significantly reduced values of LV ejection fraction and circumferential strain on CMR and mildly elevated E/e’ on Doppler echocardiogram.

3. In PKU patients, T1 native times were significantly shorter than in matched controls.

4. Plasma levels of Phe and Tyr were independently correlated with reduced T1 values, strongly supporting the idea that a stricter control of these values can be successful in preventing pathologic structural remodeling. In a multiple regression model Phe and LVM were both negatively predictive for T1 values.

5. Dyslipidemic PKU patients had more dilated LV cavity and thicker walls, reinforcing the hypothesis that an abnormal lipid profile, possibly associated with other metabolic dysfunctions or oxidative stress may be responsible for the observed cardiac changes.

This investigation demonstrates cardiac abnormalities in adult patients with PKU. The thinner and more dilated heart of the patient with PKU likely represents a relatively early stage of dilated cardiomyopathy.[24] Even if within generically normal range, the ejection fraction was reduced compared with age-matched individuals. Moreover, GCS was also reduced in PKU patients. Because of the structural preponderance of the circumferentially distributed fibers, systolic strain at this level is responsible for most of the resultant ejection force. [122] While longitudinally distributed fibers are more sensitive to inflammation, microvascular dysfunction or metabolic alteration, a selective reduction in circumferential deformation is typically observed in dilated cardiomyopathies with an intrinsic contractile deficit. [276] Aortic distensibility and diastolic function were within the normal parameters in PKU subjects, however a comparatively worse, higher E/e´ ratio was seen in poorly controlled compared to well-controlled patients.

On the other hand, paradoxically increased cardiac index (**Figure 6.1 C**), coupled with a relation between the lipid abnormal concentrations and ventricular dilatation, suggest

that the pathophysiological model of dysfunction in PKU has some common traits with the one found in obesity cardiomyopathy. [277] In contrast with cardiac remodeling observed in obese subjects, myocardial mass was severely reduced in PKU patients, and intriguingly, in subjects with a relatively higher LV mass, closer to or within the normal mean, this could be due to potential intra-myocardial substrate deposition or infiltration.

Cardiovascular risk in PKU patients may result from the cumulative effects of abnormal production of toxic metabolites, in particular free oxygen species, intermittent nutritional deficiencies resulting from specific diet intake and, in some cases, episodes of non-compliant behavior and poor metabolic control of the disease. Recent studies confirm increased plasma levels of oxidative stress markers and resultant specific vascular effects such as arterial stiffness[278] and endothelial dysfunction in PKU patients.[148] Within the cardiac tissue, oxidative stress is responsible for depressed contractility, myocyte apoptosis and interstitial and focal fibrotic deposition. [279] We could not identify any increased CMR marker of focal or interstitial fibrosis, however we observed shorter myocardial T1 native times in a majority of patients with PKU and in particular in the subgroups with an intermediate and poor adherence to diet (900≤Phe≤1200 µmol/L and Phe>1200 µmol/L). LVM and wall thicknesses correlated negatively with T1, moreover, in a multiple regression model Phe levels and LVM are, in tandem, independent negative predictors for T1. Even if globally reduced when compared with normal subjects, in PKU patients an increase in LVM likely represents an adverse structural remodeling of the heart. So far, while multiple cardiac diseases have been associated with T1 native prolongation, shorter T1 is observed only in lipid accumulation (typically seen in cardiomyopathy associated with Anderson-Fabry disease) or cardiac siderosis.[123]

Strong molecular and histological evidence of deleterious effects produced per se by elevated plasma levels of phenylalanine on the myocardial structure, were recently produced in a murine model. According with these findings, excess phenylalanine induces hypertrophy of the myocytes, premature senescence traits with diminished contractile performance and activation of the local myofibroblasts with excessive interstitial collagen deposition driven through Tgfb1, osteopontin, and leptin activation [149]. Here we showed both an important deficit of myocardial mass in PKU patients and respectively an inverse correlation between LVM and Phe concentrations, however the molecular details remain unclear. Leptin was found to be elevated in PKU patients, in particular in those with less well controlled Phe levels[280], despite their higher BMI[5,281] and higher fat/non-fat tissue ratio[282]. It is however less clear whether higher Phe levels mediate directly an increase in leptin concentrations or this is mostly due to an abnormal lipid anabolism. [222,283] On the other hand, higher leptin levels enable an antihypertrophic effect[284] which may explain strikingly low myocardial mass seen in PKU patients. Taken together these data raise the hypothesis of an effector role of the leptin downstream pathway[285] in the regulation of LVM in PKU patients and this should make the object of future investigations.

Long-standing lipid profile modifications coupled with other metabolic abnormalities (such as deficit in carnitine), a more pronounced LV dilatation and hypertrophy make us speculate that an intramyocyte deposition of lipids[286] may be at least in part responsible for abnormalities detected by parametric mapping. The precise structural abnormality underlying these CMR findings is yet to be established by further studies, in particular histological analysis on biopsy samples or heart tissue from animal models of treated PKU. An intriguing alternative hypothesis, would be that higher plasma levels of phenylalanine deposit in the myocardium, self-assembled as cytotoxic amyloid-like

fibrils, in a similar pattern to those identified in brain tissue from PKU patients and transgenic animal models of phenylketonuria. [150]

In other pathologies such as Anderson-Fabry, aortic stenosis[287] or DM[288], cardiac steatosis has a progressive negative impact on the mechanical function of the heart. [289] With this study we did not manage to show conclusively a relationship between lower T1 values and reduced mechanical contraction (assessed by myocardial strain or ejection fraction). However, given the incipient dilative pattern seen in PKU patients with abnormal lipid profile, our data suggest that this may be a plausible outcome in the evolution of this disease, in particular in patients with more pronounced lipid abnormalities. In the Framingham cohort, both increased LDL and decreased HDL-cholesterol are risk factors for developing HF, independent of co-existence of coronary artery disease. [290] In addition, prolonged dyslipidemic abnormalities, frequently present in adults with PKU, may determine per se a progressive worsening of cardiac function. [291]

Several clinical perspectives result from our findings and represent theoretical premises for modifications in the current clinical care:

- Adult patients with “classical” PKU, treated life-long with a specific phenylalanine-restrictive diet, present cardiac changes with reduced myocardial mass, thin myocardial walls, mildly impaired systolic function and undetermined structural modifications

- Structural modifications detected by parametric mapping are related to mean plasma levels of phenylalanine and tyrosine, measured frequently over a period of 10 years, suggesting a toxic effect of these abnormal concentrations, at present accepted by the American and European guidelines in place.

- As the nature of this modifications, which may indicate an early model of cardiomyopathy, is not clearly understood and neither are the long-term consequences of these modifications, in the light of these findings, cardiac follow-up of adult patients with PKU, ideally with CMR, and developing larger multi-centric studies are recommended.

6.6 Limitations

PKU is a rare disease in which metabolic control and avoiding neuropsychological complications have been so far the clinical priorities. In consequence, our proof-of-principle study was limited in size and was cross-sectional. We could not establish a direct correlation between the deficit in cardiac contraction and structural modifications such as decreased T1 values or between lipid plasma concentrations and T1 values. Myocardial samples for histology were not available and therefore what is the nature of structural changes leading to abnormal T1 remains to be established. Apart from Phe levels, an indirect indicator of compliance with the recommended restrictive diet, our analysis did not include more specific details regarding various amino-acid levels, prophylactic food supplements and nutrition status of these patients, therefore we could not exclude the possibility that complex metabolic abnormalities are responsible for cardiac changes. Further studies including systematic proteomic and lipidomic approaches are warranted. Information about potential tissue inflammation and edema given by CMR tools such as T2 mapping[183] are missing for this cohort. The blood tests available for the PKU patients at the time of the initial CMR scan did not include biomarkers of cardiac dysfunction such as N-terminal prohormone of brain natriuretic peptide (NT-proBNP) or cardiac troponin T (cTnT) with a proven role in early detection of myocardial impairment[292,293] that more recently have become part of routine evaluation in cardiovascular medicine. We anticipate that, with an increased age range

as was available in this study, these correlations will become apparent. We would also expect more pronounced modification of the cardiac phenotype at a follow-up visit. At this stage, larger multicentric longitudinal studies are warranted to further test these presumptions.

6.7 Conclusions

Adult patients with PKU present a mild form of cardiomyopathy with dilated heart with thinner ventricular walls and reduced LVM. Reduced T1 values likely reflect pathological intra-myocardial substrate deposition which has the potential to contribute further to flare up chronic inflammation, induce interstitial fibrosis and further decrease contractility. We advocate that regular follow up of these patients should include frequent echocardiograms or, ideally, CMR evaluation, in particular in cases where concentrations of Phe remain high or the compliance with the specific diet is reduced.

Chapter Seven:

Cardiac Phenotype in Adult Patients with Phenylketonuria: Follow-up Study

7.1 Abstract

Notwithstanding the maintenance of a phenylalanine (Phe) restrictive diet, adult patients with phenylketonuria (PKU) have plasma Phe concentrations much above the physiological levels and higher toxic compounds resulting from its alternative catabolism. In contrast the tyrosine (Tyr) levels are low leading in turn to complex metabolic abnormalities involving adrenergic mediators and TCA cycle. In Chapter 6 of this thesis, we showed that adult PKU patients exhibit early cardiomyopathic traits. A longitudinal evaluation of cardiac phenotype is warranted to establish the progressiveness of these changes.

Fifteen PKU patients who had participated in the baseline study underwent a comprehensive follow-up CMR scan. The mean follow-up interval was 8.3±0.3 years. On average the left ventricular (LV) end-diastolic volume (EDV) (158±29 vs 143±29 ml, p=0.013), end-systolic (ESV) (68±18 vs 62±18 ml, p=0.011) were lower at follow-up and LV mass (LVM) (72±25 vs 82±29 g, p<0.001) and the ratio LVM/EDV (0.46±0.12 vs 0.58±0.23 g/mL, p=0.005) were increased, while T1 times were longer (940±42 vs 1010±35 ms, p<0.001). LV EF (57±6 vs 57±7%, p=0.90), longitudinal (GLS) and circumferential (GCS) systolic strain remained unchanged but early diastolic hemodynamic forces were increased (-19.4±7.0 vs -26.5±12.2 %, p=0.012) while LA strain 43.8±11.3 vs 37.3±9.6 %, p=0.031) and aortic distensibility (6.38±1.75 vs 5.21±1.17 10^{-3}mmHg^{-1}, p=0.008) decreased at follow-up. A higher decrease in Phe concentration (ΔPhe) was associated with prolonged ΔT1 (β=-0.78, p<0.001), increased ΔECV (β=-0.61, p=0.016) and a decrease in systolic function. Differences in Tyr concentrations did not show to have an effect on any of these parameters. In conclusion, lowering the Phe levels while beneficial for reducing the intrinsic toxicity and oxidative stress, might associate in turn detrimental cardiac remodelling with

decreased LV systolic function and more myocardial diffuse fibrosis. Clinically, adult patients with PKU would require periodical cardiovascular evaluation while more cardiometabolic data to account for incipient cardiomyopathic changes observed in some patients remain warranted.

7.2 Introduction

During adulthood, PKU patients are advised to follow a life-long Phe restricted diet and undergo close periodic monitoring of phenylalanine (Phe) levels, clinical review and dietitian consultation. Current guidelines in place[140,265,294] recommend keeping the Phe values under 1200μmol/L[295] but clinical practice regarding optimal accepted range of Phe and vigilance in checking these values into adult life vary significantly among different European countries and in the US. [180,261,296] While multicentric clinical data demonstrate the high efficacy of these regimes in avoiding significant neurological damage and ensuring normal development, intelligence and social interaction[297], recent reports using advanced brain imaging CMR reveal subtle white matter modifications, demyelination [298,299] and persistent inflammation[17,146,300-302] in adult PKU patients with mean Phe levels as low as 600 μmol/L. with more pronounced modifications found in older patients.

Several important risk factors such as abnormal metabolite accumulation, increased oxidative stress, impaired protein and cholesterol synthesis persist in adult life, are associated with Phe levels and may concur[303] to induce and exacerbate structural and functional modification at the levels of multiple organs and tissues of the human body such as the heart and vascular system. It is expected that these modifications, progressive in nature, will become apparent or more pronounced with age and therefore longitudinal evaluation is warranted.

In Chapter 6 my data showed incipient cardiac remodeling traits in adult patients with PKU predisposing to early cardiomyopathy and HF and related these traits to higher Phe levels but also related to the presence of dyslipidemic changes. PKU patients had lower LV EF and GCS when compared with healthy subjects but I did not find any correlation between Phe or Tyr levels and any component of the cardiac function (LV EF, GLS, GCS, HD forces etc.).

Cardiac phenotype characterized by enlarged end-diastolic volume and eccentric remodeling is frequently progressive and precedes functional decompensation and heart failure in the general population. [24] As data regarding the mechanism of these modifications and their progression, in animal disease models or humans with PKU are currently missing, it is important to assess longitudinally these changes in order to direct specific clinical management.

In this chapter we aim to give an insight into the progressiveness of cardiac modifications observed at baseline in adult patients with PKU and compare the biochemical phenotype (Phe, Tyr) with the cardiac phenotype characterized by advanced CMR.

7.3 Specific Methods

7.3.1 Study Population

All PKU patients included in the baseline study received an invitation to participate for the follow-up study from the Interdisciplinary Centre for Metabolism: Endocrinology, Diabetes and Metabolism of Charité University Berlin, in agreement with the local Ethics Committee approval. The study content and purposes were explained in full to all the invited patients and a patient information leaflet has been provided. 15 out of 36 patients who had a complete initial set of CMR data (see **Chapter 6**, **Chapter 2**) agreed

to participate in a follow-up CMR study. Additionally, to compare the phenylalanine and tyrosine and respectively the lipid profile all 39 patients agreed and gave permission to access retrospectively all the clinical and laboratory data available on the dedicated database.

7.3.2 Cardiac magnetic resonance

All images were acquired using the same clinical system and acquisition protocol as for the baseline study (details are presented in **Chapter 6**, and in detail in **Chapter 2**)

7.3.3 Image analysis

Image analysis protocols were identical with those used for the baseline study and are described in detail in **Chapter 2**.

7.3.5 Biochemistry

Similarly to the baseline study, during the follow-up visit routine haematological and biochemical parameters, were determined. Phe and Tyr concentrations were measured in dried blood spots using mass spectrometry. A number of 20-60 single determinations were performed for each individual timepoint. Phe and Tyr plasma concentrations were obtained for the period between the two visits, baseline and follow-up. As individual Phe and Tyr can vary between several consecutive measurements, in order to offer more physiologically relevant values, we chose to average all the available data over a period of 2 years prior to baseline and respectively follow-up time points. All these data were restrospectively collected from the local database of the Interdisciplinary Centre for Metabolism of the Charité University Berlin. In addition, data obtained in the same laboratory unit, the most recent serum levels of total cholesterol, low-density lipoprotein (LDL) cholesterol, high-density lipoprotein (HDL) cholesterol, triglycerides, carnitine free fraction and total, glucose were obtained similarly and using an identical measurement method as for the baseline data reported

in **Chapter 6**. For this chapter the baseline data corresponding to the patients included in the follow-up study was paired with the follow-up results. All routine determinations were performed in duplicate by the Hospital laboratory as part of the standard clinical evaluation of the patients (Labor Berlin - Charité Vivantes GmbH.).

7.3.6 Statistical Analysis

Normality of distribution for continuous variables was assessed by visual assessment of normality curves and the Shapiro-Wilk test. Where a variable failed to satisfy the normality distribution condition, log transformation or non-parametric equivalent tests were used. Comparison between groups for continuous variables was performed with a 2-sided, paired-samples Student t test for normally distributed data and Wilcoxon test for skewed data. When multiple comparisons were applied to the same set of variables, Bonferroni corrections were made. For categorical variables, comparison was done with a $\chi 2$ test and statistical significance evaluated with Fisher's exact test. Results are presented as mean±SD. Values of $P < 0.05$ were considered statistically significant.

7.4 Results

7.4.1 Population Characteristics

To find out if there are systematic changes in the concentrations of Phe and Tyr and respectively the concentrations of plasma lipids between baseline and follow-up we compared their plasma concentrations between baseline and follow-up. These results are presented in **Figure 7.1** and **7.2**. The numerical data for the patients included in the follow-up study are also shown in **Table 7.1**. On average, there was no difference between Phe concentration between baseline and follow-up (961±304 vs 909±338µmol/L, p=0.24 for all patients, and 967±360 vs 815±326µmol/L, p=0.06 for the patients included in the CMR follow-up study), even if the mean value tended to be lower. There were also no significant differences between baseline and follow-up

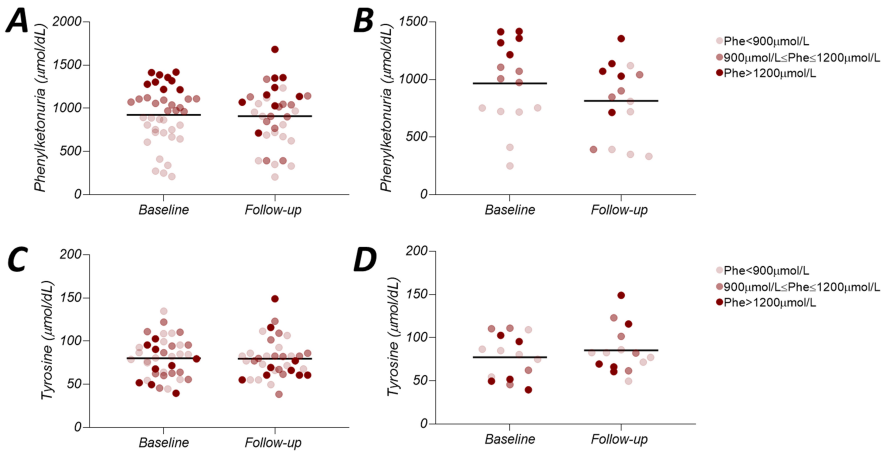


Figure 7.1 Baseline and Follow-up Plasma Concentrations of phenylalanine (Phe) and tyrosine (Tyr) in PKU Patients: **A.** Phe concentrations in the entire PKU cohort (N=39), **B.** Phe concentrations in the follow-up cohort (N=15), **C.** Tyr concentrations in the entire PKU cohort (N=39), D. Tyr concentrations in the follow-up cohort.

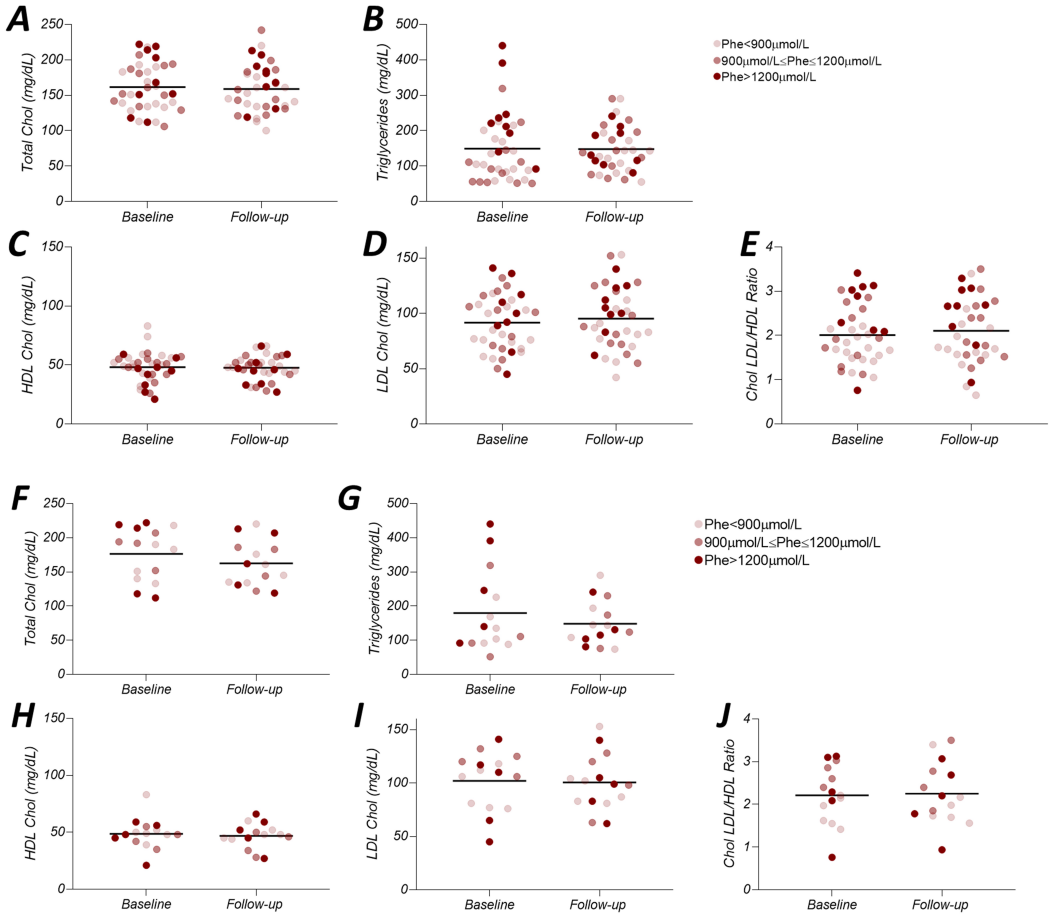


Figure 7.2 Baseline and Follow-up Plasma Concentrations in all PKU patients (N=39): **A.** total cholesterol, **B.** triglycerides, **C.** HDL cholesterol, **D.** LDL cholesterol, **E.** LDL/HDL and only in the follow-up subgroup (N=15):): **F.** total cholesterol, **G.** triglycerides, **H.** HDL cholesterol, **I.** LDL cholesterol, **J.** LDL/HDL

Table 7.1 Characteristics of Study Population (Baseline and Follow-up)

	PKU Patients (N=15)		
	Baseline	Follow-up	P Value
Demographics			
Age, y	31.5±8.1	39.8±8.1	
Males, n (%)	9 (60%)	9 (60%)	
Anthropometrics			
Height (cm)	173±11	173±11	
Weight, kg	77±14	84±20	***0.029***
BMI, kg/m2	25.7±3.8	28.7±6.3	***0.016***
BSA, m2	1.92±0.22	2.00±0.26	***0.027***
Fat mass, kg	21.6±9.7	21.2±1.5	0.62
Fat-free mass, kg	57.0±11.7	58.2±13.0	0.45
Ratio	0.39±0.19	0.38±0.19	0.47
Visceral fat, kg	6.1±2.6	7.1±3.7	0.13
BMR, J/(h·kg)	1706±329	1732±372	0.54
Muscle mass	54.2±11.2	55.5±12.4	0.42
Body Water	41.7±8.6	42.8±9.6	0.35
Clinical			
Heart Rate, bpm	66±10	64±12	0.62
Systolic BP, mmHg	115±17	114±19	0.82
Diastolic BP, mmHg	71±10	68±12	0.54
Pulse pressure, mmHg	44±12	46±12	0.75
Biochemistry			
Phe Mean, µmol/L	967±360	815±326	0.06
Phe Median, µmol/L	968±357	818±324	0.06
Phe SD, µmol/L	192±102	204±95	0.48
Tyr Mean, µmol/L	77±25	85±27	0.39
Tyr Median, µmol/L	77±25	85±27	0.37
Tyr SD, µmol/L	32±16	34±17	0.74
Carnitin free, mg/dL	37.9±11.3	41.6±11.7	0.22
Carnitin total, mg/dL	53.6±9.6	55.0±14.9	0.93
Carnitin ratio free/total	0.71±0.17	0.76±0.12	0.18
Cholesterol total, mg/dL	176±39	163±34	0.10
HDL-Cholesterol, mg/dL	49±13	47±11	0.56
LDL-Cholesterol, mg/dL	102±27	101±26	0.79
Triglycerides, mg/dL	180±120	149±65	0.30
Glucose, mg/dL	74±7	79±12	0.27

Abbreviations: BMI – body mass index, BSA – body surface area, BMR – basal metabolic rate, BP – blood pressure, Phe – phenylalanine, Tyr – tyrosine. Phe and Tyr are for baseline averaged for a 10 year period for baseline and for a 2 year period for follow-up.

Table 7.2 CMR Parameters: Volumes, Paraemtric (Baseline and Follow-up)

	PKU Patients (N=15)		
	Baseline	Follow-up	P Value
Left Ventricle			
LV EDV, mL	158±29	143±29	***0.013***
LV ESV, mL	68±18	62±18	***0.011***
LV SV, mL	90±17	81±16	0.08
LV EF, %	57±6	57±7	0.90
LV CO, L/min	6.15±1.21	6.01±1.56	0.68
Septal ED WT, mm	7.0±1.7	7.2±1.8	***0.006***
Lateral ED WT, mm	6.1±1.5	6.2±1.5	***0.011***
Relative WT	1.2±0.1	1.2±0.1	0.72
LV Mass, g	72±25	82±29	***<0.001***
LV Mass/EDV, g/mL	0.46±0.12	0.58±0.23	***0.005***
LV ED maximal diameter, mm	53±5	53±5	0.65
Left Atrium			
LA Volume max, mL	64±12	67±14	0.42
LA Volume min, mL	20±7	22±7	0.32
LA emptying fraction %	70±6	68±6	0.37
Right Ventricle			
RV EDV, mL	167±36	156±36	***0.049***
RV ESV, mL	80±24	78±22	0.23
RV SV, mL	87±17	78±17	***0.022***
RV ejection fraction, %	52±6	51±4	0.24
RV CO, mL	5.89±1.03	5.79±1.41	0.70
Ascending Aorta			
Systolic aortic area, cm2	4.53±0.88	4.53±0.92	0.99
Diastolic aortic area, cm2	3.58±0.77	3.72±0.87	0.10
Ao distens, 10-3mmHg-1	6.38±1.75	5.21±1.17	***0.008***
Parametric Imaging			
T1 native, ms	940±42	1010±35	***<0.001***
ECV (%)	26.5±2.6	26.5±3.7	0.77
T2, ms		48.9±3.1	

Abbreviations: LV left ventricle, EDV end-diastolic volume, ESV end-systolic volume, ED end-diastolic, ES end-systolic, CO cardiac output, WT wall thickness, LA left atrium, RV right ventricle, ECV extracellular volume.

according to the baseline categories of severity (Phe≤900μmol/L, 900μmol/L<Phe≤1200μmol/L, Phe>1200μmol/L). Similarly, Tyr values were not different between baseline and follow-up (78±22 vs 80±23μmol/L, p=0.78 for all patients, and 77±25 vs 85±27μmol/L, p=0.39 for the patients included in the CMR follow-up study). Total (161±35 vs 159±34mg/dL, p=0.52), HDL (47±12 vs

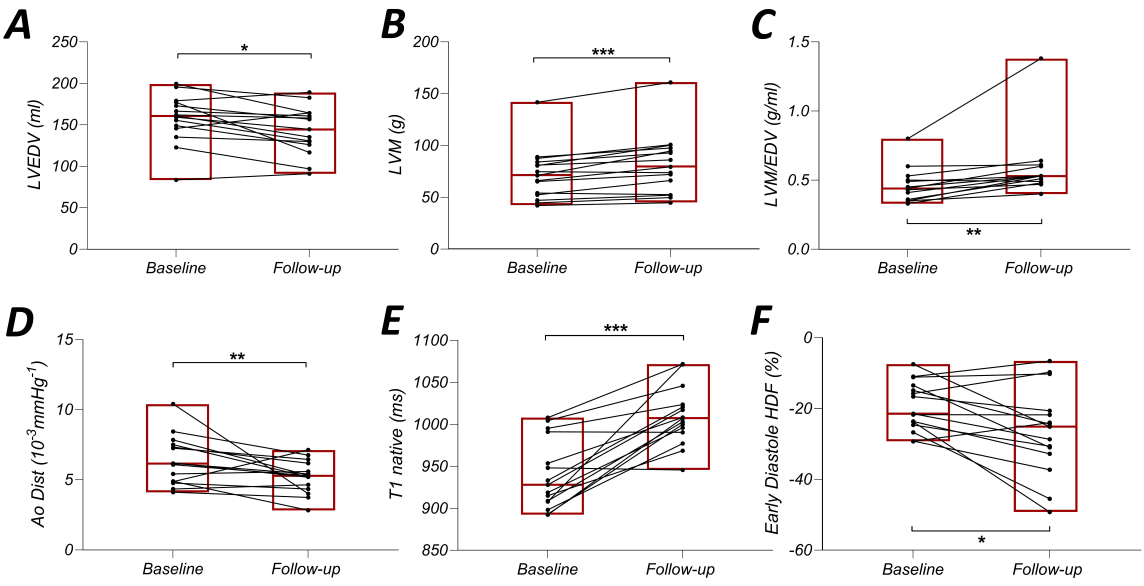


Figure 7.3 Cardiac Structural and Functional Remodeling in Adult Patients with Phenylketonuria at Baseline and Follow-up: **A.** LV End-Diastolic Volume, **B.** LV Mass , **C.** Ratio LV Mass to End-Diastolic Volume, **D.** Aortic Distensibility, **E.** T1 native , **F.** Early Diastolic Hemodynamic Force. A P<0.05 was considered statistically significant. *P<0.05, **P<0.01, ***P<0.001.

48±11mg/dL, p=0.57), LDL (91±26 vs 95±28mg/dL, p=0.30) cholesterol, LDL/HDL ratio (2.04±0.68 vs 2.10±0.74mg/dL, p=0.44) and triglycerides (154±95 vs 148±64mg/dL, p=0.72) were not changed between baseline and follow-up timepoints. 15 out of 39 patients participated in the follow-up CMR. The average follow-up period was 8.3±0.3 years. The general characteristics of these patients at follow-up and baseline timepoints is presented in **Table 7.1**. At baseline, PKU patients had a slightly higher BMI than control (25.7±5.0 vs 23.7±3.3, p=0.030, N=39), with 7 of 39 (18%) being obese (according to the WHO guidelines [304] BMI ≥ 30 kg/m^2), and none of them severely obese (BMI ≥ 40 kg/m^2). Taking into consideration the 15 patients who participated in follow-up study, at baseline 2 (13%) were obese, of which at follow-up 1 remained obese and the other one became severely obese at follow-up, and 3 overweight subjects became obese. In the follow-up cohort, BMI increased on average compared with baseline (25.7±3.8 vs 28.7±6.3, p=0.016, N=15). On the data reported

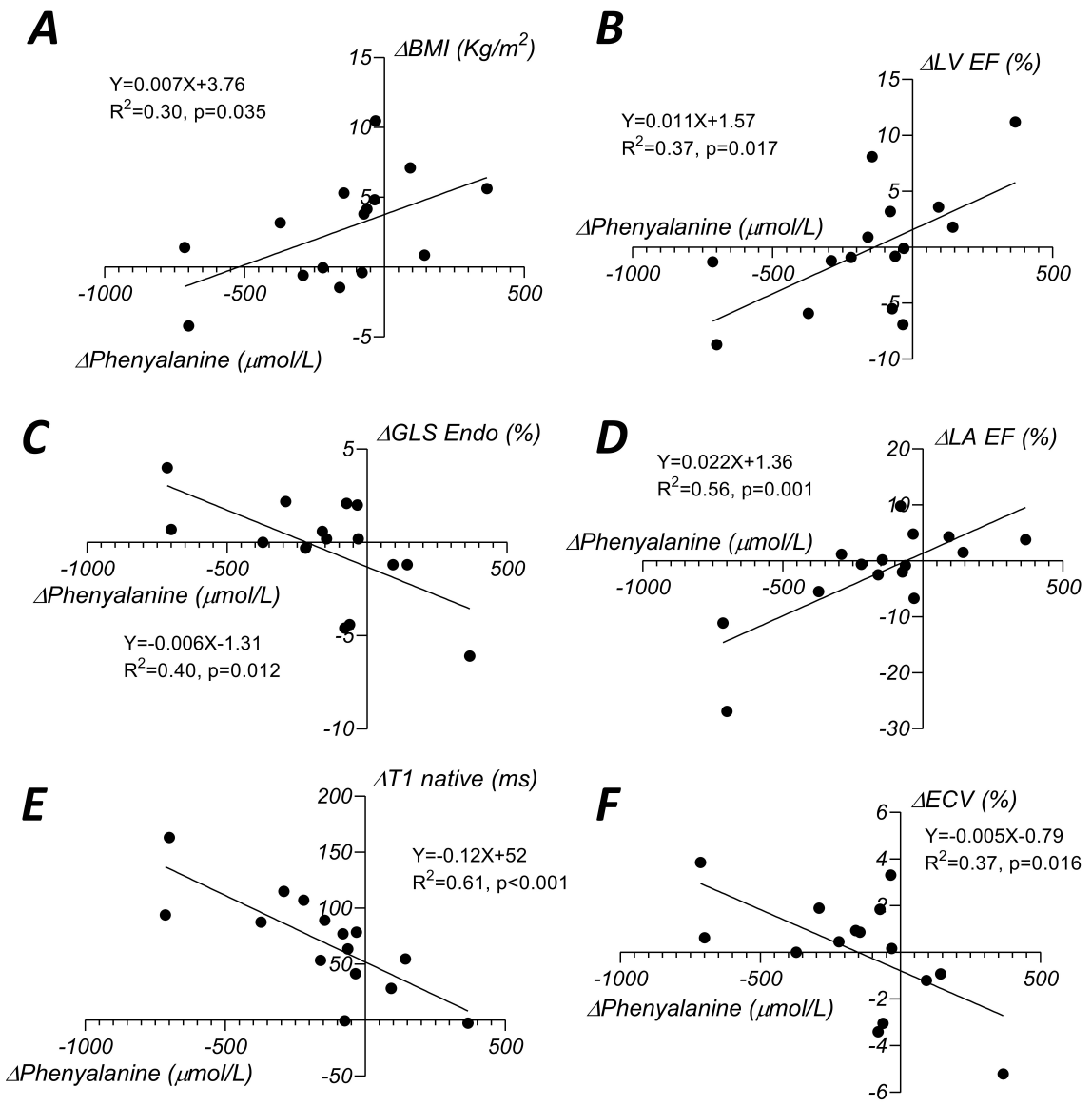


Figure 7.4 Relation between variation (Δ) between phenylalanine plasma concentrations between baseline (averaged over 10 years) and follow-up (averaged over 2 years) and variation (Δ) in **A.** body mass index (BMI), **B.** left ventricular ejection fraction (LV EF) **C.** global longitudinal strain measured subendocardially (GLS Endo) **D.** left atrial emptying fraction (LA EF), **E.** T1 native times, **F.** extracellular volume (ECV). Bivariate linear regression indicate that a larger decrease in plasma concentrations of phenylalanine between follow-up and baseline associate lower ejection fraction, more impaired longitudinal strain, prolonged T1 native times and increased extracellular volume (taken together these likely represent a negative cardiac remodelling with likely more fibrosis and depressed systolic contraction, in patients with a higher decrease in phenylalanine levels. Patients with lower Phe plasma levels at follow-up had a lower increase in BMI.

Table 7.3 CMR Parameters: Strain, Haemodynamic Forces (Baseline and Follow-up)

	PKU Patients (N=15)		
	Baseline	Follow-up	P Value
Left Ventricle			
GLS Endo, %	-26.5±5.6	-26.9±5.8	0.60
GLS Myo, %	-25.3±2.9	-24.9±3.1	0.50
GLS Endo-Epi Gradient, %	-3.0±6.0	-4.3±6.0	***0.030***
GCS Endo, %	-30.0±5.3	-31.1±5.2	0.13
GCS Myo, %	-20.5±2.8	-20.7±2.5	0.61
GCS Endo-Epi Gradient, %	-15.3±5.4	-16.9±5.5	***0.036***
HD Syst Force (%)	34.1±9.6	33.4±8.0	0.83
HD Syst Work (%)	4.3±1.5	5.0±2.4	0.30
HD Syst Work (mJ)	3.9±1.3	4.1±1.5	0.62
HD Syst Power (mJ/s)	47.0±22.7	48.8±20.6	0.77
HD Early Diast Force (%)	-19.4±7.0	-26.5±12.2	***0.012***
HD Early Diast Work (%)	-1.3±0.5	-1.4±1.0	0.57
HD Early Diast Work (mJ)	-1.1±0.42	-1.2±0.8	0.69
HD Early Diast Power (mJ/s)	-18.6±7.6	-20.1±13.5	0.59
HD Late Diast Force (%)	-6.8±3.0	-12.1±6.2	***0.004***
Left Atrium			
LA strain, %	43.8±11.3	37.3±9.6	***0.031***
Right Ventricle			
RV longitudinal strain, %	-26.7±3.4	-34.1±5.2	***<0.001***

Abbreviations: GLS global longitudinal strain, GCS global circumferential strain, Endo subendocardial, Myo mid-myocardium, Epi subepicardial layers, HD hemodynamic, Syst systolic, Diast diastolic, LV left ventricle, LA left atrium, RV right ventricle

by the bioelectrical impedance analysis and collected from the clinical files of the patients there was no significant difference in body distribution of fat, muscle or water but a noticeable trend of elevated visceral fat component. On average the concentration of Phe tends to be lower but given variability between the subjects this does not reach significance. Of note, a considerable number of patients with higher values of Phe at baseline improved the adherence to Phe-free diet and managed to control better their Phe and Tyr concentrations.

7.4.2 Cardiac anatomy, function and structural modfications in PKU patients

Because of a significant increase in weight and implicitly BMI and BSA between baseline and follow-up, I did not present here the indexed volumes of mass of cardiac chambers as I did in the other parts of this thesis but kept the measured, unindexed values. These data are presented in detail in **Table 7.2**. Compared to baseline, at follow-up timepoint PKU patients had lower LV EDV (158±29 vs 143±29 mL, p=0.013) (**Figure 7.3 A**), lower ESV (68±18 vs 62±18 mL, p=0.011) , there was a non-significant trend for a lower stroke volume (90±17 vs 81±16 mL, p=0.08) but no change in EF (57±6 vs 57±7 %, p=0.90) which remained at follow-up borderline lower than the expected average value for this age group.[188] LV Mass (72±25 vs 82±29 g, p<0.001 (**Figure 7.3 B**) and LV septal and lateral wall thickness (septum: 7.0±1.7 vs 7.2±1.8 mm , p=0.006, lateral wall: 6.1±1.5 vs 6.2±1.5 mm, p=0.011) were increased and, as a resultant, the LV Mass/EDV index was largely increased (0.46±0.12 vs 0.58±0.23 g/mL, p=0.005) (**Figure 7.3 C**), indicating a more concentric pattern of the LV remodeling compared with baseline. RV EDV (167±36 vs 156±36 mL, p=0.049) and RV SV (87±17 vs 78±17 mL, p=0.022) but not RV ESV (80±24 vs 78±22 mL, p=0.23) followed a similar pattern and were decreased compared with baseline. Aortic distensibility was also decreased at follow-up (6.38±1.75 vs 5.21±1.17 $10^{-3}mmHg^{-1}$, p=0.008) (**Figure 7.3 D**). Importantly, T1 times were increased at follow-up (940±42 vs 1010±35 ms, p<0.001) (**Figure 7.3 E**).

7.4.3 Assessment of cardiac deformation and hemodynamic forces in PKU patients

To analyse further the changes in the cardiac function, we assessed the systolic peak deformation (strain) of the myocardium at multiple layer levels. We also derived the hemodynamic forces for systole, early and late diastole. The detailed numerical values are shown in **Table 7.3**. GLS and GCS values were not different from baseline at

neither Endo (GLS: -26.5±5.6 vs -26.9±5.8 %, p=0.60, GCS: -30.0±5.3 vs -31.1±5.2 %, p=0.13) or Myo (GLS: -25.3±2.9 vs -24.9±3.1 %, p=0.50, GCS: -20.5±2.8 vs -20.7±2.5 %, p=0.61) levels but both GLS and GCS Endo-Epi gradients were increased at follow-up (-3.0±6.0 vs -4.3±6.0 %, p=0.030 and -15.3±5.4 vs -16.9±5.5, p=0.036). HD early diastolic force was markedly increased (-19.4±7.0 vs-26.5±12.2 %, p=0.012) (**Figure 7.3 F**). Of note, at baseline these values measured in all 39 patients were already higher than in control subjects (-24.3±9.8 vs -17.6±9.0, p=0.002, N=39). In addition, HD late diastolic force is higher at follow-up (-6.8±3.0 vs -12.1±6.2 %, p=0.004), LA strain was lower (43.8±11.3 vs 37.3±9.6 %, p=0.031) and RV longitudinal strain was higher (-26.7±3.4 vs -34.1±5.2, p<0.001) at follow-up.

7.4.4. Relation between phenylalanine levels and cardiac phenotype

In order to establish if an improved control of Phe and Tyr values was associated with improved cardiac phenotype we compared the differences (Δ) between follow-up and baseline in Phe and Tyr with the differences observed in cardiovascular parameters. These data are presented in **Table 7.4**. Variation (Δ) in Phe concentrations between follow-up and baseline, but not variation Δ Tyr concentrations were positively correlated with weight gain (β=0.56, p=0.031) and corollary with the BSA (β=0.58, p=0.023) and BMI (β=0.55, p=0.035) (**Figure 7.4 A**), calculated as functions of weight. Δ Phe correlated moderately with the Δ LV EF (β=0.61, p=0.017) (**Figure7.4 B**), Δ LV GLS Endo (β=-0.63, p=0.012) (**Figure7.4 C**), variation in ECV (β=-0.61, P=0.016) (**Figure7.4 F**), and correlated strongly with T1 native (β=-0.78, P<0.001) (**Figure 7.4 E**) and with LA emptying fraction (β=0.75, p=0.001) (**Figure 7.4 D**). Taken together these data suggest that a higher decrease in Phe levels associate, intriguingly, with a maladaptive cardiac phenotype at follow-up with impaired LV systolic function, increased interstitial diffuse collagen deposition (evidence supported by prolonged T1

Table 7.4 Influence of Long-Term Variation of Phenylalanine and Tyrosine on the Variation in CMR Parameters between Baseline and Follow-up Intervals

	Phenylalanine Gradient		Tyrosine Gradient	
	β	P Value	β	P Value
Anthropometrics				
Δ Weight, kg	0.56	***0.031***	-0.29	0.29
Δ BMI, kg/m2	0.55	***0.035***	-0.30	0.28
Δ BSA, m2	0.58	***0.023***	-0.30	0.28
Left Ventricle				
Δ LV EDV, mL	0.11	0.69	0.02	0.94
Δ LV ESV, mL	0.51	***0.050***	0.14	0.62
Δ LV SV, mL	0.34	0.22	-0.04	0.88
Δ LV EF, %	0.61	***0.017***	0.08	0.78
Δ LV CO, L/min	0.28	0.31	-0.16	0.56
Δ Septal ED WT, mm	-0.42	0.12	0.05	0.86
Δ Lateral ED WT, mm	-0.35	0.38	0.22	0.44
Δ LV Mass (g)	-0.15	0.59	-0.08	0.76
Δ LV Mass/ED volume, g/mL	-0.06	0.83	-0.02	0.94
Δ GLS Endo, %	-0.63	***0.012***	0.35	0.20
Δ GCS Endo, %	-0.28	0.32	0.39	0.15
Δ HD Syst Force (%)	-0.17	0.54	0.11	0.70
Δ HD Syst Work (%)	0.01	0.98	0.04	0.89
Δ HD Syst Work (mJ)	-0.12	0.66	0.14	0.62
Δ HD Syst Power (mJ/s)	-0.19	0.50	0.16	0.58
Δ HD Early Diast Force (%)	-0.06	0.82	0.35	0.21
Δ HD Early Diast Work (%)	0.06	0.85	0.19	0.51
Δ HD Early Diast Work (mJ)	0.23	0.40	0.05	0.87
Δ HD Early Diast Power (mJ/s)	0.40	0.14	0.05	0.86
Δ HD Late Diast Force (%)	0.08	0.78	0.04	0.88
Left Atrium				
Δ LA max Vol, mL	-0.24	0.39	0.41	0.13
Δ LA emptying fraction %	0.75	***0.001***	-0.12	0.67
Δ LA strain, %	0.51	0.05	0.21	0.46
Right Ventricle				
Δ RV EDV, mL	0.27	0.33	-0.04	0.90
Δ RV ESV, mL	0.10	0.73	-0.41	0.13
Δ RV SV, mL	0.27	0.34	0.15	0.60
Δ RV EF, %	0.21	0.46	0.30	0.27
Δ RV CO , L/min	0.20	0.47	0.07	0.80
Δ RV GLS, %	-0.17	0.55	-0.02	0.96
Ascending Aorta				
Δ Ao distens, 10-3mmHg-1	-0.11	0.70	0.51	0.05

Table 7.4 Influence of Long-Term Variation of Phenylalanine and Tyrosine on the Variation in CMR Parameters between Baseline and Follow-up Intervals (cont.)

Parametric Imaging				
Δ T1 native, ms	-0.78	***<0.001***	-0.02	0.96
Δ ECV, %	-0.61	***0.016***	0.32	0.24
Biochemistry				
Δ Carnitin free, mg/dL	0.07	0.82	0.20	0.47
Δ Carnitin total, mg/dL	0.08	0.79	0.19	0.50
Δ Carnitin ratio free/total	0.13	0.64	-0.09	0.75
Δ Cholesterol total, mg/dL	-0.08	0.78	-0.22	0.42
Δ HDL-Cholesterol, mg/dL	-0.02	0.94	0.06	0.84
Δ LDL-Cholesterol, mg/dL	0.00	0.99	0.41	0.13
Δ Triglycerides, mg/dL	-0.13	0.65	-0.40	0.14

Abbreviations:BMI body mass index, BSA body surface area, LV left ventricle, EDV end-diastolic volume, ESV end-systolic volume, SV stroke volume, CO cardiac output, WT wall thickness,, GLS global longitudinal strain, GCS global circumferential strain, Endo subendocardial, HD hemodynamic, Syst systolic, Diast diastolic, LA left atrium, RV right ventricle, Ao disten aortic distensibility, ECV extracellular volume. As ΔPhe is correlated to estimated ΔBSA, measured and not indexed values of CMR parameters were included in this analysis

times and increased ECV) and lower atrial emptying (likely in relation to an increased ventricular stiffness but also directly to atrial fibrosis).

We further tested the hypothesis that age [305,306] of the patients may contribute to some of the changes observed. All these correlations were maintained with age as a cofactor in bivariate regressions: (BMI: β=0.53, p=0.049, LVEF: β=0.53, p=0.012, GLS Endo: β=-0.58, p=0.016, T1 native: β=-0.77, p=0.001, ECV: β=-0.56, p=0.021). In contrast, Δ Tyr did not correlate with any of the parameters evaluated by this study. The only variation that showed a strong trend to be correlated with Δ Tyr is Aortic distensibility (β=0.51, p=0.052, non-significant). The complete numerical values are presented in **Table 7.4**.

7.5 Discussion

Following the data presented in the previous chapter where I characterized using CMR the cardiac phenotype of adult patients with PKU in a cross-sectional study, in this

chapter I investigated longitudinally, over a time span of 8.3±0.3 years, the changes produced in cardiac phenotype and related them to the biochemical control of the disease. There was an increase in BMI on average at follow-up but no significant change in the body composition ratios. Cardiac remodeling was observed at baseline with dilated LV and the largely reduced LV mass shifts, on average, towards a more concentric distribution with reduced LV EDV and ESV. EF of PKU patients remains unchanged with values that nevertheless remain mildly lower than expected in this age interval. [188] In keeping with the preservation of EF, LV GLS and GCS were also unchanged between baseline and follow-up. Regarding the parametric mapping, T1 native times, strikingly low in some patients at baseline, were significantly longer on average at follow-up but ECV remained unchanged. When we examined the correlation between the variation between Phe and respectively Tyr and the parameters characterizing the cardiovascular phenotype, we brought evidence of an adverse cardiac remodelling with decreased EF, GLS and LA strain, longer T1 and elevated ECV in patients in which the Phe levels were decreased the most at follow-up. Additionally, in agreement with previous data, maintaining or even lowering the Phe values at follow-up was associated with a more stable BMI.

Adult patients with PKU have their levels of Phe measured periodically and, accordingly are advised to maintain levels below an accepted limited, stated by national guidelines or local protocols. These levels are subject to variation depending on multiple parameters such as age, dietary adherence and therapeutic adjustments particularly dosing of protein substitutes and their energy content, genotype of phenylalanine mutation, adjacent changes in protein metabolism. [307] It was observed previously that in some individuals these values vary widely, however, the causes and implications of such reductions over longer periods of time are incompletely

understood. Some studies suggested that in addition to maintain low plasma concentrations, stability of Phe over time may be also important in avoiding neurological developmental and functional complications associated with the disease[308,309], however the mechanistic details as to how larger variations in Phe concentrations may produce tissue damage are still missing. On average, the mean Phe concentrations at follow-up showed a marked trend to be lower than at baseline, however this did not reach significance in our 15 patient cohort due to a large intersubject variability of this gradient. In contrast, Tyr concentrations remain more stable, probably do to a more efficient diet supplementation control that is not dependent of the unsupervised food intake. Due to previously documented variability between consecutive measurements in this study I chose to average the Phe values over a 2 year-period at both baseline and follow-up time-points, in this way offering a relevant picture of long-term variability of these concentrations and correcting for the short-term fluctuations which are less important from a clinical perspective and mostly due to secondary factors such as timing of the blood sample collection or recent food intake composition.

As part of the current clinical guidelines, PKU patients are advised to control long-term Phe intake as much as possible by restricting food rich in proteins such as meat, milk and dairy and eggs. [140] Even if national and local practices regarding the acceptable range vary, achieving lower Phe values through a better adherence to a Phe-free diet is widely considered a positive therapeutic course. [310] However, despite controlled nutritional adjustments under specialist guidance, a protein depleted food intake profile tends to switch towards an excessive lipid and carbohydrates dominated diet and further leads to higher BMI and particularly higher fat/muscular tissue mass. [281] Dietary hypercholesterolemia and a high LDL/HDL cholesterol ratio, frequently present in adult

PKU patients, was previously linked to systolic and diastolic contractile deficit induced through direct effect on SERCA-2 expression and intracellular Ca^{2+} handling. [311]

In **Chapter 5** I showed the importance of HD diastolic forces in non-invasively diagnosing raised LVEDP and in **Chapter 6** I showed that early diastolic HD forces were higher in PKU patients than in healthy subjects, indicating incipient diastolic dysfunction. Here we brought evidence that these values are even higher at follow-up suggesting the sustained nature of these changes that will require further investigation. Moreover, we also found that LV late diastolic HD forces are elevated and LA strain is reduced at follow-up compared with baseline. Taken together these findings support the idea of a progressive worsening of the diastolic function in adult PKU patients, with more strained diastolic hemodynamics most likely related to elevated pro-fibrotic mechanisms leading to chamber stiffness, decreased compliance and elevated filling pressures. In addition, aortic distensibility decreased at follow-up, this being in keeping with recent findings correlating the levels of oxidative stress with endothelial dysfunction and vascular impaired flow-mediated dilatation in peripheric circulation. Arterial stiffness precipitates and contributes to the development of HF amplifying hemodynamic stress and increasing energy demands on the heart muscle.

At baseline we found that the PKU patients had a more dilated LV with thinner walls and a severely reduced myocardial mass compared with matched healthy individuals. At follow-up we noted a decrease in EDV and an increase, albeit modest, in LVM, and in correlation the ratio LVM/EDV – an index used to discriminate between concentric and dilatative remodeling patterns [312] – was markedly higher. An increase of mass-to-volume ratio and impairment in systolic and diastolic parameters but not significant changes in EF were observed in physiological cardiac aging and, if prematurely present, associate with an increased risk of major cardiovascular events.[305] In

accordance with previous data, through an analysis of variance, I found that a marked decrease in Phe between baseline and follow-up associated a lower weight gain reflected by a lower increase in BMI, suggesting that in PKU patients who managed to decrease the average Phe levels, in doing so also manage better to control their BMI. Surprisingly, regarding the cardiac phenotype, in these patients I found the traits of a more pronounced maladaptive cardiac remodeling with reduced LV EF, impaired LV GLS and atrial strain, prolonged T1 native times and increased ECV. At follow-up, on average, the T1 native times were prolonged but ECV remained unchanged. In comparing the variations, ΔT1 and ΔECV were increased in patients with decreased Phe levels. Following the accepted parametric mapping interpretation, a chornic increase in both T1 native and ECV is an indication of diffuse collagen deposition [123] in the myocardium. Multiple evidence previously documented increased oxidative stress levels in adult PKU patients[143], and these were further correlated these with endothelial dysfunction and impaired vascular function.[148] Concurrently, persistent dyslipidemia per se can amplify fibrosis, determine microvascular dysfunction and depress myocyte contractility independently of hemodynamic overcharge associated with obesity. [313] Even if we did not find here a direct relation between ΔBMI and lipid fractions plasma concentrations, many PKU patients from our initial cohort presented and maintained over follow-up interval a certain degree of dyslipidemia, mostly resulting from decreased HDL-cholesterol and increased LDL/HDL-cholesterol ratio.

The relation between adipose tissue and cardiac remodelling remains controversial[314] with some studies underlining the positive roles of some adipokines such as adiponection, leptin, apelin and visfatin on various aspects of cardiovascular functions.[315] On the other hand, the daily diet of adult PKU patients is scarce in proteins and in compensation richer in lipid and carbohydrates compared with the normal age-

related diet. Both low-protein intake[316] and increased insulin resistance[317] associate worse diastolic and systolic cardiac function and are related to a higher incidence of heart failure. Lower Phe levels are mostly achieved and maintained through further protein-restriction[5] and that might be an important contributor to a negative cardiac remodeling and functional impairment. [318]

7.6 Limitations

I acknowledge the low number of participants in our follow-up study which may hide some of the significant differences at follow-up, larger studies comprising patients with a variety of Phe levels are required to give a more definitive answer. In order to discriminate better the effect of natural aging on cardiac remodeling, a comparison with a matched group of healthy controls at follow-up would have been ideal, however none of the changes observed correlated with the actual age of the patients in univariate regressions. As for the baseline study, due to local hardware limitations and ethical constraints I could not include a comprehensive cardiac spectroscopy exam in our follow-up visit and no histology or biomarker data were available to support the structural changes reported using parametric mapping. This could have offered an important insight into the lipid infiltration of the heart and respectively energetic balance and substrate utilization in the PKU heart and represents an important line of further work. Similarly, I could not include an echocardiography examination in the follow-up visit and this could have provided a more well-validated and detailed evaluation of the diastolic function.

7.7 Conclusions

Adult PKU patients may carry an increased risk for developing heart failure compared with the same age group of healthy individuals. Maintaining Phe values at a lower level

during adulthood but also a tight control of Phe values over time may be overall beneficial in precluding the neurological modifications, however a Phe restrictive diet creates the long-term risk of obesity which, due to additional risk factors and metabolic particularities, may have especially important effects for cardiac remodeling and prevalence of heart failure. Data presented here bring new details about cardiac phenotype of adult PKU patients with potentially important implications for the clinical management of these patients but further careful scrutiny of cardiovascular phenotype in larger cohorts are necessary in order to establish the optimal strategy. Moreover, mechanistic approaches on available disease models are warranted to determine the pathophysiological mechanisms responsible for these changes.

Chapter Eight:

Cardiac Involvement in COVID-19. Comparison with non-SARS CoV2 myocarditis

The work presented in this chapter is based on the article “COVID-19 vs. Classical Myocarditis Associated Myocardial Injury Evaluated by Cardiac Magnetic Resonance and Endomyocardial Biopsy” previously published in Frontiers in Cardiovascular Medicine. [319] I am the first author of this study and had the main contribution in study design, analysis and presentation of scientific data and in writing the manuscript. Endomyocardial biopsies were processed and analysed in collaboration with Professor Karin Klingel from the Universitätsklinikum Tübingen, and an expert opinion regarding the diagnostic outcome was certified by Professor Carsten Tschöpe from the Charité – Universitätsmedizin Berlin. Parametric maps quantification method and respectively compliance with updated Lake Louise Criteria have been agreed upon and verified by myself and Dr Patrick Doeblin, Consultant Cardiologist with CMR expertise, from the Cardiology and Internal Medicine Department, Deutsches Herzzentrum Berlin and followed scrupulously the current expert recommendations of the SCMR.

8.1 Abstract

Despite high mortality and worldwide spread, the impact of COVID-19 on cardiac structure and function is not completely understood. Myocarditis is a rare but potentially serious complication of other viral infections with variable recovery, and is in some cases being associated with long-term cardiac remodelling and functional impairment.

The aim of this study was to assess myocardial injury in patients, who recently recovered from an acute SARS-CoV-2 infection with advanced cardiac magnetic resonance imaging (CMR) and endomyocardial biopsy (EMB).

In total, 32 patients post COVID-19 with persistent cardiac symptoms, an additional 22 patients with acute classical myocarditis not related to COVID-19 and 16 healthy subjects were included and underwent a comprehensive baseline CMR scan. Of these,

10 patients post COVID-19 and 13 with non-COVID-19 myocarditis underwent a follow-up scan. In 10 of the post COVID-19 and 15 of the non-COVID-19 myocarditis patients endomyocardial biopsy (EMB) with histological, immunohistological and molecular analysis was performed.

10 (31%) patients with COVID-19 presented evidence of myocardial injury, 8 (25%) presented myocardial oedema, 8 (25%) exhibited global or regional systolic left ventricular (LV) dysfunction, and 9 (28%) reduced right ventricular (RV) function. However, only 3 (9%) of the COVID-19 patients fulfilled updated CMR - Lake Louise criteria (LLC) for acute myocarditis. Regarding EMB, none of the COVID-19 patients, but 87% of the non-COVID-19 myocarditis patients presented histological findings in keeping with acute or chronic inflammation. COVID-19 patients with severe disease on the WHO scale have a decreased biventricular longitudinal function, increased RV Mass and longer T1 native times compared with those with only mild or moderate disease.

In our cohort, CMR and EMB findings revealed that SARS-CoV-2 infection was related to a relatively mild but variable cardiac involvement. More symptomatic patients and those with higher clinical care demands were more likely to exhibit impaired myocardial function and chronic inflammation compared to patients with acute myocarditis during the acute and convalescent phases.

8.2 Background

The systemic response to a SARS-CoV-2 infection varies widely, ranging from asymptomatic or mildly symptomatic respiratory infection to a systemic life-threatening condition involving multiple organ failure. A three-phase model of pathogenesis of COVID-19 has been proposed[320] where a significant minority of patients progress to a

critical hyperinflammation phase characterised by a systemic host response with elevated IL-2, IL-6, IL-7, TNF-α, C-reactive protein and D-dimer levels. Some previous studies[168,321,322] demonstrated cardiac pathologic modifications, reflected by elevated troponin and N-terminal pro B-type natriuretic peptide in 10-28% of COVID-19 patients requiring hospitalisation. In a large multicentric study[176], myocardial injury was diagnosed in 62% of cases presenting with troponin elevation at admission or during hospitalisation and associated with higher frequency of structural and functional abnormalities on echocardiogram and higher mortality. In reverse, patients with cardiovascular comorbidities are more susceptible to develop severe forms of COVID-19. [321,322]

Several pathogenic mechanisms may explain the specific cardiac findings post-COVID-19: triggered pan-endotheliitis[168] or macrophage activation[323] precipitating acute plaque rupture and coronary events[324], imbalanced activation of T helper cells leading to cytokine storm and direct myocardial injury[3], sepsis or hypoxia induced myocyte apoptosis.[325] A brief review of the proposed mechanisms by which SARS-CoV2 infection triggers cardiovascular changes is presented in **Chapter 1** and summarised in **Figure 1.7**.

A recent cardiac magnetic resonance (CMR) cross-sectional study[177] suggested that COVID-19 might be responsible for a sustained subacute or chronic inflammatory state of the myocardium, comparable with cases of viral myocarditis, and prone to cause long-standing cardiac impairment by downstream activation of ventricular remodelling and fibrosis. However, the clinical relevance of these findings has been discussed controversially, given the lack of a matched comparison group.[326] In the same line, limited studies are to date available, comparing CMR findings including LGE

and mapping with histology, whereas longitudinal analyses are completely missing in this context. [327]

In this chapter, we used a tailored CMR protocol to examine potential effects of COVID-19 on cardiac function and structural remodelling in consecutive patients with recent SARS-CoV-2-infection, using endomyocardial biopsy (EMB) data as the reference standard. In addition, we sought to compare these findings to healthy volunteers and a cohort of 'classical' myocarditis patients. We also presented data on follow-up CMR assessment of patients with COVID-19 and of those with 'classic' myocarditis that satisfied the clinical criteria for cardiac imaging investigation. Parametric mapping methods (T1, ECV and T2) and respectively FT CMR offered an insight into the effects that structural modifications may have on the biventricular function in COVID-19 patients and report the reversibility of these findings over several months of convalescence. In order to validate better these findings, I sought to additionally compare the histological/immuno-histological findings between COVID-19 and myocarditis patients in which all available EMB samples were evaluated according to the current diagnostic criteria for myocarditis.[328]

8.3 Specific Methods

8.3.1. Study population

All post-COVID-19 patients referred to our clinic with a clinical indication for CMR [181] were asked for consent to be included in our observational study. Healthy control subjects were identified from an existing database available at our institution. [181] This study was previously reviewed and approved by an Ethics Committee (Charité – Universitätsmedizin Berlin) and complies with the Declaration of Helsinki.

In total, 32 patients with a previous COVID-19 infection were included in the study. For comparison, we also retrospectively included 22 patients with a clinically confirmed diagnosis of acute non-COVID-19 myocarditis and an available baseline CMR scan, as well as 16 healthy subjects. Ten of the post-COVID-19 patients underwent a clinically indicated follow-up scan. Thirteen of the 22 patients with acute myocarditis had an available follow-up CMR. Inclusion criteria for the COVID-19 patients were: (I) a previously diagnosed[329] SARS-CoV-2 infection with COVID-19 disease, (II) clinical indication for CMR such as suspected myocardial injury (elevated troponin), reduced LVEF and/or presence of pericardial effusion on echocardiogram, persistent arrhythmia, persistent dyspnoea, reduced exercise capacity or fatigue, (III) resolution of the acute COVID-related symptoms to allow the end of self-isolation or a confirmation of a negative swab test. Exclusion criteria were absolute generic contraindications to CMR, and impossibility to obtain consent. The non-COVID-19 myocarditis cases were retrospectively identified from our local database, inclusion criteria followed the most recent ESC guidelines and recommendations[179] and exclusion criteria were: coexistence of a previously known cardiac pathology (myocardial infarction, cardiomyopathy, haemodynamically relevant valvulopathy).[182] More comprehensive details of inclusion and exclusion criteria are presented in **Chapter 2**.

8.3.2. WHO Score Description

WHO (World Health Organization) guidance on clinical management of COVID-19 (https://www.who.int/publications/i/item/clinical-management-of-covid-19) was used to define disease severity as follows: mild and moderate disease – symptomatic patients meeting the case definition for COVID-19 without evidence of viral pneumonia or hypoxia, or some clinical signs of pneumonia (fever, cough, dyspnoea, fast breathing)

without other criteria of severity and SpO2 ≥ 90% on room air. Severe and critical disease were defined as presence of additional severity signs and respiratory distress: respiratory rate > 30 breaths/min; severe respiratory distress; or SpO2 < 90% on room air or presence of acute respiratory distress syndrome or specific signs on radiograph, CT scan, or lung ultrasound: bilateral opacities, not fully explained by volume overload, lobar or lung collapse, or nodules.

8.3.3 Cardiac magnetic resonance

CMR images were acquired using 3 clinical MRI scanners as follows: 25 COVID-19 patients, 18 myocarditis patients and all 16 healthy controls with a clinical 3T system (Ingenia, Philips Healthcare, Best, the Netherlands), 4 COVID-19 patients and 4 myocarditis patients with a 1.5T system (Achieva, Philips Healthcare, Best, the Netherlands) and 3 COVID-19 patients with a 1.5T system (Magnetom Aera, Siemens Inc.). All study participants were scanned with a comprehensive imaging protocol and appropriate local receiver coil arrays in accordance with SCMR guidelines.[17] (**Figure 8.1**) All CMR scans were acquired with ECG-gating or retrospective gating (cine) in one breath hold (8-15s). Typical imaging parameters and acquisitions protocols are detailed in **Chapter 2**.

8.3.4 Image analysis

All images were analyzed offline using commercially available software (Medis Suite, version 3.1, Leiden, The Netherlands) in accordance to a recent consensus document for the quantification of LV function using CMR. [182] To assess whether the updated Lake Louise Criteria (LLC) for myocarditis were fulfilled, the proposed updated analysis algorithm[128] was scrupulously followed.

8.3.5 Biopsy samples

All patients, including those with COVID-19 undergoing EMB, had a clinical suspicion for myocarditis. Indications followed the recent guideline recommendations[179]. Analysis of endomyocardial biopsy (EMB) samples was performed in specialized laboratories by experienced cardio-pathologists as described previously.[193] Details can be found in **Chapter 2**.

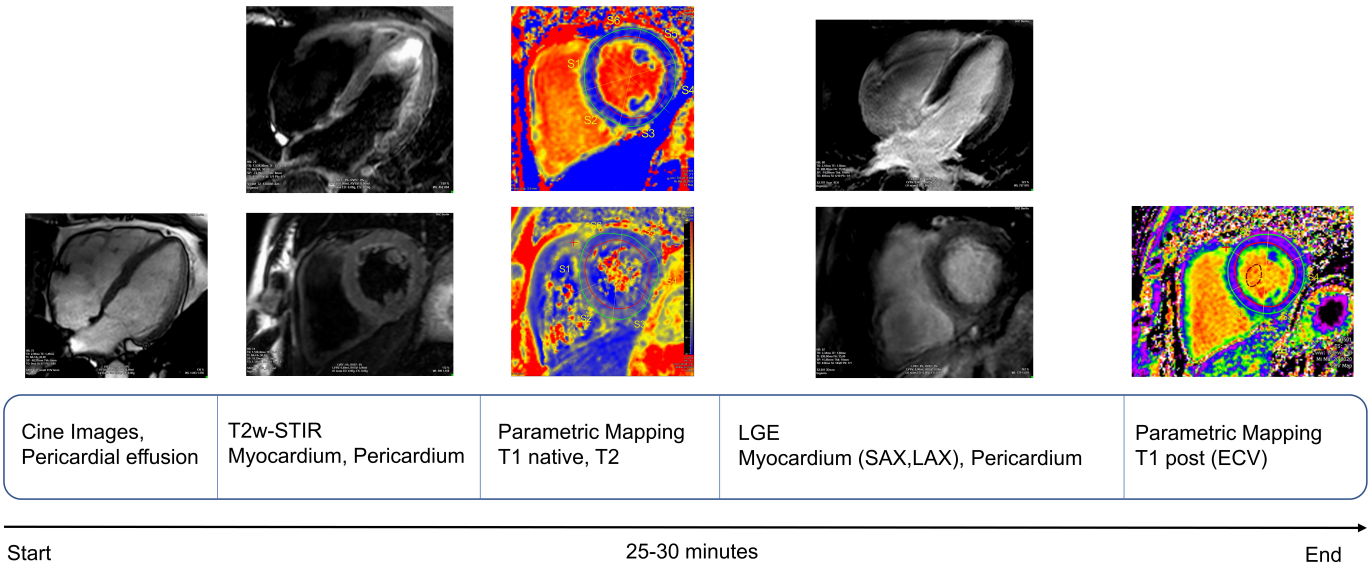


Figure 8.1 Schematic representation of CMR protocol workflow used for our study, in keeping with recent SCMR recommendations for evaluation of patients with COVID-19 (Kelle et al., *J Cardiovasc Magn Reson.* 2020 Sep 3;22(1):61.).

8.3.6 Statistical analysis

All the data within the text, tables or figures is presented as mean ± SD, unless stated otherwise. Shapiro-Wilk test was used to decide the normal distribution of data for every dataset included. To compare the three subgroups, a one-way ANOVA for normally distributed data or Kruskal-Wallis for non-normally distributed data was performed followed by Tukey post-hoc tests to compare differences among subgroups. The Wilcoxon test was used to assess the differences between baseline and follow-up

groups. The Welch correction was applied for unequal sample sizes or if the assumption of homogeneity of variance was infirmed. For differences between categorical variables Fisher's exact and χ^2 test were used. A two-tailed P value below 0.05 was considered statistically significant. All statistical tests were performed using SPSS version 27.0.

8.4 Results

8.4.1 Study Population Characteristics

Demographics, clinical and biochemical characteristics of the patients included in our study are presented in **Table 8.1**. 12 (38%) of 32 COVID-19 and respectively, 17 (77%) of 22 patients with non-COVID-19 myocarditis required hospitalisation. According to the WHO disease severity criteria for COVID-19, 20 out of 32 (63%) COVID-19 patients had mild or moderate, 7 (22%) had severe and 5 (16%) had critical disease. While fever, cough and loss of taste or smell were dominant in COVID-19 patients, some of them also suffered from palpitations (1, 3%), chest pain (8, 25%), arrhythmia (9, 28%) or had elevated troponin (9, 28%) or NT-proBNP (6, 24%). During the convalescence phase, fatigue persisted in 9 (28%), loss of taste or smell in 2 (6%) and amnesia in 2 (6%) in COVID-19 patients. COVID-19 patients were scanned for a baseline visit at 95±59 days after a first positive test and for a follow-up visit at 68±40 days after the baseline scan. Myocarditis patients were initially scanned shortly after onset of symptoms and had a longer and more variable follow-up interval of 156±124 days. There was an age discrepancy between the healthy control, COVID-19 and myocarditis groups (24±5 vs 48±14 vs 32±15 years, $p < 0.001$). Healthy controls had a lower BMI than COVID-19 and myocarditis patients. The risk factors were largely similar between COVID-19 and myocarditis groups. (**Table 8.1**)

Table 8.1 Demographics. Clinical parameters

	Healthy Control N=16	COVID-19 N=32	Myocarditis N=22	P ANOVA	P† Control vs COVID-19	P‡ Control vs Myocarditis	P# COVID-19 vs Myocarditis
Patient characteristics							
Age, y	24±5	48±14	32±15	***<0.001***	***<0.001***	***0.031***	***0.004***
Male, N (%)	8 (50)	19 (59)	17 (77)		0.54	0.08	0.17
BMI	22±3	26±5	26±5	***0.005***	***0.004***	***0.030***	0.75
Hypertension, N (%)	0 (0)	13 (42)	3 (19), N=16		***0.012***	0.12	0.14
Diabetes, N (%)	0 (0)	1 (3)	1 (6), N=16		0.48	0.31	0.22
Hypercholesterolemia, N (%)	0 (0)	8 (26)	2 (13), N=16		***0.029***	0.14	0.31
Known CAD, N (%)	0 (0)	3 (10)	1 (6), N=16		0.21	0.31	0.71
Smoking, N (%)	0 (0)	13 (41)	5 (31), N=16		***0.003***	***0.015***	0.53
COPD or asthma, N (%)	0 (0)	3 (10)	2 (13), N=16		0.21	0.14	0.74
Systolic BP (mm Hg)	112±17	119±15	114±19		0.50	0.92	0.72
Diastolic BP (mm Hg)	68±11	73±11	66±10		0.26	0.90	0.09
Heart rate, beats per min	65±5	78±15	88±22		0.83	0.94	0.91
Blood test results							
High-sensitivity CRP, mg/dL		4 ± 9, N=23	8 ± 12, N=18				0.17
Elevated hsCRP, N (%)		5 (22), N=23	10 (56), N=18				***0.033***
Elevated Troponin, N (%)		9 (45), N=20	10 (71), N=14				0.17
CK (U/L)		70±37, N=22	343±396, N=20				***<0.001***
CK-MB (U/L)		18±5, N=15	37±25, N=20				***<0.001***
NT-proBNP (ng/L)		1291±2484, N=23	2194±2360, N=17				0.19
Elevated NT-proBNP, N (%)		6 (24), N=25	15 (88), N=17				***<0.001***
eGFR (mL/min)		83±24, N=26	95±16, N=17				***0.045***
Medication		**N=32**	**N=16**				
Oral Anticoagulants, N (%)		4 (13)	2 (13)				0.70
Statins, N (%)		3 (9)	1 (6)				0.51
β-blockers, N (%)		14 (44)	8 (50)				0.59
Diuretics, N (%)		12 (38)	6 (38)				0.43
Nitrates, N (%)		0 (0)	0 (0)				0.99
ACEi, N (%)		10 (31)	3 (19)				0.14
Sartans, N (%)		5 (16)	1 (6)				0.20
Calcium Antagonists, N (%)		2 (6)	0 (0)				0.23
Symptoms		**N=32**	**N=16**				
Initial Presentation							
Fever, N (%)		19 (59)	5 (31)				0.07
Chest pain, N (%)		8 (25)	9 (56)				***0.033***
Dyspnea, N (%)		20 (63)	9 (56)				0.68
Arrythmia, N (%)		1 (3)	7 (44)				***<0.001***
Cough, N (%)		24 (75)	1 (6)				***<0.001***
Nausea/vomiting/diarrhea, N (%)		11 (34)	3 (19)				0.26
Fatigue/weakness, N (%)		24 (75)	11 (69)				0.65
Amnesia, N (%)		10 (31)	5 (31)				0.99
Lack of taste or smell, N (%)		21 (66)	0 (0)				***<0.001***
Persistent							
Fatigue/weakness, N (%)		9 (28)	0 (0)				***0.019***
Amnesia, N (%)		2 (6)	0 (0)				0.31
Lack of taste or smell, N (%)		2 (6)	0 (0)				0.31
Arrythmia , N (%)		9 (28)	3 (19)				0.48

Abbreviations: BMI, body mass index, CAD, coronary artery disease, COPD chronic obstructive pulmonary disease, COVID-19 coronavirus disease, hsCRP – high sensitivity C-reactive protein, CK – creatin-kinase, NT-proBNP – N-terminal pro-b type natriuretic peptide, eGFR – estimated glomerular filtration rate, ACEi – angiotensin-converting enzyme inhibitors. For incomplete set of data, N represents the number of subjects included in the analysis.

8.4.2 CMR parameters. Comparison between COVID-19, myocarditis and healthy volunteers

CMR parameters for each of the three groups are presented in **Table 8.2**. In one of the COVID-19 patients, no contrast agent was administered, due to claustrophobia and distress during the scan; an abbreviated protocol was used in this case. Given the discrepancies between the normal range of values for parametric mapping (T1, ECV, T2 values) for these comparisons, only the subjects scanned on 3T Philips Ingenia scanner were included in the analysis (specific numbers per group are specified in brackets in **Table 8.2**).

There were no significant differences between COVID-19 and controls for any of the CMR parameters apart from T2 values, which were significantly higher in the COVID-19 (48±6 vs 43±2ms, p=0.026) and RV stroke volume, which was significantly lower in the COVID-19 group (41±9 vs 49±8ml/m^2, p=0.031). There were no differences between LV function, RV function and mass between COVID-19 patients and healthy controls (**Figure 8.2**). COVID-19 patients had a normal left ventricular ejection fraction (LVEF), compared to a significantly reduced LVEF in myocarditis patients (61±11 vs. 51±17%, p=0.016). LV dysfunction in myocarditis was also reflected by lower values of longitudinal and circumferential strain, which were normal in COVID-19 patients. LV and RV mass were both increased in myocarditis but not in COVID-19 compared with controls (**Figure8.2**). Atrial function measured as LA and RA emptying fractions and strain was impaired in myocarditis compared with controls and COVID-19. T1 native, ECV and T2 values were all higher in myocarditis compared with controls and COVID-19 (**Figure 8.3**, **Table 8.2**). In addition, in all of myocarditis patients there were areas of LGE in myocardium and pericardium, while only 6 (19%) of the COVID-19 patients had myocardial LGE, respectively 6 (19%) had pericardial LGE (**Table 8.2**).

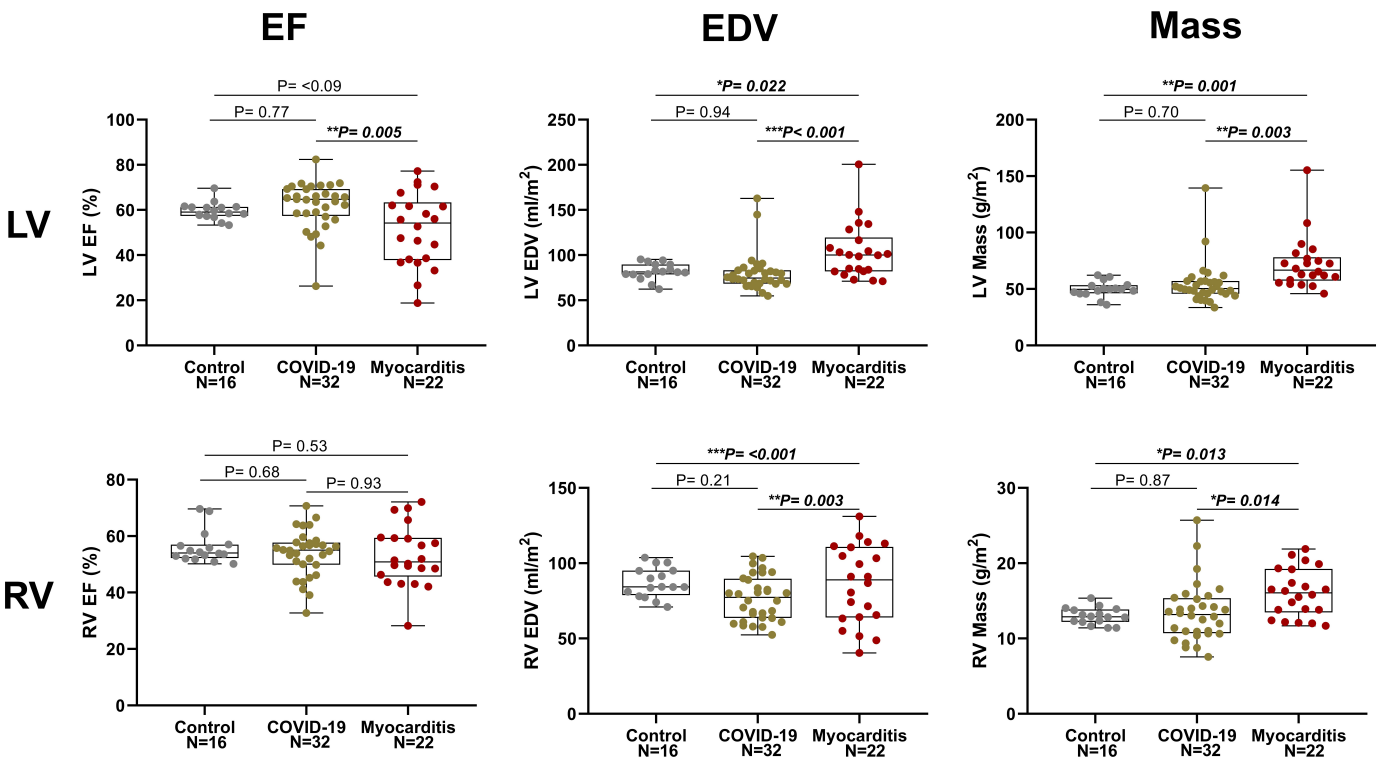


Figure 8.2 LV (upper row) and RV (lower row) EF, EDV and myocardial mass in 3 pathology groups (from left to right: Control, COVID-19, Myocarditis). There is no difference on average between COVID-19 patients and Controls however there is significant dysfunction and remodelling in some of these patients that overlaps with the myocarditis spectrum. A P value <0.05 was considered statistically significant, and indicated as follows: *< 0.05, **<0.01. ***<0.001.

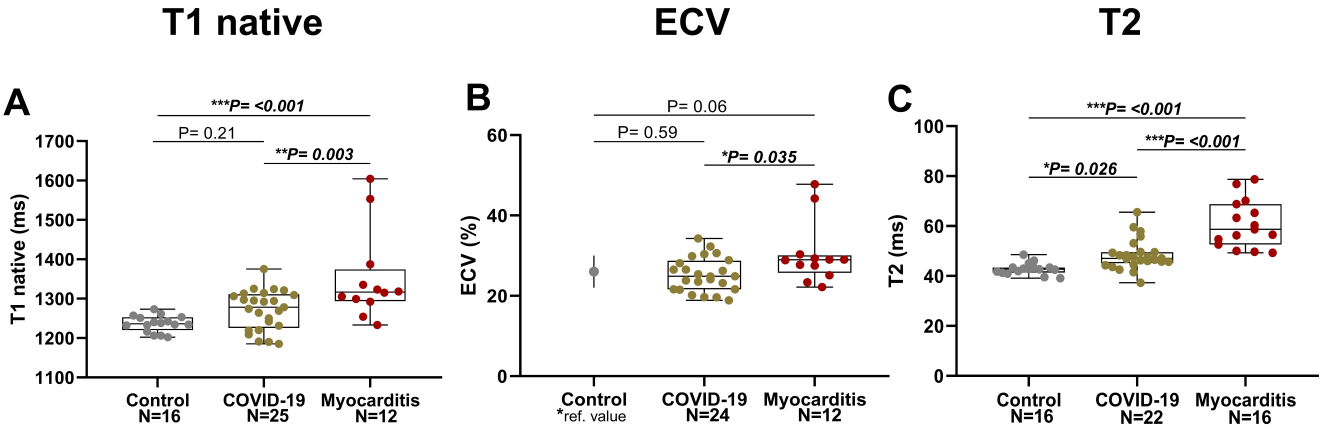


Figure 8.3 Parametric Imaging in 3 pathology groups (from left to right: Control, COVID-19, Myocarditis): **A.** T1 native, **B.** Extracellular volume (ECV) – for the Control it is represented the mean and SD referenced in literature (Dabir et al., *J Cardiovasc Magn Reson.* 2014;16:69) corresponding to similar manufacturer and magnet field strength, **C.** T2. A P value <0.05 was considered statistically significant, and indicated as follows: * < 0.05, **<0.01. ***<0.001.

Table 8.2 Cardiac Magnetic Resonance Imaging Findings. Baseline.

	Healthy Control	COVID-19	Myocarditis	P ANOVA	P† Control vs	P‡ Control vs	P# COVID-19 vs
	N=16	N=32	N=22		COVID-19	Myocarditis	Myocarditis
Left Ventricle							
LV EDV (mL/m^2)	82±9	78±25	104±31	***0.001***	0.94	***0.022***	***<0.001***
LV ESV (mL/m^2)	33±4	32±20	54±34	***0.003***	0.98	***0.023***	***0.004***
LV SV (mL/m^2)	49±7	48±8	50±11	0.66			
LV EF (%)	60±4	62±10	52±16	***0.006***	0.77	0.09	***0.005***
LV CI (L/min/m^2)	3.5±0.8	3.6±0.9	3.7±0.9	0.80			
LV GLS Endo (%)	-26.0±2.1	-24.2±4.4	-20.1±7.0	***0.001***	0.61	***0.003***	***0.008***
LV GLS Myo (%)	-24.5±2.0	-22.3±4.1	-18.3±5.8	***<0.001***	0.25	***<0.001***	***0.005***
LV GCS Endo (%)	-31.5±4.4	-32.0±7.2	-24.0±9.3	***<0.001***	0.96	***0.009***	***<0.001***
LV GCS Myo (%)	-20.9±2.7	-20.9±4.2	-17.3±6.9	***0.025***	0.99	0.08	***0.030***
LVM (g/m^2)	50±7	55±19	72±23	***<0.001***	0.70	***0.001***	***0.003***
Left Atrium							
LA max Vol (mL/m^2)	37±9	36±8	41±11	0.26			
LA EF (%)	70±6	61±12	54±17	***0.003***	0.07	***0.002***	0.19
LA strain (%)	44±11	39±12	28±16	***0.001***	0.42	***0.001***	***0.011***
Right Ventricle							
RV EDV (mL/m^2)	87±10	77±15	86±26	0.10			
RV ESV (mL/m^2)	38±7	36±10	42±19	0.26			
RV SV (mL/m^2)	49±8	41±9	44±12	***0.040***	***0.031***	0.30	0.51
RV EF (%)	56±6	54±8	53±11	0.55			
RV GLS Endo %	-29.7±7.1	-28.2±7.8	-27.1±7.3	0.56			
RV GLS Myo %	-27.9±6.5	-26.0±7.4	-25.2±6.8	0.81			
RVM (g/m^2)	13±1	13±4	16±3	***0.006***	0.87	***0.013***	***0.014***
Right Atrium							
RA max Vol (mL/m^2)	40±7	37±12	43±11	0.15			
RA EF (%)	56±9	54±11	47±13	***0.027***	0.80	***0.039***	0.07
RA strain (%)	50±16	42±13	36±13	***0.012***	0.16	***0.009***	0.25
Parametric Imaging							
T1 native (ms)	1236±21 (n=16)	1271±50 (n=25)	1352±113 (n=12)	***<0.001***	0.21	***<0.001***	***0.003***
ECV (%)	26±4* (ref)	25±4 (n=24)	30±8 (n=12)	***0.044***	0.59	0.06	***0.035***
T2 (ms)	43±2 (n=16)	48±6 (n=25)	61±10 (n=15)	***<0.001***	***0.026***	***<0.001***	***<0.001***
		N=31	N=22				
LGE No. (%)							
Ischaemic	n/a	1 (3)	3 (14)				0.17
Nonischaemic	n/a	5 (16)	19 (86)				***<0.001***
Pericardial	n/a	3 (10)	4 (18)				0.37

* Reference Value

Abbreviations: ED – end diastolic, ES – end systolic, Endo – subendocardial layer, Myo – mid-myocardial layer, LV – left ventricular RV – right ventricular, EF – ejection/emptying fraction, GLS – global longitudinal strain, GCS – global circumferential strain, LA – left atrial, RA – right atrial, ECV – extracellular volume, LGE – late gadolinium enhancement. For incomplete set of data, N represents the number of subjects included in the analysis. *Reference Values for ECV in healthy controls was taken from Dabir et al., *J Cardiovasc Magn Reson.* 2014;16:69.

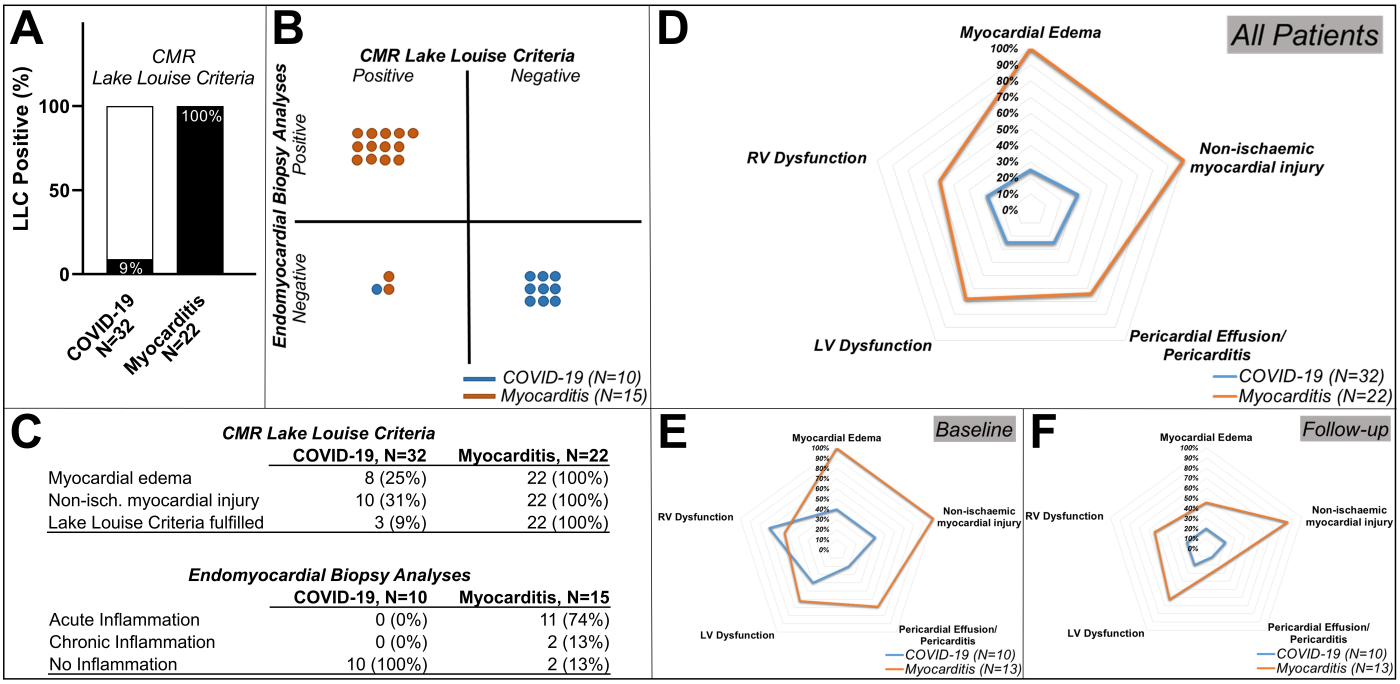


Figure 8.4 Lake Louise Criteria (LLC) and Functional Impairment in COVID-19 and Myocarditis Patients. **A.** Comparison of the CMR Lake Louise Criteria and endomyocardial biopsy findings. 3 out of 32 (9%) patients with COVID-19 and all 22 (100%) of the myocarditis patients have positive Lake Louise Criteria, **B.** from the patients in which EMB was available: none of the patients with COVID-19 and 13 (87%) out of 15 myocarditis patients with available EMB had histological findings in keeping with this diagnosis, 1 (10%) of the COVID-19 patients and 2 (13%) of the myocarditis patients have positive LLC but negative EMC diagnostic criteria. **C.** tables with numeric values for CMR LLC (upper rows) and Endomyocardial Biopsy Analyses (lower rows) **D.** spidernet representation of myocardial inflammation, injury, pericardial involvement, LV and RV dysfunctions in all COVID-19 (blue polygons) and all Myocarditis (red polygons) patients, **E.** (baseline), **F.** (follow-up) – spidernet representations of myocardial inflammation, injury, pericardial involvement, LV and RV dysfunctions in patients with COVID-19 (blue polygons) and Myocarditis (red polygons) with an available follow-up scan.

8.4.3 CMR - Lake Louise Criteria and EMB histological analyses.

In total, only 3 (9%) of the COVID-19 patients fulfilled the updated LLC for acute myocarditis: 4 (13%) presented signs of myocardia oedema (areas of elevated signal on T2 maps or T2-weighted images), 10 (31%) had signs of myocardial injury (abnormal T1, ECV or LGE). Additionally, 8 (25%) had LV wall motion abnormalities, 9 (28%) had an impaired RV function, and 8 (25%) had evidence of pericardial effusion and/or pericarditis (**Figure 8.4 A., C., Table 8.3**).All myocarditis cases (100%) fulfilled

the updated LLC with evidence of myocardial oedema and non-ischaemic myocardial injury. Additionally, 8 (25%) showed signs of pericarditis or pericardial effusion. Fifteen (68%) had systolic LV dysfunction and 13 (59%) LV dilatation. RV impairment was present in 13 (59%) and RV dilatation in 9 (41%) (**Figure 8.4 A., C. Table 8.3**). EMB was available in 10 out of 32 patients with COVID-19. None of these samples presented evidence of acute or chronic myocarditis, as usually observed in viral myocarditis. (**Figure 8.4**) In 5 (50%) of these patients traces of previous myocardial inflammation was identifiable, but no evidence of ongoing inflammation (<14 infiltrating cells/mm^2). [328] EMB was available in 15 out of 22 patients with myocarditis. Of these eleven (74%) showed evidence of acute inflammation and two (13%) of chronic inflammation (**Figure 8.5**).

Table 8.3 Summary of Lake Louise Criteria and Ventricular dysfunction

A

	All Patients, Baseline	
	COVID-19 (N=32)	**Myocarditis (N=22)**
2018 Lake Louise for Myocarditis fulfilled, N (%)	3 (9)	22 (100)
Myocardial edema (T2-mapping or T2W images)	8 (25)	22 (100)
Non-ischaemic Myocardial Injury (abnormal T1, ECV or LGE)	10 (31)	22 (100)
Pericarditis (effusion in cine images or abnormal LGE, T2 STIR)	8 (25)	14 (64)
Systolic LV Dysfunction (regional and or global WMA)	8 (25)	15 (68)
Depressed LVEF, N (%)	6 (19)	11 (50)
LV dilatation, N (%)	3 (9)	13 (59)
LV increased wall thickness, N (%)	7 (22)	4 (18)
Depressed RV EF, N (%)	9 (28)	13 (59)
RV dilatation, N (%)	4 (13)	9 (41)

B

	Only Patients will Follow-up			
	COVID-19 (N=10)		**Myocarditis (N=13)**	
	Baseline	**Follow-up**	**Baseline**	**Follow-up**
2018 Lake Louise for Myocarditis fulfilled, N (%)	2(20)	1(10)	13 (100)	5 (38)
Myocardial edema (T2-mapping or T2W images)	4 (40)	2 (20)	13 (100)	6 (46)
Non-ischaemic Myocardial Injury (abnormal T1, ECV or LGE)	4 (40)	2 (20)	13 (100)	11(85)
Pericarditis (effusion in cine images or abnormal LGE, T2 STIR)	2 (20)	1 (10)	9 (69)	3 (23)
Systolic LV Dysfunction (regional and or global WMA)	4 (40)	2 (20)	8 (62)	8 (62)
Depressed LVEF, N (%)	3 (30)	1 (10)	5 (38)	4 (31)
LV dilatation, N (%)	1 (10)	0 (0)	7 (54)	4 (31)
LV increased wall thickness, N (%)	3 (30)	3 (30)	2 (15)	2 (15)
Depressed RV EF, N (%)	7 (70)	2 (20)	7 (54)	7 (54)
RV dilatation, N (%)	2 (20)	1 (10)	6 (46)	5 (38)

A: All patients with COVID-19 (N=32) and Myocarditis (N=22), **B**: only patients with follow-up with COVID-19 (N=10) and Myocarditis (N=13). Abbreviations: T2W – T2 weighted, STIR – Short-TI Inversion Recovery, LGE – late gadolinium enhancement, WMA – wall motion abnormalities, LV – left ventricle, RV right ventricle, EF – ejection fraction.

Table 8.4 WHO Criteria of Disease Severity.

COVID-19 Patients (N=32)	WHO Disease Severity Scale		
	WHO mild, moderate disease (N=20)	WHO severe disease (N=12)	P
Initial Presentation			
Fever, N (%)	9 (45)	10 (83)	***0.033***
Chest Pain, N (%)	6 (30)	2 (17)	0.40
Dyspnea, N (%)	12 (60)	8 (67)	0.71
Arrythmia, N (%)	0 (0)	1 (8)	0.19
Cough, N (%)	14 (70)	10 (83)	0.40
Nausea/Vomiting/Diarrhea, N (%)	8 (40)	3 (25)	0.39
Fatigue, weakness, N (%)	17 (85)	7 (58)	0.09
Amnesia, N (%)	6 (30)	4 (33)	0.99
Lack of taste or smell, N (%)	16 (80)	5 (42)	***0.027***
Persistent			
Fatigue/weakness, N (%)	9 (45)	0 (0)	***0.006***
Amnesia, N (%)	1 (5)	1 (8)	0.99
Lack of taste or smell, N (%)	2 (10)	0 (0)	0.26
Arrythmia, N (%)	6 (30)	4 (33)	0.84
Left Ventricle			
LV EDV (mL/m^2)	78±27	79±23	0.85
LV ESV (mL/m^2)	31±22	34±16	0.71
LV SV (mL/m^2)	50±6	46±10	0.19
LV EF (%)	64±10	59±11	0.23
LV CI (L/min/m^2)	3.5±0.8	3.7±1.2	0.50
LV GLS Endo (%)	-26.3±4.1	-21.6±4.3	***0.004***
LV GLS Myo (%)	-24.0±3.3	-19.5±3.8	***0.001***
LV GCS Endo (%)	-32.8±6.1	-31.0±8.9	0.49
LV GCS Myo (%)	-21.8±3.8	-19.4±4.5	0.13
LVM (g/m^2)	50±12	62±25	0.07
Left Atrium			
LA max Vol mL	37±7	36±11	0.84
LA emptying fraction %	65±8	54±15	***0.030***
LA strain %	42±11	33±12	***0.029***
Right Ventricle			
RV EDV (mL/m^2)	77±14	77±17	0.97
RV ESV (mL/m^2)	34±8	39±13	0.27
RV SV (mL/m^2)	43±9	38±7	0.16
RV EF (%)	55±7	51±9	0.14
RV GLS Endo %	-30.5±5.9	-24.2±9.1	***0.048***
RV GLS Myo %	-28.3±5.3	-22.1±8.9	***0.044***
RVM (g/m^2)	12±3	16±5	***0.011***
Right Atrium			
RA max Vol mL	37±12	37±12	0.85
RA emptying fraction %	53±11	55±11	0.65
RA strain %	46±11	36±14	***0.034***
Parametric Imaging			
T1 native (ms)	1258±55 (N=16)	1296±30 (N=9)	***0.035***
ECV (%)	26±5 (N=16)	27±3 (N=9)	0.64
T2 (ms)	47±4 (N=16)	51±7 (N=9)	0.06
	(N=20)	(N=11)	P
LGE No. (%)			
Ischaemic	0 (0)	1 (9)	0.19
Nonischaemic	3 (15)	2 (18)	0.90
Pericardial	3 (15)	0 (0)	0.16
	(N=20)	(N=12)	
Lake Louise Criteria			
2018 LLC fulfilled, N (%)	0 (0)	3 (19)	
Myocardial edema	3 (15)	5 (42)	
Non-ischaemic Myocardial Injury	6 (30)	4 (33)	
Pericarditis/ pericardial effusion	3 (15)	5 (42)	
Systolic LV Dysfunction (global or regional)	2 (10)	6 (50)	
Depressed LV EF, N (%)	1 (5)	5 (42)	
LV dilatation, N (%)	2 (10)	1 (8)	
LV increased wall thickness, N (%)	2 (10)	5 (42)	
Depressed RV EF, N (%)	2 (5)	7 (58)	
RV dilatation, N (%)	2 (10)	2 (17)	

Abbreviations: WHO (World Health Organization), ED – end diastolic, ES – end systolic, SV – stroke volume, GLS – global longitudinal strain, GCS global circumferential strain, Endo – subendocardial layer, Myo – mid-myocardial layer, LV – left ventricular RV – right ventricular, LA – left atrial, RA – right atrial, ECV – extracellular volume, LLC – 2018 updated Lake Louise Criteria for acute myocarditis. For incomplete set of data, N represents the number of subjects included in the analysis.

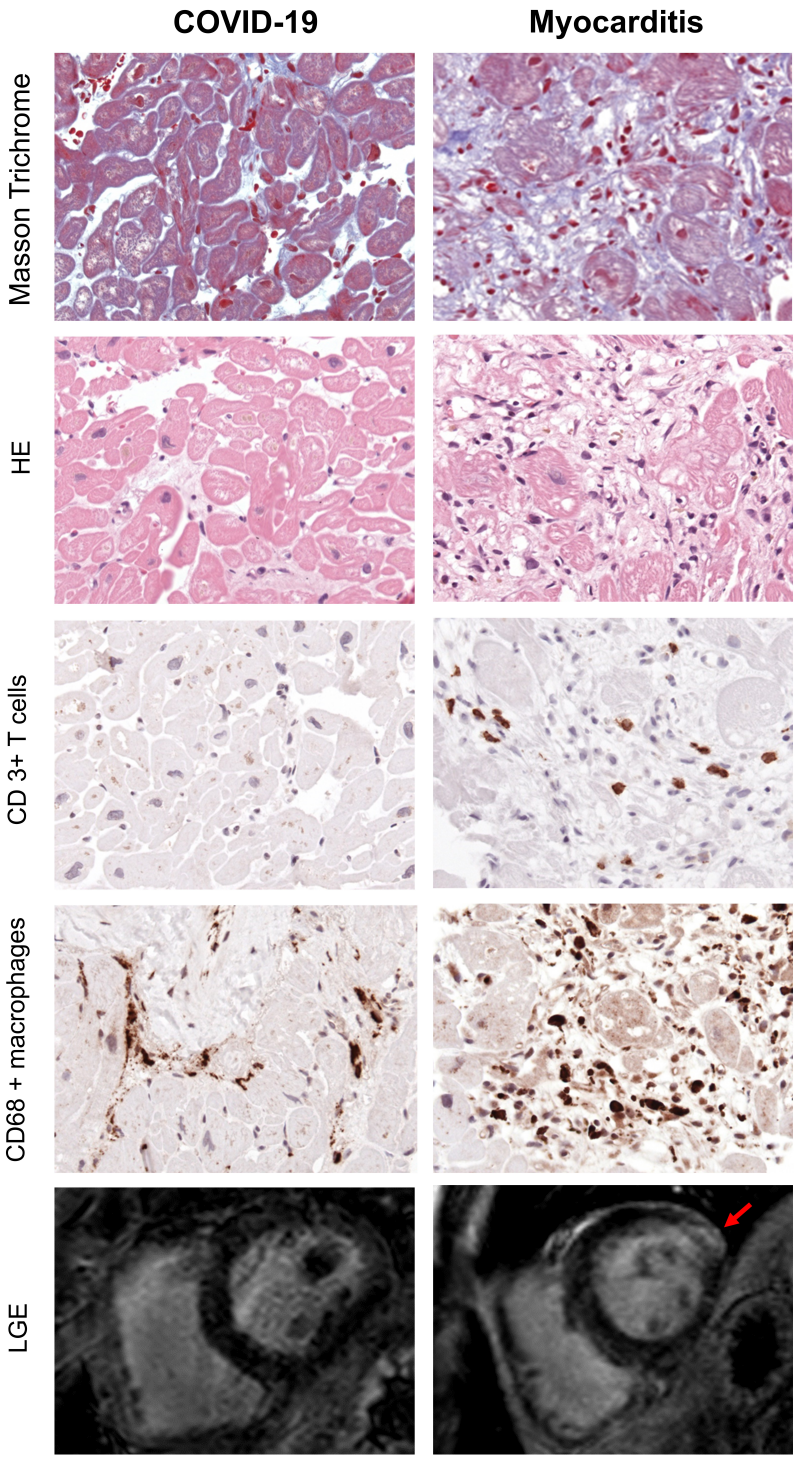


Figure 8.5 Exemplary EMB and CMR findings in COVID-19 (left) and Myocarditis (Right). First 4 rows from top represent respectively: Masson Trichrome, hematoxylin/eosin and immunohistological stainings of CD3+ T cells and CD68+ macrophages. In myocarditis, numerous T cells and macrophages are detected in presence of myocyte necrosis and fibrosis. In contrast, the majority of COVID-19 patients often show fibrosis but no myocyte necrosis or significant T cell infiltration; however, the amount of macrophages is enhanced (x400). Bottom row represents CMR short-axis LGE images: there is evidence of fibrosis in the lateral wall (indicated by the red arrow) in myocarditis patient (right), while in COVID-19 there are no LGE positive areas in keeping with the absence of active inflammation and fibrosis indicated by the histology.

In 2 patients with myocarditis no histological evidence of inflammation was present (**Figure 8.4 B**). Of note, CMR LLC were positive in one patient (10%) with COVID-19 and respectively in two patients (13%) with myocarditis, in which EMB samples were negative. (**Figure 8.4 B**).

8.4.4 CMR parameters and WHO Classification

We compared the CMR parameters between patients with mild and moderate forms of the disease (as defined by WHO) and respectively complicated or critical stages. Both LV and RV longitudinal systolic deformation is lower, RV Mass and LV T1 native values are higher in COVID-19 patients with complicated or critical disease compared with those with mild or moderate disease. LA and RA strains were lower in more severely affected patients. Additionally, there were trends for higher LVM and longer T2 in complicated or critical compared with mild or moderate disease. Detailed results are presented in **Table 8.4**.

8.4.5 CMR parameters. Comparison follow-up

A complete description of these data is presented in **Table 8.5**. In COVID-19 patients, the difference in LVEF and Endo GCS (-31.7±8.9 vs -34.2±8.6 %, p=0.21) was not significant but showed a trend for improvement (60±11 vs 64±8%, p=0.13). There was however significant improvement in Endo GLS (-23.4±3.8 vs -26.5±3.7 %, p=0.034) and in right ventricular ejection fraction (RVEF, 48±7 vs 54±5%, p=0.032), whereas LV mass (p=0.002) and RV mass (P=0.040) significantly decreased (**Figure 8.6**). Similar differences in terms of GLS improvement and LV mass reduction were detected in the myocarditis subgroup (**Figure 8.6**) In addition, a significant reduction of T1 native values (1306±39 vs 1257±49 ms, p=0.033, n=8) but not of ECV or T2 was seen with COVID-19, whereas in the myocarditis group there was a significant reduction in T2 values (58±10 vs 50±5, p=0.043, n=10) and non-significant trends for

reduction in native T1 and ECV. (**Figure 8.7**) Two examples of patients with COVID-19 and one with myocarditis to illustrate the complexity of structural modifications induced by the disease and the variability in recovery at follow-up are shown in **Figure 8.8**.

Table 8.5 Cardiac Magnetic Resonance Imaging Findings. Follow-up.

	COVID-19 N=10		P	Myocarditis N=13		P
	Baseline	Follow-up		Baseline	Follow-up	
Left Ventricle						
LV EDV (mL/m^2)	76±11	75±16	0.88	105±35	94±24	***0.042***
LV ESV (mL/m^2)	31±10	28±10	0.10	52±39	46±25	0.24
LV SV (mL/m^2)	45±8	47±7	0.40	52±13	48±11	0.13
LV EF (%)	60±11	64±8	0.13	54±16	53±12	0.79
LV CI (L/min/m^2)	3.5±1.0	3.2±0.4	0.32	3.8±1.0	3.1±1.0	***<0.001***
LV GLS Endo (%)	-23.4±3.8	-26.5±3.7	***0.034***	-20.4±7.4	-23.8±4.3	***0.039***
LV GLS Myo (%)	-21.3±3.0	-23.6±3.2	0.07	-18.8±6.5	-22.0±3.9	***0.022***
LV GCS Endo (%)	-31.7±8.9	-34.2±8.6	0.21	-25.4±9.5	-25.8±5.6	0.79
LV GCS Myo (%)	-20.1±4.0	-21.1±4.1	0.35	-18.2±7.1	-17.3±3.7	0.56
LVM (g/m^2)	55±7	50±8	***0.002***	74±27	59±13	***0.005***
Left Atrium						
LA max Vol mL	35±9	33±10	0.53	42±13	38±11	0.13
LA emptying fraction %	55±15	65±6	0.10	52±20	60±12	***0.026***
LA strain %	39±14	39±9	0.99	27±18	32±13	0.29
Right Ventricle						
RV EDV (mL/m^2)	82±17	82±20	0.87	85±28	92±16	0.44
RV ESV (mL/m^2)	43±12	38±12	0.05	37±14	44±9	0.13
RV SV (mL/m^2)	39±7	44±8	***0.032***	44±14	48±11	0.22
RV EF (%)	48±7	54±5	***0.032***	53±12	52±8	0.60
RV GLS Endo %	-24.7±8.0	-29.0±5.9	0.32	-27.4±8.6	-28.9±5.5	0.41
RV GLS Myo %	-23.2±8.1	-28.2±6.1	0.26	-25.5±8.1	-25.8±5.3	0.84
RVM (g/m^2)	16±4	12±3	***0.040***	16±3	14±3	0.06
Right Atrium						
RA max Vol mL	37±13	40±17	0.27	45±12	42±11	0.34
RA emptying fraction %	55±11	56±9	0.94	48±15	44±9	0.46
RA strain %	39±14	42±13	0.70	36±15	30±10	0.14
Parametric Imaging						
T1 native (ms)	1306±39 (n=8)	1257±49 (n=8)	***0.033***	1294±24 (n=5)	1224±42 (n=5)	***0.015***
ECV (%)	26±4 (n=10)	25±2 (n=10)	0.27	28±5 (n=5)	26±3 (n=5)	0.31
T2 (ms)	48±6 (n=8)	50±5 (n=8)	0.66	58±10 (n=10)	50±5 (n=10)	***0.043***
LGE No. (%)						
Ischaemic	1(10)	1 (10)	0.99	2 (15)	2(15)	0.99
Nonischaemic	2(20)	0 (0)	0.14	11 (85)	4 (31)	***0.015***
Pericardial	1 (10)	0 (0)	0.30	11 (92)	2 (15)	0.20

Abbreviations: ED – end diastolic, ES – end systolic, SV – stroke volume, GLS global longitudinal strain, GCS – global circumferential strain, Endo – subendocardial layer, Myo – mid-myocardial layer, LV – left ventricular RV – right ventricular, LA – left atrial, RA – right atrial, ECV – extracellular volume, LGE – late gadolinium enhancement.

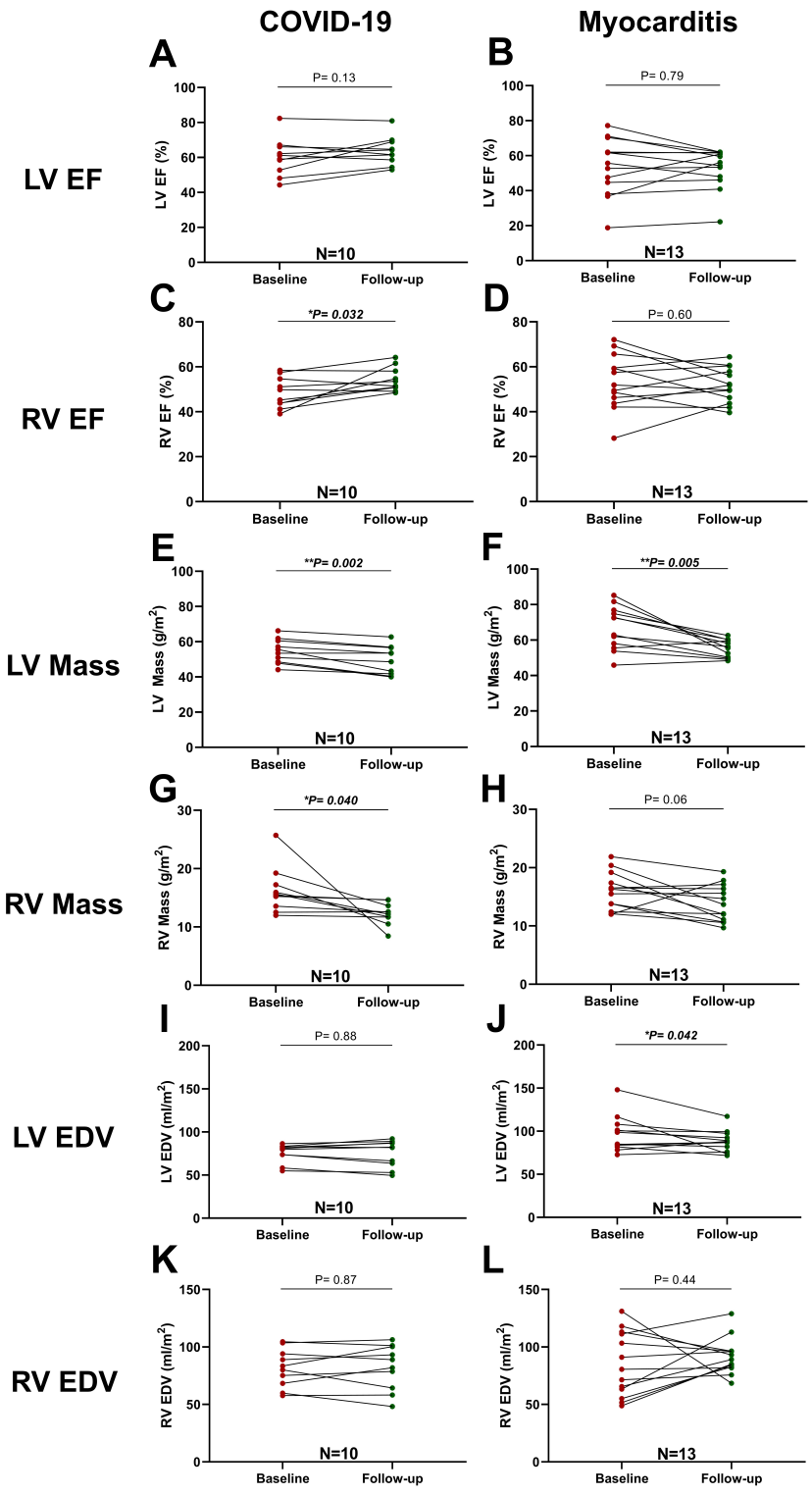


Figure 8.6 Comparison between LV and RV function and mass at baseline and follow-up in patients with COVID-19 and Myocarditis. On the left column, COVID-19 patients: **A.** LV EF, **C.** RV EF, **E.** LV Mass, **G.** RV Mass, on the right column, Myocarditis patients: **B.** LV EF, **D.** RV EF, **F.** LV Mass, **H.** RV Mass. A P value <0.05 was considered statistically significant, and indicated as follows: *< 0.05, **<0.01. ***<0.001.

Dichotomized data (**Figure 8.4 D, E, F, Table 8.3**) indicated that LLC criteria, fulfilled in 2 (20%) of the patients with COVID-19 at baseline, were fulfilled only in 1 (10%) at follow-up interval, with improvements in both myocardial oedema and myocardial injury from 4 (40%) to 2 (20%). Pericardial involvement was present in (2 (20%)) of the COVID-19 patients, and at follow-up persisted only in 1(10%). Importantly, the RV function, impaired in 7 (70%) of patients remained impaired only in 2 (20%) of these patients at the follow-up visit. In myocarditis patients there was a marked improvement of myocardial inflammation at follow-up in a majority of patients (from 13 (100%) to 6 (46%)) with 5 (38%) still fulfilling the LLC criteria at follow-up, the LV dysfunction (8(62%) and RV (7(54%)) impairment persisted in all patients initially affected. Pericardial pathology improved in 6 patients (from 9 (69%) at baseline to 3 (23%) at follow-up). (**Figure 8.4 D, E, F, Table 8.3**).

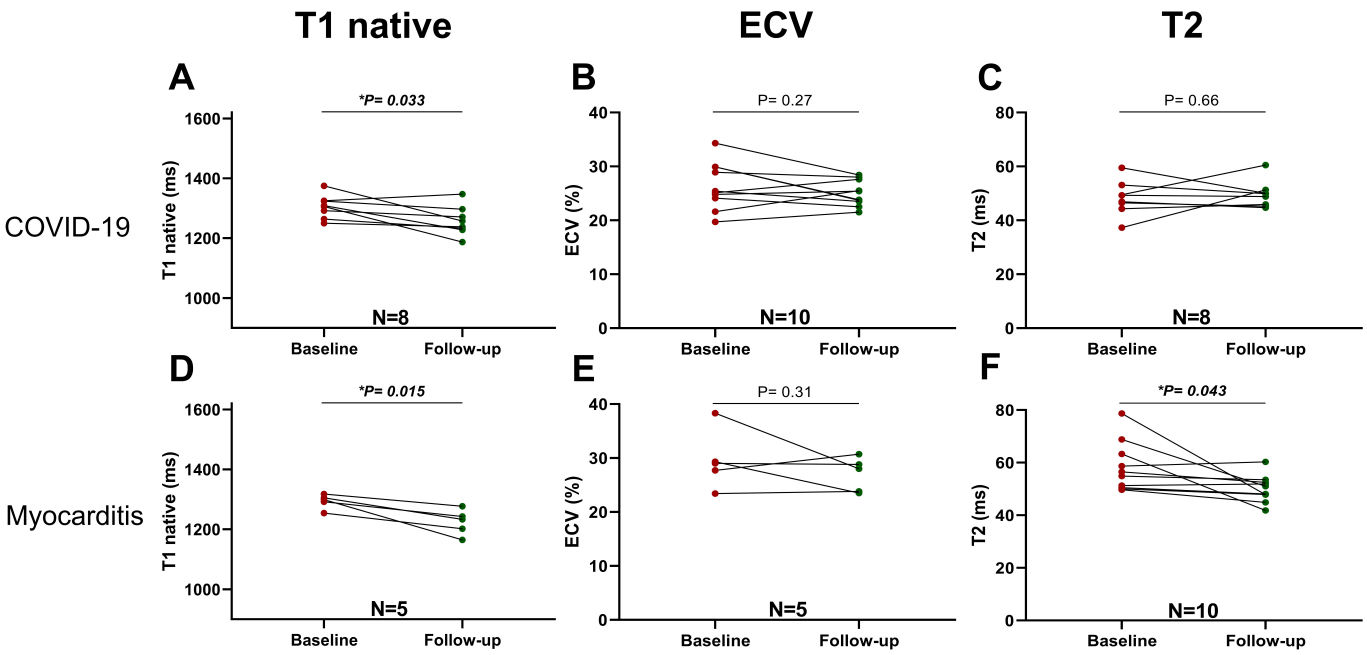


Figure 8.7 Parametric Imaging at baseline and follow-up in COVID-19 (upper row): **A.** T1 native, **B.** Extracellular volume (ECV), and Myocarditis (lower row): C. T2, **D.** T1 native, **E.** Extracellular volume (ECV), **F.** T2: A P value <0.05 was considered statistically significant, and indicated as follows: *< 0.05, **<0.01. ***<0.001.

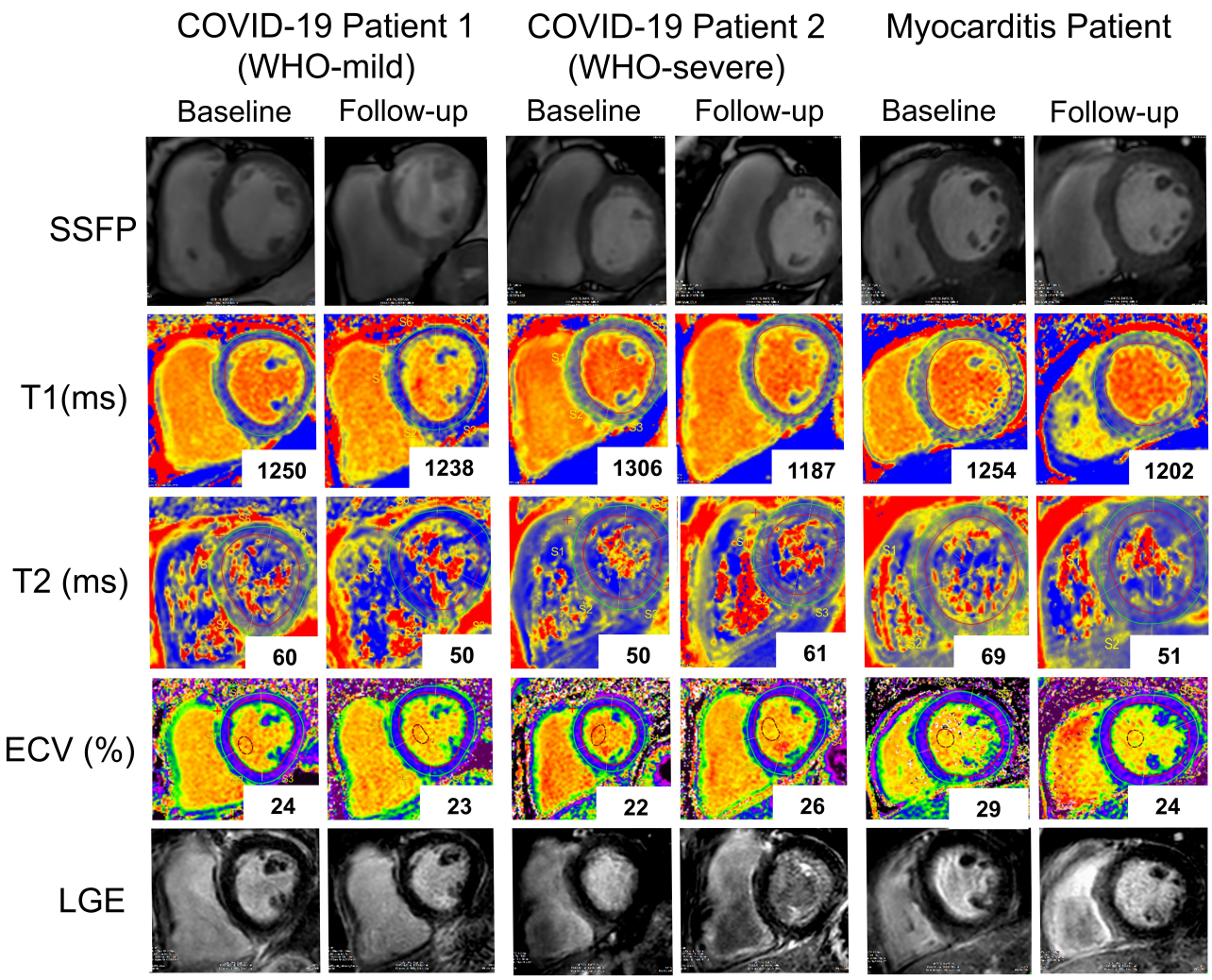


Figure 8.8 Representative baseline and follow-up CMR images of two COVID-19 patients (COVID-19 patient 1 with a WHO-score: mild and COVID-19 patient 2 with a WHO-score: severe and a Myocarditis patient. Rows (from top to bottom): SSFP-cine images, T1 native maps, T2 maps, Extracellular volume maps, late gadolinium enhancement images. While in the first COVID-19 patient (first and second columns from the left), T1 native (from 1250 to 1238ms) and T2 (from 60ms to 50ms) signals improved at follow-up in the second COVID-19 patient (third and fourth columns) T1 native signal improved (from 1306 to 1187ms) while T2 (from 50 to 61ms) and ECV (from 22 to 26%) worsened. In the myocarditis patient (fifth and sixth columns) there is at follow-up a marked improvement in all the parameters.

8.5 Discussion

My findings can be summarized as follows:

1. Patients with cardiac symptoms and COVID-19 infection of different severity grades showed only subtle changes in cardiac structure and function. On average, standard LV-ejection fraction and mass did not differ from control subjects, however, significant

differences were observed with slightly elevated mean T2 relaxation times and decreased RV stroke volumes in COVID-19 patients.

2. In comparison, the morphological changes observed in COVID-19 patients were less pronounced than in patients with “classic” lymphocytic virus-associated myocarditis or eosinophilic myocarditis, the latter exhibiting marked myocardial and pericardial inflammation and injury in EMB and impairment RV- and LV-function on CMR.

3. In COVID-19 patients, a more severe clinical presentation (WHO severe or critical disease) was associated with lower biventricular longitudinal function, prolonged T1 native times and higher RV mass.

4. Only 3 (9%) of the COVID-19 patients fulfilled the CMR - LLC diagnostic criteria for acute myocarditis. More frequently, supportive criteria such as pericarditis and pericardial effusion (25%), LV (25%) and RV (28%) dysfunction were present, these findings altogether suggesting a *sui generis* “myocarditis-like” pattern, the prognostic implications of which are yet to be established.

5. On EMB analyses, none of the COVID-19 patients presented evidence of acute or persistent inflammation, in contrast, the majority of myocarditis patients (13 of 15 (87%)) showed ongoing myocardial inflammation.

6. In COVID-19 patients, LV GLS, LVM, RV EF, T1 mildly improved at follow-up while T2 values remained elevated.

Although these results indicated that in consecutive patients, who have successfully recovered from SARS-CoV-2 infection, the cardiac function was on the whole unaffected, we found significant functional impairment in a subset of patients: out of 32 patients, 8 (25%) showed global or regional LV dysfunction, 9 (28%) depressed RV function, 10 (31%) structural myocardial alterations and 8 (25%)

pericardial effusion or pericarditis on CMR. However, these changes seem to ameliorate over time and already might have been partially resolved at the time of the first scan in comparison with the acute phase of COVID-19. These changes could be more severe in patients with pre-existing cardiac disease, in particular HF. [330] In particular, RV remodelling, diagnosed and assessed with transthoracic echocardiography, increased the mortality risk in COVID-19 patients more than 2-fold. [331] Using CMR, we showed that decreased RV function is present in one in four COVID-19 patients (9(28%)), in approximately half of whom (4(13%)) RV dilatation is also present.

In agreement with recent data[177], we found elevated myocardial T2 relaxation times in COVID-19 patients that did not seem to recede at follow-up. Possibly, this is related to a certain degree of reactive myocardial inflammation triggered by an abnormal immune response that persists even months after infection. [332] However, since almost all other functional markers improve over time, the clinical significance of this findings remains questionable and merits further investigation in future longer-term trials.

Previous reports signal the particular targeting of the endothelium by the SARS-CoV2[167,168], in particular, during the systemic, complicated, development of the infection. Reduced longitudinal function of the heart is a primary hallmark of a dysfunctional myocardial microvasculature. [333] Our findings indicate that, selectively both LV and RV long-axis deformation are depressed in more severe forms of COVID-19. This corresponds to increased values of native T1 relaxation times in these patients, a marker of persistent inflammatory response, possibly accompanied with diffuse structural changes. Taken together these findings may provide a link to capillary endothelial damage in patients with more severe forms of COVID-19. However, all

patients with COVID-19 included in this study improved clinically over time and attended the CMR examinations in an ambulatory outpatient setting. Thus, more pronounced myocardial injury may be present in more acute presentation of the disease, in older patients and patients with underlying cardiac conditions.

In a multi-centre analysis of 68 hospitalised patients that succumbed to COVID-19 in Wuhan, China, extensive myocardial damage was identified as the main cause of death in 5 (7%) of cases.[334] In contrast, the largest whole heart study to date[335] examined explanted hearts from 39 patients who died following a COVID-19 infection, identified the intra-myocardial presence of the virus in 24 and signs of viral replication in 5 samples but failed to demonstrate the presence of any acute inflammatory infiltration of the myocardium even in patients with clinically significant virus load (more than 1000 copies). In a similar study, an unexpectedly high density of macrophages was identified in the cardiac tissue of a majority of patients who died of COVID-19 and overt lymphocytic myocarditis was identified in 14%.[329] In our COVID-19 patients we also observed increased amounts of CD68+ macrophages, but not of CD3+ lymphocytes or other specific immune cells. However, it remains uncertain if these dire consequences are the direct effects of viral penetration of the cardiac structures and intra-myocardial viral replication or rather part of an exacerbated systemic response, such as autoimmune virus-triggered cytokine storm or sepsis.[336]

In our study, on EMB analyses none of the samples obtained from the ten COVID-19 patients showed any sign of acute or chronic lymphocytic inflammation or viral RNA in the myocardium. In contrast thirteen (87%) out of 15 patients with myocarditis showed evidence of acute inflammation or clinically relevant virus presence in the myocardial tissue. However, importantly, one (10%) of the COVID-19 and two (13%) of the myocarditis patients showed positive CMR LLC criteria but had a negative EMB

sample. (**Figure 8.4 A., B.**) Our results are in agreement with a recently published meta-analysis[337], scrutinizing 277 post-mortem histopathology reports in COVID-19 cases, which identified a very low prevalence of myocarditis if strict diagnostic criteria were applied, however any abnormalities at the level of myocardium were present in as many as half of the cases.

This current study provides further evidence for the role of CMR in the diagnosis of cardiac complications in COVID-19 patients. Yet, due to the small number of included patients, the results of our study should still be interpreted with caution.[327] Nonetheless we believe that our study shows that a greater number of post COVID patients would benefit from comprehensive CMR[181] and should ideally be included in a multi-centre, national or international CMR COVID-19 database with stringent long-term follow-up. Patients included in these longitudinal studies should include patients with pre-existing cardiovascular pathologies and risk factors, in whom myocardial injury and dysfunction may prove to be more severe, recovery slower and long-term sequelae more pronounced. In addition, our study also underlines the complex and incomplete overlap of CMR and EMB criteria in the diagnosis of acute myocarditis and suggests their complementary diagnostic role. [336]

8.6 Limitations

COVID-19 is currently an expanding pandemic and results to support clinical guidelines are warranted in a short time. Our study was primarily designed to assess what appears to be the most important alteration observed with CMR in post-COVID-19 patients, namely, parametric mapping (T1, T2 relaxation times). T1 and T2 values notoriously vary between different manufacturers and field strengths. Thus, in order to increase the sensitivity, for comparing parametric mapping between the 3 groups we included only subjects scanned with the same 3T Philips Ingenia scanner. Importantly,

we acknowledge the age disparity between healthy controls, COVID-19 and myocarditis groups. There was more variability in the follow-up interval within in the myocarditis group compared with the COVID-19 group, due to a more complex clinical management, frequently involving hospitalization and clinically indicated multiple scans. Despite the best of our efforts, some of the data sets remain incomplete, in particular clinical data collected retrospectively from COVID-19 and myocarditis patients – to overcome this limitation, we indicated clearly the exact number of datasets available per each subgroup. As our study design did not permit to investigate hyper-acute cardiac manifestations of COVID-19, our main purpose was to investigate whether persistent cardiac changes, as proposed previously, can induce structural or functional remodelling of the heart and hamper complete recovery.

8.7 Conclusions

In this cohort, CMR and EMB findings revealed that a SARS-CoV-2 infection shows relatively mild but variable cardiac involvement. More symptomatic patients and those with higher clinical care demands are more likely to exhibit impaired myocardial function and chronic inflammation compared to patients with ‘classic’ acute myocarditis during the acute and convalescent phases. This study highlights the importance of collecting large multicentre cardiac imaging data from patients with and recovering from COVID-19.

Chapter Nine:

Summary and Perspectives

The main task of CMR is to characterise cardiac remodelling as early as possible and as precisely as possible. This would allow a more successful earlier and more specific (phenotype-based) therapeutic intervention which would ideally lead to a partial or complete recovery of cardiac function. [338] Thanks to technical improvement in image acquisition and image processing algorithms provided by biomedical engineering, these abilities have augmented greatly over the last decade.[339] However, the clinical usefulness of these methods needs careful, sometimes laborious testing in the clinical arena, ideally including studies with large numbers of participants and strict standardisation of image acquisition and processing guidelines. My thesis comprises several clinical evaluations of two complementary methods derived from CMR acquisition which hold a high promise for evaluation of cardiac remodelling: evaluation of systolic and diastolic myocardial deformation using FT and parametric mapping.

With my investigation:

1. I brought further evidence about the importance of myocardial strain in the diagnosis of HF patients and the difficulties of mere functional assessment in the diagnosis of patients with HFpEF
2. I demonstrated the feasibility of multilayer myocardial strain assessment using FT and show that, in particular GCS Endo, yields a high sensitivity and specificity in staging of the pump deficit in HFmrEF and HFrEF.
3. Applying FT to assess the atrial phasic volumes, emptying fractions and strains, I showed that LAV is not a very sensitive marker in HF and demonstrate that emptying fractions and strain may bring more diagnostic gain. I proposed for the first time new criteria to define atrial failure, a recently proposed distinct pathological entity in heart disease. Following these criteria I indicated what

factors, involved in cardiac remodelling are the most important contributors to the atrial remodelling in HF

4. I showed the importance of HDF in characterising the filling impairment in patients with normal EF and suspected diastolic dysfunction
5. I characterised for the first type an early cardiomyopathy phenotype in adult patients with PKU with lower LV mass, lower EF and dilated LV with thin walls.
6. In PKU patients, at long-term follow-up, I showed that a marked decrease in Phe concentrations, while overall considered beneficial for avoiding neurological complications, is associated with a worse cardiac remodelling, including increased markers of diffuse fibrosis, systolic and diastolic impairment.
7. I brought evidence that convalescent patients with COVID-19, present higher T2 values, but no persistent myocardial or pericardial changes and in majority recover functionally ad integrum.

The data presented here demonstrated for the first time using CMR FT that myocardial deformation is not uniform across the myocardium with higher values observed in the subendocardium. A spatial evaluation of myocardial mechanics can be added to existing current 3D models of ventricular architecture [340]. Indeed, such models were elaborated already for myocardial tagging [341,342], and other CMR derived methods such as cine displacement encoding with stimulated echoes (DENSE) and cine strain encoding (SENC) imaging. [343] To date, no such model using FT is available even if the technology allows a pixel-based rapid numeric computation. An obvious advantage of such a technique is the correction of inter-plane movement to which a 2D evaluation remains subject.

A flexible and detailed numerical output opens the possibility for CMR FT to characterise parameters of diastolic deformation such as early relaxation tissue

velocity and torsional mechanics (diastolic untwisting), and some evidence regarding a good agreement with invasively measured parameters and diastolic 3D deformation measured by echocardiography started to emerge recently, however, more validation is required to establish feasibility and accuracy.

Diffusion tensor imaging[344,345] is a novel technique, developed for the first time in brain imaging[346], able to track directly the muscular fibres and represent the myofibrillar architecture of the myocardium. Quantification algorithms such as fractional anisotropy have been developed to measure degrees of myocyte disarray (a typical feature of hypertrophic cardiomyopathy)[347] and focal distortion after myocardial infarction.[348] Coupled with CMR FT, these methods hold a great potential in making the connection between deformation properties (velocity and force vectors) and the exact anatomical tracks on which these are applied. In this way, a fundamental and still unmet step towards quantifying myocardial contractility in vivo could be made.

One of the pending limitations of T1 mapping continues to be the insufficient or inconclusive validation against histology samples. [349] Imminent obstacles such as reduced availability of endomyocardial biopsy samples, and their only partial account of the total content of collagen of the entire myocardium hamper an exhaustive analysis and validation. [350] On the other hand, whole heart histology in a post-transplant excised specimen[351] or post-mortem CMR studies[352] are laborious and pose multiple ethical issues. However, the agreement is generally acceptable, but increased caution needs to be maintained, in the particular case of cardiomyopathies where collagen accumulation is triggered by multiple concurrent mechanisms. [353,354] A whole range of techniques of labelling and imaging molecular effectors of myocardial fibrosis such as activated myofibroblasts, matricellular proteins (MMPs and TIMPs) that are enzymes involved in trimming and respectively preserving interstitial collagen network[355], or

directly various subtypes of collagen assemblies[356], are expected to revolutionise the in vivo detection and quantification of fibrosis in the next decade.

Quantitative assessment of LV hypertrophy represents a very important outcome in cardiovascular disease directly correlated with morbidity and mortality in HF. Moreover, per se it represents a therapeutic target and numerous efforts and resources are currently spent to find adequate treatments and reverse maladaptive hypertrophic cardiac remodelling. Current assessment is based on the assumption that myocardial volume measured by imaging methods represents mostly myocytic mass. [357] This assumption is not always adequate, large amounts of fibrosis or myocardial inflammatory exudate occupying instead significant myocardial volume content. Therefore, imaging methods to assess rather the cellular hypertrophy of the myocytes may provide more correct results and improve thus the clinical management. Indeed, recent proposed protocols[32] used myocardial mapping to correct the volumetric assessment of LV hypertrophy and give results that were closer to gold standard histological measurements.

Dedicated acquisition protocols[36,358] and respectively the support offered by machine learning algorithms[359] hold a great promise to replace the use of contrast substances for parametric mapping making them more accessible with patients with generic contraindications (e.g. end-stage renal disease, severe allergic reactions to gadolinium) and improve accuracy and specificity of CMR outcomes.

I expect that all of these imminent progresses in image analysis will greatly improve our ability to use imaging, particularly CMR, to develop a phenotype-based more individualised approach to HF treatment and track more specific parameters (e.g. microvascular dysfunction, impaired relaxation, diffuse fibrosis) in monitoring longitudinal efficiency of therapy.

The findings presented here represent the first characterisation of cardiac phenotype in adult patients with PKU. Several questions arising from our work remained unanswered and warrant further investigations. Primarily, the mechanisms by which metabolic abnormalities present in the adult life of these patients lead to cellular injury and dysfunction. A recent insight into the cytopathic and histopathological changes produced by supraphysiological concentrations of Phe demonstrated its direct toxic effects on the heart and skeletal muscle. [149] However, PKU offers a more complex registry of changes such as accumulation of toxic catabolites of Phe and respectively interferences with the TCA cycle, at the centre of cellular energy machinery. These emerging hypotheses can be only partially tested further on human subjects (e.g. spectroscopy MR could reveal a reduced PCr/ATP ratio in PKU patients, or could elucidate the nature of a putative deposition substrate in the heart such as lipids or amyloid-like Phe build-up[302]) but could be successfully interrogated in animal models of PKU.[360,361] Intriguingly, our data further suggest that a drastic decrease in Phe concentrations could be deleterious. This hypothesis needs to be tested in larger cohorts and more data about fat tissue distributions and downstream pathways such as leptin and other adipokines involved in regulation of cardiac mechanics and the energetic metabolism of cardiomyocytes are warranted.

Since we performed the study and I wrote the chapter on COVID-19 (Chapter 8), a plethora of information, both clinical and mechanistic about the pathogenesis of cardiac modifications associated with this disease, has been published. Our main findings resonate with the conclusions of a recent meta-analysis. [362] COVID-19 does affect the heart in a significant number of cases and the severity of cardiac complications is higher in patients who required hospital admission and increased health care demands. The cardiovascular risk remains significantly higher in all recovered COVID-

19 patients. [162] Long COVID-19 can burden the life of many who suffered from an initial acute infection and cardiac complications may play a role in persistence of symptoms and slowness of recovery. [363] A big data approach including a large CMR longitudinal study, such as UK Biobank [364], is likely to offer a more accurate picture of the dynamics of these changes and inform a more adequate clinical management.[365]

References

1. Writing Committee M, Yancy CW, Jessup M, Bozkurt B, Butler J, Casey DE, Jr., Drazner MH, Fonarow GC, Geraci SA, Horwich T, et al. 2013 ACCF/AHA guideline for the management of heart failure: a report of the American College of Cardiology Foundation/American Heart Association Task Force on practice guidelines. *Circulation*. 2013;128:e240-327. doi: 10.1161/CIR.0b013e31829e8776
2. Writing C, Maddox TM, Januzzi JL, Jr., Allen LA, Breathett K, Butler J, Davis LL, Fonarow GC, Ibrahim NE, Lindenfeld J, et al. 2021 Update to the 2017 ACC Expert Consensus Decision Pathway for Optimization of Heart Failure Treatment: Answers to 10 Pivotal Issues About Heart Failure With Reduced Ejection Fraction: A Report of the American College of Cardiology Solution Set Oversight Committee. *J Am Coll Cardiol*. 2021;77:772-810. doi: 10.1016/j.jacc.2020.11.022
3. Yancy CW, Jessup M, Bozkurt B, Butler J, Casey DE, Jr., Colvin MM, Drazner MH, Filippatos GS, Fonarow GC, Givertz MM, et al. 2017 ACC/AHA/HFSA Focused Update of the 2013 ACCF/AHA Guideline for the Management of Heart Failure: A Report of the American College of Cardiology/American Heart Association Task Force on Clinical Practice Guidelines and the Heart Failure Society of America. *Circulation*. 2017;136:e137-e161. doi: 10.1161/CIR.0000000000000509
4. Merlo M, Pivetta A, Pinamonti B, Stolfo D, Zecchin M, Barbati G, Di Lenarda A, Sinagra G. Long-term prognostic impact of therapeutic strategies in patients with idiopathic dilated cardiomyopathy: changing mortality over the last 30 years. *Eur J Heart Fail*. 2014;16:317-324. doi: 10.1002/ejhf.16
5. Conrad N, Judge A, Tran J, Mohseni H, Hedgecott D, Crespillo AP, Allison M, Hemingway H, Cleland JG, McMurray JJV, et al. Temporal trends and patterns in heart failure incidence: a population-based study of 4 million individuals. *Lancet*. 2018;391:572-580. doi: 10.1016/S0140-6736(17)32520-5
6. Writing Group M, Mozaffarian D, Benjamin EJ, Go AS, Arnett DK, Blaha MJ, Cushman M, Das SR, de Ferranti S, Despres JP, et al. Heart Disease and Stroke Statistics-2016 Update: A Report From the American Heart Association. *Circulation*. 2016;133:e38-360. doi: 10.1161/CIR.0000000000000350
7. Virani SS, Alonso A, Aparicio HJ, Benjamin EJ, Bittencourt MS, Callaway CW, Carson AP, Chamberlain AM, Cheng S, Delling FN, et al. Heart Disease and Stroke Statistics-2021 Update: A Report From the American Heart Association. *Circulation*. 2021;143:e254-e743. doi: 10.1161/CIR.0000000000000950
8. van Riet EE, Hoes AW, Wagenaar KP, Limburg A, Landman MA, Rutten FH. Epidemiology of heart failure: the prevalence of heart failure and ventricular dysfunction in older adults over time. A systematic review. *Eur J Heart Fail*. 2016;18:242-252. doi: 10.1002/ejhf.483

9. Hunt SA, Baker DW, Chin MH, Cinquegrani MP, Feldman AM, Francis GS, Ganiats TG, Goldstein S, Gregoratos G, Jessup ML, et al. ACC/AHA Guidelines for the Evaluation and Management of Chronic Heart Failure in the Adult: Executive Summary A Report of the American College of Cardiology/American Heart Association Task Force on Practice Guidelines (Committee to Revise the 1995 Guidelines for the Evaluation and Management of Heart Failure): Developed in Collaboration With the International Society for Heart and Lung Transplantation; Endorsed by the Heart Failure Society of America. *Circulation*. 2001;104:2996-3007. doi: 10.1161/hc4901.102568
10. Pezel T, Viallon M, Croisille P, Sebbag L, Bochaton T, Garot J, Lima JAC, Mewton N. Imaging Interstitial Fibrosis, Left Ventricular Remodeling, and Function in Stage A and B Heart Failure. *JACC Cardiovasc Imaging*. 2021;14:1038-1052. doi: 10.1016/j.jcmg.2020.05.036
11. Paulus WJ, Tschope C. A novel paradigm for heart failure with preserved ejection fraction: comorbidities drive myocardial dysfunction and remodeling through coronary microvascular endothelial inflammation. *J Am Coll Cardiol*. 2013;62:263-271. doi: 10.1016/j.jacc.2013.02.092
12. Paulus WJ, Zile MR. From Systemic Inflammation to Myocardial Fibrosis: The Heart Failure With Preserved Ejection Fraction Paradigm Revisited. *Circ Res*. 2021;128:1451-1467. doi: 10.1161/CIRCRESAHA.121.318159
13. Yusuf S, Pfeffer MA, Swedberg K, Granger CB, Held P, McMurray JJ, Michelson EL, Olofsson B, Ostergren J, Investigators C, et al. Effects of candesartan in patients with chronic heart failure and preserved left-ventricular ejection fraction: the CHARM-Preserved Trial. *Lancet*. 2003;362:777-781. doi: 10.1016/S0140-6736(03)14285-7
14. Cleland JG, Tendera M, Adamus J, Freemantle N, Polonski L, Taylor J, Investigators P-C. The perindopril in elderly people with chronic heart failure (PEP-CHF) study. *Eur Heart J*. 2006;27:2338-2345. doi: 10.1093/eurheartj/ehl250
15. Massie BM, Carson PE, McMurray JJ, Komajda M, McKelvie R, Zile MR, Anderson S, Donovan M, Iverson E, Staiger C, et al. Irbesartan in patients with heart failure and preserved ejection fraction. *N Engl J Med*. 2008;359:2456-2467. doi: 10.1056/NEJMoa0805450
16. Pitt B, Pfeffer MA, Assmann SF, Boineau R, Anand IS, Claggett B, Clausell N, Desai AS, Diaz R, Fleg JL, et al. Spironolactone for heart failure with preserved ejection fraction. *N Engl J Med*. 2014;370:1383-1392. doi: 10.1056/NEJMoa1313731
17. Lund LH, Benson L, Dahlstrom U, Edner M, Friberg L. Association between use of beta-blockers and outcomes in patients with heart failure and preserved ejection fraction. *JAMA*. 2014;312:2008-2018. doi: 10.1001/jama.2014.15241
18. Watkins H, Ashrafian H, Redwood C. Inherited cardiomyopathies. *N Engl J Med*. 2011;364:1643-1656. doi: 10.1056/NEJMra0902923
19. Ponikowski P, Voors AA, Anker SD, Bueno H, Cleland JGF, Coats AJS, Falk V, Gonzalez-Juanatey JR, Harjola VP, Jankowska EA, et al. 2016 ESC Guidelines for the diagnosis and treatment of acute and chronic heart failure: The Task Force for the diagnosis and treatment of acute and chronic heart failure of the European Society of Cardiology (ESC)Developed with the special contribution of the Heart Failure Association (HFA) of the ESC. *Eur Heart J*. 2016;37:2129-2200. doi: 10.1093/eurheartj/ehw128
20. Adamo L, Yu J, Rocha-Resende C, Javaheri A, Head RD, Mann DL. Proteomic Signatures of Heart Failure in Relation to Left Ventricular Ejection Fraction. *J Am Coll Cardiol*. 2020;76:1982-1994. doi: 10.1016/j.jacc.2020.08.061
21. Kim GH, Uriel N, Burkhoff D. Reverse remodelling and myocardial recovery in heart failure. *Nat Rev Cardiol*. 2018;15:83-96. doi: 10.1038/nrcardio.2017.139
22. Jacob R, Dierberger B, Kissling G. Functional significance of the Frank-Starling mechanism under physiological and pathophysiological conditions. *Eur Heart J*. 1992;13 Suppl E:7-14. doi: 10.1093/eurheartj/13.suppl_e.7
23. Gaudron P, Eilles C, Kugler I, Ertl G. Progressive left ventricular dysfunction and remodeling after myocardial infarction. Potential mechanisms and early predictors. *Circulation*. 1993;87:755-763. doi: 10.1161/01.cir.87.3.755
24. Vasan RS, Larson MG, Benjamin EJ, Evans JC, Levy D. Left ventricular dilatation and the risk of congestive heart failure in people without myocardial infarction. *N Engl J Med*. 1997;336:1350-1355. doi: 10.1056/NEJM199705083361903
25. Reiter G, Reiter U, Rienmuller R, Gagarina N, Ryabikin A. On the value of geometry-based models for left ventricular volumetry in magnetic resonance imaging and electron beam tomography: a Bland-Altman analysis. *Eur J Radiol*. 2004;52:110-118. doi: 10.1016/j.ejrad.2003.10.003
26. Farber NJ, Reddy ST, Doyle M, Rayarao G, Thompson DV, Olson P, Glass J, Williams RB, Yamrozik JA, Murali S, et al. Ex vivo cardiovascular magnetic resonance measurements of right

and left ventricular mass compared with direct mass measurement in excised hearts after transplantation: a first human SSFP comparison. *J Cardiovasc Magn Reson*. 2014;16:74. doi: 10.1186/s12968-014-0074-0
27. Nakamura M, Sadoshima J. Mechanisms of physiological and pathological cardiac hypertrophy. *Nat Rev Cardiol*. 2018;15:387-407. doi: 10.1038/s41569-018-0007-y
28. Ruwhof C, van der Laarse A. Mechanical stress-induced cardiac hypertrophy: mechanisms and signal transduction pathways. *Cardiovasc Res*. 2000;47:23-37. doi: 10.1016/s0008-6363(00)00076-6
29. Wang J, Chen H, Seth A, McCulloch CA. Mechanical force regulation of myofibroblast differentiation in cardiac fibroblasts. *Am J Physiol Heart Circ Physiol*. 2003;285:H1871-1881. doi: 10.1152/ajpheart.00387.2003
30. Gerdes AM, Kellerman SE, Moore JA, Muffly KE, Clark LC, Reaves PY, Malec KB, McKeown PP, Schocken DD. Structural remodeling of cardiac myocytes in patients with ischemic cardiomyopathy. *Circulation*. 1992;86:426-430. doi: 10.1161/01.cir.86.2.426
31. Onodera T, Tamura T, Said S, McCune SA, Gerdes AM. Maladaptive remodeling of cardiac myocyte shape begins long before failure in hypertension. *Hypertension*. 1998;32:753-757. doi: 10.1161/01.hyp.32.4.753
32. Coelho-Filho OR, Shah RV, Mitchell R, Neilan TG, Moreno H, Jr., Simonson B, Kwong R, Rosenzweig A, Das S, Jerosch-Herold M. Quantification of cardiomyocyte hypertrophy by cardiac magnetic resonance: implications for early cardiac remodeling. *Circulation*. 2013;128:1225-1233. doi: 10.1161/CIRCULATIONAHA.112.000438
33. Shekhar A, Heeger P, Reutelingsperger C, Arbustini E, Narula N, Hofstra L, Bax JJ, Narula J. Targeted Imaging for Cell Death in Cardiovascular Disorders. *JACC Cardiovasc Imaging*. 2018;11:476-493. doi: 10.1016/j.jcmg.2017.11.018
34. Kim RJ, Wu E, Rafael A, Chen EL, Parker MA, Simonetti O, Klocke FJ, Bonow RO, Judd RM. The use of contrast-enhanced magnetic resonance imaging to identify reversible myocardial dysfunction. *N Engl J Med*. 2000;343:1445-1453. doi: 10.1056/NEJM200011163432003
35. Dall'Armellina E, Karamitsos TD, Neubauer S, Choudhury RP. CMR for characterization of the myocardium in acute coronary syndromes. *Nat Rev Cardiol*. 2010;7:624-636. doi: 10.1038/nrcardio.2010.140
36. Piechnik SK, Ferreira VM, Dall'Armellina E, Cochlin LE, Greiser A, Neubauer S, Robson MD. Shortened Modified Look-Locker Inversion recovery (ShMOLLI) for clinical myocardial T1-mapping at 1.5 and 3 T within a 9 heartbeat breathhold. *J Cardiovasc Magn Reson*. 2010;12:69. doi: 10.1186/1532-429X-12-69
37. Chen Z, Sohal M, Voigt T, Sammut E, Tobon-Gomez C, Child N, Jackson T, Shetty A, Bostock J, Cooklin M, et al. Myocardial tissue characterization by cardiac magnetic resonance imaging using T1 mapping predicts ventricular arrhythmia in ischemic and non-ischemic cardiomyopathy patients with implantable cardioverter-defibrillators. *Heart Rhythm*. 2015;12:792-801. doi: 10.1016/j.hrthm.2014.12.020
38. Gao P, Yee R, Gula L, Krahn AD, Skanes A, Leong-Sit P, Klein GJ, Stirrat J, Fine N, Pallaveshi L, et al. Prediction of arrhythmic events in ischemic and dilated cardiomyopathy patients referred for implantable cardiac defibrillator: evaluation of multiple scar quantification measures for late gadolinium enhancement magnetic resonance imaging. *Circ Cardiovasc Imaging*. 2012;5:448-456. doi: 10.1161/CIRCIMAGING.111.971549
39. Moore-Morris T, Guimaraes-Camboa N, Banerjee I, Zambon AC, Kisseleva T, Velayoudon A, Stallcup WB, Gu Y, Dalton ND, Cedenilla M, et al. Resident fibroblast lineages mediate pressure overload-induced cardiac fibrosis. *J Clin Invest*. 2014;124:2921-2934. doi: 10.1172/JCI74783
40. Moore-Morris T, Cattaneo P, Guimaraes-Camboa N, Bogomolovas J, Cedenilla M, Banerjee I, Ricote M, Kisseleva T, Zhang L, Gu Y, et al. Infarct Fibroblasts Do Not Derive From Bone Marrow Lineages. *Circ Res*. 2018;122:583-590. doi: 10.1161/CIRCRESAHA.117.311490
41. Weber KT, Sun Y, Bhattacharya SK, Ahokas RA, Gerling IC. Myofibroblast-mediated mechanisms of pathological remodelling of the heart. *Nat Rev Cardiol*. 2013;10:15-26. doi: 10.1038/nrcardio.2012.158
42. Spinale FG. Matrix metalloproteinases: regulation and dysregulation in the failing heart. *Circ Res*. 2002;90:520-530. doi: 10.1161/01.res.0000013290.12884.a3
43. Lopez B, Ravassa S, Moreno MU, Jose GS, Beaumont J, Gonzalez A, Diez J. Diffuse myocardial fibrosis: mechanisms, diagnosis and therapeutic approaches. *Nat Rev Cardiol*. 2021;18:479-498. doi: 10.1038/s41569-020-00504-1
44. Mohammed SF, Hussain S, Mirzoyev SA, Edwards WD, Maleszewski JJ, Redfield MM. Coronary microvascular rarefaction and myocardial fibrosis in heart failure with preserved ejection fraction. *Circulation*. 2015;131:550-559. doi: 10.1161/CIRCULATIONAHA.114.009625

45. Kim JB, Porreca GJ, Song L, Greenway SC, Gorham JM, Church GM, Seidman CE, Seidman JG. Polony multiplex analysis of gene expression (PMAGE) in mouse hypertrophic cardiomyopathy. *Science*. 2007;316:1481-1484. doi: 10.1126/science.1137325
46. Ho CY, Lopez B, Coelho-Filho OR, Lakdawala NK, Cirino AL, Jarolim P, Kwong R, Gonzalez A, Colan SD, Seidman JG, et al. Myocardial fibrosis as an early manifestation of hypertrophic cardiomyopathy. *N Engl J Med*. 2010;363:552-563. doi: 10.1056/NEJMoa1002659
47. Moreo A, Ambrosio G, De Chiara B, Pu M, Tran T, Mauri F, Raman SV. Influence of myocardial fibrosis on left ventricular diastolic function: noninvasive assessment by cardiac magnetic resonance and echo. *Circ Cardiovasc Imaging*. 2009;2:437-443. doi: 10.1161/CIRCIMAGING.108.838367
48. Kranias EG, Hajjar RJ. Modulation of cardiac contractility by the phospholamban/SERCA2a regulatome. *Circ Res*. 2012;110:1646-1660. doi: 10.1161/CIRCRESAHA.111.259754
49. Crea F, Camici PG, Bairey Merz CN. Coronary microvascular dysfunction: an update. *Eur Heart J*. 2014;35:1101-1111. doi: 10.1093/eurheartj/eht513
50. Camici PG, Crea F. Coronary microvascular dysfunction. *N Engl J Med*. 2007;356:830-840. doi: 10.1056/NEJMra061889
51. Camici PG, d'Amati G, Rimoldi O. Coronary microvascular dysfunction: mechanisms and functional assessment. *Nat Rev Cardiol*. 2015;12:48-62. doi: 10.1038/nrcardio.2014.160
52. Litvinukova M, Talavera-Lopez C, Maatz H, Reichart D, Worth CL, Lindberg EL, Kanda M, Polanski K, Heinig M, Lee M, et al. Cells of the adult human heart. *Nature*. 2020;588:466-472. doi: 10.1038/s41586-020-2797-4
53. Hiramatsu O, Goto M, Yada T, Kimura A, Chiba Y, Tachibana H, Ogasawara Y, Tsujioka K, Kajiya F. In vivo observations of the intramural arterioles and venules in beating canine hearts. *J Physiol*. 1998;509 (Pt 2):619-628. doi: 10.1111/j.1469-7793.1998.619bn.x
54. Figueredo VM, Brandes R, Weiner MW, Massie BM, Camacho SA. Endocardial versus epicardial differences of intracellular free calcium under normal and ischemic conditions in perfused rat hearts. *Circ Res*. 1993;72:1082-1090. doi: 10.1161/01.res.72.5.1082
55. Prestle J, Dieterich S, Preuss M, Bieligk U, Hasenfuss G. Heterogeneous transmural gene expression of calcium-handling proteins and natriuretic peptides in the failing human heart. *Cardiovasc Res*. 1999;43:323-331. doi: 10.1016/s0008-6363(99)00119-4
56. Bers DM. Cardiac excitation-contraction coupling. *Nature*. 2002;415:198-205. doi: 10.1038/415198a
57. Zareian M, Ciuffo L, Habibi M, Opdahl A, Chamera EH, Wu CO, Bluemke DA, Lima JA, Venkatesh BA. Left atrial structure and functional quantitation using cardiovascular magnetic resonance and multimodality tissue tracking: validation and reproducibility assessment. *J Cardiovasc Magn Reson*. 2015;17:52. doi: 10.1186/s12968-015-0152-y
58. Prati G, Vitrella G, Allocca G, Muser D, Buttignoni SC, Piccoli G, Morocutti G, Delise P, Pinamonti B, Proclemer A, et al. Right Ventricular Strain and Dyssynchrony Assessment in Arrhythmogenic Right Ventricular Cardiomyopathy: Cardiac Magnetic Resonance Feature-Tracking Study. *Circ Cardiovasc Imaging*. 2015;8:e003647; discussion e003647. doi: 10.1161/CIRCIMAGING.115.003647
59. Kowallick JT, Kutty S, Edelmann F, Chiribiri A, Villa A, Steinmetz M, Sohns JM, Staab W, Bettencourt N, Unterberg-Buchwald C, et al. Quantification of left atrial strain and strain rate using Cardiovascular Magnetic Resonance myocardial feature tracking: a feasibility study. *J Cardiovasc Magn Reson*. 2014;16:60. doi: 10.1186/s12968-014-0060-6
60. Mehta BB, Auger DA, Gonzalez JA, Workman V, Chen X, Chow K, Stump CJ, Mazimba S, Kennedy JL, Gay E, et al. Detection of elevated right ventricular extracellular volume in pulmonary hypertension using Accelerated and Navigator-Gated Look-Locker Imaging for Cardiac T1 Estimation (ANGIE) cardiovascular magnetic resonance. *J Cardiovasc Magn Reson*. 2015;17:110. doi: 10.1186/s12968-015-0209-y
61. Beinart R, Khurram IM, Liu S, Yarmohammadi H, Halperin HR, Bluemke DA, Gai N, van der Geest RJ, Lima JA, Calkins H, et al. Cardiac magnetic resonance T1 mapping of left atrial myocardium. *Heart Rhythm*. 2013;10:1325-1331. doi: 10.1016/j.hrthm.2013.05.003
62. Redfield MM, Jacobsen SJ, Burnett JC, Jr., Mahoney DW, Bailey KR, Rodeheffer RJ. Burden of systolic and diastolic ventricular dysfunction in the community: appreciating the scope of the heart failure epidemic. *JAMA*. 2003;289:194-202. doi: 10.1001/jama.289.2.194
63. Owan TE, Hodge DO, Herges RM, Jacobsen SJ, Roger VL, Redfield MM. Trends in prevalence and outcome of heart failure with preserved ejection fraction. *N Engl J Med*. 2006;355:251-259. doi: 10.1056/NEJMoa052256

64. Andersen OS, Smiseth OA, Dokainish H, Abudiab MM, Schutt RC, Kumar A, Sato K, Harb S, Gude E, Remme EW, et al. Estimating Left Ventricular Filling Pressure by Echocardiography. *J Am Coll Cardiol*. 2017;69:1937-1948. doi: 10.1016/j.jacc.2017.01.058
65. Lancellotti P, Galderisi M, Edvardsen T, Donal E, Goliasch G, Cardim N, Magne J, Laginha S, Hagendorff A, Haland TF, et al. Echo-Doppler estimation of left ventricular filling pressure: results of the multicentre EACVI Euro-Filling study. *Eur Heart J Cardiovasc Imaging*. 2017;18:961-968. doi: 10.1093/ehjci/jex067
66. Sharifov OF, Schiros CG, Aban I, Denney TS, Gupta H. Diagnostic Accuracy of Tissue Doppler Index E/e' for Evaluating Left Ventricular Filling Pressure and Diastolic Dysfunction/Heart Failure With Preserved Ejection Fraction: A Systematic Review and Meta-Analysis. *J Am Heart Assoc*. 2016;5. doi: 10.1161/JAHA.115.002530
67. Chamsi-Pasha MA, Zhan Y, Debs D, Shah DJ. CMR in the Evaluation of Diastolic Dysfunction and Phenotyping of HFpEF: Current Role and Future Perspectives. *JACC Cardiovasc Imaging*. 2020;13:283-296. doi: 10.1016/j.jcmg.2019.02.031
68. Baan J, van der Velde ET, de Bruin HG, Smeenk GJ, Koops J, van Dijk AD, Temmerman D, Senden J, Buis B. Continuous measurement of left ventricular volume in animals and humans by conductance catheter. *Circulation*. 1984;70:812-823. doi: 10.1161/01.cir.70.5.812
69. Chaliki HP, Hurrell DG, Nishimura RA, Reinke RA, Appleton CP. Pulmonary venous pressure: relationship to pulmonary artery, pulmonary wedge, and left atrial pressure in normal, lightly sedated dogs. *Catheter Cardiovasc Interv*. 2002;56:432-438. doi: 10.1002/ccd.10203
70. Benjamin EJ, D'Agostino RB, Belanger AJ, Wolf PA, Levy D. Left atrial size and the risk of stroke and death. The Framingham Heart Study. *Circulation*. 1995;92:835-841. doi: 10.1161/01.cir.92.4.835
71. Santos AB, Roca GQ, Claggett B, Sweitzer NK, Shah SJ, Anand IS, Fang JC, Zile MR, Pitt B, Solomon SD, et al. Prognostic Relevance of Left Atrial Dysfunction in Heart Failure With Preserved Ejection Fraction. *Circ Heart Fail*. 2016;9:e002763. doi: 10.1161/CIRCHEARTFAILURE.115.002763
72. Malagoli A, Rossi L, Bursi F, Zanni A, Sticozzi C, Piepoli MF, Villani GQ. Left Atrial Function Predicts Cardiovascular Events in Patients With Chronic Heart Failure With Reduced Ejection Fraction. *J Am Soc Echocardiogr*. 2019;32:248-256. doi: 10.1016/j.echo.2018.08.012
73. Inciardi RM, Claggett B, Minamisawa M, Shin SH, Selvaraj S, Goncalves A, Wang W, Kitzman D, Matsushita K, Prasad NG, et al. Association of Left Atrial Structure and Function With Heart Failure in Older Adults. *J Am Coll Cardiol*. 2022;79:1549-1561. doi: 10.1016/j.jacc.2022.01.053
74. Pathan F, Sivaraj E, Negishi K, Rafiudeen R, Pathan S, D'Elia N, Galligan J, Neilson S, Fonseca R, Marwick TH. Use of Atrial Strain to Predict Atrial Fibrillation After Cerebral Ischemia. *JACC Cardiovasc Imaging*. 2018;11:1557-1565. doi: 10.1016/j.jcmg.2017.07.027
75. Melenovsky V, Hwang SJ, Redfield MM, Zakeri R, Lin G, Borlaug BA. Left atrial remodeling and function in advanced heart failure with preserved or reduced ejection fraction. *Circ Heart Fail*. 2015;8:295-303. doi: 10.1161/CIRCHEARTFAILURE.114.001667
76. Hohendanner F, Messroghli D, Bode D, Blaschke F, Parwani A, Boldt LH, Heinzel FR. Atrial remodelling in heart failure: recent developments and relevance for heart failure with preserved ejection fraction. *ESC Heart Fail*. 2018;5:211-221. doi: 10.1002/ehf2.12260
77. Hoit BD. Left atrial size and function: role in prognosis. *J Am Coll Cardiol*. 2014;63:493-505. doi: 10.1016/j.jacc.2013.10.055
78. Vaziri SM, Larson MG, Benjamin EJ, Levy D. Echocardiographic predictors of nonrheumatic atrial fibrillation. The Framingham Heart Study. *Circulation*. 1994;89:724-730. doi: 10.1161/01.cir.89.2.724
79. Wang TJ, Larson MG, Levy D, Vasan RS, Leip EP, Wolf PA, D'Agostino RB, Murabito JM, Kannel WB, Benjamin EJ. Temporal relations of atrial fibrillation and congestive heart failure and their joint influence on mortality: the Framingham Heart Study. *Circulation*. 2003;107:2920-2925. doi: 10.1161/01.CIR.0000072767.89944.6E
80. Potter EL, Ramkumar S, Kawakami H, Yang H, Wright L, Negishi T, Marwick TH. Association of Asymptomatic Diastolic Dysfunction Assessed by Left Atrial Strain With Incident Heart Failure. *JACC Cardiovasc Imaging*. 2020;13:2316-2326. doi: 10.1016/j.jcmg.2020.04.028
81. Burstein B, Nattel S. Atrial fibrosis: mechanisms and clinical relevance in atrial fibrillation. *J Am Coll Cardiol*. 2008;51:802-809. doi: 10.1016/j.jacc.2007.09.064
82. Dernellis JM, Stefanadis CI, Zacharoulis AA, Toutouzas PK. Left atrial mechanical adaptation to long-standing hemodynamic loads based on pressure-volume relations. *Am J Cardiol*. 1998;81:1138-1143. doi: 10.1016/s0002-9149(98)00134-9
83. Verheule S, Sato T, Everett Tt, Engle SK, Otten D, Rubart-von der Lohe M, Nakajima HO, Nakajima H, Field LJ, Olgin JE. Increased vulnerability to atrial fibrillation in transgenic mice

with selective atrial fibrosis caused by overexpression of TGF-beta1. *Circ Res*. 2004;94:1458-1465. doi: 10.1161/01.RES.0000129579.59664.9d
84. Antonini-Canterin F, Poli S, Vriz O, Pavan D, Bello VD, Nicolosi GL. The Ventricular-Arterial Coupling: From Basic Pathophysiology to Clinical Application in the Echocardiography Laboratory. *J Cardiovasc Echogr*. 2013;23:91-95. doi: 10.4103/2211-4122.127408
85. Thomas L, Marwick TH, Popescu BA, Donal E, Badano LP. Left Atrial Structure and Function, and Left Ventricular Diastolic Dysfunction: JACC State-of-the-Art Review. *J Am Coll Cardiol*. 2019;73:1961-1977. doi: 10.1016/j.jacc.2019.01.059
86. Chirinos JA, Sardana M, Ansari B, Satija V, Kuriakose D, Edelstein I, Oldland G, Miller R, Gaddam S, Lee J, et al. Left Atrial Phasic Function by Cardiac Magnetic Resonance Feature Tracking Is a Strong Predictor of Incident Cardiovascular Events. *Circ Cardiovasc Imaging*. 2018;11:e007512. doi: 10.1161/CIRCIMAGING.117.007512
87. Thomas L, Muraru D, Popescu BA, Sitges M, Rosca M, Pedrizzetti G, Henein MY, Donal E, Badano LP. Evaluation of Left Atrial Size and Function: Relevance for Clinical Practice. *J Am Soc Echocardiogr*. 2020;33:934-952. doi: 10.1016/j.echo.2020.03.021
88. Olsen FJ, Bertelsen L, de Knegt MC, Christensen TE, Vejlstrup N, Svendsen JH, Jensen JS, Biering-Sorensen T. Multimodality Cardiac Imaging for the Assessment of Left Atrial Function and the Association With Atrial Arrhythmias. *Circ Cardiovasc Imaging*. 2016;9. doi: 10.1161/CIRCIMAGING.116.004947
89. Oakes RS, Badger TJ, Kholmovski EG, Akoum N, Burgon NS, Fish EN, Blauer JJ, Rao SN, DiBella EV, Segerson NM, et al. Detection and quantification of left atrial structural remodeling with delayed-enhancement magnetic resonance imaging in patients with atrial fibrillation. *Circulation*. 2009;119:1758-1767. doi: 10.1161/CIRCULATIONAHA.108.811877
90. Harrison JL, Jensen HK, Peel SA, Chiribiri A, Grondal AK, Bloch LO, Pedersen SF, Bentzon JF, Kolbitsch C, Karim R, et al. Cardiac magnetic resonance and electroanatomical mapping of acute and chronic atrial ablation injury: a histological validation study. *Eur Heart J*. 2014;35:1486-1495. doi: 10.1093/eurheartj/eht560
91. Kuppahally SS, Akoum N, Burgon NS, Badger TJ, Kholmovski EG, Vijayakumar S, Rao SN, Blauer J, Fish EN, Dibella EV, et al. Left atrial strain and strain rate in patients with paroxysmal and persistent atrial fibrillation: relationship to left atrial structural remodeling detected by delayed-enhancement MRI. *Circ Cardiovasc Imaging*. 2010;3:231-239. doi: 10.1161/CIRCIMAGING.109.865683
92. Hopman L, Mulder MJ, van der Laan AM, Demirkiran A, Bhagirath P, van Rossum AC, Allaart CP, Gotte MJW. Impaired left atrial reservoir and conduit strain in patients with atrial fibrillation and extensive left atrial fibrosis. *J Cardiovasc Magn Reson*. 2021;23:131. doi: 10.1186/s12968-021-00820-6
93. Bisbal F, Baranchuk A, Braunwald E, Bayes de Luna A, Bayes-Genis A. Atrial Failure as a Clinical Entity: JACC Review Topic of the Week. *J Am Coll Cardiol*. 2020;75:222-232. doi: 10.1016/j.jacc.2019.11.013
94. Santhanakrishnan R, Wang N, Larson MG, Magnani JW, McManus DD, Lubitz SA, Ellinor PT, Cheng S, Vasan RS, Lee DS, et al. Atrial Fibrillation Begets Heart Failure and Vice Versa: Temporal Associations and Differences in Preserved Versus Reduced Ejection Fraction. *Circulation*. 2016;133:484-492. doi: 10.1161/CIRCULATIONAHA.115.018614
95. Kotecha D, Lam CS, Van Veldhuisen DJ, Van Gelder IC, Voors AA, Rienstra M. Heart Failure With Preserved Ejection Fraction and Atrial Fibrillation: Vicious Twins. *J Am Coll Cardiol*. 2016;68:2217-2228. doi: 10.1016/j.jacc.2016.08.048
96. Wijesurendra RS, Liu A, Eichhorn C, Ariga R, Levelt E, Clarke WT, Rodgers CT, Karamitsos TD, Bashir Y, Ginks M, et al. Lone Atrial Fibrillation Is Associated With Impaired Left Ventricular Energetics That Persists Despite Successful Catheter Ablation. *Circulation*. 2016;134:1068-1081. doi: 10.1161/CIRCULATIONAHA.116.022931
97. Zafrir B, Lund LH, Laroche C, Ruschitzka F, Crespo-Leiro MG, Coats AJS, Anker SD, Filippatos G, Seferovic PM, Maggioni AP, et al. Prognostic implications of atrial fibrillation in heart failure with reduced, mid-range, and preserved ejection fraction: a report from 14 964 patients in the European Society of Cardiology Heart Failure Long-Term Registry. *Eur Heart J*. 2018;39:4277-4284. doi: 10.1093/eurheartj/ehy626
98. Thomas L, Abhayaratna WP. Left Atrial Reverse Remodeling: Mechanisms, Evaluation, and Clinical Significance. *JACC Cardiovasc Imaging*. 2017;10:65-77. doi: 10.1016/j.jcmg.2016.11.003
99. Folse R, Braunwald E. Determination of fraction of left ventricular volume ejected per beat and of ventricular end-diastolic and residual volumes. Experimental and clinical observations with a precordial dilution technic. *Circulation*. 1962;25:674-685. doi: 10.1161/01.cir.25.4.674

100. McDermott MM, Feinglass J, Lee PI, Mehta S, Schmitt B, Lefevre F, Gheorghiade M. Systolic function, readmission rates, and survival among consecutively hospitalized patients with congestive heart failure. *Am Heart J*. 1997;134:728-736. doi: 10.1016/s0002-8703(97)70057-7
101. St John Sutton M, Pfeffer MA, Moye L, Plappert T, Rouleau JL, Lamas G, Rouleau J, Parker JO, Arnold MO, Sussex B, et al. Cardiovascular death and left ventricular remodeling two years after myocardial infarction: baseline predictors and impact of long-term use of captopril: information from the Survival and Ventricular Enlargement (SAVE) trial. *Circulation*. 1997;96:3294-3299. doi: 10.1161/01.cir.96.10.3294
102. Solomon SD, Anavekar N, Skali H, McMurray JJ, Swedberg K, Yusuf S, Granger CB, Michelson EL, Wang D, Pocock S, et al. Influence of ejection fraction on cardiovascular outcomes in a broad spectrum of heart failure patients. *Circulation*. 2005;112:3738-3744. doi: 10.1161/CIRCULATIONAHA.105.561423
103. Senni M, Redfield MM. Heart failure with preserved systolic function. A different natural history? *J Am Coll Cardiol*. 2001;38:1277-1282. doi: 10.1016/s0735-1097(01)01567-4
104. Zerhouni EA, Parish DM, Rogers WJ, Yang A, Shapiro EP. Human heart: tagging with MR imaging--a method for noninvasive assessment of myocardial motion. *Radiology*. 1988;169:59-63. doi: 10.1148/radiology.169.1.3420283
105. Gotte MJ, Germans T, Russel IK, Zwanenburg JJ, Marcus JT, van Rossum AC, van Veldhuisen DJ. Myocardial strain and torsion quantified by cardiovascular magnetic resonance tissue tagging: studies in normal and impaired left ventricular function. *J Am Coll Cardiol*. 2006;48:2002-2011. doi: 10.1016/j.jacc.2006.07.048
106. Ibrahim el SH. Myocardial tagging by cardiovascular magnetic resonance: evolution of techniques--pulse sequences, analysis algorithms, and applications. *J Cardiovasc Magn Reson*. 2011;13:36. doi: 10.1186/1532-429X-13-36
107. Edvardsen T, Urheim S, Skulstad H, Steine K, Ihlen H, Smiseth OA. Quantification of left ventricular systolic function by tissue Doppler echocardiography: added value of measuring pre- and postejection velocities in ischemic myocardium. *Circulation*. 2002;105:2071-2077. doi: 10.1161/01.cir.0000014614.63980.ba
108. Helle-Valle T, Crosby J, Edvardsen T, Lyseggen E, Amundsen BH, Smith HJ, Rosen BD, Lima JA, Torp H, Ihlen H, et al. New noninvasive method for assessment of left ventricular rotation: speckle tracking echocardiography. *Circulation*. 2005;112:3149-3156. doi: 10.1161/CIRCULATIONAHA.104.531558
109. Urheim S, Edvardsen T, Torp H, Angelsen B, Smiseth OA. Myocardial strain by Doppler echocardiography. Validation of a new method to quantify regional myocardial function. *Circulation*. 2000;102:1158-1164.
110. Ommen SR, Nishimura RA, Appleton CP, Miller FA, Oh JK, Redfield MM, Tajik AJ. Clinical utility of Doppler echocardiography and tissue Doppler imaging in the estimation of left ventricular filling pressures: A comparative simultaneous Doppler-catheterization study. *Circulation*. 2000;102:1788-1794. doi: 10.1161/01.cir.102.15.1788
111. Nagueh SF, Appleton CP, Gillebert TC, Marino PN, Oh JK, Smiseth OA, Waggoner AD, Flachskampf FA, Pellikka PA, Evangelista A. Recommendations for the evaluation of left ventricular diastolic function by echocardiography. *J Am Soc Echocardiogr*. 2009;22:107-133. doi: 10.1016/j.echo.2008.11.023
112. Pohost GM, Hung L, Doyle M. Clinical use of cardiovascular magnetic resonance. *Circulation*. 2003;108:647-653. doi: 10.1161/01.CIR.0000083233.86078.3E
113. Pennell DJ. Cardiovascular magnetic resonance. *Circulation*. 2010;121:692-705. doi: 10.1161/CIRCULATIONAHA.108.811547
114. Ng MY, Tong X, He J, Lin Q, Luo L, Chen Y, Shen XP, Wan EYF, Yan AT, Yiu KH. Feature tracking for assessment of diastolic function by cardiovascular magnetic resonance imaging. *Clin Radiol*. 2020;75:321 e321-321 e311. doi: 10.1016/j.crad.2019.11.013
115. Wang J, Khoury DS, Yue Y, Torre-Amione G, Nagueh SF. Left ventricular untwisting rate by speckle tracking echocardiography. *Circulation*. 2007;116:2580-2586. doi: 10.1161/CIRCULATIONAHA.107.706770
116. Guerra M, Bras-Silva C, Amorim MJ, Moura C, Bastos P, Leite-Moreira AF. Intraventricular pressure gradients in heart failure. *Physiol Res*. 2013;62:479-487. doi: 10.33549/physiolres.932531
117. Stoll VM, Hess AT, Rodgers CT, Bissell MM, Dyverfeldt P, Ebbers T, Myerson SG, Carlhall CJ, Neubauer S. Left Ventricular Flow Analysis. *Circ Cardiovasc Imaging*. 2019;12:e008130. doi: 10.1161/CIRCIMAGING.118.008130

118. Vallelonga F, Airale L, Tonti G, Argulian E, Milan A, Narula J, Pedrizzetti G. Introduction to Hemodynamic Forces Analysis: Moving Into the New Frontier of Cardiac Deformation Analysis. *J Am Heart Assoc*. 2021;10:e023417. doi: 10.1161/JAHA.121.023417
119. Pedrizzetti G, Arvidsson PM, Toger J, Borgquist R, Domenichini F, Arheden H, Heiberg E. On estimating intraventricular hemodynamic forces from endocardial dynamics: A comparative study with 4D flow MRI. *J Biomech*. 2017;60:203-210. doi: 10.1016/j.jbiomech.2017.06.046
120. Airale L, Vallelonga F, Forni T, Leone D, Magnino C, Avenatti E, Iannaccone A, Astarita A, Mingrone G, Cesareo M, et al. A Novel Approach to Left Ventricular Filling Pressure Assessment: The Role of Hemodynamic Forces Analysis. *Front Cardiovasc Med*. 2021;8:704909. doi: 10.3389/fcvm.2021.704909
121. Backhaus SJ, Metschies G, Billing M, Kowallick JT, Gertz RJ, Lapinskas T, Pieske B, Lotz J, Bigalke B, Kutty S, et al. Cardiovascular magnetic resonance imaging feature tracking: Impact of training on observer performance and reproducibility. *PLoS One*. 2019;14:e0210127. doi: 10.1371/journal.pone.0210127
122. Stokke TM, Hasselberg NE, Smedsrud MK, Sarvari SI, Haugaa KH, Smiseth OA, Edvardsen T, Remme EW. Geometry as a Confounder When Assessing Ventricular Systolic Function: Comparison Between Ejection Fraction and Strain. *J Am Coll Cardiol*. 2017;70:942-954. doi: 10.1016/j.jacc.2017.06.046
123. Puntmann VO, Peker E, Chandrashekhar Y, Nagel E. T1 Mapping in Characterizing Myocardial Disease: A Comprehensive Review. *Circ Res*. 2016;119:277-299. doi: 10.1161/CIRCRESAHA.116.307974
124. Bloch F. The Principle of Nuclear Induction. *Science*. 1953;118:425-430. doi: 10.1126/science.118.3068.425
125. Ferreira VM, Holloway CJ, Piechnik SK, Karamitsos TD, Neubauer S. Is it really fat? Ask a T1-map. *Eur Heart J Cardiovasc Imaging*. 2013;14:1060. doi: 10.1093/ehjci/jet095
126. Abdel-Aty H, Zagrosek A, Schulz-Menger J, Taylor AJ, Messroghli D, Kumar A, Gross M, Dietz R, Friedrich MG. Delayed enhancement and T2-weighted cardiovascular magnetic resonance imaging differentiate acute from chronic myocardial infarction. *Circulation*. 2004;109:2411-2416. doi: 10.1161/01.CIR.0000127428.10985.C6
127. Friedrich MG, Sechtem U, Schulz-Menger J, Holmvang G, Alakija P, Cooper LT, White JA, Abdel-Aty H, Gutberlet M, Prasad S, et al. Cardiovascular magnetic resonance in myocarditis: A JACC White Paper. *J Am Coll Cardiol*. 2009;53:1475-1487. doi: 10.1016/j.jacc.2009.02.007
128. Ferreira VM, Schulz-Menger J, Holmvang G, Kramer CM, Carbone I, Sechtem U, Kindermann I, Gutberlet M, Cooper LT, Liu P, et al. Cardiovascular Magnetic Resonance in Nonischemic Myocardial Inflammation: Expert Recommendations. *J Am Coll Cardiol*. 2018;72:3158-3176. doi: 10.1016/j.jacc.2018.09.072
129. Garg P, Broadbent DA, Swoboda PP, Foley JRJ, Fent GJ, Musa TA, Ripley DP, Erhayiem B, Dobson LE, McDiarmid AK, et al. Acute Infarct Extracellular Volume Mapping to Quantify Myocardial Area at Risk and Chronic Infarct Size on Cardiovascular Magnetic Resonance Imaging. *Circ Cardiovasc Imaging*. 2017;10. doi: 10.1161/CIRCIMAGING.117.006182
130. Kellman P, Hansen MS. T1-mapping in the heart: accuracy and precision. *J Cardiovasc Magn Reson*. 2014;16:2. doi: 10.1186/1532-429X-16-2
131. von Knobelsdorff-Brenkenhoff F, Prothmann M, Dieringer MA, Wassmuth R, Greiser A, Schwenke C, Niendorf T, Schulz-Menger J. Myocardial T1 and T2 mapping at 3 T: reference values, influencing factors and implications. *J Cardiovasc Magn Reson*. 2013;15:53. doi: 10.1186/1532-429X-15-53
132. Dabir D, Child N, Kalra A, Rogers T, Gebker R, Jabbour A, Plein S, Yu CY, Otton J, Kidambi A, et al. Reference values for healthy human myocardium using a T1 mapping methodology: results from the International T1 Multicenter cardiovascular magnetic resonance study. *J Cardiovasc Magn Reson*. 2014;16:69. doi: 10.1186/s12968-014-0069-x
133. Blau N, van Spronsen FJ, Levy HL. Phenylketonuria. *Lancet*. 2010;376:1417-1427. doi: 10.1016/S0140-6736(10)60961-0
134. Lichter-Konecki U, Hipke CM, Konecki DS. Human phenylalanine hydroxylase gene expression in kidney and other nonhepatic tissues. *Mol Genet Metab*. 1999;67:308-316. doi: 10.1006/mgme.1999.2880
135. Kaufman S. A model of human phenylalanine metabolism in normal subjects and in phenylketonuric patients. *Proc Natl Acad Sci U S A*. 1999;96:3160-3164. doi: 10.1073/pnas.96.6.3160
136. de Baulny HO, Abadie V, Feillet F, de Parscau L. Management of phenylketonuria and hyperphenylalaninemia. *J Nutr*. 2007;137:1561S-1563S; discussion 1573S-1575S. doi: 10.1093/jn/137.6.1561S

137. Cederbaum S. Phenylketonuria: an update. *Curr Opin Pediatr*. 2002;14:702-706. doi: 10.1097/00008480-200212000-00010
138. MacDonald A. Diet and compliance in phenylketonuria. *Eur J Pediatr*. 2000;159 Suppl 2:S136-141. doi: 10.1007/pl00014375
139. Macleod EL, Ney DM. Nutritional Management of Phenylketonuria. *Ann Nestle Eng*. 2010;68:58-69. doi: 10.1159/000312813
140. MacDonald A, van Wegberg AMJ, Ahring K, Beblo S, Belanger-Quintana A, Burlina A, Campistol J, Coskun T, Feillet F, Gizewska M, et al. PKU dietary handbook to accompany PKU guidelines. *Orphanet J Rare Dis*. 2020;15:171. doi: 10.1186/s13023-020-01391-y
141. Ahring K, Belanger-Quintana A, Dokoupil K, Gokmen-Ozel H, Lammardo AM, MacDonald A, Motzfeldt K, Nowacka M, Robert M, van Rijn M. Blood phenylalanine control in phenylketonuria: a survey of 10 European centres. *Eur J Clin Nutr*. 2011;65:275-278. doi: 10.1038/ejcn.2010.258
142. Burton BK, Jones KB, Cederbaum S, Rohr F, Waisbren S, Irwin DE, Kim G, Lilienstein J, Alvarez I, Jurecki E, et al. Prevalence of comorbid conditions among adult patients diagnosed with phenylketonuria. *Mol Genet Metab*. 2018;125:228-234. doi: 10.1016/j.ymgme.2018.09.006
143. Sirtori LR, Dutra-Filho CS, Fitarelli D, Sitta A, Haeser A, Barschak AG, Wajner M, Coelho DM, Llesuy S, Bello-Klein A, et al. Oxidative stress in patients with phenylketonuria. *Biochim Biophys Acta*. 2005;1740:68-73. doi: 10.1016/j.bbadis.2005.02.005
144. Huemer M, Simma B, Mayr D, Moslinger D, Muhl A, Schmid I, Ulmer H, Bodamer OA. Free asymmetric dimethylarginine (ADMA) is low in children and adolescents with classical phenylketonuria (PKU). *J Inherit Metab Dis*. 2012;35:817-821. doi: 10.1007/s10545-011-9448-8
145. Moraes TB, Jacques CE, Rosa AP, Dalazen GR, Terra M, Coelho JG, Dutra-Filho CS. Role of catalase and superoxide dismutase activities on oxidative stress in the brain of a phenylketonuria animal model and the effect of lipoic acid. *Cell Mol Neurobiol*. 2013;33:253-260. doi: 10.1007/s10571-012-9892-5
146. Sitta A, Barschak AG, Deon M, de Mari JF, Barden AT, Vanzin CS, Biancini GB, Schwartz IV, Wajner M, Vargas CR. L-carnitine blood levels and oxidative stress in treated phenylketonuric patients. *Cell Mol Neurobiol*. 2009;29:211-218. doi: 10.1007/s10571-008-9313-y
147. Bortoluzzi VT, Dutra Filho CS, Wannmacher CMD. Oxidative stress in phenylketonuria-evidence from human studies and animal models, and possible implications for redox signaling. *Metab Brain Dis*. 2021;36:523-543. doi: 10.1007/s11011-021-00676-w
148. Azabdaftari A, van der Giet M, Schuchardt M, Hennermann JB, Plockinger U, Querfeld U. The cardiovascular phenotype of adult patients with phenylketonuria. *Orphanet J Rare Dis*. 2019;14:213. doi: 10.1186/s13023-019-1188-0
149. Czibik G, Mezdari Z, Murat Altintas D, Brehat J, Pini M, d'Humieres T, Delmont T, Radu C, Breau M, Liang H, et al. Dysregulated Phenylalanine Catabolism Plays a Key Role in the Trajectory of Cardiac Aging. *Circulation*. 2021;144:559-574. doi: 10.1161/CIRCULATIONAHA.121.054204
150. Adler-Abramovich L, Vaks L, Carny O, Trudler D, Magno A, Caflisch A, Frenkel D, Gazit E. Phenylalanine assembly into toxic fibrils suggests amyloid etiology in phenylketonuria. *Nat Chem Biol*. 2012;8:701-706. doi: 10.1038/nchembio.1002
151. Ercal N, Aykin-Burns N, Gurer-Orhan H, McDonald JD. Oxidative stress in a phenylketonuria animal model. *Free Radic Biol Med*. 2002;32:906-911. doi: 10.1016/s0891-5849(02)00781-5
152. Wurtz P, Havulinna AS, Soininen P, Tynkkynen T, Prieto-Merino D, Tillin T, Ghorbani A, Artati A, Wang Q, Tiainen M, et al. Metabolite profiling and cardiovascular event risk: a prospective study of 3 population-based cohorts. *Circulation*. 2015;131:774-785. doi: 10.1161/CIRCULATIONAHA.114.013116
153. Guerra IMS, Ferreira HB, Neves B, Melo T, Diogo LM, Domingues MR, Moreira ASP. Lipids and phenylketonuria: Current evidences pointed the need for lipidomics studies. *Arch Biochem Biophys*. 2020;688:108431. doi: 10.1016/j.abb.2020.108431
154. Couce ML, Vitoria I, Aldamiz-Echevarria L, Fernandez-Marmiesse A, Roca I, Llarena M, Sanchez-Pintos P, Leis R, Hermida A. Lipid profile status and other related factors in patients with Hyperphenylalaninaemia. *Orphanet J Rare Dis*. 2016;11:123. doi: 10.1186/s13023-016-0508-x
155. Lohner S, Fekete K, Decsi T. Lower n-3 long-chain polyunsaturated fatty acid values in patients with phenylketonuria: a systematic review and meta-analysis. *Nutr Res*. 2013;33:513-520. doi: 10.1016/j.nutres.2013.05.003
156. Sundstrom J, Lind L, Vessby B, Andren B, Aro A, Lithell H. Dyslipidemia and an unfavorable fatty acid profile predict left ventricular hypertrophy 20 years later. *Circulation*. 2001;103:836-841. doi: 10.1161/01.cir.103.6.836

157. Anan F, Yonemochi H, Masaki T, Takahashi N, Fukunaga N, Teshima Y, Iwao T, Kaneda K, Eshima N, Saikawa T, et al. High-density lipoprotein cholesterol and insulin resistance are independent and additive markers of left ventricular hypertrophy in essential hypertension. *Hypertens Res*. 2007;30:125-131. doi: 10.1291/hypres.30.125
158. Horio T, Miyazato J, Kamide K, Takiuchi S, Kawano Y. Influence of low high-density lipoprotein cholesterol on left ventricular hypertrophy and diastolic function in essential hypertension. *Am J Hypertens*. 2003;16:938-944. doi: 10.1016/s0895-7061(03)01015-x
159. Schillaci G, Vaudo G, Reboldi G, Verdecchia P, Lupattelli G, Pasqualini L, Porcellati C, Mannarino E. High-density lipoprotein cholesterol and left ventricular hypertrophy in essential hypertension. *J Hypertens*. 2001;19:2265-2270. doi: 10.1097/00004872-200112000-00021
160. Siripanthong B, Asatryan B, Hanff TC, Chatha SR, Khanji MY, Ricci F, Muser D, Ferrari VA, Nazarian S, Santangeli P, et al. The Pathogenesis and Long-Term Consequences of COVID-19 Cardiac Injury. *JACC Basic Transl Sci*. 2022;7:294-308. doi: 10.1016/j.jacbts.2021.10.011
161. Nalbandian A, Sehgal K, Gupta A, Madhavan MV, McGroder C, Stevens JS, Cook JR, Nordvig AS, Shalev D, Sehrawat TS, et al. Post-acute COVID-19 syndrome. *Nat Med*. 2021;27:601-615. doi: 10.1038/s41591-021-01283-z
162. Xie Y, Xu E, Bowe B, Al-Aly Z. Long-term cardiovascular outcomes of COVID-19. *Nat Med*. 2022;28:583-590. doi: 10.1038/s41591-022-01689-3
163. Sharma A, Garcia G, Jr., Wang Y, Plummer JT, Morizono K, Arumugaswami V, Svendsen CN. Human iPSC-Derived Cardiomyocytes Are Susceptible to SARS-CoV-2 Infection. *Cell Rep Med*. 2020;1:100052. doi: 10.1016/j.xcrm.2020.100052
164. Ishikura H, Maruyama J, Hoshino K, Matsuoka Y, Yano M, Arimura T, Katano H, Kato S, Kitamura T, Nakamura Y. Coronavirus disease (COVID-19) associated delayed-onset fulminant myocarditis in patient with a history of severe acute respiratory syndrome coronavirus 2 (SARS-CoV-2) infection. *J Infect Chemother*. 2021;27:1760-1764. doi: 10.1016/j.jiac.2021.08.007
165. Lindner D, Fitzek A, Brauninger H, Aleshcheva G, Edler C, Meissner K, Scherschel K, Kirchhof P, Escher F, Schultheiss HP, et al. Association of Cardiac Infection With SARS-CoV-2 in Confirmed COVID-19 Autopsy Cases. *JAMA Cardiol*. 2020;5:1281-1285. doi: 10.1001/jamacardio.2020.3551
166. Tavazzi G, Pellegrini C, Maurelli M, Belliato M, Sciutti F, Bottazzi A, Sepe PA, Resasco T, Camporotondo R, Bruno R, et al. Myocardial localization of coronavirus in COVID-19 cardiogenic shock. *Eur J Heart Fail*. 2020;22:911-915. doi: 10.1002/ejhf.1828
167. Varga Z, Flammer AJ, Steiger P, Haberecker M, Andermatt R, Zinkernagel AS, Mehra MR, Schuepbach RA, Ruschitzka F, Moch H. Endothelial cell infection and endotheliitis in COVID-19. *Lancet*. 2020;395:1417-1418. doi: 10.1016/S0140-6736(20)30937-5
168. Teuwen LA, Geldhof V, Pasut A, Carmeliet P. COVID-19: the vasculature unleashed. *Nat Rev Immunol*. 2020;20:389-391. doi: 10.1038/s41577-020-0343-0
169. Sala S, Peretto G, Gramegna M, Palmisano A, Villatore A, Vignale D, De Cobelli F, Tresoldi M, Cappelletti AM, Basso C, et al. Acute myocarditis presenting as a reverse Tako-Tsubo syndrome in a patient with SARS-CoV-2 respiratory infection. *Eur Heart J*. 2020;41:1861-1862. doi: 10.1093/eurheartj/ehaa286
170. Patra T, Meyer K, Geerling L, Isbell TS, Hoft DF, Brien J, Pinto AK, Ray RB, Ray R. SARS-CoV-2 spike protein promotes IL-6 trans-signaling by activation of angiotensin II receptor signaling in epithelial cells. *PLoS Pathog*. 2020;16:e1009128. doi: 10.1371/journal.ppat.1009128
171. Jiang Y, Duffy F, Hadlock J, Raappana A, Styrchak S, Beck I, Mast FD, Miller LR, Chour W, Houck J, et al. Angiotensin II receptor I auto-antibodies following SARS-CoV-2 infection. *PLoS One*. 2021;16:e0259902. doi: 10.1371/journal.pone.0259902
172. Arthur JM, Forrest JC, Boehme KW, Kennedy JL, Owens S, Herzog C, Liu J, Harville TO. Development of ACE2 autoantibodies after SARS-CoV-2 infection. *PLoS One*. 2021;16:e0257016. doi: 10.1371/journal.pone.0257016
173. Rodriguez-Perez AI, Labandeira CM, Pedrosa MA, Valenzuela R, Suarez-Quintanilla JA, Cortes-Ayaso M, Mayan-Conesa P, Labandeira-Garcia JL. Autoantibodies against ACE2 and angiotensin type-1 receptors increase severity of COVID-19. *J Autoimmun*. 2021;122:102683. doi: 10.1016/j.jaut.2021.102683
174. Petersen SE, Friedrich MG, Leiner T, Elias MD, Ferreira VM, Fenski M, Flamm SD, Fogel M, Garg R, Halushka MK, et al. Cardiovascular Magnetic Resonance for Patients With COVID-19. *JACC Cardiovasc Imaging*. 2022;15:685-699. doi: 10.1016/j.jcmg.2021.08.021
175. Kelle S, Bucciarelli-Ducci C, Judd RM, Kwong RY, Simonetti O, Plein S, Raimondi F, Weinsaft JW, Wong TC, Carr J. Society for Cardiovascular Magnetic Resonance (SCMR) recommended CMR protocols for scanning patients with active or convalescent phase COVID-19 infection. *J Cardiovasc Magn Reson*. 2020;22:61. doi: 10.1186/s12968-020-00656-6

176. Giustino G, Croft LB, Stefanini GG, Bragato R, Silbiger JJ, Vicenzi M, Danilov T, Kukar N, Shaban N, Kini A, et al. Characterization of Myocardial Injury in Patients With COVID-19. *J Am Coll Cardiol*. 2020;76:2043-2055. doi: 10.1016/j.jacc.2020.08.069
177. Puntmann VO, Carerj ML, Wieters I, Fahim M, Arendt C, Hoffmann J, Shchendrygina A, Escher F, Vasa-Nicotera M, Zeiher AM, et al. Outcomes of Cardiovascular Magnetic Resonance Imaging in Patients Recently Recovered From Coronavirus Disease 2019 (COVID-19). *JAMA Cardiol*. 2020. doi: 10.1001/jamacardio.2020.3557
178. Wang H, Li R, Zhou Z, Jiang H, Yan Z, Tao X, Li H, Xu L. Cardiac involvement in COVID-19 patients: mid-term follow up by cardiovascular magnetic resonance. *J Cardiovasc Magn Reson*. 2021;23:14. doi: 10.1186/s12968-021-00710-x
179. Caforio AL, Pankuweit S, Arbustini E, Basso C, Gimeno-Blanes J, Felix SB, Fu M, Helio T, Heymans S, Jahns R, et al. Current state of knowledge on aetiology, diagnosis, management, and therapy of myocarditis: a position statement of the European Society of Cardiology Working Group on Myocardial and Pericardial Diseases. *Eur Heart J*. 2013;34:2636-2648, 2648a-2648d. doi: 10.1093/eurheartj/eht210
180. Reddy YNV, Carter RE, Obokata M, Redfield MM, Borlaug BA. A Simple, Evidence-Based Approach to Help Guide Diagnosis of Heart Failure With Preserved Ejection Fraction. *Circulation*. 2018;138:861-870. doi: 10.1161/CIRCULATIONAHA.118.034646
181. Erley J, Zieschang V, Lapinskas T, Demir A, Wiesemann S, Haass M, Osman NF, Simonetti OP, Liu Y, Patel AR, et al. A multi-vendor, multi-center study on reproducibility and comparability of fast strain-encoded cardiovascular magnetic resonance imaging. *Int J Cardiovasc Imaging*. 2020;36:899-911. doi: 10.1007/s10554-020-01775-y
182. Kramer CM, Barkhausen J, Bucciarelli-Ducci C, Flamm SD, Kim RJ, Nagel E. Standardized cardiovascular magnetic resonance imaging (CMR) protocols: 2020 update. *J Cardiovasc Magn Reson*. 2020;22:17. doi: 10.1186/s12968-020-00607-1
183. Doeblin P, Hashemi D, Tanacli R, Lapinskas T, Gebker R, Stehning C, Motzkus LA, Blum M, Tahirovic E, Dordevic A, et al. CMR Tissue Characterization in Patients with HFmrEF. *J Clin Med*. 2019;8. doi: 10.3390/jcm8111877
184. Farrelly C, Shah S, Davarpanah A, Keeling AN, Carr JC. ECG-gated multiecho Dixon fat-water separation in cardiac MRI: advantages over conventional fat-saturated imaging. *AJR Am J Roentgenol*. 2012;199:W74-83. doi: 10.2214/AJR.11.7759
185. Schulz-Menger J, Bluemke DA, Bremerich J, Flamm SD, Fogel MA, Friedrich MG, Kim RJ, von Knobelsdorff-Brenkenhoff F, Kramer CM, Pennell DJ, et al. Standardized image interpretation and post-processing in cardiovascular magnetic resonance - 2020 update : Society for Cardiovascular Magnetic Resonance (SCMR): Board of Trustees Task Force on Standardized Post-Processing. *J Cardiovasc Magn Reson*. 2020;22:19. doi: 10.1186/s12968-020-00610-6
186. Messroghli DR, Moon JC, Ferreira VM, Grosse-Wortmann L, He T, Kellman P, Mascherbauer J, Nezafat R, Salerno M, Schelbert EB, et al. Clinical recommendations for cardiovascular magnetic resonance mapping of T1, T2, T2* and extracellular volume: A consensus statement by the Society for Cardiovascular Magnetic Resonance (SCMR) endorsed by the European Association for Cardiovascular Imaging (EACVI). *J Cardiovasc Magn Reson*. 2017;19:75. doi: 10.1186/s12968-017-0389-8
187. Suinesiaputra A, Bluemke DA, Cowan BR, Friedrich MG, Kramer CM, Kwong R, Plein S, Schulz-Menger J, Westenberg JJ, Young AA, et al. Quantification of LV function and mass by cardiovascular magnetic resonance: multi-center variability and consensus contours. *J Cardiovasc Magn Reson*. 2015;17:63. doi: 10.1186/s12968-015-0170-9
188. Kawel-Boehm N, Hetzel SJ, Ambale-Venkatesh B, Captur G, Francois CJ, Jerosch-Herold M, Salerno M, Teague SD, Valsangiacomo-Buechel E, van der Geest RJ, et al. Reference ranges ("normal values") for cardiovascular magnetic resonance (CMR) in adults and children: 2020 update. *J Cardiovasc Magn Reson*. 2020;22:87. doi: 10.1186/s12968-020-00683-3
189. Cerqueira MD, Weissman NJ, Dilsizian V, Jacobs AK, Kaul S, Laskey WK, Pennell DJ, Rumberger JA, Ryan T, Verani MS, et al. Standardized myocardial segmentation and nomenclature for tomographic imaging of the heart. A statement for healthcare professionals from the Cardiac Imaging Committee of the Council on Clinical Cardiology of the American Heart Association. *Circulation*. 2002;105:539-542.
190. Lapinskas T, Pedrizzetti G, Stoiber L, Dungen HD, Edelmann F, Pieske B, Kelle S. The Intraventricular Hemodynamic Forces Estimated Using Routine CMR Cine Images: A New Marker of the Failing Heart. *JACC Cardiovasc Imaging*. 2019;12:377-379. doi: 10.1016/j.jcmg.2018.08.012

191. Faganello G, Collia D, Furlotti S, Pagura L, Zaccari M, Pedrizzetti G, Di Lenarda A. A new integrated approach to cardiac mechanics: reference values for normal left ventricle. *Int J Cardiovasc Imaging*. 2020;36:2173-2185. doi: 10.1007/s10554-020-01934-1
192. Rommel KP, von Roeder M, Latuscynski K, Oberueck C, Blazek S, Fengler K, Besler C, Sandri M, Lucke C, Gutberlet M, et al. Extracellular Volume Fraction for Characterization of Patients With Heart Failure and Preserved Ejection Fraction. *J Am Coll Cardiol*. 2016;67:1815-1825. doi: 10.1016/j.jacc.2016.02.018
193. Grun S, Schumm J, Greulich S, Wagner A, Schneider S, Bruder O, Kispert EM, Hill S, Ong P, Klingel K, et al. Long-term follow-up of biopsy-proven viral myocarditis: predictors of mortality and incomplete recovery. *J Am Coll Cardiol*. 2012;59:1604-1615. doi: 10.1016/j.jacc.2012.01.007
194. Tanacli R, Hashemi D, Lapinskas T, Edelmann F, Gebker R, Pedrizzetti G, Schuster A, Nagel E, Pieske B, Dungen HD, et al. Range Variability in CMR Feature Tracking Multilayer Strain across Different Stages of Heart Failure. *Sci Rep*. 2019;9:16478. doi: 10.1038/s41598-019-52683-8
195. Tanacli R, Hashemi D, Neye M, Motzkus LA, Blum M, Tahirovic E, Dordevic A, Kraft R, Zamani SM, Pieske B, et al. Multilayer myocardial strain improves the diagnosis of heart failure with preserved ejection fraction. *ESC Heart Fail*. 2020;7:3240-3245. doi: 10.1002/ehf2.12826
196. Smiseth OA, Torp H, Opdahl A, Haugaa KH, Urheim S. Myocardial strain imaging: how useful is it in clinical decision making? *Eur Heart J*. 2016;37:1196-1207. doi: 10.1093/eurheartj/ehv529
197. Scatteia A, Baritussio A, Bucciarelli-Ducci C. Strain imaging using cardiac magnetic resonance. *Heart Fail Rev*. 2017;22:465-476. doi: 10.1007/s10741-017-9621-8
198. Bogaert J, Rademakers FE. Regional nonuniformity of normal adult human left ventricle. *Am J Physiol Heart Circ Physiol*. 2001;280:H610-620. doi: 10.1152/ajpheart.2001.280.2.H610
199. Buckberg G, Hoffman JI, Mahajan A, Saleh S, Coghlan C. Cardiac mechanics revisited: the relationship of cardiac architecture to ventricular function. *Circulation*. 2008;118:2571-2587. doi: 10.1161/CIRCULATIONAHA.107.754424
200. Voit D, Zhang S, Unterberg-Buchwald C, Sohns JM, Lotz J, Frahm J. Real-time cardiovascular magnetic resonance at 1.5 T using balanced SSFP and 40 ms resolution. *J Cardiovasc Magn Reson*. 2013;15:79. doi: 10.1186/1532-429X-15-79
201. Claus P, Omar AMS, Pedrizzetti G, Sengupta PP, Nagel E. Tissue Tracking Technology for Assessing Cardiac Mechanics: Principles, Normal Values, and Clinical Applications. *JACC Cardiovasc Imaging*. 2015;8:1444-1460. doi: 10.1016/j.jcmg.2015.11.001
202. Sengupta PP, Narula J. Reclassifying heart failure: predominantly subendocardial, subepicardial, and transmural. *Heart Fail Clin*. 2008;4:379-382. doi: 10.1016/j.hfc.2008.03.013
203. Stanton T, Leano R, Marwick TH. Prediction of all-cause mortality from global longitudinal speckle strain: comparison with ejection fraction and wall motion scoring. *Circ Cardiovasc Imaging*. 2009;2:356-364. doi: 10.1161/CIRCIMAGING.109.862334
204. Russo C, Jin Z, Elkind MS, Rundek T, Homma S, Sacco RL, Di Tullio MR. Prevalence and prognostic value of subclinical left ventricular systolic dysfunction by global longitudinal strain in a community-based cohort. *Eur J Heart Fail*. 2014;16:1301-1309. doi: 10.1002/ejhf.154
205. Medvedofsky D, Kebed K, Laffin L, Stone J, Addetia K, Lang RM, Mor-Avi V. Reproducibility and experience dependence of echocardiographic indices of left ventricular function: Side-by-side comparison of global longitudinal strain and ejection fraction. *Echocardiography*. 2017;34:365-370. doi: 10.1111/echo.13446
206. Adamu U, Schmitz F, Becker M, Kelm M, Hoffmann R. Advanced speckle tracking echocardiography allowing a three-myocardial layer-specific analysis of deformation parameters. *Eur J Echocardiogr*. 2009;10:303-308. doi: 10.1093/ejechocard/jen238
207. Alcidi GM, Esposito R, Evola V, Santoro C, Lembo M, Sorrentino R, Lo Iudice F, Borgia F, Novo G, Trimarco B, et al. Normal reference values of multilayer longitudinal strain according to age decades in a healthy population: A single-centre experience. *Eur Heart J Cardiovasc Imaging*. 2018;19:1390-1396. doi: 10.1093/ehjci/jex306
208. Leitman M, Lysiansky M, Lysyansky P, Friedman Z, Tyomkin V, Fuchs T, Adam D, Krakover R, Vered Z. Circumferential and longitudinal strain in 3 myocardial layers in normal subjects and in patients with regional left ventricular dysfunction. *J Am Soc Echocardiogr*. 2010;23:64-70. doi: 10.1016/j.echo.2009.10.004
209. Shi J, Pan C, Kong D, Cheng L, Shu X. Left Ventricular Longitudinal and Circumferential Layer-Specific Myocardial Strains and Their Determinants in Healthy Subjects. *Echocardiography*. 2016;33:510-518. doi: 10.1111/echo.13132
210. Sarvari SI, Haugaa KH, Zahid W, Bendz B, Aakhus S, Aaberge L, Edvardsen T. Layer-specific quantification of myocardial deformation by strain echocardiography may reveal significant CAD

in patients with non-ST-segment elevation acute coronary syndrome. *JACC Cardiovasc Imaging*. 2013;6:535-544. doi: 10.1016/j.jcmg.2013.01.009
211. Shiino K, Yamada A, Scalia GM, Putrino A, Chamberlain R, Poon K, Walters DL, Chan J. Early Changes of Myocardial Function After Transcatheter Aortic Valve Implantation Using Multilayer Strain Speckle Tracking Echocardiography. *Am J Cardiol*. 2018. doi: 10.1016/j.amjcard.2018.12.008
212. Petutschnigg J, Edelmann F. Heart failure with mid-range ejection fraction and with preserved ejection fraction. *Herz*. 2018;43:392-405. doi: 10.1007/s00059-018-4729-8
213. Vigneault DM, Yang E, Jensen PJ, Tee MW, Farhad H, Chu L, Noble JA, Day SM, Colan SD, Russell MW, et al. Left Ventricular Strain Is Abnormal in Preclinical and Overt Hypertrophic Cardiomyopathy: Cardiac MR Feature Tracking. *Radiology*. 2019;290:640-648. doi: 10.1148/radiol.2018180339
214. Altiok E, Neizel M, Tiemann S, Krass V, Kuhr K, Becker M, Zwicker C, Koos R, Lehmacher W, Kelm M, et al. Quantitative analysis of endocardial and epicardial left ventricular myocardial deformation-comparison of strain-encoded cardiac magnetic resonance imaging with two-dimensional speckle-tracking echocardiography. *J Am Soc Echocardiogr*. 2012;25:1179-1188. doi: 10.1016/j.echo.2012.07.019
215. Carlsson M, Heiberg E, Ostenfeld E, Steding-Ehrenborg K, Kovacs SJ, Flachskampf F, Arheden H. Functional Contribution of Circumferential Versus Longitudinal Strain: Different Concepts Suggest Conflicting Results. *J Am Coll Cardiol*. 2018;71:254-255. doi: 10.1016/j.jacc.2017.09.1156
216. Matthews SD, Rubin J, Cohen LP, Maurer MS. Myocardial Contraction Fraction: A Volumetric Measure of Myocardial Shortening Analogous to Strain. *J Am Coll Cardiol*. 2018;71:255-256. doi: 10.1016/j.jacc.2017.09.1157
217. Streeter DD, Jr., Spotnitz HM, Patel DP, Ross J, Jr., Sonnenblick EH. Fiber orientation in the canine left ventricle during diastole and systole. *Circ Res*. 1969;24:339-347.
218. Romano S, Judd RM, Kim RJ, Kim HW, Klem I, Heitner JF, Shah DJ, Jue J, White BE, Indorkar R, et al. Feature-Tracking Global Longitudinal Strain Predicts Death in a Multicenter Population of Patients With Ischemic and Nonischemic Dilated Cardiomyopathy Incremental to Ejection Fraction and Late Gadolinium Enhancement. *JACC Cardiovasc Imaging*. 2018;11:1419-1429. doi: 10.1016/j.jcmg.2017.10.024
219. Onishi T, Saha SK, Delgado-Montero A, Ludwig DR, Onishi T, Schelbert EB, Schwartzman D, Gorcsan J, 3rd. Global longitudinal strain and global circumferential strain by speckle-tracking echocardiography and feature-tracking cardiac magnetic resonance imaging: comparison with left ventricular ejection fraction. *J Am Soc Echocardiogr*. 2015;28:587-596. doi: 10.1016/j.echo.2014.11.018
220. Raafs AG, Boscutti A, Henkens M, van den Broek WWA, Verdonschot JAJ, Weerts J, Stolfo D, Nuzzi V, Manca P, Hazebroek MR, et al. Global Longitudinal Strain is Incremental to Left Ventricular Ejection Fraction for the Prediction of Outcome in Optimally Treated Dilated Cardiomyopathy Patients. *J Am Heart Assoc*. 2022;11:e024505. doi: 10.1161/JAHA.121.024505
221. Sengelov M, Jorgensen PG, Jensen JS, Bruun NE, Olsen FJ, Fritz-Hansen T, Nochioka K, Biering-Sorensen T. Global Longitudinal Strain Is a Superior Predictor of All-Cause Mortality in Heart Failure With Reduced Ejection Fraction. *JACC Cardiovasc Imaging*. 2015;8:1351-1359. doi: 10.1016/j.jcmg.2015.07.013
222. Shah SJ, Kitzman DW, Borlaug BA, van Heerebeek L, Zile MR, Kass DA, Paulus WJ. Phenotype-Specific Treatment of Heart Failure With Preserved Ejection Fraction: A Multiorgan Roadmap. *Circulation*. 2016;134:73-90. doi: 10.1161/CIRCULATIONAHA.116.021884
223. Nagueh SF. Classification of Left Ventricular Diastolic Dysfunction and Heart Failure Diagnosis and Prognosis. *J Am Soc Echocardiogr*. 2018;31:1209-1211. doi: 10.1016/j.echo.2018.09.011
224. DeVore AD, McNulty S, Alenezi F, Ersboll M, Vader JM, Oh JK, Lin G, Redfield MM, Lewis G, Semigran MJ, et al. Impaired left ventricular global longitudinal strain in patients with heart failure with preserved ejection fraction: insights from the RELAX trial. *Eur J Heart Fail*. 2017;19:893-900. doi: 10.1002/ejhf.754
225. Kraigher-Krainer E, Shah AM, Gupta DK, Santos A, Claggett B, Pieske B, Zile MR, Voors AA, Lefkowitz MP, Packer M, et al. Impaired systolic function by strain imaging in heart failure with preserved ejection fraction. *J Am Coll Cardiol*. 2014;63:447-456. doi: 10.1016/j.jacc.2013.09.052
226. Ardekani S, Jain S, Sanzi A, Corona-Villalobos CP, Abraham TP, Abraham MR, Zimmerman SL, Wu KC, Winslow RL, Miller MI, et al. Shape analysis of hypertrophic and hypertensive heart

disease using MRI-based 3D surface models of left ventricular geometry. *Med Image Anal*. 2016;29:12-23. doi: 10.1016/j.media.2015.11.004
227. Wu MT, Tseng WY, Su MY, Liu CP, Chiou KR, Wedeen VJ, Reese TG, Yang CF. Diffusion tensor magnetic resonance imaging mapping the fiber architecture remodeling in human myocardium after infarction: correlation with viability and wall motion. *Circulation*. 2006;114:1036-1045. doi: 10.1161/CIRCULATIONAHA.105.545863
228. Tamura H, Watanabe T, Nishiyama S, Sasaki S, Arimoto T, Takahashi H, Shishido T, Miyashita T, Miyamoto T, Nitobe J, et al. Increased left atrial volume index predicts a poor prognosis in patients with heart failure. *J Card Fail*. 2011;17:210-216. doi: 10.1016/j.cardfail.2010.10.006
229. Li D, Fareh S, Leung TK, Nattel S. Promotion of atrial fibrillation by heart failure in dogs: atrial remodeling of a different sort. *Circulation*. 1999;100:87-95. doi: 10.1161/01.cir.100.1.87
230. Blume GG, McLeod CJ, Barnes ME, Seward JB, Pellikka PA, Bastiansen PM, Tsang TS. Left atrial function: physiology, assessment, and clinical implications. *Eur J Echocardiogr*. 2011;12:421-430. doi: 10.1093/ejechocard/jeq175
231. Nattel S, Burstein B, Dobrev D. Atrial remodeling and atrial fibrillation: mechanisms and implications. *Circ Arrhythm Electrophysiol*. 2008;1:62-73. doi: 10.1161/CIRCEP.107.754564
232. Mamas MA, Caldwell JC, Chacko S, Garratt CJ, Fath-Ordoubadi F, Neyses L. A meta-analysis of the prognostic significance of atrial fibrillation in chronic heart failure. *Eur J Heart Fail*. 2009;11:676-683. doi: 10.1093/eurjhf/hfp085
233. Sartipy U, Dahlstrom U, Fu M, Lund LH. Atrial Fibrillation in Heart Failure With Preserved, Mid-Range, and Reduced Ejection Fraction. *JACC Heart Fail*. 2017;5:565-574. doi: 10.1016/j.jchf.2017.05.001
234. Son MK, Park JJ, Lim NK, Kim WH, Choi DJ. Impact of atrial fibrillation in patients with heart failure and reduced, mid-range or preserved ejection fraction. *Heart*. 2020;106:1160-1168. doi: 10.1136/heartjnl-2019-316219
235. Li W, Wan K, Han Y, Liu H, Cheng W, Sun J, Luo Y, Yang D, Chung YC, Chen Y. Reference value of left and right atrial size and phasic function by SSFP CMR at 3.0 T in healthy Chinese adults. *Sci Rep*. 2017;7:3196. doi: 10.1038/s41598-017-03377-6
236. Funk S, Kermer J, Doganguezel S, Schwenke C, von Knobelsdorff-Brenkenhoff F, Schulz-Menger J. Quantification of the left atrium applying cardiovascular magnetic resonance in clinical routine. *Scand Cardiovasc J*. 2018;52:85-92. doi: 10.1080/14017431.2017.1423107
237. Hudsmith LE, Petersen SE, Francis JM, Robson MD, Neubauer S. Normal human left and right ventricular and left atrial dimensions using steady state free precession magnetic resonance imaging. *J Cardiovasc Magn Reson*. 2005;7:775-782. doi: 10.1080/10976640500295516
238. Petersen SE, Aung N, Sanghvi MM, Zemrak F, Fung K, Paiva JM, Francis JM, Khanji MY, Lukaschuk E, Lee AM, et al. Reference ranges for cardiac structure and function using cardiovascular magnetic resonance (CMR) in Caucasians from the UK Biobank population cohort. *J Cardiovasc Magn Reson*. 2017;19:18. doi: 10.1186/s12968-017-0327-9
239. Fisher RA. *Statistical methods for research workers*. 14th ed. Darien, Conn.,: Hafner Pub. Co.; 1970.
240. Tsang TS, Abhayaratna WP, Barnes ME, Miyasaka Y, Gersh BJ, Bailey KR, Cha SS, Seward JB. Prediction of cardiovascular outcomes with left atrial size: is volume superior to area or diameter? *J Am Coll Cardiol*. 2006;47:1018-1023. doi: 10.1016/j.jacc.2005.08.077
241. Ristow B, Ali S, Whooley MA, Schiller NB. Usefulness of left atrial volume index to predict heart failure hospitalization and mortality in ambulatory patients with coronary heart disease and comparison to left ventricular ejection fraction (from the Heart and Soul Study). *Am J Cardiol*. 2008;102:70-76. doi: 10.1016/j.amjcard.2008.02.099
242. Triposkiadis F, Pieske B, Butler J, Parissis J, Giamouzis G, Skoularigis J, Brutsaert D, Boudoulas H. Global left atrial failure in heart failure. *Eur J Heart Fail*. 2016;18:1307-1320. doi: 10.1002/ejhf.645
243. Nagendran J, Norris CM, Appoo JJ, Ross DB, Nagendran J, Alberta Provincial Project for Outcome Assessment in Coronary Heart Disease I. Left ventricular end-diastolic pressure predicts survival in coronary artery bypass graft surgery patients. *Ann Thorac Surg*. 2014;97:1343-1347. doi: 10.1016/j.athoracsur.2013.10.047
244. Kobayashi A, Misumida N, Fox JT, Kanei Y. Prognostic Value of Left Ventricular End-Diastolic Pressure in Patients With Non-ST-Segment Elevation Myocardial Infarction. *Cardiol Res*. 2015;6:301-305. doi: 10.14740/cr406w
245. Salem R, Denault AY, Couture P, Belisle S, Fortier A, Guertin MC, Carrier M, Martineau R. Left ventricular end-diastolic pressure is a predictor of mortality in cardiac surgery independently of left ventricular ejection fraction. *Br J Anaesth*. 2006;97:292-297. doi: 10.1093/bja/ael140

246. Nagueh SF, Smiseth OA, Appleton CP, Byrd BF, 3rd, Dokainish H, Edvardsen T, Flachskampf FA, Gillebert TC, Klein AL, Lancellotti P, et al. Recommendations for the Evaluation of Left Ventricular Diastolic Function by Echocardiography: An Update from the American Society of Echocardiography and the European Association of Cardiovascular Imaging. *J Am Soc Echocardiogr*. 2016;29:277-314. doi: 10.1016/j.echo.2016.01.011
247. Pieske B, Tschope C, de Boer RA, Fraser AG, Anker SD, Donal E, Edelmann F, Fu M, Guazzi M, Lam CSP, et al. How to diagnose heart failure with preserved ejection fraction: the HFA-PEFF diagnostic algorithm: a consensus recommendation from the Heart Failure Association (HFA) of the European Society of Cardiology (ESC). *Eur Heart J*. 2019;40:3297-3317. doi: 10.1093/eurheartj/ehz641
248. Faragli A, Tanacli R, Kolp C, Abawi D, Lapinskas T, Stehning C, Schnackenburg B, Lo Muzio FP, Fassina L, Pieske B, et al. Cardiovascular magnetic resonance-derived left ventricular mechanics-strain, cardiac power and end-systolic elastance under various inotropic states in swine. *J Cardiovasc Magn Reson*. 2020;22:79. doi: 10.1186/s12968-020-00679-z
249. Backhaus SJ, Lange T, George EF, Hellenkamp K, Gertz RJ, Billing M, Wachter R, Steinmetz M, Kutty S, Raaz U, et al. Exercise Stress Real-Time Cardiac Magnetic Resonance Imaging for Noninvasive Characterization of Heart Failure With Preserved Ejection Fraction: The HFpEF-Stress Trial. *Circulation*. 2021;143:1484-1498. doi: 10.1161/CIRCULATIONAHA.120.051542
250. Obokata M, Kane GC, Reddy YN, Olson TP, Melenovsky V, Borlaug BA. Role of Diastolic Stress Testing in the Evaluation for Heart Failure With Preserved Ejection Fraction: A Simultaneous Invasive-Echocardiographic Study. *Circulation*. 2017;135:825-838. doi: 10.1161/CIRCULATIONAHA.116.024822
251. Borlaug BA, Olson TP, Lam CS, Flood KS, Lerman A, Johnson BD, Redfield MM. Global cardiovascular reserve dysfunction in heart failure with preserved ejection fraction. *J Am Coll Cardiol*. 2010;56:845-854. doi: 10.1016/j.jacc.2010.03.077
252. Burrage MK, Hundertmark M, Valkovic L, Watson WD, Rayner J, Sabharwal N, Ferreira VM, Neubauer S, Miller JJ, Rider OJ, et al. Energetic Basis for Exercise-Induced Pulmonary Congestion in Heart Failure With Preserved Ejection Fraction. *Circulation*. 2021;144:1664-1678. doi: 10.1161/CIRCULATIONAHA.121.054858
253. Zile MR, Brutsaert DL. New concepts in diastolic dysfunction and diastolic heart failure: Part II: causal mechanisms and treatment. *Circulation*. 2002;105:1503-1508. doi: 10.1161/hc1202.105290
254. Zile MR, Baicu CF, Ikonomidis JS, Stroud RE, Nietert PJ, Bradshaw AD, Slater R, Palmer BM, Van Buren P, Meyer M, et al. Myocardial stiffness in patients with heart failure and a preserved ejection fraction: contributions of collagen and titin. *Circulation*. 2015;131:1247-1259. doi: 10.1161/CIRCULATIONAHA.114.013215
255. Westermann D, Kasner M, Steendijk P, Spillmann F, Riad A, Weitmann K, Hoffmann W, Poller W, Pauschinger M, Schultheiss HP, et al. Role of left ventricular stiffness in heart failure with normal ejection fraction. *Circulation*. 2008;117:2051-2060. doi: 10.1161/CIRCULATIONAHA.107.716886
256. Mordi IR, Singh S, Rudd A, Srinivasan J, Frenneaux M, Tzemos N, Dawson DK. Comprehensive Echocardiographic and Cardiac Magnetic Resonance Evaluation Differentiates Among Heart Failure With Preserved Ejection Fraction Patients, Hypertensive Patients, and Healthy Control Subjects. *JACC Cardiovasc Imaging*. 2018;11:577-585. doi: 10.1016/j.jcmg.2017.05.022
257. Yang EY, Ghosn MG, Khan MA, Gramze NL, Brunner G, Nabi F, Nambi V, Nagueh SF, Nguyen DT, Graviss EA, et al. Myocardial Extracellular Volume Fraction Adds Prognostic Information Beyond Myocardial Replacement Fibrosis. *Circ Cardiovasc Imaging*. 2019;12:e009535. doi: 10.1161/CIRCIMAGING.119.009535
258. Peng H, Carretero OA, Vuljaj N, Liao TD, Motivala A, Peterson EL, Rhaleb NE. Angiotensin-converting enzyme inhibitors: a new mechanism of action. *Circulation*. 2005;112:2436-2445. doi: 10.1161/CIRCULATIONAHA.104.528695
259. Bastos MB, Burkhoff D, Maly J, Daemen J, den Uil CA, Ameloot K, Lenzen M, Mahfoud F, Zijlstra F, Schreuder JJ, et al. Invasive left ventricle pressure-volume analysis: overview and practical clinical implications. *Eur Heart J*. 2020;41:1286-1297. doi: 10.1093/eurheartj/ehz552
260. Fukuta H, Goto T, Wakami K, Kamiya T, Ohte N. Effect of beta-blockers on heart failure severity in patients with heart failure with preserved ejection fraction: a meta-analysis of randomized controlled trials. *Heart Fail Rev*. 2021;26:165-171. doi: 10.1007/s10741-020-10013-5
261. de Groot MJ, Hoeksma M, Blau N, Reijngoud DJ, van Spronsen FJ. Pathogenesis of cognitive dysfunction in phenylketonuria: review of hypotheses. *Mol Genet Metab*. 2010;99 Suppl 1:S86-89. doi: 10.1016/j.ymgme.2009.10.016

262. McCombe PA, McLaughlin DB, Chalk JB, Brown NN, McGill JJ, Pender MP. Spasticity and white matter abnormalities in adult phenylketonuria. *J Neurol Neurosurg Psychiatry*. 1992;55:359-361. doi: 10.1136/jnnp.55.5.359
263. Thompson AJ, Smith I, Brenton D, Youl BD, Rylance G, Davidson DC, Kendall B, Lees AJ. Neurological deterioration in young adults with phenylketonuria. *Lancet*. 1990;336:602-605. doi: 10.1016/0140-6736(90)93401-a
264. Guthrie R, Susi A. A Simple Phenylalanine Method for Detecting Phenylketonuria in Large Populations of Newborn Infants. *Pediatrics*. 1963;32:338-343.
265. van Wegberg AMJ, MacDonald A, Ahring K, Belanger-Quintana A, Blau N, Bosch AM, Burlina A, Campistol J, Feillet F, Gizewska M, et al. The complete European guidelines on phenylketonuria: diagnosis and treatment. *Orphanet J Rare Dis*. 2017;12:162. doi: 10.1186/s13023-017-0685-2
266. Schulpis KH, Tsakiris S, Traeger-Synodinos J, Papassotiriou I. Low total antioxidant status is implicated with high 8-hydroxy-2-deoxyguanosine serum concentrations in phenylketonuria. *Clin Biochem*. 2005;38:239-242. doi: 10.1016/j.clinbiochem.2004.11.006
267. Deon M, Sitta A, Faverzani JL, Guerreiro GB, Donida B, Marchetti DP, Mescka CP, Ribas GS, Coitinho AS, Wajner M, et al. Urinary biomarkers of oxidative stress and plasmatic inflammatory profile in phenylketonuric treated patients. *Int J Dev Neurosci*. 2015;47:259-265. doi: 10.1016/j.ijdevneu.2015.10.001
268. Rocha JC, van Spronsen FJ, Almeida MF, Soares G, Quelhas D, Ramos E, Guimaraes JT, Borges N. Dietary treatment in phenylketonuria does not lead to increased risk of obesity or metabolic syndrome. *Mol Genet Metab*. 2012;107:659-663. doi: 10.1016/j.ymgme.2012.10.006
269. Colome C, Artuch R, Lambruschini N, Cambra FJ, Campistol J, Vilaseca M. Is there a relationship between plasma phenylalanine and cholesterol in phenylketonuric patients under dietary treatment? *Clin Biochem*. 2001;34:373-376. doi: 10.1016/s0009-9120(01)00249-1
270. Schulpi KH, Scarpalezou A. Triglycerides, cholesterol, HDL, LDL, and VLDL cholesterol in serum of phenylketonuric children under dietary control. *Clin Pediatr (Phila)*. 1989;28:466-469. doi: 10.1177/000992288902801007
271. Schulpis KH, Karakonstantakis T, Bartzeliotou A, Karikas GA, Papassotiriou I. The association of serum lipids, lipoproteins and apolipoproteins with selected trace elements and minerals in phenylketonuric patients on diet. *Clin Nutr*. 2004;23:401-407. doi: 10.1016/j.clnu.2003.09.006
272. Haaf P, Garg P, Messroghli DR, Broadbent DA, Greenwood JP, Plein S. Cardiac T1 Mapping and Extracellular Volume (ECV) in clinical practice: a comprehensive review. *J Cardiovasc Magn Reson*. 2016;18:89. doi: 10.1186/s12968-016-0308-4
273. Giusca S, Korosoglou G, Zieschang V, Stoiber L, Schnackenburg B, Stehning C, Gebker R, Pieske B, Schuster A, Backhaus S, et al. Reproducibility study on myocardial strain assessment using fast-SENC cardiac magnetic resonance imaging. *Sci Rep*. 2018;8:14100. doi: 10.1038/s41598-018-32226-3
274. Burgard P, Bremer HJ, Buhrdel P, Clemens PC, Monch E, Przyrembel H, Trefz FK, Ullrich K. Rationale for the German recommendations for phenylalanine level control in phenylketonuria 1997. *Eur J Pediatr*. 1999;158:46-54. doi: 10.1007/s004310051008
275. Sanayama Y, Nagasaka H, Takayanagi M, Ohura T, Sakamoto O, Ito T, Ishige-Wada M, Usui H, Yoshino M, Ohtake A, et al. Experimental evidence that phenylalanine is strongly associated to oxidative stress in adolescents and adults with phenylketonuria. *Mol Genet Metab*. 2011;103:220-225. doi: 10.1016/j.ymgme.2011.03.019
276. Hor KN, Wansapura J, Markham LW, Mazur W, Cripe LH, Fleck R, Benson DW, Gottliebson WM. Circumferential strain analysis identifies strata of cardiomyopathy in Duchenne muscular dystrophy: a cardiac magnetic resonance tagging study. *J Am Coll Cardiol*. 2009;53:1204-1210. doi: 10.1016/j.jacc.2008.12.032
277. Wong C, Marwick TH. Obesity cardiomyopathy: pathogenesis and pathophysiology. *Nat Clin Pract Cardiovasc Med*. 2007;4:436-443. doi: 10.1038/ncpcardio0943
278. Hermida-Ameijeiras A, Crujeiras V, Roca I, Calvo C, Leis R, Couce ML. Arterial stiffness assessment in patients with phenylketonuria. *Medicine (Baltimore)*. 2017;96:e9322. doi: 10.1097/MD.0000000000009322
279. Tsutsui H, Kinugawa S, Matsushima S. Oxidative stress and heart failure. *Am J Physiol Heart Circ Physiol*. 2011;301:H2181-2190. doi: 10.1152/ajpheart.00554.2011
280. Schulpis KH, Papakonstantinou ED, Tzamouranis J. Plasma leptin concentrations in phenylketonuric patients. *Horm Res*. 2000;53:32-35. doi: 10.1159/000023510
281. Robertson LV, McStravick N, Ripley S, Weetch E, Donald S, Adam S, Micciche A, Boocock S, MacDonald A. Body mass index in adult patients with diet-treated phenylketonuria. *J Hum Nutr Diet*. 2013;26 Suppl 1:1-6. doi: 10.1111/jhn.12054

282. Doulgeraki A, Skarpalezou A, Theodosiadou A, Monopolis I, Schulpis K. Body composition profile of young patients with phenylketonuria and mild hyperphenylalaninemia. *Int J Endocrinol Metab*. 2014;12:e16061. doi: 10.5812/ijem.16061
283. Stern JH, Rutkowski JM, Scherer PE. Adiponectin, Leptin, and Fatty Acids in the Maintenance of Metabolic Homeostasis through Adipose Tissue Crosstalk. *Cell Metab*. 2016;23:770-784. doi: 10.1016/j.cmet.2016.04.011
284. Barouch LA, Berkowitz DE, Harrison RW, O'Donnell CP, Hare JM. Disruption of leptin signaling contributes to cardiac hypertrophy independently of body weight in mice. *Circulation*. 2003;108:754-759. doi: 10.1161/01.CIR.0000083716.82622.FD
285. Friedman JM. Leptin and the endocrine control of energy balance. *Nat Metab*. 2019;1:754-764. doi: 10.1038/s42255-019-0095-y
286. Goldberg IJ, Trent CM, Schulze PC. Lipid metabolism and toxicity in the heart. *Cell Metab*. 2012;15:805-812. doi: 10.1016/j.cmet.2012.04.006
287. Mahmod M, Bull S, Suttie JJ, Pal N, Holloway C, Dass S, Myerson SG, Schneider JE, De Silva R, Petrou M, et al. Myocardial steatosis and left ventricular contractile dysfunction in patients with severe aortic stenosis. *Circ Cardiovasc Imaging*. 2013;6:808-816. doi: 10.1161/CIRCIMAGING.113.000559
288. Rijzewijk LJ, van der Meer RW, Smit JW, Diamant M, Bax JJ, Hammer S, Romijn JA, de Roos A, Lamb HJ. Myocardial steatosis is an independent predictor of diastolic dysfunction in type 2 diabetes mellitus. *J Am Coll Cardiol*. 2008;52:1793-1799. doi: 10.1016/j.jacc.2008.07.062
289. Weidemann F, Breunig F, Beer M, Sandstede J, Turschner O, Voelker W, Ertl G, Knoll A, Wanner C, Strotmann JM. Improvement of cardiac function during enzyme replacement therapy in patients with Fabry disease: a prospective strain rate imaging study. *Circulation*. 2003;108:1299-1301. doi: 10.1161/01.CIR.0000091253.71282.04
290. Velagaleti RS, Massaro J, Vasan RS, Robins SJ, Kannel WB, Levy D. Relations of lipid concentrations to heart failure incidence: the Framingham Heart Study. *Circulation*. 2009;120:2345-2351. doi: 10.1161/CIRCULATIONAHA.109.830984
291. Brunner FJ, Waldeyer C, Ojeda F, Salomaa V, Kee F, Sans S, Thorand B, Giampaoli S, Brambilla P, Tunstall-Pedoe H, et al. Application of non-HDL cholesterol for population-based cardiovascular risk stratification: results from the Multinational Cardiovascular Risk Consortium. *Lancet*. 2019;394:2173-2183. doi: 10.1016/S0140-6736(19)32519-X
292. de Lemos JA, McGuire DK, Drazner MH. B-type natriuretic peptide in cardiovascular disease. *Lancet*. 2003;362:316-322. doi: 10.1016/S0140-6736(03)13976-1
293. Wallace TW, Abdullah SM, Drazner MH, Das SR, Khera A, McGuire DK, Wians F, Sabatine MS, Morrow DA, de Lemos JA. Prevalence and determinants of troponin T elevation in the general population. *Circulation*. 2006;113:1958-1965. doi: 10.1161/CIRCULATIONAHA.105.609974
294. Hellekson KL, National Institutes of H. NIH consensus statement on phenylketonuria. *Am Fam Physician*. 2001;63:1430-1432.
295. Griffiths PV, Demellweek C, Fay N, Robinson PH, Davidson DC. Wechsler subscale IQ and subtest profile in early treated phenylketonuria. *Arch Dis Child*. 2000;82:209-215. doi: 10.1136/adc.82.3.209
296. Blau N, Belanger-Quintana A, Demirkol M, Feillet F, Giovannini M, MacDonald A, Trefz FK, van Spronsen F, European PKUc. Management of phenylketonuria in Europe: survey results from 19 countries. *Mol Genet Metab*. 2010;99:109-115. doi: 10.1016/j.ymgme.2009.09.005
297. Klimek A, Baerwald C, Schwarz M, Rutsch F, Parhofer KG, Plockinger U, Heddrich-Ellerbrok M, Vom Dahl S, Schone K, Ott M, et al. Everyday Life, Dietary Practices, and Health Conditions of Adult PKU Patients: A Multicenter, Cross-Sectional Study. *Ann Nutr Metab*. 2020;76:251-258. doi: 10.1159/000510260
298. Vermathen P, Robert-Tissot L, Pietz J, Lutz T, Boesch C, Kreis R. Characterization of white matter alterations in phenylketonuria by magnetic resonance relaxometry and diffusion tensor imaging. *Magn Reson Med*. 2007;58:1145-1156. doi: 10.1002/mrm.21422
299. Gonzalez MJ, Polo MR, Ripolles P, Gassio R, Ormazabal A, Sierra C, Roura RC, Artuch R, Campistol J. White matter microstructural damage in early treated phenylketonuric patients. *Orphanet J Rare Dis*. 2018;13:188. doi: 10.1186/s13023-018-0912-5
300. Brito-Martins M, Harding SE, Ali NN. beta(1)- and beta(2)-adrenoceptor responses in cardiomyocytes derived from human embryonic stem cells: comparison with failing and non-failing adult human heart. *Br J Pharmacol*. 2008;153:751-759. doi: 10.1038/sj.bjp.0707619
301. Ding XQ, Fiehler J, Kohlschutter B, Wittkugel O, Grzyska U, Zeumer H, Ullrich K. MRI abnormalities in normal-appearing brain tissue of treated adult PKU patients. *J Magn Reson Imaging*. 2008;27:998-1004. doi: 10.1002/jmri.21289

302. Hudsmith LE, Neubauer S. Magnetic resonance spectroscopy in myocardial disease. *JACC Cardiovasc Imaging*. 2009;2:87-96. doi: 10.1016/j.jcmg.2008.08.005
303. Schuck PF, Malgarin F, Cararo JH, Cardoso F, Streck EL, Ferreira GC. Phenylketonuria Pathophysiology: on the Role of Metabolic Alterations. *Aging Dis*. 2015;6:390-399. doi: 10.14336/AD.2015.0827
304. Global BMIMC, Di Angelantonio E, Bhupathiraju Sh N, Wormser D, Gao P, Kaptoge S, Berrington de Gonzalez A, Cairns BJ, Huxley R, Jackson Ch L, et al. Body-mass index and all-cause mortality: individual-participant-data meta-analysis of 239 prospective studies in four continents. *Lancet*. 2016;388:776-786. doi: 10.1016/S0140-6736(16)30175-1
305. Cheng S, Fernandes VR, Bluemke DA, McClelland RL, Kronmal RA, Lima JA. Age-related left ventricular remodeling and associated risk for cardiovascular outcomes: the Multi-Ethnic Study of Atherosclerosis. *Circ Cardiovasc Imaging*. 2009;2:191-198. doi: 10.1161/CIRCIMAGING.108.819938
306. Rosmini S, Bulluck H, Captur G, Treibel TA, Abdel-Gadir A, Bhuva AN, Culotta V, Merghani A, Fontana M, Maestrini V, et al. Myocardial native T1 and extracellular volume with healthy ageing and gender. *Eur Heart J Cardiovasc Imaging*. 2018;19:615-621. doi: 10.1093/ehjci/jey034
307. Cleary M, Trefz F, Muntau AC, Feillet F, van Spronsen FJ, Burlina A, Belanger-Quintana A, Gizewska M, Gasteyger C, Bettiol E, et al. Fluctuations in phenylalanine concentrations in phenylketonuria: a review of possible relationships with outcomes. *Mol Genet Metab*. 2013;110:418-423. doi: 10.1016/j.ymgme.2013.09.001
308. Arnold GL, Kramer BM, Kirby RS, Plumeau PB, Blakely EM, Sanger Cregan LS, Davidson PW. Factors affecting cognitive, motor, behavioral and executive functioning in children with phenylketonuria. *Acta Paediatr*. 1998;87:565-570. doi: 10.1080/08035259850158308
309. Anastasoaie V, Kurzius L, Forbes P, Waisbren S. Stability of blood phenylalanine levels and IQ in children with phenylketonuria. *Mol Genet Metab*. 2008;95:17-20. doi: 10.1016/j.ymgme.2008.06.014
310. Okano Y, Nagasaka H. Optimal serum phenylalanine for adult patients with phenylketonuria. *Mol Genet Metab*. 2013;110:424-430. doi: 10.1016/j.ymgme.2013.09.007
311. Huang Y, Walker KE, Hanley F, Narula J, Houser SR, Tulenko TN. Cardiac systolic and diastolic dysfunction after a cholesterol-rich diet. *Circulation*. 2004;109:97-102. doi: 10.1161/01.CIR.0000109213.10461.F6
312. Bang CN, Gerdts E, Aurigemma GP, Boman K, de Simone G, Dahlof B, Kober L, Wachtell K, Devereux RB. Four-group classification of left ventricular hypertrophy based on ventricular concentricity and dilatation identifies a low-risk subset of eccentric hypertrophy in hypertensive patients. *Circ Cardiovasc Imaging*. 2014;7:422-429. doi: 10.1161/CIRCIMAGING.113.001275
313. Yao YS, Li TD, Zeng ZH. Mechanisms underlying direct actions of hyperlipidemia on myocardium: an updated review. *Lipids Health Dis*. 2020;19:23. doi: 10.1186/s12944-019-1171-8
314. Rayner JJ, Neubauer S, Rider OJ. The paradox of obesity cardiomyopathy and the potential for weight loss as a therapy. *Obes Rev*. 2015;16:679-690. doi: 10.1111/obr.12292
315. Ha EE, Bauer RC. Emerging Roles for Adipose Tissue in Cardiovascular Disease. *Arterioscler Thromb Vasc Biol*. 2018;38:e137-e144. doi: 10.1161/ATVBAHA.118.311421
316. Streng KW, Hillege HL, Ter Maaten JM, van Veldhuisen DJ, Dickstein K, Ng LL, Samani NJ, Metra M, Ponikowski P, Cleland JG, et al. Clinical implications of low estimated protein intake in patients with heart failure. *J Cachexia Sarcopenia Muscle*. 2022;13:1762-1770. doi: 10.1002/jcsm.12973
317. Banerjee D, Biggs ML, Mercer L, Mukamal K, Kaplan R, Barzilay J, Kuller L, Kizer JR, Djousse L, Tracy R, et al. Insulin resistance and risk of incident heart failure: Cardiovascular Health Study. *Circ Heart Fail*. 2013;6:364-370. doi: 10.1161/CIRCHEARTFAILURE.112.000022
318. Hu FB. Protein, body weight, and cardiovascular health. *Am J Clin Nutr*. 2005;82:242S-247S. doi: 10.1093/ajcn/82.1.242S
319. Tanacli R, Doeblin P, Gotze C, Zieschang V, Faragli A, Stehning C, Korosoglou G, Erley J, Weiss J, Berger A, et al. COVID-19 vs. Classical Myocarditis Associated Myocardial Injury Evaluated by Cardiac Magnetic Resonance and Endomyocardial Biopsy. *Front Cardiovasc Med*. 2021;8:737257. doi: 10.3389/fcvm.2021.737257
320. Siddiqi HK, Mehra MR. COVID-19 illness in native and immunosuppressed states: A clinical-therapeutic staging proposal. *J Heart Lung Transplant*. 2020;39:405-407. doi: 10.1016/j.healun.2020.03.012
321. Guo T, Fan Y, Chen M, Wu X, Zhang L, He T, Wang H, Wan J, Wang X, Lu Z. Cardiovascular Implications of Fatal Outcomes of Patients With Coronavirus Disease 2019 (COVID-19). *JAMA Cardiol*. 2020;5:811-818. doi: 10.1001/jamacardio.2020.1017

322. Zhou F, Yu T, Du R, Fan G, Liu Y, Liu Z, Xiang J, Wang Y, Song B, Gu X, et al. Clinical course and risk factors for mortality of adult inpatients with COVID-19 in Wuhan, China: a retrospective cohort study. *Lancet*. 2020;395:1054-1062. doi: 10.1016/S0140-6736(20)30566-3
323. Nishiga M, Wang DW, Han Y, Lewis DB, Wu JC. COVID-19 and cardiovascular disease: from basic mechanisms to clinical perspectives. *Nat Rev Cardiol*. 2020;17:543-558. doi: 10.1038/s41569-020-0413-9
324. Tschope C, Sherif M, Anker MS, Geisel D, Kuehne T, Kelle S. COVID-19-convalescence phase unmasks a silent myocardial infarction due to coronary plaque rupture. *ESC Heart Fail*. 2021. doi: 10.1002/ehf2.13186
325. Clerkin KJ, Fried JA, Raikhelkar J, Sayer G, Griffin JM, Masoumi A, Jain SS, Burkhoff D, Kumaraiah D, Rabbani L, et al. COVID-19 and Cardiovascular Disease. *Circulation*. 2020;141:1648-1655. doi: 10.1161/CIRCULATIONAHA.120.046941
326. Clark DE, Parikh A, Dendy JM, Diamond AB, George-Durrett K, Fish FA, Slaughter JC, Fitch W, Hughes SG, Soslow JH. COVID-19 Myocardial Pathology Evaluation in AthleTEs with Cardiac Magnetic Resonance (COMPETE CMR). *Circulation*. 2020. doi: 10.1161/CIRCULATIONAHA.120.052573
327. Frangogiannis NG. The significance of COVID-19-associated myocardial injury: how overinterpretation of scientific findings can fuel media sensationalism and spread misinformation. *Eur Heart J*. 2020;41:3836-3838. doi: 10.1093/eurheartj/ehaa727
328. Kociol RD, Cooper LT, Fang JC, Moslehi JJ, Pang PS, Sabe MA, Shah RV, Sims DB, Thiene G, Vardeny O, et al. Recognition and Initial Management of Fulminant Myocarditis: A Scientific Statement From the American Heart Association. *Circulation*. 2020;141:e69-e92. doi: 10.1161/CIR.0000000000000745
329. Basso C, Leone O, Rizzo S, De Gaspari M, van der Wal AC, Aubry MC, Bois MC, Lin PT, Maleszewski JJ, Stone JR. Pathological features of COVID-19-associated myocardial injury: a multicentre cardiovascular pathology study. *Eur Heart J*. 2020;41:3827-3835. doi: 10.1093/eurheartj/ehaa664
330. Sisti N, Valente S, Mandoli GE, Santoro C, Sciaccaluga C, Franchi F, Cameli P, Mondillo S, Cameli M. COVID-19 in patients with heart failure: the new and the old epidemic. *Postgrad Med J*. 2020. doi: 10.1136/postgradmedj-2020-138080
331. Kim J, Volodarskiy A, Sultana R, Pollie MP, Yum B, Nambiar L, Tafreshi R, Mitlak HW, RoyChoudhury A, Horn EM, et al. Prognostic Utility of Right Ventricular Remodeling Over Conventional Risk Stratification in Patients With COVID-19. *J Am Coll Cardiol*. 2020;76:1965-1977. doi: 10.1016/j.jacc.2020.08.066
332. Poland GA, Ovsyannikova IG, Kennedy RB. SARS-CoV-2 immunity: review and applications to phase 3 vaccine candidates. *Lancet*. 2020;396:1595-1606. doi: 10.1016/S0140-6736(20)32137-1
333. Taqueti VR, Di Carli MF. Coronary Microvascular Disease Pathogenic Mechanisms and Therapeutic Options: JACC State-of-the-Art Review. *J Am Coll Cardiol*. 2018;72:2625-2641. doi: 10.1016/j.jacc.2018.09.042
334. Ruan Q, Yang K, Wang W, Jiang L, Song J. Clinical predictors of mortality due to COVID-19 based on an analysis of data of 150 patients from Wuhan, China. *Intensive Care Med*. 2020;46:846-848. doi: 10.1007/s00134-020-05991-x
335. Lindner D, Fitzek A, Brauninger H, Aleshcheva G, Edler C, Meissner K, Scherschel K, Kirchhof P, Escher F, Schultheiss HP, et al. Association of Cardiac Infection With SARS-CoV-2 in Confirmed COVID-19 Autopsy Cases. *JAMA Cardiol*. 2020. doi: 10.1001/jamacardio.2020.3551
336. Tschope C, Ammirati E, Bozkurt B, Caforio ALP, Cooper LT, Felix SB, Hare JM, Heidecker B, Heymans S, Hubner N, et al. Myocarditis and inflammatory cardiomyopathy: current evidence and future directions. *Nat Rev Cardiol*. 2020. doi: 10.1038/s41569-020-00435-x
337. Halushka MK, Vander Heide RS. Myocarditis is rare in COVID-19 autopsies: cardiovascular findings across 277 postmortem examinations. *Cardiovasc Pathol*. 2021;50:107300. doi: 10.1016/j.carpath.2020.107300
338. Wilcox JE, Fonarow GC, Ardehali H, Bonow RO, Butler J, Sauer AJ, Epstein SE, Khan SS, Kim RJ, Sabbah HN, et al. "Targeting the Heart" in Heart Failure: Myocardial Recovery in Heart Failure With Reduced Ejection Fraction. *JACC Heart Fail*. 2015;3:661-669. doi: 10.1016/j.jchf.2015.04.011
339. Salerno M, Sharif B, Arheden H, Kumar A, Axel L, Li D, Neubauer S. Recent Advances in Cardiovascular Magnetic Resonance: Techniques and Applications. *Circ Cardiovasc Imaging*. 2017;10. doi: 10.1161/CIRCIMAGING.116.003951

340. Yang D, Wu P, Tan C, Pohl KM, Axel L, Metaxas D. 3D Motion Modeling and Reconstruction of Left Ventricle Wall in Cardiac MRI. *Funct Imaging Model Heart*. 2017;10263:481-492. doi: 10.1007/978-3-319-59448-4_46
341. O'Dell WG, Moore CC, Hunter WC, Zerhouni EA, McVeigh ER. Three-dimensional myocardial deformations: calculation with displacement field fitting to tagged MR images. *Radiology*. 1995;195:829-835. doi: 10.1148/radiology.195.3.7754016
342. Deng X, Denney TS, Jr. Three-dimensional myocardial strain reconstruction from tagged MRI using a cylindrical B-spline model. *IEEE Trans Med Imaging*. 2004;23:861-867. doi: 10.1109/TMI.2004.827961
343. Hess AT, Zhong X, Spottiswoode BS, Epstein FH, Meintjes EM. Myocardial 3D strain calculation by combining cine displacement encoding with stimulated echoes (DENSE) and cine strain encoding (SENC) imaging. *Magn Reson Med*. 2009;62:77-84. doi: 10.1002/mrm.21984
344. Scollan DF, Holmes A, Winslow R, Forder J. Histological validation of myocardial microstructure obtained from diffusion tensor magnetic resonance imaging. *Am J Physiol*. 1998;275:H2308-2318. doi: 10.1152/ajpheart.1998.275.6.H2308
345. Reese TG, Weisskoff RM, Smith RN, Rosen BR, Dinsmore RE, Wedeen VJ. Imaging myocardial fiber architecture in vivo with magnetic resonance. *Magn Reson Med*. 1995;34:786-791. doi: 10.1002/mrm.1910340603
346. Basser PJ, Mattiello J, LeBihan D. Estimation of the effective self-diffusion tensor from the NMR spin echo. *J Magn Reson B*. 1994;103:247-254. doi: 10.1006/jmrb.1994.1037
347. Ariga R, Tunnicliffe EM, Manohar SG, Mahmod M, Raman B, Piechnik SK, Francis JM, Robson MD, Neubauer S, Watkins H. Identification of Myocardial Disarray in Patients With Hypertrophic Cardiomyopathy and Ventricular Arrhythmias. *J Am Coll Cardiol*. 2019;73:2493-2502. doi: 10.1016/j.jacc.2019.02.065
348. Das A, Kelly C, Teh I, Stoeck CT, Kozerke S, Chowdhary A, Brown LAE, Saunderson CED, Craven TP, Chew PG, et al. Acute Microstructural Changes after ST-Segment Elevation Myocardial Infarction Assessed with Diffusion Tensor Imaging. *Radiology*. 2021;299:86-96. doi: 10.1148/radiol.2021203208
349. Diao KY, Yang ZG, Xu HY, Liu X, Zhang Q, Shi K, Jiang L, Xie LJ, Wen LY, Guo YK. Histologic validation of myocardial fibrosis measured by T1 mapping: a systematic review and meta-analysis. *J Cardiovasc Magn Reson*. 2016;18:92. doi: 10.1186/s12968-016-0313-7
350. Kammerlander AA, Marzluf BA, Zotter-Tufaro C, Aschauer S, Duca F, Bachmann A, Knechtelsdorfer K, Wiesinger M, Pfaffenberger S, Greiser A, et al. T1 Mapping by CMR Imaging: From Histological Validation to Clinical Implication. *JACC Cardiovasc Imaging*. 2016;9:14-23. doi: 10.1016/j.jcmg.2015.11.002
351. Ide S, Riesenkampff E, Chiasson DA, Dipchand AI, Kantor PF, Chaturvedi RR, Yoo SJ, Grosse-Wortmann L. Histological validation of cardiovascular magnetic resonance T1 mapping markers of myocardial fibrosis in paediatric heart transplant recipients. *J Cardiovasc Magn Reson*. 2017;19:10. doi: 10.1186/s12968-017-0326-x
352. Aquaro GD, Di Paolo M, Guidi B, Ghabisonia K, Pucci A, Aringheri G, Gorgodze N, Veronica M, Chiti E, Burchielli S, et al. Post-mortem CMR in a model of sudden death due to myocardial ischemia: validation with connexin-43. *Eur Radiol*. 2021;31:8098-8107. doi: 10.1007/s00330-021-07890-1
353. Tanacli R, Tschope C, Pieske B, Kelle S. CMR Assessment of Myocyte Disarray in HCM: Matching Another Piece in the Puzzle. *J Am Coll Cardiol*. 2019;74:1847-1848. doi: 10.1016/j.jacc.2019.06.079
354. Galati G, Leone O, Pasquale F, Olivotto I, Biagini E, Grigioni F, Pilato E, Lorenzini M, Corti B, Foa A, et al. Histological and Histometric Characterization of Myocardial Fibrosis in End-Stage Hypertrophic Cardiomyopathy: A Clinical-Pathological Study of 30 Explanted Hearts. *Circ Heart Fail*. 2016;9. doi: 10.1161/CIRCHEARTFAILURE.116.003090
355. de Haas HJ, Arbustini E, Fuster V, Kramer CM, Narula J. Molecular imaging of the cardiac extracellular matrix. *Circ Res*. 2014;114:903-915. doi: 10.1161/CIRCRESAHA.113.302680
356. Ezeani M, Noor A, Alt K, Lal S, Donnelly PS, Hagemeyer CE, Niego B. Collagen-Targeted Peptides for Molecular Imaging of Diffuse Cardiac Fibrosis. *J Am Heart Assoc*. 2021;10:e022139. doi: 10.1161/JAHA.121.022139
357. Armstrong AC, Gidding S, Gjesdal O, Wu C, Bluemke DA, Lima JA. LV mass assessed by echocardiography and CMR, cardiovascular outcomes, and medical practice. *JACC Cardiovasc Imaging*. 2012;5:837-848. doi: 10.1016/j.jcmg.2012.06.003
358. Taylor AJ, Salerno M, Dharmakumar R, Jerosch-Herold M. T1 Mapping: Basic Techniques and Clinical Applications. *JACC Cardiovasc Imaging*. 2016;9:67-81. doi: 10.1016/j.jcmg.2015.11.005

359. Zhang Q, Burrage MK, Lukaschuk E, Shanmuganathan M, Popescu IA, Nikolaidou C, Mills R, Werys K, Hann E, Barutcu A, et al. Toward Replacing Late Gadolinium Enhancement With Artificial Intelligence Virtual Native Enhancement for Gadolinium-Free Cardiovascular Magnetic Resonance Tissue Characterization in Hypertrophic Cardiomyopathy. *Circulation*. 2021;144:589-599. doi: 10.1161/CIRCULATIONAHA.121.054432
360. Singh K, Cornell CS, Jackson R, Kabiri M, Phipps M, Desai M, Fogle R, Ying X, Anarat-Cappillino G, Geller S, et al. CRISPR/Cas9 generated knockout mice lacking phenylalanine hydroxylase protein as a novel preclinical model for human phenylketonuria. *Sci Rep*. 2021;11:7254. doi: 10.1038/s41598-021-86663-8
361. Shedlovsky A, McDonald JD, Symula D, Dove WF. Mouse models of human phenylketonuria. *Genetics*. 1993;134:1205-1210. doi: 10.1093/genetics/134.4.1205
362. Kim JY, Han K, Suh YJ. Prevalence of abnormal cardiovascular magnetic resonance findings in recovered patients from COVID-19: a systematic review and meta-analysis. *J Cardiovasc Magn Reson*. 2021;23:100. doi: 10.1186/s12968-021-00792-7
363. Chidambaram V, Kumar A, Calcaterra G, Mehta JL. Persistent cardiac injury - An important component of long COVID-19 syndrome. *EBioMedicine*. 2022;77:103892. doi: 10.1016/j.ebiom.2022.103892
364. Petersen SE, Matthews PM, Bamberg F, Bluemke DA, Francis JM, Friedrich MG, Leeson P, Nagel E, Plein S, Rademakers FE, et al. Imaging in population science: cardiovascular magnetic resonance in 100,000 participants of UK Biobank - rationale, challenges and approaches. *J Cardiovasc Magn Reson*. 2013;15:46. doi: 10.1186/1532-429X-15-46
365. Douaud G, Lee S, Alfaro-Almagro F, Arthofer C, Wang C, McCarthy P, Lange F, Andersson JLR, Griffanti L, Duff E, et al. SARS-CoV-2 is associated with changes in brain structure in UK Biobank. *Nature*. 2022. doi: 10.1038/s41586-022-04569-5